C Journal of Carbon Research

MDPI

Review

Nanostructured Graphene Oxide-Based Hybrids as Anodes for Lithium-Ion Batteries

Poonam Sehrawat [1], Abid Abid [1], Saikh S. Islam [1], Alain Mauger [2] and Christian M. Julien [2,]*

[1] Centre for Nanoscience and Nanotechnology, Jamia Millia Islamia (A Central University), New Delhi 110025, India; sehrawatpoonam@gmail.com (P.S.); abid.zak@gmail.com (A.A.); sislam@jmi.ac.in (S.S.I.)

[2] Institut de Minéralogie, de Physique des Matériaux et de Cosmochimie (IMPMC), Sorbonne Université, CNRS-UMR 7590, 4 Place Jussieu, CEDEX 05, 75252 Paris, France; alain.mauger@sorbonne-universite.fr

* Correspondence: christian.julien@sorbonne-universite.fr

Received: 28 November 2020; Accepted: 14 December 2020; Published: 16 December 2020

Abstract: Presently, the negative electrodes of lithium-ion batteries (LIBs) are constituted by carbon-based materials, which exhibit a limited specific capacity 372 mAh g^{-1} associated with the cycle in the composition between C and LiC_6. Therefore, many efforts are currently made towards the technological development of nanostructured graphene materials because of their extraordinary mechanical, electrical, and electrochemical properties. Recent progress on advanced hybrids based on graphene oxide (GO) and reduced graphene oxide (rGO) has demonstrated the synergistic effects between graphene and an electroactive material (silicon, germanium, metal oxides (MO_x)) as electrode for electrochemical devices. In this review, attention is focused on advanced materials based on GO and rGO and their composites used as anode materials for lithium-ion batteries.

Keywords: carbonaceous materials; graphene oxide; reduced graphene oxide; composite anodes; lithium-ion batteries; supercapacitors

1. Introduction

Recently, researchers' quest for advanced devices for storing and converting sustainable energy is increasing day by day due to the demand for renewable and clean energy resources. Among all power sources, lithium-ion batteries (LIBs), sodium-ion batteries (SIBs), and electrochemical supercapacitors (ESCs) have become the most important and efficient devices for storing the electricity produced from solar cells and windmills, and they are currently in use to solve the problem of intermittency of these renewable energy sources for their integration in grid-scale stationary storage [1,2]. Anode materials for rechargeable batteries can be classified in three main groups depending on the mechanism of lithiation [3–9]:

(i) Alloying materials such as Si, Ge, Sn, Al, Bi, etc.,
(ii) Conversion materials like transition-metal oxides (Mn_xO_y, NiO, Fe_xO_y, CuO, Cu_2O, MoO_2, etc.), metal sulfides, metal phosphides, and metal nitrides (M_xX_y; here X = S, P, N),
(iii) Insertion materials, such as carbonaceous compounds (graphite, porous carbon, carbon nanotubes, graphene), TiO_2, $Li_4Ti_5O_{12}$, etc.

Presently, the negative electrodes of lithium-ion batteries (LIBs) are constituted by graphite-based materials, which exhibit a limited specific capacity of 372 mAh g^{-1} associated with the cycle in the composition between C and LiC_6. As promising anode materials for LIBs, silicon and transition-metal oxides have many advantages over graphite currently in use, such as very high capacity, wide availability, good stability, and environmental friendliness. However, certain obstacles prevent the use of these materials, namely low electronic/ionic conductivity, large volume variations, poor cycling performance, and low faradaic efficiency in the first cycle. To solve these issues, many strategies have been proposed such as the fabrication of composite electrode including a carbon-type compound like graphene and its derivatives [10,11].

Since the first experimental investigation in 2004, mono-layer graphite, known as graphene [12], has attracted considerable interest to replace graphite due to its outstanding properties. Graphene has an exceptional chemical architecture, i.e., a two-dimensional (2D) monolayer sp^2 hybridized conjugated carbon atoms with a tight packing of honeycomb lattice and displays remarkable electronic, thermal, optical, and mechanical properties [13]. It is a material that has attained tremendous attention due to its large surface area of 2630 m^2 g^{-1}, giant electrical conductivity of 6000 S cm^{-1}, and high tensile strength of 130 GPa [14]. A large number of materials have been combined with graphene, i.e., metals, semiconductors, metal oxides, polymers, alloys, etc., and applied in energy storage devices, such as lithium-based batteries, especially lithium-ion (LIBs), lithium sulfur (Li-S), and lithium-air (Li-O_2) (for a review, see Ref. [15]). However, the 2D-sheets of graphene tend restacking and irreversible aggregation due to the strong p–p interaction, hydrophobic interaction, and van der Waals force, which induce small specific surface area and poor electrochemical performance (i.e., low Li-ion diffusion rate) [16]. These issues can be overcome by the elaboration of graphene oxide (GO) and reduced graphene oxide (rGO).

Why use reduced graphene oxide in batteries instead of just graphene? Graphene is hydrophobic and difficult to handle in chemical processes, while graphene oxide has superior hydrophylic behavior; thus, graphene oxide is easy to deposit on any surface with any methods. Due to the simple and fast reduction of GO (which results in an increase of the conductivity desirable in batteries), this suggests the possibility of producing low-cost graphene battery by using cost effective rGO. Moreover, rGO can be easily fabricated in terms of mass production [17].

Therefore, using GO or rGO, many efforts are currently being made towards the technological development of new nanostructured hybrid anode materials for LIBs, which exhibit better cycling stability than graphite. We guide the reader to older review papers on graphene-based hybrids as anode materials for prior works [11,18,19]. For a historical overview related to GO and rGO synthesis and their electrochemical applications, see Refs. [20,21].

Transition-metal oxides (MO_x) have been widely studied as elements of composite electrode due to their different oxidation states and heterogeneous electrochemical activity. The combination of a nanostructured MO_x with a graphene network has met the ever-growing requirements for energy storage applications. In such hybrids, the graphene component plays several roles including stabilization of nanosized particles, inhibition of the unwanted volumetric changes, increase of the electrical conductivity and enhancement of the mechanical strength, both are improving cyclability and rate capability. Anode hybrids have been extensively investigated including various MO_x such as MnO [22], Mn_3O_4 [23], SnO_2 [24,25], MoO_2 [26], Co_3O_4 [27], Fe_3O_4 [28], and Fe_2O_3 [29]. Single elements embedded in carbonaceous matrix have been also actively investigated such silicon [30], germanium [31,32], and tin [33]. For the works related to graphene/metal oxide composites before 2012, we just guide the reader to the review article by Wu et al. [34]. The synthesis of graphene–transition metal oxide hybrid nanoparticles and their application in various fields have been reviewed in 2017 by Jana et al. [35].

In this review, we present the recent five-year developments of graphene-supported nanocomposites for advanced energy storage devices. The electrochemical performances of several rGO-based composites are discussed in relation with their methods of preparation and morphology. Graphene-supported materials are used not only as components of electrodes for batteries, but also for supercapacitors as well. However, recent reviews have been already devoted to such electrodes for supercapacitors [36,37], so that attention in the present work is focused on anode materials for lithium-ion batteries. The paper is organized as follows. A brief introduction to graphene oxide materials is given in Section 2. In Section 3, we examine the synthesis and properties of composites of graphene oxide and reduced graphene oxide with a single element, such as silicon, germanium, or tin, the technology of which is currently developed to increase the delivered specific energy, the rate capability, and the cycle life. Similar issues are treated in Section 4 for composites with metal oxides. For each system, we highlight the synthesis, morphology (particle size, porosity, specific surface area), and electrochemical parameters (initial capacity, initial coulombic efficiency (ICE), long-term cycling, and rate capability).

2. Graphene Oxide Materials

2.1. Properties of Graphene Oxides

Graphite oxide is derived from graphite by introducing a range of oxygen-containing functional groups including carboxylic acid, phenol, hydroxyl, and epoxide [38]. These functional groups attach themselves to carbon atoms in basal planes resulting in widening of the interlayer spacing. This material with an ideal chemical formula of $C_8O_2(OH)_2$ has been investigated since the 1850s by the English chemist Brodie [39]. It is an insulator with a large portion of *sp*^{3} hybridized carbon atoms, which results in a sheet resistance of ~10^{12} W sq^{-1} [40] depending on the oxygen content. GO is generally prepared from natural graphite via a modified Hummers' method [41]. The entire process is achieved within a few hours at temperature $T < 45$ °C. Typically, 100 gr powdered flake graphite and 50 g $NaNO_3$ into 2.3 L H_2SO_4 are mixed at 0 °C in an ice-bath to form a suspension and then vigorously agitated with 300 g $KMnO_4$. The exothermic reaction was controlled to prevent the suspension temperature lower than 20 °C. Then, the obtained brownish grey paste is diluted in water and treated with 3% hydrogen peroxide to reduce the residual $KMnO_4$. Finally, the yellowish-brown cake is washed in warm water and the dry from of GO is obtained by centrifugation and dehydration at 40 °C.

Reduced graphene oxide (rGO) is a layered, two-dimensional sheet of *sp*^{2}-hybridized carbon with ultrahigh specific surface area and excellent electrical conductivity [42,43]. In contrast to GO, rGO transforms into semiconductor or even into graphene-like semimetal [20]. The conductivity of rGO can reach ~10^3 S m^{-1} [44]. Rao et al. [45] investigated the effect of reducing agents on the electrical resistivity: The average resistivity for GO samples treated with hydroiodic acid appear to be in the range of 0.003–0.022 Ω·cm, followed by those treated with hydrobromic acid (0.056–0.347 Ω·cm), and finally with hydrochloric acid (0.33–0.641 Ω·cm). Wang et al. [46] found that the conductivity of rGO could be tuned in the range 2–15 S m^{-1} by changing the synthesis alkaline solution ($8 \leq \text{pH} \leq 14$). Tokarczyk et al. [47] reported that rGO samples reduced by combined thermal and pressure treatment exhibit values of surface resistivity of 1–128 W sq^{-1}. Marquez et al. [48] measured the sheet resistance of 226 W sq^{-1} for rGO prepared by laser-assisted photothermal reduction process. The properties of rGO depend on the electronic band gap, which depends on the *sp*^{2} cluster size. They are controlled by performing reversible functionalization of rGO with oxygen species. The reversible functionalization of rGO results in its partial transformation to GO such that the size of *sp*^{2} clusters within *sp*^{3} matrix varies, thereby affecting the π-π band structure [49].

Three-dimensional (3D) rGO can be easily synthesized by chemical reduction of GO by using reducing agents such as hydrazine hydrate [50,51], sodium borohydride [52], ethylene glycol [53], ascorbic acid [54], and metal powders [55], which endows them with unique properties. rGO was also prepared by reduction of GO using mild green agents, i.e., extract of fruits or vegetables containing plant polyphenols [56]. During the reduction reaction, the structure of graphene (p-conjugated structure) is substantially restored by eliminating oxygen-containing groups in GO. Birch's reaction, which entails the use of ammonia, alkali metal, and an alcohol is another efficient method to reduce GO [57]. As compared with pure graphene, many advantages endow graphene oxide (GO) and reduced graphene oxide (rGO) as a preferred conductive agent in LIBs, such as lower cost, facile preparation processes, large-scale production, and easy functionalization [58–60]. The 2D-layered structures of GO and rGO sheets anchored with metal oxide nanoparticles (NPs) are used to facilitate the electron transport and Li$^+$ diffusion in negative electrodes of LIBs [61,62]. rGO proved to be a highly versatile conductive and structure stabilizing additive in many hybrids used in LIBs. It is believed that rGO plays an essential role to enhance the electrochemical performance of composite electrodes by serving as the electrical conductive medium for the electron transfer process, providing a synergistic effect between active particles, alleviating the agglomeration of dispersed nanocrystals during the lithiation/delithiation process, and facilitating the reaction by generating well-mixed Li_2S in rGO matrix [3,9,23,63,64]. In addition, in the particular case of lithium-sulfur batteries, which will not be considered in this review, it facilitates the reaction by generating well-mixed Li_2S in rGO matrix [65].

In September 2020, the price of GO in the form of aqueous acidic paste (C/O atomic ratio 2.5–2.6) is 1600 US$ per kg, while 50 g of rGO (fully reduced) in a volume of 4–5 L costs 1200 US$ [66].

To evidence the reduction of GO to rGO, the as-synthesized samples are currently characterized by thermogravimetry analysis (TGA), X-ray diffraction (XRD), and Raman spectroscopy. Figure 1a displays the TGA profiles of GO prepared via the Hummers' method and rGO obtained by hydrothermal process. The initial weight loss of GO from 100 °C to 200 °C was attributed to the decomposition of residual oxygen-containing functional groups. On another hand, the rGO phase is stable up to 350 °C, which indicates that the main oxygenated functional groups were removed from the network by the reduction process during the synthesis. Above 200 °C, the loss results from the decomposition of carboxyl, hydroxyl, and epoxy groups at the edge and basal planes. Figure 1b presents the typical XRD patterns, in which the reflections from the stacked atomic planes of GO and rGO appear at the 2θ angle of ~12.5° and 24.0°, respectively, corresponding to the interlayer spacing of 7.08 Å for GO and 3.71 Å for rGO. Figure 1c shows the typical Raman spectra of GO and rGO samples, showing characteristic D band (at ca. 1348 cm^{-1}) and G band (at ca. 1588 cm^{-1}). The peak intensity ratio I_D/I_G increases upon reduction, which reveals the removal of oxygenated functional groups attached on carbon backbones. The I_D/I_G ratio in Raman spectroscopy can be used to evaluate the distance between defects in graphene, which is about 1 for pristine graphene and increases with the decrease in average size of the sp^2 domain and average crystalline size (L_a): $L_a = (2.4 \times 10^{-10})\ \lambda^4\ (I_D/I_G)^{-1}$, where λ is the laser wavelength in nm [67,68]. In the present case, the calculated average crystalline sizes of GO and RGO are 22 and 13 nm, respectively, indicating the decrease in average crystalline size of RGO compared with GO.

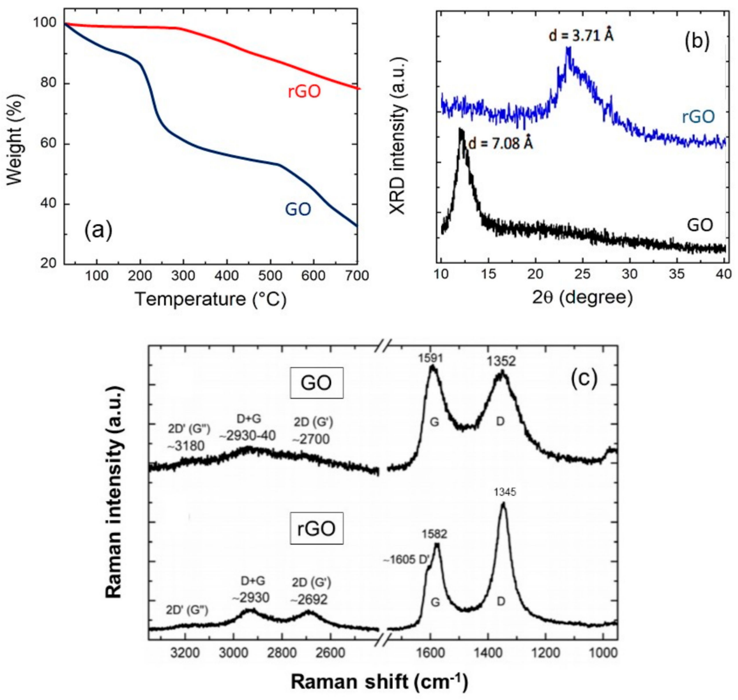

Figure 1. Characterization of graphene oxide (GO) prepared via the Hummers' method and reduced graphene oxide (rGO) obtained by hydrothermal process by (**a**) thermogravimetry analysis, (**b**) X-ray diffraction, and (**c**) Raman spectroscopy.

2.2. Lithiation of rGO

The lithiation mechanism and lithium storage capacity of rGO have been the subject of numerous investigations by means of first-principle calculations and by experimental studies such as galvanostatic charge/discharge (GCD) measurements, cyclic voltammetry (CV), and differential capacity curves [69–77]. The theoretical capacity of graphene is 744 mAh g^{-1} if Li can be absorbed on both sides up to the chemical formula Li_2C_6, and 1116 mAh g^{-1} if Li can be trapped at the benzene rings up to LiC_2, but these targets have not been achieved by using pure graphene materials [78]. Pan et al. [72] have investigated the mechanism of the lithiation of the rGO anode. The GCD profiles show a first cycle lithiation peak at 800 mV and a secondary lithiation event beginning around 250 mV and intensifying down to the cutoff voltage of 10 mV. The first cycle charge capacity at a rate of C/20 was nearly 1200 mAh g^{-1} and then dropped steadily to 350 mAh g^{-1}, where it stabilized after 20 cycles. The rate capability leads the capacity of ~200 mAh g^{-1} at a rate of C/5 and ~100 mAh g^{-1} at a rate of 1C. Wang et al. [79] observed a first cycle capacity of 700 mAh g^{-1} with an immediate decrease to 100 mAh g^{-1} in the second cycle at a rate of C/7.5. The high irreversible first cycle capacity is due to the electrochemical reactions contributing to solid-electrolyte interphase (SEI) layer formation. It is also well known that the capacity of rGO anodes is sensitive to the preparation method. Solar reduced graphene oxide (SrGO) proved to be an excellent anode material in Li-ion batteries. The SrGO material was obtained by a thermal reduction and exfoliation of GO spread over Petri disk and sun-lighted [80]. This material exhibits first cycle discharge and charge capacities as high as 1480 and 880 mAh g^{-1}, respectively. Moreover, the coulombic efficiency (CE) was found to be >95% and the specific capacity after 60 cycles was >500 mAh g^{-1} [81].

2.3. rGO-Based Composites

Currently, the typical process to fabricate a MO_x/rGO composite consists in the preparation of GO by the modified Hummers' method and then attach/grow MO_x nanoparticles (NPs) on the GO, followed by a reduction process to transform GO to rGO [82,83]. Various strategies for the fabrication of nanostructured composites have been proposed, including mixed model [84], encapsulated model [85], wrapped model [86], anchored model [87], sandwich-like model [88], and layer model [34]. Among them, the sandwich-like model appears to be a smart choice to take combinations of both the electrochemically active material and the rGO matrix in an ordered arrangement. Figure 2 shows the different structural models of *M*Ox-based composites [34].

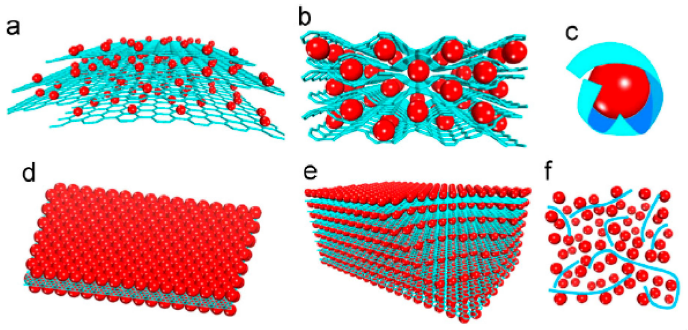

Figure 2. Schematic of structural models of GO/MO_x composites. (**a**) Anchored model. (**b**) Wrapped model. (**c**) Encapsulated model. (**d**) Sandwich-like model. (**e**) Layered model. (**f**) Mixed model (red: Metal oxide particles; blue: Graphene sheets). Reproduced with permission from [34]. Copyright 2012 Elsevier.

The theoretical specific capacity, C_{theor}, of the hypothetical metal oxide/reduced graphene oxide mixture (MO_x/rGO) can be calculated through the equation:

$$C_{\text{theor}} = C_{MOx} \times m_{MOx} + C_{\text{rGO}} \times m_{\text{rGO}}, \quad (1)$$

where C_{MOx} and m_{MOx} are the theoretical specific capacity and mass percentage of metal oxide (wt%), respectively, and C_{rGO} and m_{rGO} are the theoretical specific capacity and mass percentage of rGO, respectively. The value of C_{rGO} in the potential range of 1–3 V (744 mAh g^{-1}) is used to estimate the theoretical capacity of these composites [89].

3. Single Element/GO or rGO Composites

3.1. Silicon

Among all existing anode materials, silicon has the high theoretical specific capacity of 4200 mAh g^{-1}, which corresponds to 4.4Li^+ per Si atom to form $Li_{4.4}Si$ alloy. The huge volume change (~400%) in the lithiation/delithiation process results in loss of electrical contact of Si powders and structural cracking, implying poor cycle ability of Si anodes. To overcome this problem, the best anodes consist in Si nanoparticles dispersed in a carbon matrix, referred to as Si/C anodes. Nano-size is needed to alleviate the volume change during cycling, and the dispersion of carbon is needed to maintain electrical contact [90–95]. Since the first preparation of Si/graphene hybrid by Chou et al. in 2010 [96] constant progress in the preparation of Si/C electrodes for LIBs has been obtained through the years, even though some drawbacks still exist, such as low first coulombic efficiency [97].

As mentioned in the introduction, this review is focused on rGO-supported anodes, which are closer to commercial use than graphene-supported anodes. However, it may be useful to mention few results obtained this year on Si/graphene anodes, which illustrate the best results observed with such a composite, for comparison with the results obtained with Si/rGO anodes detailed hereunder. Jamaluddin at al. reported a Si@graphene composite with a ball-like structure [98]. The graphene sheets were obtained by an electrochemical exfoliation method from natural graphite. The Si@graphene composite was then obtained by a spray drying process, with a void space in the core-shelled ball structure inside the site. The void space helps in the accommodation of the volume change during cycling. 2882.3 mAh g^{-1} and an initial coulombic efficiency of 86.9% at 0.2 A g^{-1} was observed. At 0.5 A g^{-1}, the capacity maintained at 1063 mAh g^{-1} after 100 cycles. Si/multilayer graphene (thickness controlled to 2 nm) delivered a capacity of 990 mAh g^{-1} at 1 A g^{-1} after 500 cycles. At 4 A g^{-1}, the capacity was 1164.5 mAh g^{-1} [99]. This result was attributed to the formation of a silicon oxycarbide interlayer formed by a rapid cooling during the synthesis process of the composite. Both graphene and GO can also be used in the same anode in combination with Si. Spherical graphite/silicon/graphene oxides/carbon (Gr/Si/GO/C) composite was prepared by Huang et al. by electrostatic self-assembly and spray drying process [100]. This composite delivered a capacity of 1212 mAh g^{-1} at 200 mA g^{-1} with a capacity retention rate of 81.7% after 100 cycles.

Si@rGO composites are considered as promising anodes for the next generation of LIBs. It was shown that the particle morphology, specific surface area, and architecture of hybrids are the key issues optimizing the electrochemical performance. For example, Kim et al. have recently prepared a 2D multi-layered Si/rGO hybrid anode by direct growth of Si intercalated into a porous multi-layered rGO film, in which the porous rGO network acts as a cushion against the expansion of the Si layer during lithiation [101]. The templated self-assembly (TSA) strategy seems to be another efficient way for the preparation of Si/rGO composite [102–105]. In a typical TSA method, the self-assembled rGO/Si solution was acquired by mild stirring for 2 h and dialysis in absolute ethanol several times and then transferred to a hydrothermal reactor for reduction at 80 °C for 3 h by sodium borohydride [105].

In 2012, Chockla et al. [32] investigated the lithiation/delithiation process in binder-free rGO-supported Ge and Si nanowires (NWs) as negative electrode materials in LIBs. In the Si/Ge NWs/rGO composite, there is a competition between rGO and Si/Ge lithiation. At a high cycling rate (>0.1 C) the rGO lithiation dominates, while at low cycle rates (<0.1 C) and high Si/Ge loading only Si and Ge are lithiated. The Si NWs/rGO electrode was stabilized to a small extent but the specific capacity was low and dropped to less than 100 mAh g^{-1} for when the rate was increased from C/20 to C/10. Wang et al. [88] developed a novel type of self-supporting binder free silicon-based negative electrode through the encapsulation of silicon nanowires (SiNWs) with dual adaptable apparels (overlapped graphene sheaths and rGO overcoats). The resulting SiNWs@G/rGO composite gave high reversible capacity of 1600 mAh g^{-1} at 2.1 A g^{-1} current rate and 80% capacity retention over 100 cycles. A rate capability of 500 mAh g^{-1} at 8.4 A g^{-1} (on the basis of the total electrode weight) was demonstrated. Two advantages of such an architecture were discussed. Firstly, sealed and adaptable coated graphene sheets avoid the direct contact of encapsulated silicon and electrolyte, enabling the structural and interfacial stabilization. Secondly, the flexible and conductive rGO network controls the pulverization of the electrode and provides the conductive homogeneity to the composite. It is generally accepted that the creation of defects in the graphitic planes of graphene by replacing the carbon atom with heteroatoms increases its electrochemical performance. [106]. Chang et al. [107] prepared a Si/rGO hybrid composite anode with over 20 layers with excellent electrochemical performance at 3C rate. A control sample of Si/rGO composite was prepared using pristine Si nanoparticles and GO (weight ratio of Si to GO = 3:2) by self-assembly process mediated by electrostatic attraction [103]. The Si/rGO composite containing 64.6 wt% Si exhibits a capacity of 512 mAh g^{-1} after 40 cycles at current density of 200 mA g^{-1} between voltage limits of 0.05–1.2 V vs. Li^+/Li. In 2015, Chang et al. fabricated an anode constituted by 3D carbon-coated Si/rGO nanostructure anchored by nickel foam with carbon nanotubes using Si NPs and GO sheets in poly(methyl methacrylate solution [87]. The carbon-coated Si NPs/rGO hybrid displays a high reversible capacity up to 2700 mAh g^{-1} at a current density of 0.05 C (130 mA g^{-1}) and 70% capacity retention (up to 1311 mAh g^{-1}) at 2.6 A g^{-1} current rate after 900 cycles. Lin et al. [108] developed a Si@carbon/rGO composite with the assistance of polyaniline (PANI), which can glue to combine Si nanoparticles with GO and can be pyrolyzed as carbon coating layer. The Li storage performance of this assembled hybrid, which delivers a reversible capacity of 1121 mAh g^{-1} at a current density of 0.9 A g^{-1} over 230 cycles with CE of 81.1%, comparing well with that of the Si@carbon anode (495 mAh g^{-1} at 0.3 A g^{-1} after 50 cycles). A CNT/rGO/Si nanoparticle composite anode showing high rate and long cycle life was prepared by a layer-by-layer assembly process. In this structure, rGO completely wrapped the entire Si/CNT networks by different layers and CNT networks provide fast electron transport pathways. The CNT/rGO/Si-NPs composite exhibits high performances with long cycle life; it delivers a specific capacity of 455 mAh g^{-1} at 15 A g^{-1} after 2000 cycles, high specific charge capacity of 2250 and 650 mAh g^{-1} at 0.2 and 15 A g^{-1} current rate, respectively, and fast charge/discharge rates up to 16 A g^{-1} [109].

Recently, a multi-layered structure obtained by tuning the interface chemistries of GO and siloxene sheets as anode delivered 3880 mAh g^{-1} at 205 mA g^{-1}, and still 1040 mAh g^{-1} after 1000 cycles at 4.1 A g^{-1} [110]. The fabrication of Si@SnS_2/rGO composite anodes for high-capacity Li-ion batteries was achieved by Dai et al. [111]. The composite is formed by Si nanoparticles (30 nm in size) anchored on a 3D rGO network and mixed with $SnS_{2,}$ which provides space-constraining effects to accommodate volume expansion and particle aggregation. The Si@SnS_2/rGO composite presents a high specific capacity of 1480 mAh g^{-1} after 200 cycles at a current density of 0.2 A g^{-1} and a high stability at rates of 0.2–3.0 A g^{-1}. A stable specific capacity of 425 mAh g^{-1} was achieved after 600 cycles at a current density of 3 A g^{-1}. Deng et al. [112] reported the properties of a layer-by-layer coated nanocomposite anode fabricated by a scalable laser shock assisted roll-to-roll deposition process. The Si NPS/rGO hybrid can deliver a high specific capacity of 1956 mAh g^{-1} at a high cyclic rate of 15 A g^{-1} and can retain 71.3% of the initial capacity after 1000 cycles. A prototype full-cell using a slurry-cast $LiNi_{0.6}Mn_{0.2}Co_{0.2}O_2$ (NMC622) cathode with a mass loading of 7 mg cm^{-2} was built to demonstrate the performance of the Si/rGO composite anode (with mass loading of 0.5 mg cm^{-2}) to form the full-cell. The NMC622||Si/rGO full-cell delivers a good areal capacity of 0.95 mAh cm^{-2} at a charge/discharge rate of 0.25 mA cm^{-2} and 0.70 mAh cm^{-2} at 1 mA cm^{-2} in a voltage window 2.0–4.3 V. In addition, a 98% capacity retention after 50 cycles at 0.25 mA cm^{-2} and a high energy density of 467 Wh kg^{-1} with an average voltage of ~3.58 V are achieved. A Si/rGO composite used as an active element of an anode with mass loading of 1.0–1.2 mg cm^{-2} delivered a capacity of 894 mAh g^{-1} over 100 cycles at 0.2 A g^{-1}, and demonstrated a high-rate capability, with a capacity of 513 mAh g^{-1} retained at 5 A g^{-1} [113].

Si nanoparticles veiled with ultrathin rGO film reduced directly by precoated Ni template delivered capacity of 975 and 717 mAh g^{-1} after 300 cycles at 1 and 3 A g^{-1}, respectively [114].

Several reports are related to the Si/rGO mesoporous-like architectures [115–120]. A 3D porous micro-size pomegranate shaped nano-silicon and rGO composite delivered a capacity of 1200 mAh g^{-1} after 300 cycles at 0.5 A g^{-1} [121]. Si particles encapsulated by rGO and forming a mesoporous structure delivered 1548 mAh g^{-1} at 200 mA g^{-1} after 100 cycles, and 905 mAh g^{-1} after 100 cycles at 1 A g^{-1} [116]. A lower cost and scalable synthesis of Si@rGO composite was proposed by Benzait et al. [122]. First, low-cost Al–Si (80:20) powder was chosen as the precursor instead of the higher-priced Si. Then, nanostructured porous Si was obtained by chemical dealloying with etching of Al using hydrochloric acid. This Al-etching reaction produces hydrogen allowing the reduction of GO to rGO simultaneously. This process thus avoids the post-treatment usually needed to reduce GO. This composite delivered a capacity of 1080 mAh g^{-1} at 0.2 A g^{-1} after 250 cycles, and 840 mAh g^{-1} at 4 A g^{-1}. Liang et al. reported the fabrication of highly porous Si@C network derived from rice husks through activation and subsequent calcinations and consolidation by rGO introduced via ultrasonication [119]. The 3D carbon-coated mesoporous Si nanospheres@graphene foam (C@Si/GF) nanoarchitectures, synthesized by a thermal bubble ejection assisted chemical-vapor-deposition and magnesiothermic reduction method, exhibits superior anode performance including a specific capacity of 1200 mAh g^{-1} at 1 A g^{-1} current rate and shows stable morphology after 200 cycles [120].

The Si@C/rGO product having a high specific surface area of 539 m^2 g^{-1} and pore volume of 0.693 cm^3 g^{-1} achieved enhanced electrochemical properties with a stable capacity of 760 mAh g^{-1} after 80 cycles and a capacity of 317 mAh g^{-1} at 1 A g^{-1} current rate. Another highly porous composite was prepared by a templated self-assembly procedure with xrGO:Si ratios (x = 5, 10, 15) and optimized by calcination. The specific surface area of 482 m^2 g^{-1} for rGO/Si composite (x = 10) increased to 539 m^2 g^{-1} after a calcination at 600 °C for 4 h in Ar environment. The optimized composite displayed an initial discharge capacity of 2317 mAh g^{-1} (ICE of 93.2%) and a capacity retention of 85% after 100 cycles at 0.1 A g^{-1} rate. At a higher current density of 2 A g^{-1}, this electrode delivered a specific capacity of 728 mAh g^{-1} after 100 cycles [105]. Song's group [123] prepared Si nanoparticles (Si-NPs) enwrapped in N-doped carbon and combine with N-doped rGO and CNTs by solution-mixing and subsequent carbonization process using pyrolyzing melamine formaldehyde resin (MFR). The Si-NPs/rGO/CNTs composite, in which N-doped carbon outside Si-NPs buffers the volume change, exhibited a high reversible capacity of 892 mAh g^{-1} after 100 cycles at a current density of 100 mA g^{-1}, good rate capability, and cycling stability.

Zhang et al. [124] proposed a facile template-sacrificing method to fabricate bowl-like Si@rGO hybrids using uniform SiO_2 spheres wrapped by GO. The reduced 3D bowl-like nanoarchitecture resulting in Si nanoparticles distributed on the flexible rGO layer exhibited a high first discharge capacity of ~1890 mAh g^{-1} with a CE of 90.79% at a current density of 0.1 A g^{-1}. A stable specific capacity of 450 mAh g^{-1} was achieved after 100 cycles. More recently, Majeed et al. [116] fabricated a clay-derived mesoporous Si/rGO composite using a cost-effective and scalable process (i.e., one-pot magnesiothermic reduction), in which Si nanoparticles are encapsulated by rGO. Montmorillonite clay were used as natural resource for Si. This suitable mesoporous (with 89.2 m^2 g^{-1} specific surface area) anode material for LIBs shows an enhanced capacity of 1548 mAh g^{-1} after 100 cycles at 200 mA g^{-1} current rate.

Since 2016, a large amount of research was focused on ternary composites showing superior electrochemical performance with long-term stability. Chen et al. [125] reported the fabrication of an electrospun sandwich-structured silicon-based anode with an architecture of rGO-protected silicon/carbon nanofibers (CNF) inhibiting the fragmentation of silicon electrodes typically caused by the large volume changes during charge/discharge reactions. This composite exhibited a high specific capacity of 1055 mAh g^{-1} up to 130 cycles at 0.1 A g^{-1}. The Si/CNFs@rGO electrode also demonstrated outstanding rate behavior with a reversible capacity of 358 mAh g^{-1} at 5.0 A g^{-1}. Pan et al. [126] prepared a micro-sized ternary Si@C@rGO spherical composite by a scalable spray drying technique and a subsequent calcination process. The obtained Si@C@rGO anode delivered a high initial reversible specific capacity of 1599 mAh g^{-1} at a current density of 0.1 A g^{-1} with a good capacity retention of 94.9% at a higher current rate of 0.2 A g^{-1}. Moreover, the Si@C@rGO anode demonstrated a good rate capability with a capacity of 951 mAh g^{-1} at 2 A g^{-1}. According to the EIS results, the incorporation of graphene inhibited the growth of the SEI layer and enhanced the cycling stability of the electrode. The Si/rGO/C composite was prepared by encapsulating graphene-coated Si nanoparticles in the interconnected carbon nanofibers based on electrospinning technology [127]. This hierarchical core-shell nanofibers Si/rGO/C NFs demonstrated excellent electrochemical performance with a reversible capacity of 1228 mAh g^{-1} and a capacity retention of 72% after 100 cycles with a current density of 0.8 A g^{-1}. When the current rate increased to 4 A g^{-1}, the anode displayed superior rate capability with a specific capacity of 954 mAh g^{-1}. Lee and coworkers [128] synthesized rGO/Si composite via a simple dip-coating method with nickel foam as a current collector and template for the electrode fabrication. The rGO/Si hybrid anode with 0.03 wt% Si delivered a capacity of 778 mAh g^{-1} after 100 cycles.

Porous Si/C/reduced graphene oxide (Si/C/rGO) microspheres were prepared by the Tao's group [129] using spray drying and subsequent carbonization process with polyvinyl alcohol (PVA) as cross-linking agent. The rGO wrapped Si/C ball structure offers a buffer space for the volume change of Si during the charge–discharge process. The as-prepared Si/C/rGO anode exhibited a high reversible capacity of 928 mAh g^{-1} after 70 cycles at a current density of 0.1 A g^{-1}, and a good rate capability. An electrostatic self-assembly method was proposed to fabricate ball-milling-silicon@carbon/rGO composite (bmSi@C/rGO) using chitosan as a charged bridge [104]. The composite with 5-nm thick carbon coating and 20.4 wt% rGO tested as anode material displayed high reversible capacity of 935 mAh g^{-1} at 0.2 A g^{-1} current rate in the potential range of 0.02–1.5 V vs. Li^{+}/Li and 71.9% capacity retention after 100 cycles. In 2017, Qin et al. [130] reported the preparation of binder-free, conductive agent-free Si/rGO anode on nickel foam via one-step hydrothermal method with subsequent post-annealing process. This anode material demonstrated a remarkable cycle ability and rate performance, i.e., reversible specific capacity of 1500 mAh g^{-1} at 2 A g^{-1} current rate after 2500 cycles and over 600 mAh g^{-1} at 4 A g^{-1} after 2500 cycles. The rate capability of 500 mAh g^{-1} was still maintained at high current density of 16 A g^{-1} (Figure 3).

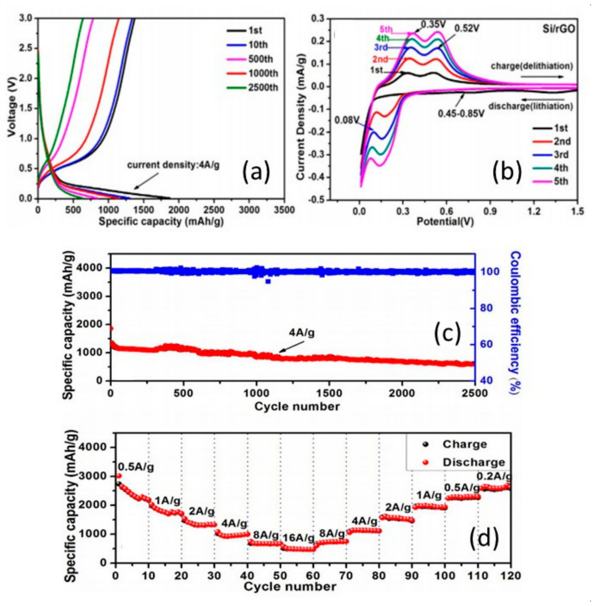

Figure 3. Electrochemical characterization of the binder-free, conductive agent-free Si/rGO anode. (**a**) Galvanostatic discharge/charge profiles from the 1st to 2500th cycle at 4 A g^{-1} current rate. (**b**) Cyclic voltammograms for the first five cycles. (**c**) Cyclability upon 2500 cycles at 4 A g^{-1} current rate. (**d**) Rate capability at various current densities from 0.5 to 16 A g^{-1} and finally back to 0.2 A g^{-1}. Reproduced with permission from [130]. Copyright 2018 Elsevier.

Recently, 3D-framework Si@N-doped C/rGO composite was synthesized by a novel polymer network method using acrylic amide and *N*,*N*′-methylene bisacrylamide as the crosslinker [131]. After the crosslinking process, Si nanoparticles (30 nm in size) were embedded in a N-doped C/rGO sheet-like network. As an anode, this composite delivered a first discharge capacity of 2609 mAh g^{-1}, an ICE of 69% and demonstrated a capacity of ~479 mAh g^{-1} after 200 cycles at 2 A g^{-1} with a CE of 99.6%. A yolk-shell structured rGO/multi-walled carbon nanotubes (MWCNT)-based hybrid as binder-free anode material was designed and investigated for different MWCNT:rGO ratios by Toçoğlu and coworkers [132]. In this configuration, the void space between Si nanoparticles (50–150 nm) and carbon coating created by the yolk-shell architecture buffered the Si volume expansion. The rGO/MWCNT/Si@void@C free-standing composite with MWCNT:rGO of 2:1 tested at 200 mA g^{-1} current rate in the voltage range 0.05–2.5 V delivered specific discharge capacities of 2472 and 1621 mAh g^{-1} at the first and second cycle, respectively. After 500 cycles at the current rate of 200 mA g^{-1}, the composite anodes with MWCNT:rGO ratios of 1:1, 1:2, 2:1 delivered capacities of 820, 503, and 951 mAhg^{-1}, respectively, while the rGO/Si@void@C (without MWCNT) exhibited only 500 mAhg^{-1}. A green-synthetic spiderweb-like hybrid composed of Si nanoparticles encapsulated by a multifunctional citric acid binder (SiNPs@CA) anchored on rGO sheets through chemical bonds was characterized as anode material [133]. The SiNPs@CA@rGO anode retained a capacity of 2566 mAh g^{-1} after 100 cycles at a current density of 1 A g^{-1} with an ICE of 81%. Kinetic measurements by EIS and GITT methods showed that Li^+ diffusion coefficients are in the range 10^{-8}–10^{-10} cm^2 s^{-1}. Wu et al. [134] prepared ternary hierarchical Si/rGO/C composites by encapsulating Si nanoparticles into the rGO/C dual-carbon matrix via self-assembling, ball milling, polystyrene sphere (PSS) template-assisting, and spray drying techniques. When cycled at 0.4 A g^{-1} for 500 cycles, the Si/rGO/C anode showed a capacity retention of ~75% and CE of ~99.7% retaining a specific capacity of ~602 mAh g^{-1}. Yu et al. [135] employed a synthesis process in mild conditions free of reducing agent to fabricate rGO/Si and N-doped rGO/C@Si composites. Analysis of the peak strength ratio of D- and G-Raman band (I_D/I_G) showed that rGO/C@Si had the higher degree of graphitization (I_D/I_G = 0.87) compared with rGO/Si (I_D/I_G = 1.04). Due to the increased affinity to lithium of amorphous carbon, the designed N-doped rGO/C@Si anode material (29.1 wt% GO; specific surface area of ~86 m^2 g^{-1}; pore volume of 0.13 cm^3 g^{-1}) showed superior cycling performance, i.e., specific capacity of 1115.8 mAh g^{-1} after 150 cycles at 0.42 A g^{-1} and better rate capability of 1077 mAh g^{-1} at 4.2 mA g^{-1}. Pomegranate-like Si@N-doped C/rGO composites were successfully fabricated by in-situ nitrogen doped carbon coating and freeze-drying processes [116]. The composite anode with ~84% Si (spherical nanoparticles with average diameter of 50 nm) presented an initial discharge capacity of ~1717 mAh g^{-1}, an ICE of 70.7%, and a charge specific capacity of 709 mAh g^{-1} at 1 A g^{-1} after 400 cycles. The capacity was still 532 mAh g^{-1} at 3 A g^{-1}. The Si@N-doped C/rGO anode demonstrated a slightly increasing $D_{Li}{}^+$ from 8.08×10^{-14} to 8.50×10^{-14} cm^2 s^{-1} after 100 cycles. Recently, Zhu et al. fabricated an anode with yolk-void-shell Si-C particles strongly anchored on rGO [136]. The Si@void@C/rGO with a void size of 5 nm delivered a capacity of 1294 mAh g^{-1} after 100 cycles at 0.5 A g^{-1}. Electrochemical performance of Si/rGO composite anodes from the recent literature are summarized in Table 1.

Table 1. Electrochemical performance of Si/rGO composites. The relevant cycle number is displayed in brackets.

Material	Synthesis	Specific Capacity (mAh g^{-1})	Current Density (A g^{-1})	Ref.
SiNWs@G/rGO	sandwich procedure	1280	2.1 (100)	[88]
Si NPs/rGO	polymer-assisted	1311	2.6 (900)	[87]
Si/CNFs@rGO	layer-by-layer assembly	455	15 (2000)	[109]
CNT/rGO/Si-NPs	electrostatic method	1480	0.2 (200)	[111]
Si@C/rGO	sonication + calcination	780	1.0 (80)	[119]
Si NPS/rGO	roll-to-roll deposition	1394	15 (1000)	[112]
Si/rGO	self-assembly	1481	0.5 (50)	[102]

Table 1. *Cont.*

Material	Synthesis	Specific Capacity (mAh g^{-1})	Current Density (A g^{-1})	Ref.
3D Si/rGO	evaporation	1406	0.05 (100)	[117]
Si@SnS$_2$/rGO	electrostatic self-assembly	1055	0.1 (130)	[125]
Si@C@rGO	spray drying + calcination	1567	0.2 (100)	[126]
Si@N-doped C/rGO	polymer network method	479	2.0 (200)	[131]
Si/C/rGO	spray-drying + carbonization	928	0.1 (70)	[129]
Si/rGO/C NFs	electrospinning	884	0.8 (100)	[127]
bmSi@C/rGO	ball-milling + pyrolysis	935	0.2 (100)	[104]
Si@N-doped C/rGO	freeze drying	709	1.0 (400)	[117]
N-doped rGO/C@Si	freeze-drying + pyrolysis	1115	0.42 (150)	[135]
Si/rGO/C	self-assembling + spray-drying	602	0.4 (500)	[134]
rGO/MWCNT/Si@void@C	dispersion + ultrasonication	951	0.2 (500)	[116]
rGO/Si@void@C	dispersion + ultrasonication	500	0.2 (500)	[132]
SiNPs@CA@rGO	suspension + freeze drying	2566	1.0 (100)	[133]
Si@rGO (bowl-like)	templating	450	0.1 (100)	[124]
Si/rGO @ Ni foam	hydrothermal	1500	2 (2500)	[130]
Si@Void@C/rGO	surface carbonization + etching	1294	0.5 (100)	[136]

3.2. Germanium

Germanium has important advantages over Si: A better electronic conductivity (2.1 S cm^{-1}) and higher Li-ion diffusivity (6.5 × 10^{-12} cm^2 s^{-1}), and a huge theoretical capacity of 1624 mAh g^{-1}; since it can be lithiated to $Li_{15}Ge_4$ (4.4 Li$^+$ per Ge atom) at low operating voltage (0.3 V vs. Li$^+$/Li) [137]. Reported phases of Li–Ge alloys include Li_7Ge_{12}, LiGe, $Li_{11}Ge_6$, Li_9Ge_4, Li_7Ge_2, $Li_{15}Ge_4$, and $Li_{22}Ge_5$ [138]. In addition, the dilatation/contraction of the lattice upon lithiation/delithiation is isotropic (~260% volume change) so that the particles avoid cracking even at a high C-rate and big particles 620 nm in size, which result in remarkable rate capability of Ge [139]. However, Ge has a disadvantage with respect to Si: A much higher cost of production. For a recent review on Ge-nanomaterials as anodes for LIBs, see Ref. [140,141].

Since 2012, improvements on Ge anodes have been made by the fabrication of hybrids with graphene oxide using different synthesis routes. Xue et al. [142] proposed a double carbon protection strategy, in which Ge is combined with amorphous carbon and graphene. When cycled under the high current density of 3.6 mA g^{-1}, the Ge@C/rGO nanocomposites still displayed a specific capacity of 380 mAh g^{-1} after 50 cycles, which is still higher than the specific capacity of 100 mAh g^{-1} of Ge@C NPs hybrid. Later, another Ge@C/rGO composite was fabricated by simply distributing Ge@C on the rGO sheets using a low-pressure thermal deposition approach. Such a hybrid anode exhibited a reversible capacity of ~940 mAh g^{-1} at a current density of 50 mA g^{-1} after 50 cycles. Germanium-graphene composites retained a capacity of 675 mAh g^{-1} after 400 cycles at current density to 400 mA g^{-1} [31]. Later, Xu et al. [143] reported the fabrication of a Ge/rGO composite made of ~5 nm Ge nanoparticles uniformly distributed within a nitrogen-doped rGO carbon matrix using a PVP-assisted hydrolysis method. The Ge/rGO composite delivered an initial discharge capacity of 1475 mAh g^{-1} and a reversible capacity of 700 mAh g^{-1} after 200 cycles at a current density of 0.5 A g^{-1}, which demonstrates that the conductive rGO carbon matrix alleviated the pulverization problem, prevented Ge particle aggregation, and facilitated lithium-ion motion. Wang et al. [144] prepared Ge@C/rGO hybrids as anode materials for Li-ion batteries by anchoring the core-shell structured germanium@carbon (Ge@C) on the reduced graphene oxide nanosheets by the strong adhesion of polydopamine (PDA). The products delivered a reversible capacity of 1074 mAh g^{-1} at 2C rate after 600 cycles (capacity retention of 96.5%) and 436 mAh g^{-1} at 20C rate after 200 cycles. An advanced anode material, which consists of sub-micron Ge crystals (200–600 nm) uniformly encapsulated in a conductive rGO matrix forming a sandwich-structured rGO/Ge/rGO, was successfully prepared through a facile thermal reduction method [145]. Enhanced reversible specific capacity of 1085 mAh g^{-1} was delivered after 500 cycles at current density of 1.6 A g^{-1} (1C rate) with the capacity loss of ~0.017% per cycle. This rGO/Ge/rGO anode was tested in a coin-type full cell with $LiNi_{0.5}Co_{0.2}Mn_{0.3}O_2$ as cathode, which exhibited a high specific capacity of 940 mAh g^{-1} after 100 cycles at 1C rate. Fang et al. [146] compared the performance of two Ge-based hybrids, namely Ge-rGO and Ge-rGO-CNTs. Ge nanoparticles anchored on rGO intertwined with carbon nanotubes (CNTs) yielded a capacity of 863 mAh g^{-1} at a current density of 100 mA g^{-1} after 100 cycles and good rate performance of 1181, 1073, 1005, 872, 767, and 644 mAh g^{-1} at current densities of 100, 200, 400, 800, 1600, and 3200 mA g^{-1}, respectively. As an example, Figure 4 presents the electrochemical performance of pure Ge, Ge-rGO, and Ge-rGO-CNTs nano-composite anodes.

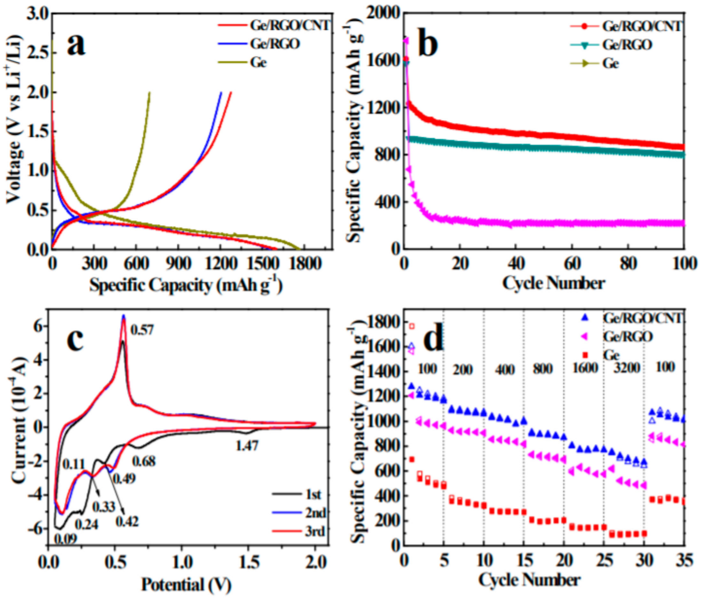

Figure 4. (**a**) Charge/discharge curves of pure Ge, Ge/rGO, and Ge/rGO/carbon nanotubes (CNTs) nanocomposite at a rate of 0.1 A g^{-1}. (**b**) Cycling performance of the three different samples at a current density of 0.1 mA g^{-1}. (**c**) Cyclic voltammetry curves of Ge/rGO/CNTs between 2.0 and 0.05 V with a scan rate of 0.1 mV s^{-1}. (**d**) Rate performance of pure Ge, Ge/rGO and Ge/rGO/CNTs nanocomposite electrodes at different current rates. Reproduced with permission from [146]. Copyright 2015 The Royal Society of Chemistry.

Recently, Chen and coworkers [147] proposed an in-situ method (i.e., chemical reaction at 60 °C for 3 h of a mixture of GO suspension and Na_2GeO_3 aqueous solution added with $NaBH_4$ solution) for the synthesis of amorphous Ge/rGO nanocomposites containing 27–37 wt% carbon, which were transformed to crystalline phase by annealing at 650 °C in reducing Ar/H_2 atmosphere. The mesoporous Ge/rGO hybrid (34.3 wt% C) had a BET specific surface area and average pore size of 81 m^2 g^{-1} and 4.2 nm, respectively. Galvanostatic measurements carried out at the current density of 0.1 A g^{-1} in the potential range of 0.01–1.5 V vs. Li^{+}/Li) showed initial discharge and charge specific capacities of 2100 and 1184 mAh g^{-1} (ICE of 56.4%) and cycling performance of 500 mAh g^{-1} is obtained at 5 A g^{-1} current rate after 100 cycles. It is believed that the small size (~5 nm) of Ge nanoparticles embedded in rGO sheets results in void space large enough to buffer the volume and maintain high structural stability during cycles. The full cell Ge/rGO||$LiFePO_4$ performed the specific capacity of ~125 mAh g^{-1} at 0.5C (85 mA g^{-1}) over 100 cycles. Zhao et al. [148] designed a double-layered protective structure in which the cubic hollow Ge@C hybrids are uniformly dispersed on rGO through dopamine-coating and subsequent carbothermal reduction. The Ge@C/rGO composite demonstrated the capacity of 1183 mAh·g^{-1} at the specific current of 0.1 A g^{-1} and 710 mAh g^{-1} at 1 A g^{-1} for 200 cycles. A few-layer methyl-terminated germanene-graphene nanocomposite ($GeCH_3$/rGO) was prepared through ultrasonic wet dispersion using $GeCH_3$ nanosheets (typical thickness 4–5 nm) prepared by liquid-phase exfoliation [149]. The resulting $GeCH_3$/rGO||Li half-cell exhibited a remaining capacity of 1058 mAh g^{-1} after 100 cycles at 0.2 A g^{-1} with CE of 98%. After 500 cycles the capacities were 439 and 288 mAh g^{-1} (CE of 98.58 and 99.31%) at current densities of 0.5 and 1.0 A g^{-1}, respectively. Electrochemical performance of Ge/rGO composite anodes from the recent literature are summarized in Table 2.

Table 2. Summary of electrochemical properties of Ge-based composite anodes. Relevant cycle number is given in brackets.

Material	Synthesis	Specific Capacity (mAh/g^{-1})	Current Density (A/g^{-1})	Ref.
Ge@C/rGO	polymerization with PDA	1074	3.2 (600)	[144]
Ge@C/rGO	dispersion + thermal reduction	380	0.1 (50)	[142]
Ge@C/rGO	low-pressure thermal deposition	940	0.05 (50)	[31]
Ge-rGO-CNTs	dispersion + thermal reduction	863	0.1 (100)	[146]
Ge/rGO	PVP-assisted hydrolysis	700	0.5 (200)	[143]
rGO/Ge/rGO	carbothermal reduction	1085	1.6 (500)	[145]
Ge@C/rGO	carbothermal reduction	710	1.0 (200)	[148]
Ge/rGO	polymeric in-situ reduction	960	1.0 (100)	[147]
$GeCH_3$/rGO	ultrasonic wet dispersion	1058	0.2 (100)	[149]
$CuGeO_3$/rGO (30 wt%)	hydrothermal reduction	909	0.1 (200)	[150]

3.3. *Tin*

Wen and Huggins showed that tin reacted with lithium to generate different alloys within the Li–Sn phase diagram [151]. Therefore, Sn has attracted great attention as anode material due to its low cost and good electrochemical activity. Upon lithiation, Sn exhibits a theoretical reversible capacity of 994 mAh g^{-1} according the reaction $Sn + xLi^+ + xe^- \leftrightarrow Li_xSn$ ($0 \leq x \leq 4.4$) with a working potential of ~0.5 V vs. $Li^{+/}Li$ [152,153]. However, during the battery cycles, Sn anodes seriously suffer from repeated large compressive and tensile stresses, which leads to fast capacity fading [154]. This problem can be solved by using Sn-graphene composites. In the early 2000s, Li and coworkers [155] investigated several nano-alloy anodes for lithium-ion batteries and showed that, with the pure nanostructured phase β-Sn-Sb prepared by co-precipitation, the reversible alloy reaction of Li with Sb(2) and Sn(3) occurs at 0.9–0.7 and 0.7–0.0 V successively. However, the use of this anode material is limited because Li alloy clusters have a very strong tendency to aggregate and form larger nano-crystallites (>20 nm) inducing a decrease of the surface energy of nano-alloy particles/clusters. In 2012, Wang et al. [156] outlined the development of Sn-based nanomaterials with a focus on their dimensionality when combined with different types of carbonaceous materials (i.e., carbon supported and carbon confined) as anode composites in LIBs. Sn/graphene composites grown by in-situ chemical reduction process (using GO and $SnCl_2$ precursors) exhibited lithium storage performance of 795 mAh g^{-1} in the 2nd cycle and 508 mAh g^{-1} in the 100th cycle, much better than that of bare Sn nanoparticles [157]. Hybridized 1D Sn nanoparticles were integrated onto the rGO surface via a hydrolysis process to form rGO-supported Sn/C nanocales (rGO/Sn@C) [158]. These rGO/Sn@C coaxial nanocables displayed an initial capacity of 760 mAh g^{-1} with a retention of 83% after 50 cycles. Submicron metallic Sn particles encapsulated in a rGO framework were used as the electrode materials for potassium-ion batteries. The Sn@rGO anode, with abundant structural defects and a high BET surface area of 136.5 m^2 g^{-1}, exhibited a capacity of 120 mAh g^{-1} after 500 cycles at 0.5 Ag^{-1} and an excellent rate capability of 67 mAh g^{-1} at 2 A g^{-1} [159]. Botas et al. developed an advanced binder-free anode material composed of 3D macroporous foams formed by rGO and submicron tin-based particles [160]. Typically, Sn/rGO samples were obtained by preparing a Sn-rGO aerogel by dissolving $SnSO_4$ in a GO suspension, with a control at pH = 9 by addition of NH_3 solution, followed by a pyrolysis process at 800 °C in argon atmosphere. The Sn/rGO anode delivered an initial capacity of 715 mAh g^{-1}, decreasing to 234 mAh g^{-1} after 50 cycles at 50 mA g^{-1}.

Two other metal/carbon would be worthy to be mentioned. A Ni@C composite, which consists of dispersed Ni nanocrystals (average size of 20 nm) encapsulated by carbon nanosheets was prepared via thermal decomposition of a nickel oleate complex at 700 °C. The composite adopts a bending structure with a good ordering of the carbon layers, forced by the Ni encapsulation. The electrode delivers an average capacity value around 723 $mAh \cdot g^{-1}$ on cycling at moderate rate of C/4. At higher rate (1C), the average specific capacity decreases to ~205 $mAh \cdot g^{-1}$ with a coulombic efficiency close to 100% after the first cycles [161]. To overcome the capacity fading of the antimony anode (theoretical capacity of 660 mAh g^{-1}, volumetric strain of 135%), a Sb/rGO anode was prepared by poly(acrylic acid) and nickel nitrate assisted electrophoretic deposition. The composite anode deposited on copper foil offers a stable discharge and charge capacity of ~498 and ~498 mAh g^{-1}, respectively, up to 100 cycles at a high current rate of 0.5 A g^{-1} [162].

4. Metal Oxide/rGO Composites

4.1. Silicon-Based Oxide Composites

Silica suboxides (SiO_x) have been regularly studied as hopeful anode materials replacing pure Si. In 2002, the Yamamoto group demonstrated the effect of both the oxygen concentration and particle size on the cycling life and on the reversible capacity of SiO_x [163]. In 2012, the Sohn group found that SiO_2 could be activated via a simple high-energy ball-milling process and could deliver a reversible capacity of ~800 mAh g^{-1} after 200 cycles [164]. The lithium battery with $SiO_{0.8}$ anode (50 nm particle size) can provide a reversible capacity of ca. 1600 mAh g^{-1} over the voltage range from 0.02 to 1.4 V vs. Li^+/Li. The success of SiO_x materials is due to their high theoretical capacity (>1600 mAh g^{-1}) and to the lithium oxygen co-ordination, which implies minimal volume change and, at the same time, lower activation energy [165].

SiO_x-based composites were synthesized by green methods such as hydrothermal route [166,167], chemical etching [168], sol-gel with subsequent annealing [169,170], solvothermal reaction [171], template route [172], and vacuum-assisted filtration and self-assembling [173,174]. Haeri et al. [169] synthesized SiO_2/GO nanohybrids through one-step sol-gel method using a mixture of tetraethylorthosilane (TEOS) and 3-aminopropyl triethoxysilane (APTES) silanes at various hydrolysis times. Structural analysis showed that amino-functionalized SiO_2 nanoparticles (~20–30 nm) were deposited on the basal plane of GO sheets. Kasimayan et al. [168] used the same method for the preparation of SiO_2@α-Fe_2O_3 core-shell decorated rGO nanocomposites with a subsequent refluxing process at 75 °C for 6 h.

Guo et al. [175] designed a SiO_x/C/rGO ternary nanocomposite using tetraethoxysilane (TEOS) as the silicon precursor. The primary SiO_x/C nanoparticles (spherical shape 50–100 nm diameter) were SiO_x particles coated with a 3-nm thick carbon layer; the disorderly stacked layer-by-layer SiO_x/C/rGO structure containing 20 wt% of amorphous carbon and rGO obtained by solvothermal reaction demonstrated very high BET specific surface area of 390.2 m^2 g^{-1}. Tested at 100 mA g^{-1} between 0.01 and 1.5 V, it exhibited a capacity of 1284 mAh g^{-1} after 100 cycles. At high rate of 3.2 A g^{-1}, the electrode retained 412 mAh g^{-1}. The electric conductivity of the SiO_x/C/RGO was 1.26×10^{-3} S cm^{-1}. Xu et al. [166] fabricated a hierarchical structure SiO_2@SnO_2/rGO by a facile hydrothermal process, which consisted of mono-dispersed SnO_2 nanoparticles (as small as 5 nm) on the surface of rGO sheets and SiO_2 spheres (~100 nm). The SiO_2@SnO_2/rGO electrode displayed a large initial discharge capacity of 1548 mAh g^{-1} at a current density of 100 mA g^{-1} and it still retained a discharge capacity of about 600 mAh g^{-1} after 100 cycles. In this hybrid, the presence of SiO_2 nanospheres mitigated the agglomeration tendency of SnO_2 nanoparticles. Zhao et al. [167] reported ternary Co_2SiO_4/SiO_2/RGO nanocomposites that exhibited a reversible capacity of 1382 mAh g^{-1} at 0.5 A g^{-1} current rate and long-life span (500 cycles), which is over 20 times higher than the SiO_2/rGO counterpart. Ex situ XPS measurements evidenced the role Co, which activates and promotes the conversion of tetravalent state of Si to low valence ones along with cycling. Guo et al. [176] reported the lithium storage performance of SiO_2@rGO hybrid, which consists of 3D interconnected SiO_2 nanoparticles (<120 nm in diameter) coated by rGO. This composite was fabricated by online hydrolysis and subsequent condensation of the precursor tetraethylorthosilicate (TEOS) in the dispersed GO sol, followed by the reduction of GO using hydrazine hydrate. The SiO_2@rGO anode material delivered a reversible discharge capacity of 708 mAh g^{-1} for the 2nd cycle and 490 mAh g^{-1} at a current density of 100 mA g^{-1} after 60 cycles with CE of ~98%.

More recently, Hu et al. [168] developed a composite with core-shell Fe_3O_4@SiO_2 particles wrapped by rGO nanosheets. Meso-/micro-porosity was produced by chemical etching, forming 3D continuous channels for Li^+ motion. The Fe_3O_4@SiO_2/GO composite delivered an initial specific capacity of 1630 mAh g^{-1} at 0.1 A g^{-1} rate over the potential range of 0.01–3.0 V vs. Li^+/Li along with a CE of 86% and retained the capacity of 514 mAh g^{-1} at 5 A g^{-1} after 1000 cycles. The fast charge/discharge process was attributed to the pseudocapacitive behavior. A multicomponent nanosheet rGO@SiO_x@NNC consisting of an inner rGO nanosheet substrate, an SiO_x intermediate layer, and an N-doped nanoporous carbon (NNC) was obtained by pyrolysis of poly(vinylpyrrolidone) [177]. The as-prepared rGO@SiO_x@NNC nanosheets with a high BET specific surface area of 360 m^2 g^{-1} and pore volume of 0.6 cm^3 g^{-1} exhibited a good cycle ability of 410 mAh g^{-1} at a current density of 1 A g^{-1} for 200 cycles as well as a specific capacity of 179 mAh g^{-1} at 5 A g^{-1} after 500 cycles. The beneficial advantage of non-stoichiometric SiO_x is evidenced by the comparison with the rGO@SiO_2@C composite, which possesses the capacity of 320 mAh g^{-1} at 1.0 A g^{-1} after 200 cycles (Figure 5).

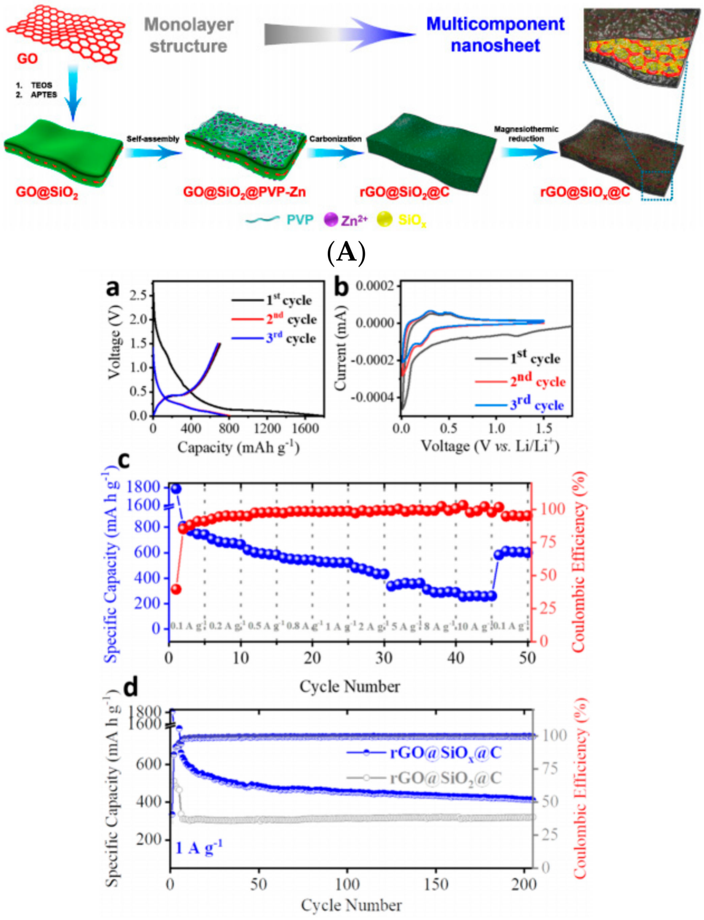

(A)

(B)

Figure 5. (**A**) Schematic illustration to fabricate rGO@SiO_x@C nanosheets. (**B**) Electrochemical properties: (a) Discharge−charge curves at 0.1 A g^{-1}, (b) cyclic voltammetry (CV) curves at 0.1 mV s^{-1} for the first three cycles, and (c) rate capability performance of the obtained rGO@SiO_x@C electrode; (d) coulombic efficiency (CE) and cycling stability at a current density of 1 A g^{-1} for 200 cycles of rGO@ SiO_2@C and rGO@SiO_x@C. Reproduced with permission from [177]. Copyright 2020 American Chemical Society.

4.2. Tin-Based Oxide Composites

SnO_2 has been widely investigated as anode for Li-ion batteries. It is abundant in nature, environmentally friendly, and has the advantage of high theoretical capacity (782 mAh g^{-1}). In 1997, Idota et al. from Fuji Photo Film Company (Japan) replaced the graphite anode of Li-ion cells by a tin-based amorphous composite oxide (TCO), which can accept 8 moles of Li^+ ions per unit mole [178]. Based on previous findings, the lithiation of SnO_2 occurs within three steps: Insertion (intermediate phase), conversion, and alloying/dealloying [179]. However, the poor electrical conductivity of SnO_2 and its severe volume expansion during lithiation hinder its wide scale utilization. Thus, the extensive study of SnO_2-graphene composites started in 2010–2011; the integration of SnO_2 with graphene has demonstrated improvement in cycling stability and rate capability [180–184].

Currently, SnO_2/graphene hybrids are fabricated using tin salts and GO via different routes, such as chemical reduction, hydrothermal growth, in situ deposition, and combined routes including calcination as the last step [25,185–190]. The most explored strategy used for the fabrication of SnO_2/rGO composite involves the hydro- or solvo-thermal deposition of very small SnO_2 nanoparticles (generally ~5 nm) on the GO layers [186,191] and its subsequent partial reduction by thermal treatments at moderate temperatures under inert atmosphere [192] or through its reaction with hydrazine [193]. For example, Hu et al. [194] designed and prepared a 3D porous rGO wrapped hollow SnO_2 nanosphere composite via a hydrothermal reaction and hydrazine reduction process. The as-developed 3D porous H-SnO_2/rGO composite was tested as anode showing a high reversible capacity of 1107 mAh g^{-1} after 100 cycles at a current density of 0.1 A g^{-1} and maintaining 552 mAh g^{-1} over 500 cycles at a current density up to 1 A g^{-1}. SnO_2NCs@N-rGO hybrid anode material was fabricated by binding SnO_2 nanocrystals (NCs) in N-doped rGO sheets by means of an in-situ hydrazine monohydrate vapor reduction method [193]. It is believed that bonds formed between graphene and SnO_2 NCs limit the aggregation of in situ formed Sn nanoparticles, leading to a stable hybrid anode material with long cycle life. A simple one-pot hydrothermal method was utilized by Wang and coworkers [195] to prepare tungsten-doped SnO_2 and reduced graphene oxide nanocomposites. The W:SnO_2/rGO hybrid exhibited an excellent long-term cycling performance. After 100 cycles, the specific discharge capacity was still as high as 1100 mAh g^{-1} at 0.1 A g^{-1} current rate (i.e., capacity retention of 90%). It still remained at 776 mAh g^{-1} after 2000 cycles at the current density of 1A g^{-1}. Wang et al. [196] prepared defect-rich crystalline SnO_2 nanoparticles with an average size of 3.5 nm homogeneously deposited on graphene nanosheets using a one-step microwave-assisted hydrothermal method. The SnO_2/graphene nanocomposites deliver a superior reversible capacity of 635 mAh g^{-1} after 100 cycles and display excellent rate performance. Shao and coworkers [197] prepared a SnO_2/rGO composite with SnO_2 nanoparticles confined by multilayered and interconnected 3D spherical rGO sheets; such hybrid anode displayed a large reversible capacity over 1000 mAh g^{-1} and long cycling life with 88% retention after 100 cycles. In situ chemical synthesis of SnO_2/rGO nanocomposites (SnO_2 crystal size of ~3–4 nm) was realized in ethanol solution. This anode material had a reversible lithium storage capacity of 1051 mAh g^{-1} [198]. Hierarchical porous SnO_2 incorporated with rGO (HP-SnO_2/rGO) was fabricated by Chen and coworkers [199] showing mesopores of 3.3 nm and macropores of ~200 nm. The half-cell using Li||SnO_2/rGO exhibited an excellent cycle performance of 850 mAh g^{-1} in 100 cycles at a current density of 0.3C and rate capability of 436 mAh g^{-1} at a current density of 4.5C. The GO/SnO_2 nanocomposite was prepared using an aqueous solution of $Sn(BF_4)_2$ with the addition of GO powders and different concentrations of reducing agent (i.e., 0–0.075 mol L^{-1} $Na_2S_2O_4$ + 0.5 mol L^{-1} HBF_4) [200]. Using low content of reducing agent (0.025 mole), the rGO-SnO_2 hybrid obtained by annealing at 500 °C under Ar atmosphere for 2 h exhibited SnO_2 nanoparticles of 15–20 nm in size and rGO Raman spectrum with I_D/I_G ratio of ~1.06 ± 0.01. It showed good Li storage performance with specific capacity of 378 mAh g^{-1} at 3.2 A g^{-1}, and cyclability of 522 mAh g^{-1} after 50 cycles at 30 mA g^{-1} current rate.

Since 2019, advanced rGO-based anodes have shown remarkable performance. Tan et al. [201] have used combined methods including in-situ metal tin oxidation for the generation of the 2D Sn/SnO/SnO_2 structure, and spray drying and thermal annealing for the transformation to 3D blueberry-shaped

SnO_2/rGO. The as-prepared hybrid containing 18.6 wt% rGO displayed a BET surface area of 218 $m^2\ g^{-1}$. Tested under a current density of 500 $mA{\cdot}g^{-1}$ in the potential window 0.01–3.0 V it exhibited a reversible capacity of 708 $mAh{\cdot}g^{-1}$ over 150 cycles. Liu et al. [202] have developed an SnO_2/GO composite composed of SnO_2 nanoparticles (200 nm in size) uniformly anchored on the surface of GO sheets using ultrasonication and calcination processes. The anode with SnO_2:GO ratio of 4:1 exhibits a discharge capacity of 492 mAh g^{-1} at 0.2C rate after 100 cycles. Tan et al. [201] reported the properties of a shrunken 3D dried blueberry shaped SnO_2/rGO composite synthesized by tin foil washed by sonification in anhydrous ethanol and placed in GO suspension in oil bath maintained at 90 °C. The SnO_2/rGO composite consisting of individual SnO_2 crystals (10 nm in size) aggregated to form larger cluster (100 nm) were well encapsulated by the few-layered rGO sheets. Electrochemical tests of this anode electrode demonstrated a high initial capacity of 737 and 128 $mAh{\cdot}g^{-1}$ under a current density of 0.2 and 10.0 $A{\cdot}g^{-1}$, respectively, over 150 cycles, and a reversible capacity of 708 $mAh{\cdot}g^{-1}$ under a current density of 0.5 $A{\cdot}g^{-1}$ over 150 cycles. Jiang et al. [203] developed a SnO_2/rGO nanocomposite, which showed an initial specific capacity of 1705 mAh g^{-1} and a capacity retention of 500 $mAh{\cdot}g^{-1}$ after 50 cycles at 250 mA g^{-1}. A free-standing SnO_2@rGO composite anode, in which SnO_2 nanoparticles were tightly wrapped within wrinkled rGO sheets, was synthesized via an anti-solvent-assisted precipitation [204]. The SnO_2@rGO anode showed significant enhanced lithium storage behavior; a high charge capacity above 700 mAh g^{-1} was achieved with 95.6% retention after 50 cycles at a current density of 0.5 A g^{-1}. The superior performance of the free-standing SnO_2@rGO electrode was evidenced by analysis of its structure after 50 cycles (Figure 6). Briefly, results are as follows: (i) The cycled composite anode displayed compressed pores and channels, attributed to the SEI formation during cycling, (ii) XRD pattern of the cycled anode revealed the co-existence of three rGO, SnO_2, and Sn components in the fully charged state, (iii) TEM image shows that, in the assembled composite, Sn-based nanoparticles remain uniformly wrapped within rGO sheets, and (iv) the observation of lattice fringes evidences the structural stability.

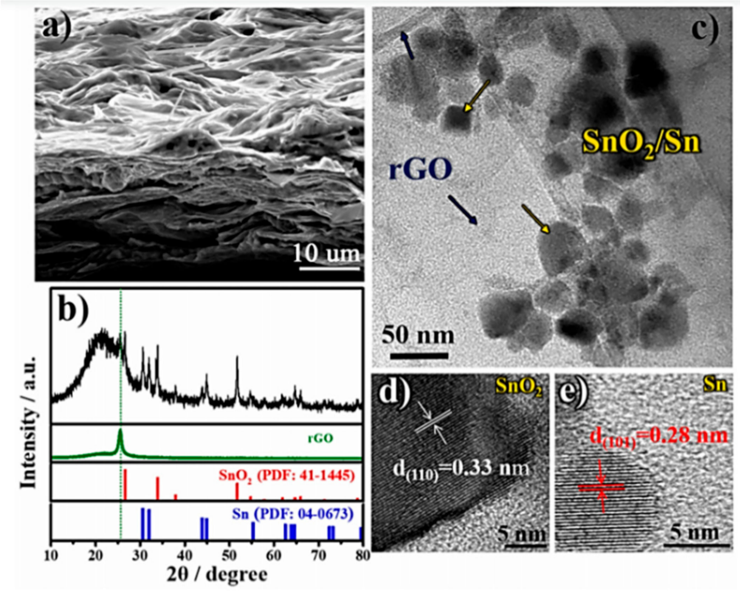

Figure 6. Morphologic and structural characteristics of cycled SnO_2@rGO nanocomposite synthesized via an anti-solvent-assisted precipitation method [204]. (**a**) FESEM image of the anode material in the fully charged state after 50 cycles at a current density of 0.5 A g^{-1}, (**b**) XRD pattern, (**c**) TEM image, and HRTEM images of (**d**) SnO_2 and (**e**) Sn particles, respectively. Copyright 2019 Jiang, Huang, Zhu, Li, Zhao, Gao, Gao, and Zhao. Under the terms of the Creative Commons Attribution License (CC BY).

Recently, rGO/SnO_x (x = 0, 1, 2) nanocomposites were prepared using a low-cost and room-temperature one-pot in-situ chemical reduction process for 30 min with $NaBH_4$ (0 mol–0.06 mol) as chelating agent [205]. SnO_x nanoparticles (2–4 nm) were uniformly distributed over rGO sheets. The rGO-SnO_x hybrid synthesized by using 0.04 mol $NaBH_4$ revealed stable specific capacity of 833 mAh g^{-1} after 50 cycles, 767 mAh g^{-1} after 100 cycles at current rate of 0.1 A g^{-1}, and good rate capability (481 mAh g^{-1} at ~1 A g^{-1}). The lithium-ion diffusion coefficient in the rGO-SnO_x anode was estimated to be 2.4×10^{-10} m^2 s^{-1}, which evidences the vital role of rGO in terms of kinetics.

Several reports have shown that doping also results in an increase of lithiation rate in SnO_2. Wang et al. [206] compared the electrochemical behavior of an Fe-doped SnO_2/rGO nanocomposite with undoped SnO_2/rGO nanoparticles prepared through a wet-chemical approach. The specific capacity of the SnO_2/rGO electrode (SnO_2 particle size of 6–8 nm) reaches 905 mAh g^{-1} after 100 cycles at 0.1 A g^{-1}, while the Fe@SnO_2/rGO nanocomposite retains a capacity of 1353 mAh g^{-1} in similar conditions. Huang et al. [207] fabricated a P-doped SnO_2/rGO/C composite by electrospinning process of a GO/(H_3PO_4)/$SnCl_4$/PVP-containing precursor solution. The cycling performance is 285 mAh g^{-1} at a rate of 0.1 A g^{-1} after 60 cycles. Zoller et al. [208] investigated the Sb-doped SnO_2(ATO)/rGO composite synthesized via a microwave-assisted in-situ method in tert-butyl alcohol. This composite featured a specific capacity of 1226 mAh g^{-1} at 1C rate and retained 577 mAh g^{-1} at very high charge rate of 60C. Fluorine-doped SnO_2 was also realized through hydrothermal process, significantly improving the electrochemical properties of the F-SnO_2 NCs/rGO composite [209]. The composite delivers a reversible capacity of 1277 mAh g^{-1} after 100 cycles at current density 0.1 A g^{-1}. The high-rate capability of 634 mAh g^{-1} after 10 cycles at current density 5 A g^{-1} was due to the reduced resistance induced by the F-doping that protects the electrode surface from the hydrolysis or decomposition of the $LiPF_6$ salt. The chemical diffusion coefficients of Li ions in F-SnO_2@rGO and SnO_2@rGO electrodes were calculated from EIS measurements as $\sim 1 \times 10^{-16}$ and $\sim 4 \times 10^{-17}$ cm^2 s^{-1}, respectively. More recently, F-SnO_2@rGO synthesized by hydrothermal process was mixed with artificial graphite and proposed as an anode by Zhang et al. [210]. It maintained specific capacities of 440 mAh g^{-1} at 500 mA g^{-1} with high capacity retention of 96.28% after 500 cycles. Electrochemical performance of SnO_2/rGO composite anodes for LIBs from the recent literature are summarized in Table 3.

Table 3. Electrochemical performance of SnO_2/GO composites as anode materials for Li-ion batteries. Relevant cycle number is given in brackets.

Material	Synthesis	Specific Capacity (mAh g^{-1})	Current Density (A g^{-1})	Ref.
SnO_2/rGO	in-situ hydrolysis	600	0.05 (20)	[198]
H-SnO_2/rGO	hydrothermal reduction	552	1.0 (500)	[194]
PS@GO/SnO_2	hydrolysis	781	0.1 (100)	[197]
SnO_2/rGO	spray drying + thermal treatment	708	0.5 (150)	[201]
SnO_{2-x}/rGO	precipitation	950	0.1 (1100)	[211]
F–SnO_2/rGO	hydrothermal @180 °C/12 h	1037	0.1 (150)	[188]
F–SnO_2/rGO	hydrothermal	440	0.5 (500)	[210]
HP-SnO_2/rGO	hydrolysis + calcination	850	0.3C (100)	[199]
W–SnO_2/rGO	hydrothermal reduction	1100	0.1 (100)	[187]
Zn–SnO_2/rGO	sol-gel + freeze-drying	628	0.1 (200)	[212]
SnO_2/GO	ultrasonication + calcination	492	2C (100)	[202]
SnO_x/rGO	chemical reduction	767	0.1 (100)	[205]
Fe@SnO_2/rGO	wet chemistry	1353	0.1 (100)	[206]
Sb-SnO_2/rGO	in-situ microwave-assisted	577	60C	[211]
F-SnO_2 NCs/rGO	hydrothermal	1277	0.1 (100)	[209]
SnO_2/rGO	precipitation + calcination	522	0.03 (50)	[200]

4.3. Manganese-Based Oxide Composites

Manganese-based oxides such as MnO, Mn_3O_4, Mn_2O_3, MnO_2, and their derivatives are attractive anode materials because of their theoretical specific capacity of 755, 936, 1018, and 1232 mAh g^{-1}, respectively [213–216]. In addition, they exhibit high safety, low cost, and environmental benignity and manganese is an abundant element. The improved performance (i.e., discharge capacity, high rate capability, kinetics of inserted ions, and long-term cyclability) of the MnO_2/rGO composite electrodes as anode materials have been evidenced by several electrochemical techniques, accounting for their extraordinary cycling properties compared with that in a simple MnO_2 electrode. Generally, the volume expansion of MnO_2 during the charge–discharge process is significantly alleviated due to the uniform dispersion and firm anchoring of MnO_2 nanoparticles on the rGO surface.

4.3.1. MnO_2-Based Composite

MnO_2 has received much attention because of its low cost, ease of fabrication, environment friendliness, low operating voltage, existence of several polymorphs with tunnel-like structure (depending on the linkage of fundamental MnO_6 octahedral units) [217]. The β-MnO_2 phase crystallizes with the rutile-like tetragonal symmetry ($P4_2/mnm$ (136) space group) and possesses 1 × 1 tunnels (0.23 nm × 0.23 nm). The α-MnO_2 phase is widely used in batteries and supercapacitors due to its large 2 × 2 tunnel structure (tetragonal, $I4/m$ (87) space group) along c-axis with MnO_6 octahedral units, which favors short diffusion path and easy ionic transport. However, the low conductivity of α-MnO_2 (~10^{-5} S cm^{-1}) inhibits its application in high power devices. To overcome these drawbacks, workers have fabricated MnO_2 nanocomposites using carbon-based materials as conducting additives. Hydrothermal method is the most popular route to prepare MnO_2/rGo composite using various reaction times [218,219]. Other techniques include in-situ electrodeposition [220], spray coating [221], ionic layer adsorption and reaction (SILAR) method [222], redox reaction [223], precipitation method [224], room temperature solution method [225], and co-electrodepossition [226].

Zhang et al. [227] reported the electrochemical performance of β-MnO_2/rGO composite anode synthesized by hydrothermal route at 160 °C for 6 h in solution containing HCl. The composite product cycled in the voltage range of 0.01–3.0 V at 100 mA g^{-1} current rate delivered an initial discharge/charge capacity of 1475/746 mAh g^{-1} and maintained a sustainable reversible capacity of 448 mAh g^{-1} over 50 cycles. The same group of researchers used the as-prepared composite as anode material in an all-solid-state lithium-ion battery with $Li_7La_3Zr_2O_{12}$ as the solid electrolyte (20 μm thick) and $LiCoO_2$ as the cathode material. When cycled at 2 μA cm^{-2} current density, the (MnO_2/rGO)/$Li_7La_3Zr_2O_{12}$/$LiCoO_2$ cell delivered a capacity of 1.87 μAh cm^{-2} [228]. Ali et al. [229] utilized a one-step electrochemical synthesis to generate MnO_2/rGO nanocomposite from Mn_3O_4 and GO starting materials. Performing a simple in-situ hydrothermal method at 160 °C for 6 h, Liu and coworkers [230] used MnO_2 nanorods (a-phase) for the fabrication of MnO_2/3D-rGO composites with a large specific surface area of ~150 m^2 g^{-1}. Galvanostatic discharge/charge measurements showed that the first discharge occurs as a long potential plateau at ca. 0.31 V attributed to the reduction of MnO_2 to Mn ($MnO_2 + 4Li^+ + 4e^- \leftrightarrow Mn + 2Li_2O$) and a weak potential plateau at ca. 0.03 V assigned to the Li insertion into graphene ($C + xLi^+ + xe^- \leftrightarrow Li_xC$). The initial discharge capacity of 1515 mAh g^{-1} decreased to 812 mAh g^{-1} in subsequent cycles and reached the value ~595 mAh g^{-1} after 60 cycles at 0.1 A g^{-1} current rate and high CE of 99%. A MnO_2 nanoflake (birnessite type)–reduced graphene oxide (MnO_2/rGO) composite was synthesized by a one-step solution method (i.e., redox reaction of $KMnO_4$ and rGO in 0.5 mol L^{-1} H_2SO_4 solution) [231]. The composite yielded a reversible capacity of 1430 and 520 mAh g^{-1} at current densities of 0.1 and 10 A g^{-1}, respectively, and a capacity retention of 1000 mAh g^{-1} after 200 cycles at the current density of 1 A g^{-1}. Lee et al. [225] synthesized rGO/a-MnO_2 nanocomposites via a simple solution method at room temperature using 1 wt% cetyltrimethylammonium bromide (CTAB) in the rGO suspension as surfactant and protection layer to prevent direct reaction between rGO and MnO_4^- ions. With a MnO_2 loading of 75 wt%, the BET surface area was 324 m^2 g^{-1} and the average pore size was evaluated as 3–4 nm. The discharge and charge capacities of the as prepared nanocomposite in the first cycle were ~1450 and ~850 mAh g^{-1}, respectively, at 100 mA g^{-1} current density in the voltage range 0.01–3.0 V. Discharge specific capacities of 222 and 115 mAh g^{-1} at a current density of 5 and 10 A g^{-1}, respectively, maintained after 400 cycles. Chae et al. [232] suggested to prepare MnO_2/rGO composites using an unrecognized chemical method by induction of intra-stacked assembly from MnO_2 NRs (birnessite d-MnO_2) and GO through polyethylenimine (PEI)-derived electrostatic modulation between both constituents. The hierarchical, 2D MnO_2/rGO hybrids (73.2:26.8 in weight) enabled highly reversible capacities of 880, 770, 630, and 460 mAh g^{-1} at current densities of 0.1, 1, 3, and 5 A g^{-1}, respectively.

Highly performing rGO/MnO_2 mesoporous nanocomposites were fabricated in a Teflon-lined stainless-steel autoclave kept at 150 °C for 15 h using pre-synthesized a-MnO_2 nanowires (diameter of 40–50 nm and length of 5–10 µm) dispersed in solution with GO sheets [233]. The rGO/a-MnO_2 composite anode featured a reversible specific capacity of 998 mAh g^{-1} at a current density of 60 mA g^{-1} after 30 cycles and rate capability of 590 mAh g^{-1} at 12 A g^{-1} current rate. The outstanding electrochemical performance is due to the increase of the BET specific surface area of the nanowires from 37.7 to 110.7 m^2 g^{-1} after graphene coverage and the inhibition of the MnO_2 nanowires agglomeration by graphene coating. Ma et al. [234] mitigated the capacity fading of MnO_2 at high cycling rates by anchoring MnO_2 nanorods (average diameter of ~100 nm and length of ~750 nm) on the surface of graphene. The composite was prepared by hydrothermal route at 160 °C for 18 h using a mixture of MnO_2 nanorods (synthesized from aqueous solution of $MnSO_4{\cdot}H_2O$ and $KMnO_4$ (ratio 2:5 in wt%)), GO sheets (prepared by the modified Hummers' method), and (3-Aminopropyl) triethoxysilane (APTES) as reducing agent. The MnO_2/rGO composite showed superior electrochemical performance with reversible capacity of 600 mAh g^{-1} after 650 cycles at 0.5 A g^{-1} current density. When cycled at a high rate of 5 A g^{-1}, a reversible specific capacity of 168 mAh g^{-1} was delivered (Figure 7). Li et al. [235] designed a polypyrrole nanoparticles (~10 nm) wrapped MnO_2/reduced graphene oxide/carbon nanotubes composite (PPy/MnO_2/rGO-CNTs). In this heterostructure, CNTs act as conductive medium and rGO nanosheets work as both reactive material and carrier for in situ growth of MnO_2. The PPy/MnO_2/rGO-CNTs shell-layer anode achieved a reversible specific capacity of 1748 mAh g^{-1} at 100 mA g^{-1} current density after 200 cycles and still features 941 mAh g^{-1} at 1 A g^{-1} current rate after 1200 cycles. Flexible graphene-wrapped carbon nanotube/graphene@MnO_2 3D multilevel porous films were fabricated via vacuum freeze-drying [236]. The outstanding nanosized pores provided vast accessible active sites and alleviated volume change. The CNT/rGO@MnO_2 porous film as an anode in lithium cell showed a high capacity of 1344.2 mAh g^{-1} over 630 cycles at 2 A g^{-1}, and superior cycling stability of 608.5 mAh g^{-1} over 1000 cycles at 7.5 A g^{-1}.

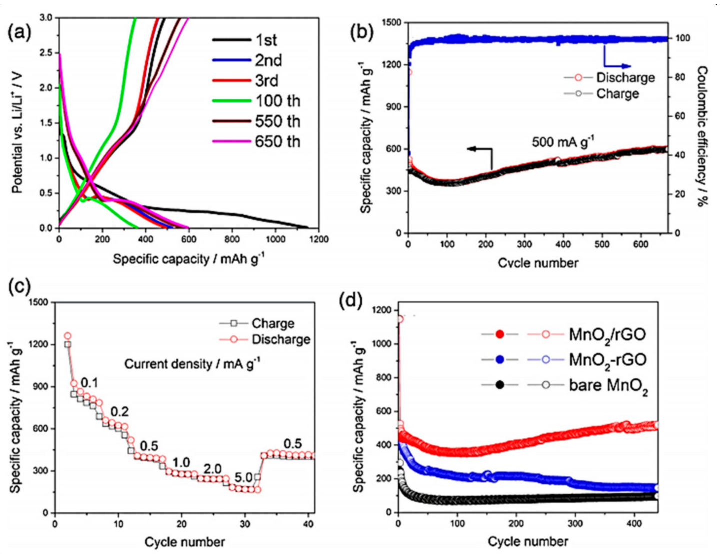

Figure 7. Electrochemical properties of MnO_2/rGO composite synthesized with (3-Aminopropyl) triethoxysilane (APTES). (**a**) Galvanostatic discharge-charge profiles of MnO_2/rGO composite at 0.5 A g^{-1} for different cycles, (**b**) cycle performance and Coulombic efficiency of MnO_2/rGO composite at a current rate of 0.5 A g^{-1}, (**c**) rate capabilities of MnO_2/rGO composite at current density ranging from 0.1 to 5A g^{-1}, (**d**) comparison of the cycle performance of MnO_2/rGO composite with MnO_2-rGO synthesized without APTES and bare MnO_2 at 0.5 A g^{-1} current density. Reproduced with permission from [234]. Copyright 2016 Elsevier.

Kim et al. [237] employed a new strategy to construct sequentially stacked a-MnO_2/rGO composites driven by surface-charge-induced mutual electrostatic interactions. The as-prepared hybrid displayed a reversible charge/discharge capacity of 1100 mAh g^{-1} without capacity fading after 100 cycles. A free-standing reduced graphene oxide/MnO_2-reduced graphene oxide-carbon nanotube nanocomposite was fabricated using vacuum filtration and thermal annealing [238]. The rGO/MnO_2/CNTS hybrid anode with 56 wt% MnO_2 cycled 100 times at 0.1 A g^{-1} current rate yielded a specific capacity of 1172 mAh g^{-1}, as 71% of the initial capacity.

Layered manganese oxides (birnessite δ-MnO_2 phase) are also considered as promising cathode materials for lithium-ion and lithium-sulfur batteries, and supercapacitors. Ultrathin layered MnO_2 nanosheets were attached on the surface of rGO sheets by one-pot precipitation method to form 2D MnO_2/rGO nanocomposites used as cathode materials for Li-ion batteries [224]. The initial discharge-specific capacity of 279.7mAh g^{-1} was maintained at 242 mAh g^{-1} after 60 cycles at 0.1C rate. The synthesis of MnO_2/rGO nanocomposites was realized using ultrasonication with Mn powder under mildly acidic conditions, which is a efficient reducing agent for GO and the MnO_2 precursor [239]. Ternary composites of GO-polyaniline (PANI)-MnO_2 nanorods were synthesized by a two-step process: (a) Coating solution-exfoliated GO nanosheets with polyaniline and (b) dispersion of graphene oxide sheets and MnO_2 nanorods in solution by ultrasonication and self-assembly during the second aniline polymerization [240]. In such a hybrid, the PANI layer anchors MnO_2 nanorods onto the surface of GO and prevents GO sheets and MnO_2 nanorods from stacking/aggregating. Chan et al. prepared rGO-wrapped MnO_2 composite electrode by an electrodeposition method using an electrolyte formed a solution of manganese acetate with L-ascorbic acid added to a dispersed solution of GO. A 13-min electrodeposition process leads spherical shaped-MnO_2 nanoparticles (~100 nm) and absence of rGO agglomeration [241]. Recently, Yang et al. [219] demonstrated that the MnO_2/rGO/S composite prepared by one-step hydrothermal method using GO and hollow MnO_2 spheres (birnessite-type) as precursors can facilitates a fast-electronic transfer. The MnO_2/rGO/S composite exhibited a BET specific surface area and the total pore volume 15.3 m^2 g^{-1} and 0.059 cm^3 g^{-1}, respectively. This cathode showed a first discharge specific capacity of 1202 mAh g^{-1} at current density of 0.2C (1C = 1675 mAh g^{-1}) and a capacity retention of 61.4% after 100 cycles at 1C rate, which corresponds to only ~0.38% decay per cycle.

The syntheses and supercapacitive behaviors of composite materials combining either GO or rGO with manganese-based oxide have been the subjects of intensive researches. The high capacitance values of MnO_2/rGO composites are most likely attributed to the synergistic effect originating from the high surface area of MnO_2 nanoparticles, the high conductivity of rGO nanosheets, and the high porosity of nanocomposites. Sawangphruk et al. [221] produced MnO_2/rGO nanocomposites on graphitized carbon fiber paper by a spray coating method. The as-prepared MnO_2/rGO composite displayed a specific surface area of 490 m^2 g^{-1}, which is slightly lower than that of pure rGO (510 m^2 g^{-1}) indicating that the composite is rather stable and still dispersed. A specific capacity of 393 F g^{-1} at a scan rate of 10 mV s^{-1} was obtained in 0.5 mol L^{-1} Na_2SO_4 electrolyte. Zhu et al. assembled an interconnected rGO/b-MnO_2 binary hybrid electrode with ultrafine MnO_2 nanostructure and precisely mass-loading control for high performance ESC [242]. The typical hybrid hydrogel also showed outstanding cycling stability with 96.3% capacitance retention after 10,000 cycles. In the work of Chen et al. [243], needle-like MnO_2-GO nanocomposites were fabricated by soft-chemical route using the double-solvent system of a water-isopropyl alcohol. These composites demonstrated the specific capacitance of 197 F g^{-1} at 0.2 A g^{-1} current density. Wang et al. synthesized MnO_2 nanowire-GO and MnOOH nanowire-GO hybrids for ESCs using a redox reaction between $KMnO_4$ and GO, and hydrothermal reaction without any extra reductants, respectively. The maximum specific capacitances of 155 and 76 F g^{-1} at current density of 0.1 A g^{-1} were obtained, respectively, in 5% ammonia aqueous solution [223]. Lu et al. [244] demonstrated that the CNTs/RGO/MnO_2 composite (with the d-MnO_2 phase) as electrode of ESC in 2 mol L^{-1} Na_2SO_4 electrolyte delivered specific capacitances of 404 and 82 F g^{-1} at 1.0 and 10 A g^{-1}

current densities. The long-term charge–discharge test indicates that the specific capacitance remained 70% after 5000 cycles under current density of 30 A g^{-1}.

In the work of Hareech and coworkers, a ternary nanocomposite, which consists of MnO_2 nanorods and reduced graphene oxide sheets supported on poly(3,4-ethylenedioxythiophene) -poly(styrenesulfonate) (PEDOT:PSS) polymer, was developed for ESC applications [245]. Electrochemical studies demonstrate a specific capacitance of 633 F g^{-1} at 0.5 A g^{-1} current density and 100% stability over 5000 cycles at 1 A g^{-1} rate in acetonitrile containing lithium perchlorate as electrolyte. Seredych et al. reported the preparation of MnO_2/GO composites containing only 10 wt% GO of different oxidation levels and low crystallization birnessite-type MnO_2; specific capacitance of 125 F g^{-1} at current density of 0.1 Ag^{-1} was obtained [246]. Nanostructured a-MnO_2/rGO composites with different weight feed ratios of graphene to MnO_2 (1:1, 1:2 and 2:1) were synthesized by coprecipitation under alkaline conditions. The a-MnO_2/rGO (1:1) hybrid, which exhibited a BET specific surface area of 174 m^2 g^{-1} and ~26 nm average pore diameter had a specific capacitance of 367 F g^{-1} at current density of 1 A g^{-1} (i.e., 4.6-fold higher than of MnO_2) [247]. Miniach et al. [248] studied a MnO_2/rGO via a hydrothermal technique with good specific capacitance of 157 F g^{-1} and energy density of 21 Wh kg^{-1}. Chen et al. [249] offered a rGO/MnO_2/carbon black ternary hybrid with desirable specific capacitance of 209 F g^{-1} and higher energy density of 24.3 Wh kg^{-1} in 0.5 mol L^{-1} Na_2SO_4 aqueous electrolyte at room temperature. In this study, the rGO/MnO_2 hybrid films were prepared using a vacuum filtration route by the mixture of the $KMnO_4$ solution with the rGO dispersion through cellulose esters filter. A flexible asymmetric ESC including CuO@MnO_2/rGO and MoS_2/rGO as positive and negative hybrid electrodes, respectively, showed only 8.1% capacitance loss after 10,000 cycles and an outstanding energy density of 165.6 Wh kg^{-1} and a power density of 1992 W kg^{-1} [250]. PANI/MnO_2/graphene composite was prepared by pulse electrodeposition method (current density of 2 mA cm^{-2}, pulse frequency of 1 kHz). The γ-phase MnO_2 nanoparticles are uniformly distributed on the PANI nanorods, which increases the specific surface area [251]. A MnO_2/rGO/CNTs framework was designed to inhibit the shuttle effect of lithium-sulfur batteries. It was fabricated by hydrothermal method at 180 °C for 12 h using $KMnO_4$, GO, CNTs, and $H_3PO_4{\cdot}H_2O$. The hybrid was composed by MnO_2 short nanorods (α-phase, diameter of 50 nm, and length of ~200 nm) compounded with carbon nanotubes (diameter of 20–50 nm) and tulle-like rGO and exhibited a mesoporous structure with average pore size of ~12 nm [252]. The MnO_2/rGO/CNTs/S cathode delivered an initial specific capacity of 1010 mAh g^{-1} at 0.5 C rate and achieved 780 mAh g^{-1} after 200 cycles (i.e., capacity decay rate of 0.11% per cycle).

4.3.2. Mn_3O_4-Based Composite

Mn_3O_4 (hausmannite, tetragonal structure) has gained much attention as anode material due to its high reversible capacity, low oxidation potential, abundance, and environmental friendliness [253]. Mn_3O_4 can react with 8 Li ions per formula unit (i.e., conversion reaction to form lithium oxide and metal nanoparticles: $Mn_3O_4 + 8Li^+ + 8e^- \leftrightarrow 3Mn + 4Li_2O$) leading to a theoretical specific capacity of about 936 mAh g^{-1} [254]. For the first time, in 2010, Wang and coworkers [255] reported the deposition of Mn_3O_4 nanoparticles onto rGO sheets as anode materials for LIBs. Mn_3O_4/rGO hybrids were fabricated by two-step solution phase reaction, i.e., hydrolysis in DMF followed by a hydrothermal process in water. The authors stated that Mn_3O_4 nanoparticles were possibly grown on the oxygen functional group on GO. With the assistance of rGO, this composite exhibited a capacity of 900 and 390 mAh g^{-1} at 40 and 1600 mA g^{-1}, respectively.

Mn_3O_4/rGO composites have been synthesized using combined techniques such as co-precipitation and subsequent flame procedure [256–258], hydrothermal method [259,260], in situ reduction by hydrazine vapour [261], sonication with subsequent heat treatment [262], gel formation and electrochemical reduction process [263], one-step reduction in aqueous phase [264,265], successive ionic layer adsorption and reaction (SILAR) method [222], flame plasma [256], and sonochemistry-assisted method [266,267]. Gund et al. investigated the capacitive performance of hybrid Mn_3O_4/GO composite prepared by the SILAR method, which implicates the sequential immersion (20 s duration) of the charged substrate in separately placed cationic ($MnSO_4$) and anionic (NaOH) solution, with the deposition of the monolayer of different species on the substrate in one cycle. The composite electrode with Mn_3O_4 nanograins of 20 nm and BET specific surface area of 94 m^2 g^{-1} showed the specific capacitance of 344 and 180 F g^{-1} at scan rate of 5 and 20 mV s^{-1}, respectively, in 1 mol L^{-1} Na_2SO_4 electrolyte [222]. Nanosized Mn_3O_4 particles grown on rGO were prepared by precipitation method via refluxing in solution containing $MnCl_2{\cdot}4H_2O$ and $KMnO_4$ added to GO dispersion with various $MnCl_2{\cdot}4H_2O$/GO ratios [268]. The Mn_3O_4/rGO hybrid with 72% Mn_3O_4 (~30 nm in size) delivered an initial discharge capacity of ~1226 mAh g^{-1} at 120 mA g^{-1} current rate, higher than the theoretical value of 989 mAh g^{-1} because of high surface area and charge accumulation at active sites commonly observed in nanomaterials [269]. However, the best rate capability and cyclability were obtained with the composition of 54% Mn_3O_4 (i.e., a capacity of 531 mAh g^{-1} was maintained after 40 cycles at 0.1 C rate) due to the minimum particle agglomeration. Seong et al. [262] compared the performance of an acid-treated rGO/Mn_3O_4 nanorods (ArGO/Mn_3O_4 NRs) composite with that of its parent rGO/Mn_3O_4 NRs synthesized by a simple mixing of GO and MnOOH (3:1 weight ratio) using sonication followed by heat treatment at 400 °C for 5 h in N_2 atmosphere. The ArGO/Mn_3O_4 NRs and rGO/Mn_3O_4 NRs had a mesoporous morphology with BET specific surface areas of 73.8 and 48.1 m^2 g^{-1}, respectively. Tests carried out at 200 mAh g^{-1} current density in the potential range 3.0–0.01 V showed that rGO/Mn_3O_4 and ArGO/Mn_3O_4 electrodes deliver an initial discharge capacity of 1100 and 1130 mAh g^{-1} and then a reversible capacity of 695 and 778 mAh g^{-1}, respectively. The first cycling capacity loss was due to the formation of the SEI and the reduction of Mn_3O_4 (Mn^{3+}) to MnO (Mn^{2+}), which occurs as a broad cathodic peak in the range 0.5–1.9 V. In the second cycle, the strong cathodic peak at ca. 0.35 V is assigned to the reduction of MnO (Mn^{2+}) to MnO, while the anodic peak at 1.3 V is the fingerprint of the oxidation reaction of Mn to MnO.

More recently, Rosaiah et al. [270] reported the Mn_3O_4@rGO composite for ESCs and LIBs. Nithya et al. demonstrated the application of the Mn_3O_4@rGO composite for K-ion Batteries [271]. The rGO/Mn_3O_4 hybrid anode reported by Nam et al. [272] delivers a reversible capacity of 1294 mAh g^{-1} at 100 mA g^{-1} after 100 cycles. A low-cost and green ultrasound-assisted method was developed by Luo [273]. For the rapid synthesis of Mn_3O_4 nanosheets supported on rGO, $Mn(OAc)_2$ and GO obtained according to the Hummers' method were dispersed in aqueous solution in the presence of tert-butylamine. Such anode materials yielded a high specific capacity of ~1400 mAh g^{-1} after 40 cycles at a current density of 100 mA g^{-1} (based on the mass of Mn_3O_4). A coprecipitation method was used to fabricate a 3D GO/Mn_3O_4 hybrid, which exhibited a large specific capacity of 949 mAh g^{-1}, CE of ~98%. After 100 cycles at 100 mA g^{-1} current rate, the specific capacity remained at 792 mAh g^{-1} with a CE of 98.1% [257]. Li et al. [274] took advantage of C-O-Mn chemical bonds to prepare graphene nanosheets dispersed in porous Mn_3O_4 making a 3D Mn_3O_4/rGO hybrid, which displayed excellent performance as anode of LIBs and electrode of ESCs by simply tuning the graphene content (<7 wt%). As LIB anode, with 6.9 wt% rGO, BET specific surface area of 153 m^2 g^{-1}, and ~5 nm pore size, the composite featured a reversible capacity of ~1500 mAh g^{-1} at 50 mA g^{-1}, and 561 mAh g^{-1} at 1 A g^{-1}. Zhang et al. [275] took advantage of the effective synergy between $MnCO_3$ and Mn_3O_4 to fabricate a multicomponent hybrid with the configuration $MnCO_3$/Mn_3O_4/rGO. In a typical experiment, a GO/Mn suspension (yellow color) was first obtained by mixing GO prepared by the modified Hummers'method with $KMnO_4$ at 0 °C for 3 h. Second, the as-prepared GO/Mn suspension was treated ultrasonically for 1 h to exfoliate the GO layers and added to Na_2CO_3 solution (1 mol L^{-1}) under stirring to adjust the pH value of the whole suspension to 11. Then, reduction of GO to rGO was obtained in an alkaline solution maintained at 95 °C for 2 h. Parents $MnCO_3$/rGO and Mn_3O_4/rGO composite were prepared using similar procedure changing the pH and the alkaline solution, respectively (Figure 8A). The $MnCO_3$/Mn_3O_4/rGO ternary composite displayed a cycling stability of 988 mAh g^{-1} after 200 cycles at 0.1 A g^{-1} current rate and 532 mAh g^{-1} after 800 cycles at 1 A g^{-1} (Figure 8B).

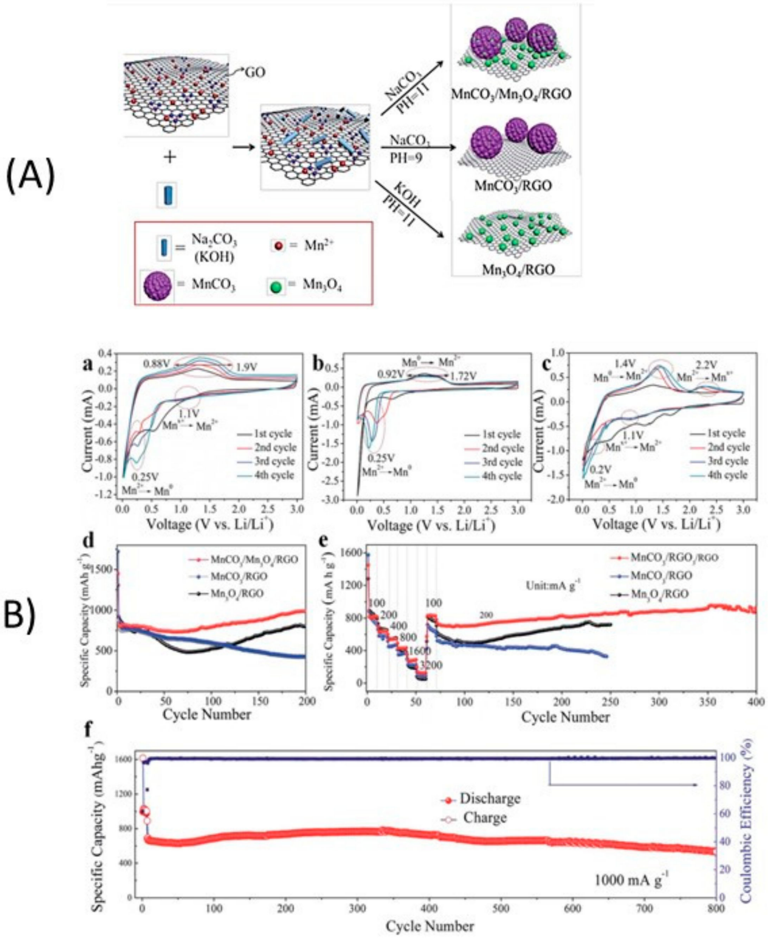

Figure 8. (**A**) Schematic illustration of the synthesis processes of multicomponent composites. (**B**) Cyclic voltammetry curves of (a) $MnCO_3/Mn_3O_4$/rGO composites, (b) $MnCO_3$/rGO composites, and (c) Mn_3O_4/rGO composites. (d) Cycling performances at 100 mA g^{-1}. (e) Rate capabilities of the $MnCO_3/Mn_3O_4$/rGO composites, $MnCO_3$/rGO composites, and Mn_3O_4/rGO composites. (f) Long-term cycling performance with coulombic efficiency of $MnCO_3/Mn_3O_4$/rGO composites at 1 A g^{-1}. Reproduced with permission from Ref. [275]. Copyright 2017 The Royal Society of Chemistry.

The Mn_3O_4/rGO designed by Shah et al. was prepared by the hydrothermal treatment at 180 °C for 18 h of an aqueous alkaline solution of $MnCl_2$, GO, and NaOH [276]. The presence of Mn_3O_4 nanoparticles on the surface of graphene nanosheets makes the structure with porous morphology. The rGO-Mn_3O_4 electrode tested over 5000 cycles displayed a high specific capacitance of 457 F g^{-1} at 1 A g^{-1} current rate. By means of a novel surfactant-free, single-step hydrothermal method, Varghese et al. [277] synthesized the Mn_3O_4 nanostructures and their rGO composites. The morphology of Mn_3O_4/rGO composite revealed that Mn_3O_4 nano-octahedrons (~100–150 nm in size) were wrapped in the graphene matrix. The Mn_3O_4/rGO||Li half-cell showed a reversible specific capacity of 474 mAh g^{-1} at 100 mA g^{-1} upon 200 cycles. Further, a high capacitive contribution of ~73% (evaluated at 1.0 mV s^{-1} sweep rate) contributed to fast Li^+ ion kinetics of this anode.

4.3.3. MnO-Based Composites

Manganese monoxide (MnO) has drawn considerable attention as anode material for LIBs due to its high theoretical capacity of 755.6 mAh g^{-1} and relatively low voltage hysteresis. However, poor cyclic performance and inferior rate capability caused by the severe particle agglomeration and large volume expansion are challenging issues. Exfoliated graphene oxide (EGO)/MnO composite (35/65 wt%) powders synthesized by simple solid state graphenothermal reduction process (specific surface area of ~82 m^2 g^{-1} and an average pore size of ~12 nm) were formed by cubic MnO crystallites that anchored onto EG surfaces. Tested as an anode in lithium-ion batteries, the EGO/MnO composite exhibited high reversible capacity of 936 mAh g^{-1} at a current rate of 75 mA g^{-1} with a capacity retention of ~84% and CE of 99% over 100 cycles [278]. The reversible conversion reactions of MnO and electrochemical absorption/desorption by EGO were evidenced by cyclic voltammetry studies showing easy lithiation kinetics. An ever-increasing surface redox capacitive lithium storage device was fabricated with a sandwich nanostructure. MnO was electrodeposited on rGO, forming interconnected nanorods (15–30 nm in diameter) with random orientation covered by depositing the top GO layer. The as-prepared RGO–Mn_xO_y–GO film was then heat treated at 600 °C for 6 h in H_2/Ar (5:95) atmosphere to achieve the RGO–MnO–RGO product. The as-designed rGO-MnO-rGO sandwich nanostructures displayed a surface pseudocapacitance dynamically in equilibrium with the diffusion-controlled process leading ultrahigh-rate capability of ~332 mAh g^{-1} at 40 A g^{-1} and ~379 mAh g^{-1} after 4000 cycles at 15 A g^{-1} was achieved due to the dynamical equilibrium between surface pseudocapacitance and diffusion-controlled ion storage [279]. Cheng et al. [280] developed a MnO-based sandwiched composite within 3D graphene-based N-doped carbon (NC) networks. The NC/MnO/rGO nanohybrid was prepared by precipitation assisted by polydopamine followed by heat treatment at 700 °C for 2 h in H_2/Ar atmosphere. HRTEM analysis showed that MnO nanoparticles (40 nm in size) were completely wrapped by a uniform amorphous carbon layer with a thickness about 2 nm, and then anchored on the rGO matrix. It demonstrated high reversible capacity of 1360 mAh g^{-1} at 0.2 A g^{-1} over 150 cycles, excellent rate capability, and good cyclability (648 mAh g^{-1} at 2 A g^{-1} without fading over 600 cycles). A composite anode, which consisted of rGO-anchored MnO within an nitrogen-codoped carbon coating (rGO/MnO@NC) was prepared under solvothermal conditions (at 180 °C for 15 h) of suspension of rGH sheets with manganese acetate followed by a two-step heat treatment with dopamine to produce the rGO/MnO@NC final hybrid (at 400 °C for 2 h with a heating rate of 1 °C min^{-1} under a pure argon flow and then at 800 °C for 2 h at a heating rate of 3 °C min^{-1}). This composite electrode presented high specific capacity of 699 mAh g^{-1} at 0.1 A g^{-1}, and excellent cycling performance of 607 mAh g^{-1} at 1 A g^{-1} over 550 cycles [281]. Table 4 summarizes the electrochemical performances of Mn-based oxide/rGO composite anodes of rechargeable lithium batteries.

Table 4. Comparison of the electrochemical behaviors of Mn-based oxide/rGO composite anodes of rechargeable lithium batteries. The relevant graphene content in wt% (a) and cycle number (b) are displayed in brackets.

Material [(a)]	**Synthesis**	**Specific Capacity (mAh g^{-1})**	**Current Density** [(b)] **(A g^{-1})**	**Ref.**
b-MnO_2/rGO	hydrothermal @160 °C/6 h	448	0.1 (50)	[227]
a-MnO_2/3D-rGO	in situ hydrothermal @ 60 °C/6 h	595	0.1 (60)	[230]
d-MnO_2 NFs/rGO	redox reaction with $KMnO_4$	1000	1 (200)	[231]
a-MnO_2/rGO	solution method with CTAB	222	5 (200)	[225]
a-MnO_2/rGO	hydrothermal @150 °C/15 h	590	12 (30)	[233]
MnO_2 NRs/rGO	hydrothermal @160 °C/18 h	600	0.5 (650)	[234]
d-MnO_2 NRs/GO	sonication	460	5 (80)	[232]
CNT/rGO@MnO_2	vacuum freeze-drying	608	7.5 (1000)	[236]
PPy/MnO_2/rGO-CNTs	vacuum filtration	941	1 (1200)	[235]
rGO/MnO_2/CNTS	vacuum filtration + thermal annealing	1172	0.1 (100)	[238]
Mn_3O_4/rGO (10)	two-step solution-phase reaction	900	0.04 (5)	[255]
MnO/GO (9.17)	impregnation + thermal reduction	500	0.2C (32)	[282]
N-MnO/rGO (8.9)	hydrothermal + ammonia annealing	772	0.1 (90)	[283]
MnO/rGO (75)	in-situ carbothermal reduction	782	0.1 (60)	[284]
$MnCO_3$/Mn_3O_4/rGO	sonication + alkaline solution	998	0.2 (100)	[275]
Mn_3O_4-MnO/rGO (12)	one-pot solvothermal	825	0.05 (30)	[285]
MnO/rGO (72.5)	two-step liquid phase deposition	665	0.1 (50)	[286]
MnO NWs/GO	dialysis	930	0.1 (470)	[287]
MnO NRs/GO (7.58)	in-situ reduction	705	0.05 (100)	[288]
MnO/rGO (6)	pyrolysis	950	0.1 (5)	[289]
MnO NSs/rGO	hydrolysis + calcination	648	0.75 (50)	[290]

4.4. Molybdenum-Based Oxide Composites

Since 1987, MoO_2 has been recognized as anode material for lithium-ion batteries [291]. Bulk MoO_2 possesses excellent physical properties with a metallic conductivity of ~10^{-4} S cm^{-1} at room temperature and a theoretical specific capacity as high as 838 mAh g^{-1}. It adopts the distorted variant of the rutile-like structure (monoclinic, $P21/c$ space group) in which the metal atoms occur in pairs along the c axis of the rutile pseudo-cell [292]. In the 0.01–3.0 V potential range, the lithiation of the MoO_2 electrode investigated by cyclic voltammetry occurs with two steps (first discharge): (1) The Li insertion ($Li_{0.98}MoO_2$) evidenced by the 1.52 and 1.24 V reduction peaks attributed to the monoclinic orthorhombic phase transition and (2) below 0.7 V reduction peaks assigned to the conversion of MoO_2 into elemental Mo with ~3Li uptake [293,294]. However, inherent disadvantages of bulk MoO_2 anode are the low reversible capacity due to sluggish lithiation/delithiation kinetics [295], the substantial volume change during lithiation process, which result in rapid capacity fading and poor capacity retention [296].

Graphene oxide was used as a reducing agent of MoO_3 (molar ratio of 4:1) and as a source for exfoliated graphene oxide (EGO) to fabricate EGO/MoO_2 composites with 46 wt% graphene [297]. The small particle size of ~33 nm indicates that agglomeration of MoO_2 has been controlled with the increased amount of EGO. The initial capacity of 713 mAh g^{-1} increased slightly to 878 mAh g^{-1} after 100 cycles at 100 mA g^{-1} current rate in the voltage window 0.005–3.0 V. Kinetics investigated by cyclic voltammetry revealed high values of the diffusion coefficients of Li ions in the range 6×10^{-10}–1×10^{-11} cm^2 s^{-1} during Li_xMoO_2 lithiation ($0 < x < 4$). Hu et al. [298] prepared MoO_2/GO composites via hydrothermal route at 200 °C for 24 h using Mo powder and exfoliated GO produced by sonication. MoO_2 nanoparticles (5−15 nm in size) were homogeneously dispersed on GO. When tested as an anode material for lithium, the MoO_2/GO composite displayed an initial specific capacity of 780 and 500 mAh g^{-1} at 0.1 and 0.5 A g^{-1}, respectively. The beneficial contribution of exfoliated GO was evidenced by EIS measurements, as the charge transfer resistance of 44 W for MoO_2/GO was much lower than 300 W for pure MoO_2 nanoparticles, due to more conductive pathway for Li-ion transportation. MnO_2/graphene composite was also synthesized by an effective polymer-assisted chemical reduction method, which provides nanosized MnO_2 particles homogeneously distributed on graphene nanosheets [299].

Huang and coworkers [300] fabricated a composite of MoO_2 nanoparticles (~100 nm) anchored on GO for sodium-ion battery anodes. This MoO_2/GO hybrid (15 wt% GO) yielded a discharge capacity of 483 mAh g^{-1} (~2318 mAh cm^{-3}) at the current density of 100 mA g^{-1} and a capacity fading of 0.019% per cycle over the first 1000 cycles. Tang et al. reported the electrochemical properties of rGO-wrapped MoO_2 porous nanobelts (rGO/MoO_2 NBs) synthesized using a reduction process of the GO-MoO_3 hybrids with Ar/ethanol vapor at 400 °C for 12 h [301]. The full-scale multi-electron conversion reaction in rGO/MoO_2 NBs (with 8 wt% rGO) led to a high reversible capacity of 974 mAh g^{-1} at the current density of 60 mA g^{-1} after the 6th cycle and, after initial activation, a specific capacity of 420 mAh g^{-1} was retained at the end of 1900 cycles at 5 A g^{-1} rate. Zhu et al. [302] demonstrated that rGO/MoO_2 nanobelt composite (with 19.4 wt% rGO) synthesized by a simple thermal reduction of MoO_3 and GO at 550 °C for 2 h in a 10% H_2/Ar atmosphere had a BET specific surface area and pore volume of 17.68 m^2 g^{-1} and 0.09 cm^3 g^{-1}, respectively. This self-assembled hybrid showed attractive electrochemical performance as LIB anodes with specific discharge capacity reaching 584 mAh g^{-1} after 100 cycles at 1 A g^{-1}.

In 2017, Ju and coworkers [303] designed a TiO_2/rGO/MoO_2@Mo composite electrode for ESC. This architectural nanostructure with 3D walnut-shape synthesized by one-step hydrothermal method was composed of amorphous TiO_2 decorating the rGO/MoO_2 surface grown on Mo foam. It exhibited a specific capacitance of 1636 F g^{-1} at 1.25 A g^{-1} with only 3.5% capacitance loss after 5000 cycles. Tightly anchored MoO_2 nanoparticles (10–20 nm in size) deposited on the basal plane of rGO were fabricated using a green supercritical methanol (scMeOH) route. When tested as an anode in lithium cells, the composite with 37 wt% MoO_2 loading (BET surface area of 14.3 m^2 g^{-1}, 15% porosity) delivered a reversible capacity of 793 mAh g^{-1} at 50 mA g^{-1} current rate [304]. Graphene oxide flexibly supported MoO_2 porous hybrids were constructed by decomposition of $(NH_4)_2MoO_4$/GO preforms with the percentage of GO at 4.3, 15.2, and 20.8 wt%. The lithium storage performance was investigated at the current density of 0.1 A g^{-1} using various MoO_2/GO architectures showing specific capacities of 901, 1127, and 967 mAh g^{-1} after 100 cycles for micrometer MoO_2/GO, MoO_2/GO nanohoneycomb, and layered MoO_2/GO, respectively. The MoO_2/GO nanohoneycomb delivered the capacity of 461 mAh g^{-1} at 5 A g^{-1} current rate with CE of 99.3% [305]. Wang et al. [306] synthesized 2D layered mesoporous-MoO_2/rGO composites (m-MoO_2/rGO) through a novel strategy using silica KIT-6/rGO as a template and ammonium molybdate as a precursor via a nanocasting method with subsequent heat treatment heated up to 600 °C for 6 h at a rate of 2 °C min^{-1} in a mixed gas flow of H_2/Ar (10:90). Analyses of the morphology validated the ordered mesoporous structure with a BET specific surface area of 86 m^2 g^{-1}, a pore size of 3–4 nm in a large domain, and a pore volume of 0.19 cm^3 g^{-1}. The m-MoO_2/rGO (1:1) electrode delivered an initial discharge capacity of 1160 mAh g^{-1} at current density of 0.1 A g^{-1} with a capacity loss of 31.9% during the first cycle and a reversible capacity is 801 mAh g^{-1} after 50 cycles.

In 2018, Chen et al. [307] investigated a hierarchical MoO_2@rGO (~10 nm MoO_2 particle size and 21.1 wt% rGO) composite prepared by hydrothermal route at 200 °C for 2 days, which exhibited outstanding electrochemical performance with a reversible capacity of 708 mAh g^{-1} at a current density of 0.5 A g^{-1} after 50 cycles. A capacity of 473 mAh g^{-1} was maintained when cycled at 2 A g^{-1} current rate. Li et al. [308] utilized Mo particles as both the reductant for GO and as the Mo source to prepare MoO_2/rGO hybrid anodes. The MoO_2/rGO composite with Mo:GO of 3:1 was used as an efficient cathode catalyst for the oxygen reduction reaction (ORR). Recently, Liu et al. [309] reported the direct growth of MoO_2/rGO hollow sphere composites through hydrothermal technique. This advanced anode materials tested in potassium-ion batteries delivered a reversible specific capacity of 219 mAh g^{-1} after 200 cycles at 50 mA g^{-1} current rate. When cycled at 0.5 A g^{-1}, a high charge specific capacity of 104 mAh g^{-1} was achieved after 500 cycles. Li et al. [310] prepared the MoO_2/Mo-GO hybrids using a freeze-drying technique, which exhibited a high ICE of 97%. A capacity of 550 mAh g^{-1} ws delivered by the MoO_2/Mo-GO anode materials after 150 cycles at 0.1 A g^{-1} rate. Devina et al. [311] used the same technique to prepare MoO_2/rGO composite attached with Mo_2C during carbothermal hydrogen reduction. The MoO_2/Mo_2C/rGO product displayed an increased initial coulombic efficiency (77%), long-term cyclability (500 mAh g^{-1} at 50 mA g^{-1} after 150 cycles), and high-rate performance (200 mAh g^{-1} at 1 A g^{-1}) compared with those of the MoO_2/rGO composite (53%; 280 mAh g^{-1} at 50 mA g^{-1} after 150 cycles; 120 mAh g^{-1} at 1 A g^{-1}).

Recently, the fabrication of submicrometer-sized MoO_2@MoS_2/rGO composite with a hierarchical core-shell structure was suggested by Zheng et al. [312]. The three-step synthesis includes: (i) The preparation of the MoO_2@MoS_2 precursor using a solid-state reaction (i.e., MoO_3 and sulfur heated at 600 °C for 1 h in a gas stream of Ar/H_2 (90:10)), (ii) a hydrothermal process at 180 °C for 4 h using a GO suspension, and (iii) a final heat treatment at 400 °C for 2 h in Ar/H_2 flowing gas. The electrochemical tests of the MoO_2@MoS_2/rGO anode showed an initial reversible capacity of 833 mAh g^{-1} with ICE of 80.6% and improved cycling stability (733 mAh g^{-1} after 80 cycles at 0.2 mA g^{-1}). The good rate capability with a capacity of 645 mAh g^{-1} at 4 A g^{-1} was also evidenced. An assembled MoO_2@MoS_2/rGO||$LiCoO_2$ full cell maintained a reversible capacity of 694 mAh g^{-1} (based on the mass of MoO_2@MoS_2/rGO) at 0.2 mA g^{-1} after 40 cycles. Electrochemical performance of MoO_2/rGO composite anodes for LIBs from the recent literature are summarized in Table 5.

Table 5. Electrochemical performance of MoO_2/GO composites as anode materials for Li-ion batteries. The relevant cycle number is displayed in brackets.

Material	Synthesis	Reversible Capacity (mAh g^{-1})	Current Rate (A g^{-1})	Ref.
MoO_2/Gr	layer-by-layer assembly	676	48 (100)	[313]
MoO_2/Gr	sonication in water (11.2)	597	1000 (70)	[26]
MoO_2/rGO	solvothermal in ethanol (10.0)	714	100 (30)	[314]
MoO_2/rGO	hydrothermal @200 °C/24 h	503	100 (30)	[298]
MoO_2/rGO	hydrothermal @400 °C/3 h (10)	1009	100 (60)	[315]
MoO_2/rGO	solid state reaction (22.0)	640	200 (50)	[316]
MoO_2/GO	thermal reduction @550 °C/2 h	752	100 (100)	[317]
MoO_2/Gr	hydrothermal @180 °C/26 h (33)	769	540 (83)	[318]
MoO_2/N-rGO	hydrothermal @180 °C/24 h	400	1000 (5)	[319]
MoO_2/exfol-rGO	solid-state graphenothermal (46)	878	100 (100)	[297]
MoO_2 NSs/rGO	in situ reduction of MoO_3	1003	100 (100)	[320]
MoO_2/GO	solvothermal @160 °C/16 h (10)	500	800 (30)	[299]
MoO_2/rGO	solid-state reaction @500 °C (15)	276	100 (1000)	[300]
MoO_2/rGO	hydrothermal @200 °C/2 days (21)	708	500 (50)	[307]
MoO_2/rGO	thermal reduction @550 °C (19)	584	1000 (100)	[308]
MoO_2/rGO/NBs	surfactant-free self-assembly	420	5000 (1900)	[302]
MoO_2 NBs/rGO	supercritical methanol route	793	50 (50)	[304]
MoO_2/Mo-GO	freeze-drying (5)	550	100 (150)	[310]
MoO_2/rGO	solid state reaction @500 °C (15)	1127	100 (150)	[305]
MoO_2 NBs/rGO	freeze-drying (8)	420	5000 (1900)	[301]
m-MoO_2/rGO	nanocasting (50)	801	100 (100)	[306]
MoO_2@MoS_2/rGO	hydrothermal @180 °C/4h	733	200 (80)	[312]

Xu et al. [314] used a solvothermal treatment of a GO suspension with $(NH_4)_6Mo_7O_{24}$ and HNO_3 in ethanol at 160 °C for 16 h. The MoO_2/GO with 10 wt% GO tested in lithium half-cell delivered an initial capacity of 800 mAh g^{-1} at current density of 0.8 A g^{-1} corresponding to Li uptake of 3.43 moles. The capacity retention was 63% after 30 cycles.

4.5. Titanium-Based Oxide Composites

4.5.1. TiO_2-Based Composites

TiO_2 has been widely investigated as anode material of LIBs due to its strong redox ability, relative non-toxicity, good stability, low cost, and abundance [321]. The insertion of Li^+ ions in the TiO_2 framework occurs at about 1.5 V with the electrochemical process $TiO_2 + xLi^+ + xe^- \leftrightarrow Li_xTiO_2$ ($0 \leq x \leq 1$) providing a theoretical capacity of 170 mAh g^{-1} (for 1 Li^+ uptake) almost equal to $Li_4Ti_5O_{12}$. However, pure TiO_2 suffers from poor electronic conductivity (~10^{-12}–10^{-7} S cm^{-1}) and low diffusion rate (10^{-15}–10^{-11} cm^2 s^{-1}) [322,323], which affects the cycling performance and rate capability. To overcome these drawbacks, researchers have tried to combine TiO_2 with high conductive carbonaceous substances such as graphene [324], GO [325], and rGO [326–329]. In this context, Wang et al. reported that the sandwich structure formed by carbon-coated mesoporous TiO_2 nanocrystals and rGO sheets with a high surface area of ~209 m^2 g^{-1}, and a large pore volume of ~0.68 cm^3 g^{-1} gives a capacity retention of 110 mAh g^{-1} after 100 cycles at 0.2 A g^{-1} current rate [330].

Several effective strategies proved that the TiO_2/GO and TiO_2/rGO composite materials exhibit enhanced electrochemical properties in comparison with pure TiO_2. In most cases, the carbonaceous support results in several advantages: It provides fast transmission channels for electronic, maintains the structural stability of the hybrid, and increases the conductivity in the presence of reduced graphene oxide. The presence of carbon also provokes a reduction of the TiO_2 particles size during synthesis, which can shorten the transport paths for both Li^+ ions and electrons and can lead to more electroactive sites due to the enlarged electrode–electrolyte contact area. In addition, the Ti-C bonds in the hybrid are crucial for fast interfacial charge transfer [331]. For instance, Etacheri et al. identified the formation of Ti^{3+} -C bonds between TiO_2(B) and rGO in chemically bonded mesoporous TiO_2(B) nanosheets to rGO sheets prepared by a photocatalytic reduction method, using EPR and XPS measurements. These TiO_2(B)/rGO nanohybrids demonstrated superior rate capability with 80% of the initial capacity retained after 1000 cycles at high rate of 40C [332].

Hydrothermal method is the most popular technique to prepare TiO_2/rGO nanocomposites [333]. TiO_2/rGO nanocomposites with small particle size were prepared via a mild hydrothermal route at 160 °C for 12 h with titanium tetrabutoxide (3 mL) and GO as the precursors in a mixture of ethanol (2.5 mL) and hydrochloric acid (3.5 mL); after heat treatment at 350 °C the final product with blue-black color was obtained [334]. This TiO_2/rGO nanocomposite delivered a first discharge capacity of 275 mAh g^{-1} corresponding to a nominal degree of lithiation of $x = 1.64$ in Li_xTiO_2 and it retained a capacity of 112 mAh g^{-1} after 100 cycles at a high charge rate of 1 A g^{-1}. Zhen et al. [327] fabricated rGO nanosheet supported anatase TiO_2 fiber bundles by hydrothermal method at 180 °C for 20 h using the mixture of the $TiCl_3$ and NaF in NaOH solution added to GO into HCl solution. This TiO_2/rGO composite showed a mesostructure with a broad pore size distribution from 5 to 50 nm, average ~21 nm pore diameter and higher specific surface area of 83.8 m^2 g^{-1}. The galvanostatic charge–discharge patterns carried out under 200 mA g^{-1} current rate in the voltage range from 3 to 0.01 V vs. Li^+/Li showed a capacity retention of 235 mAh g^{-1} after 1000 cycles. He et al. [328] used a mild seed-assisted hydrothermal method at 110 °C for 12 h with $Ti(OBu)_4$ titanium source to synthesize a sandwich-like nanocomposite consisting of rutile TiO_2 nanorods (<25 nm in size) onto rGO. The composite with specific surface area of 43 m^2 g^{-1} demonstrated reversible capacities of 145 mAh g^{-1} (1 C) and 94 mAh g^{-1} (5 C) retained up to 100 cycles (1C = 168 mAh g^{-1}), better than that of cells composed of nanosized TiO_2, i.e., 80 mAh g^{-1} at 2C rate (8 nm grain size, 5 mg cm^{-2} loading) [335]. TiO_2 nanorods (~5 nm in size, anatase phase) anchored on rGO composite were fabricated by hydrothermal method (180 °C for 12 h) after annealing treatment using GO solution, titanium trichloride ($TiCl_3$), and sodium hydroxide (NaOH) aqueous solution. The resultant R-TiO_2/rGO composites (BET surface area of ~149m^2 g^{-1}, average pore diameter of ~18 nm) were explored as anode material for LIBs displaying reversible capacities of 276 and 151 mAh g^{-1} at 1C and 10C (1 C = 168 mA g^{-1}), respectively, with an excellent cycle ability (~90 mAh g^{-1} at 10 C after 1000 cycles in the potential range 0.01–3 V) [336]. Li and coworkers [337] reported in situ growth of anatase TiO_2 nanoparticles on nitrogen-doped reduced graphene oxide (N-rGO) via hydrothermal route at 200 °C for 20 h. The properties of the TiO_2/N-rGO composite were compared with those of pure TiO_2 and TiO_2/rGO prepared in similar conditions. However, it was noted that the presence of rGO results in a decrease of the particle size from 30 nm in TiO_2 to 10–15 nm in TiO_2/rGO. The average reversible capacities of bare TiO_2, TiO_2/rGO, and TiO_2/N-rGO were 194, 210, and 226 mAh g^{-1}, respectively, at a current rate of 0.2 C. The authors discussed the effects of nitrogen doping on the electrochemical performance, in terms of defects in pyridinic graphene sheets suitable sites for lithium-ion storage. The nitrogen doping improved the conductivity by opening the bandgap and the disordered carbon structure increases the Li:C ratio. Geng et al. [338] synthesized TiO_2/rGO anode materials using hydrothermal method at 150 °C for 14 h. In a typical process, titanium oxysulfate dissolved in ethyl alcohol was mixed with multilayers GO sonically dispersed in water and hydrazine hydrate as reducing agent. The discharge specific capacity of TiO_2/rGO composite was 236 mAh g^{-1} after 100 charge–discharge cycles at 0.1 A g^{-1} rate and the coulombic efficiency was 98.5%.

In 2017, Mondal et al. [339] developed a large-scale synthesis for TiO_2-rGO nanocomposite hollow spheres by an aerosol-assisted spray-drying technique (using an aqueous titanium ammonium peroxo-carbonate complex (TAPCC) solution) with subsequent calcination. The porous TiO_2-rGO nanohybrid was composed of TiO_2 particles (10–20 nm) dispersed on the surface of rGO (10%) with a BET specific surface area of 86 m^2 g^{-1}. Specific discharge capacities of 265 and 274 mAh g^{-1} at 18.8 mA g^{-1} current rate were delivered by the synthesized TiO_2-rGO hollow spheres with rGO content of 10 and 20 wt%, respectively, against 236 mAh g^{-1} for the pristine sample with a 2D flake-like morphology. Li et al. [329] prepared TiO_2/rGO hybrids using an ethanol-type hydrothermal method at 180 °C for 12 h followed by a freeze-drying process. Samples consisted of TiO_2 spherical particles

(10 nm diameter, anatase phase) combined with the rGO matrix. The TiO_2/rGO assembly exhibited high rate capability of ~270 mAh g^{-1} at 0.1 A g^{-1}, and excellent cycling capacity of ~180 mAh g^{-1} at 0.5 A g^{-1} after 2000 cycles. The improvement of these electrodes was explained in terms of fast pseudocapacitive charge storage process. Enhancement of the transport of Li^+ ions in TiO_2/rGO composite electrode was evaluated by EIS measurements showing a diffusion coefficient of 1.14×10^{-11} cm^2 s^{-1}, against 7.4×10^{-13} cm^2 s^{-1} for pure TiO_2 electrode. A TiO_2(B)–CNTs–graphene ternary was synthesized by a three-step growth procedure, i.e., dispersion of Go and CNTs in ethanol, precipitation with titanium isopropoxide and ammonium hydroxide followed by a hydrothermal process at 200 °C for 48 h and a calcination at 350 °C for 5 h [340]. The TiO_2(B)–CNTs–GO sample with a 11.2% weight content carbon, including graphene and CNTs, had a BET surface area of 65.5 m^2 g^{-1}. It exhibited electrochemical activity within the voltage range of 0.01–3 V with a specific capacity of 388 mAh g^{-1} in the 2nd cycle at 0.1C rate and a rate capability of 76 mAh g^{-1} at 10C. A capacity of 190 mAh g^{-1} was maintained after 200 cycles at 1C rate.

Recently, the hollow TiO_2@rGO hybrid spheres as anode materials for LIBs by Zhao et al. exhibited excellent electrochemical performance, i.e., high-rate and long-life [333]. The composite with a BET surface area of 58.7 m^2 g^{-1} was in-situ constructed by using TiO_2 spheres in GO suspension as a precursor and a simple in-situ hydrothermal route with subsequent annealing at 600 °C for 3 h under an Ar atmosphere. It exhibited a specific capacity of 254 mAh g^{-1} at 1C rate after 600 cycles (1C = 188 mAh g^{-1}; voltage rand 0.01–3.0 V vs. Li^+/Li) and superior rate capacity of 159 mAh g^{-1} at 10C after 3000 cycles. Fang et al. [341] prepared a two-dimensional TiO_2/rGO composite (particle size of 15–25 nm) by a facile hydrothermal method at 160 °C for 16 h using Ti_2C and GO as precursors. HRTEM images showed a large amount of sandwich layer-space and TiO_2-rGO interfaces, which are very advantageous for electron transfer and ion transport. The average specific capacities of 302, 200, 170, 148, and 128 mAh g^{-1} were obtained at the current density of 0.5, 2.0, 10, 20, and 50C (1C = 168 mA g^{-1}), respectively. Even at the large current density of 100C, the TiO_2/rGO anode yielded a capacity of 111 mAh g^{-1}. At the current density of 1.68 A g^{-1}, a capacity of 130 mAh g^{-1} was achieved, and an outstanding cycling retention of 86% remained after 1000 cycles. Quantification of the capacitive and diffusion contributions made from cyclic voltammetry data demonstrated that, at high currents, the capacity control was the main reaction power, i.e., accounted for 69.6% of the total charge (see Figure 9). TiO_2/rGO was also used as the anode material for a K-ion cell showing remarkable capacity retention of 83% after 1000 cycles at 1 A g^{-1} current rate. Farook et al. used a microwave hydrothermal process to obtain a TiO_2–rGO nanocomposite consisted of TiO_2 particles with a size of ~100 nm, uniformly distributed on the rGO sheets. As an anode for LIBs, it delivered a capacity of a capacity of 250 mAh g^{-1} ± 5% at 0.2C for more than 200 cycles. A capacity of 100 mAh g^{-1} with >99% coulombic efficiency was recorded up to 20C [342]. Subasi et al. could increase the capacity of TiO_2–rGO owing to a surface modification of the nanocomposite by the use of H_2O_2 [343]. This composite, with TiO_2 20 nm-thick synthesized through a sol-gel method, delivered 291 mA h g^{-1} at a current of 100 mA g^{-1}.

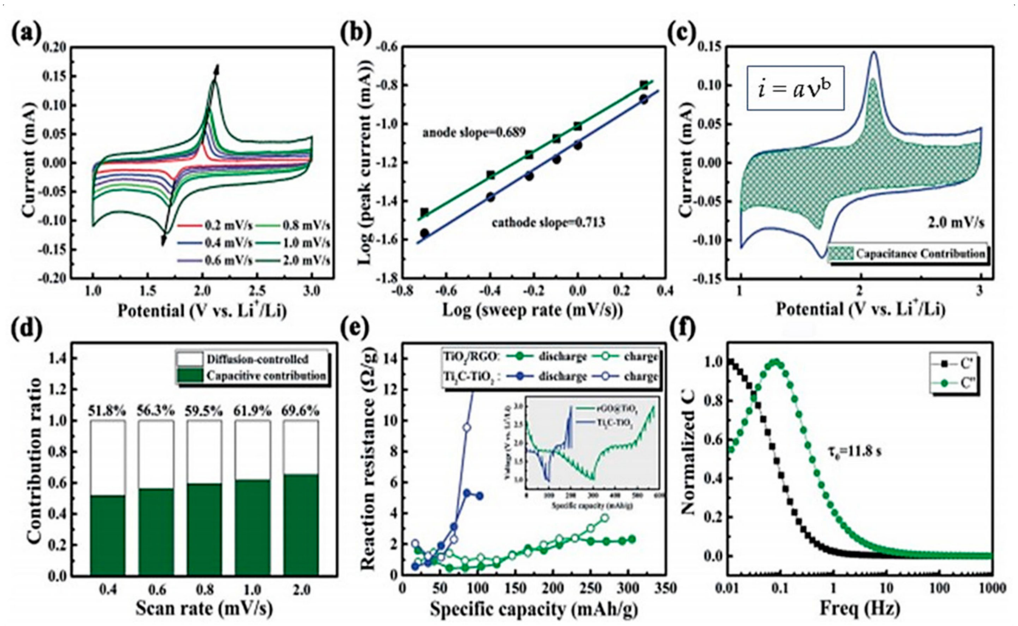

Figure 9. Quantification of the capacitive and diffusion contributions of TiO_2/rGO composite. (**a**) CV curves at different sweep rates n in the range 0.2–2.0 mV s^{-1}. (**b**) Value of the power parameter of peak currents ($i = an^b$) at different scan rates. (**c**) Area ratio of the CV curve at 2.0 mV s^{-1}. (**d**) Columnar contrast chart at different scan rates. (**e**) Reaction resistance analysis of TiO_2/rGO, inset: GITT tests. (**f**) Bode curves of normalized real and imaginary of TiO_2/rGO. Reproduced with permission from [341]. Copyright 2019 The Royal Society of Chemistry.

GO can be photocatalytically reduced by the TiO_2 nanoparticles under the UV illumination [344,345]. Qiu et al. [345] prepared the TiO_2/GO hybrids by sonication and reduced GO into rGO using the photocatalytic property of TiO_2. The suspension was illuminated under the UV light of a 1000-W exon lamp for 2–5 h producing TiO_2 nanoparticles uniformly anchored on the surface of rGO sheets. The TiO_2/rGO nanocomposites exhibited the first discharge and charge capacities of 546 and 296 mAh g^{-1} and preserved a cycling stability of ~215 mAh g^{-1} at 200 mA g^{-1} after 100 cycles. Tong et al. [346] fabricated 3D-mesoporous TiO_2/GO microspheres synthesized through an UV-assisted method of reduced graphene oxide with hydrazine. This composite possessed large surface area of 258 m^2 g^{-1} and a narrow pore size of 7.8 nm. These TiO_2/GO microspheres achieved an initial discharge capacity of 220 mAh g^{-1} with 84% (~185 mAh g^{-1}) capacity retention over 100 cycles at 0.2C rate, and 141 mAh g^{-1} at 1C rate. A 3D TiO_2–carbon–rGO composite was fabricated and post-treated with UV irradiation (254 nm) for 0.5 h. A specific discharge capacity up to 191 mAh g^{-1} was obtained after 100 cycles at a current rate of 0.2C (40 mA g^{-1}) for composite with 158 m^2 g^{-1} [347].

Ren et al. [348] constructed TiO_2-carbon-rGO composites by anchoring TiO_2 nanoparticles (10–15 nm in size, anatase phase) encapsulated in carbon shells onto rGO sheets (15 wt%). This hybrid showed a BET specific surface area of 167.2 m^2 g^{-1} and a typical bi-modal mesoporous structure with pore width of 3.8 and 32.5 nm and average pore width of 7.5 nm calculated using BJH model. The total pore volume with pore width from 1.7 to 300 nm was 0.26 cm^3 g^{-1}. Such a morphology useful for the facile diffusion of Li^+ ions in electrodes provided excellent electrochemical performance. Tested as the anode materials in Li-ion cell, the TiO_2-carbon-rGO composites exhibited an initial specific discharge capacity of 188 mAh g^{-1} and a superior capacity retention of 158 mAh g^{-1} after 100 cycles at 1 A g^{-1} current rate. Cao et al. [89] investigated the lithium-ion insertion/extraction behavior in TiO_2/rGO nanocomposites synthesized using tetrabutyl titanate ($Ti(OBu)_4$) as the titanium source via a solvothermal route as anode materials for lithium-ion batteries. The hybrid nanocomposite featured a reversible capacity of 153 mAh g^{-1} for after 100 cycles at a high charge rate of 5C (1000 mA g^{-1}). Madhusanka et al. [349] reported the electrochemical properties of TiO_2/rGO composite prepared by sonication for 5 min of a water/ethanol solution containing rGO, TiO_2 powder, Triton X-100 surfactant, and sodium carboxymethyl cellulose. TiO_2/rGO electrodes (loading of 4–6 mg cm^{-2}) delivered a first discharge capacity of 159 mAh g^{-1} and retained 143 mAh g^{-1} after 100 cycles at current density of 100 mA g^{-1} with a coulombic efficiency of 99.5%. Mesoporous anatase TiO_2 sheets/rGO sandwich-like nanocomposites were fabricated by acid-assisted $Ti(OBu)_4$ hydrolysis and subsequent thermal reduction process [350]. Three samples with different proportion of rGO were obtained by changing the volumes of $Ti(OBu)_4$ and concentrated H_2SO_4. The optimal sample (9.6 nm particle size, ~43 m^2 g^{-1} BET specific surface area) delivered an initial discharge capacity of 357 mAh g^{-1}. The reversible lithium-storage capacity reached 161 mAh g^{-1} after 50 cycles with ~70% retention at a current rate of 170 mA g^{-1} (0.5C). Park et al. have synthesized rGO-coated TiO_2 microcones as composite anode materials via simple anodization and cyclic voltammetry [351]. The obtained TiO_2/rGO hybrid showed a capacity of 157 mAh g^{-1} at 10C rate and sustained 1000 cycles with only 0.02% capacity fading per cycle. The hierarchically porous TiO_2/rGO hybrid anode material designed by Yu and coworkers [352] exhibited a reversible capacity of 250 mAh g^{-1} at 1C rate (1 C = 335 mA g^{-1}) in the voltage range of 1.0–3.0 V. After 1000 cycles, stable capacities of 176 and 160 mAh g^{-1} were delivered at 5C and 500 cycles at 10C, respectively. An ultrathin mesoporous TiO_2/rGO composite was obtained by Liang et al. via a layer-by-layer process [353]. $Ti_3O_7{}^{2-}$ nanosheets obtained by exfoliation of $Na_2Ti_3O_7$ were used as the precursor for TiO_2. Coprecipitation of GO and $Ti_3O_7{}^{2-}$ nanosheets in presence of HCl resulted in the formation of restacked $H_2Ti_3O_7$/GO. Then, annealing at 450 °C for 5 h facilitated the phase transition from $H_2Ti_3O_7$ to TiO_2 and the reduction of graphene oxide. The resulting mesoporous TiO_2/rGO composite delivered a capacity of 350 mAh g^{-1} at a current density of 0.2 A g^{-1}, and a capacity of 245 mAh g^{-1} maintained over 1000 cycles at 1 A g^{-1}.

Several studies were attempted to enhance the performance of TiO_2/rGO composites by doping with nitrogen. As experimental results, both electronic and ionic transport were significantly improved [337,354,355]. TiO_2/N-rGO hybrid was prepared via a facile one-pot hydrothermal method, in which ethylene glycol and ammonia are used as the reducing agent and nitrogen precursor, respectively [354]. The TiO_2/N-RGO nanocomposite exhibited superior electrochemical behaviors with reversible capacity of 126.8 mAh g^{-1} at 10C rate and outstanding capacity retention of 118.4 mAh g^{-1} after 100 cycles. In addition to the beneficial effect on ionic and electronic transport, the nitrogen doping enhances the nucleation and growth kinetics of TiO_2 nanoparticles uniformly anchored on the N-rGO surface. Li et al. [337] reported that the introduction of nitrogen on the rGO framework leads to more defects. A disordered structure is thus formed to accommodate more lithium ions. Another nitrogen-doped TiO_2/rGO hybrids was synthesized by hydrothermal reaction and post-annealing at 400 °C for 3 h [355]. The as-prepared samples contained anatase TiO_2 nanoparticles (~20 nm) uniformly anchored on GO lamella. The N-TiO_2/rGO electrode delivered a discharge capacity of 318 mAh g^{-1} at 0.1 A g^{-1} and maintained 117 mAh g^{-1} at 5 A g^{-1}. A high reversible capacity of 210 mAh g^{-1} was preserved after 2000 cycles at 0.5 A g^{-1}. Li^+ ion diffusion coefficient evaluated from EIS measurements for N-TiO_2/rGO was 3.8×10^{-15} cm^2 s^{-1}, which is higher than that of the TiO_2/rGO electrode (5.5×10^{-16} cm^2 s^{-1}). Electrochemical analysis finds the number of active Li-ions is increased from the formation of N-Ti-O and N-C bonds.

Ternary Si@TiO_2@rGO composite with sandwich-like structure was prepared via simple sol-gel combined with graphene encapsulation process of GO, with subsequent annealing process at 600 °C for 2 h in N_2 atmosphere to reduce GO. The composite consisted of Si nanoparticles (spherical, 50 nm diameter) covered by uniform TiO_2 shells during the sol-gel process to fabricate the Si@TiO_2 composite, which were then encapsulated by flexible graphene sheets (15 nm thick) to produce the Si@TiO_2@rGO hybrid. Due to the synergetic effects of the stable TiO_2 (anatase phase) coating and the flexible graphene network, the as-synthetized Si@TiO_2@rGO anode delivered a charge specific capacity of 1135 mAh g^{-1} under current rate of 0.2 A g^{-1} after 100 cycles with an initial CE of 76.9%. A charge specific capacity of 568 mAh g^{-1} was retained at current rate of 3 A g^{-1} (Figure 10). Results of EIS measurements in the 100th cycle showed higher diffusion coefficient of lithium ion of 8.0×10^{-11} cm^2 s^{-1} than $D_{Li^+} = 5.7 \times$

10^{-12} cm^2 s^{-1} for the fresh Si@TiO_2@rGO anode, which suggests a better lithium-ion transfer after the initial cell formation [356]. Electrochemical performance of TiO_2/rGO composite anodes for LIBs from the recent literature are summarized in Table 6.

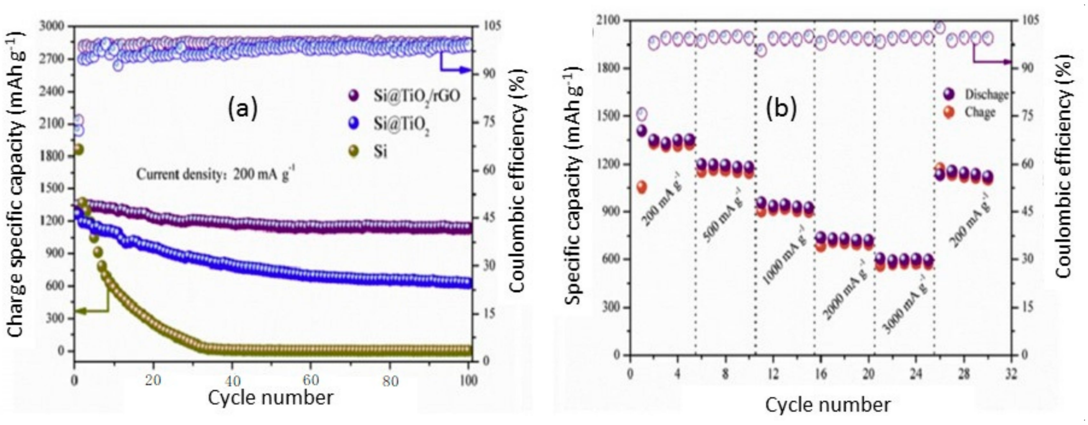

Figure 10. (**a**) Cyclability of Si@TiO_2@rGO, Si@TiO_2 and Si anodes tested at current rate of 0.2 A g^{-1}. (**b**) Rate capability and coulombic efficiency of the Si@TiO_2@rGO anode. Reproduced with permission from ref. [356]. Copyright 2020 Elsevier.

Table 6. Electrochemical properties of TiO_2/GO composites. Relevant cycle number is given in brackets.

Material	Synthesis	Specific Capacity (mAh g^{-1})	Current Rate (mA g^{-1})	Ref.
TiO_2/rGO	hydrothermal 160 °C/12 h	112	1700 (100)	[334]
TiO_2/GO	UV photocatalysis	130	200 (100)	[345]
TiO_2/rGO	UV photocatalysis	215	200 (100)	[345]
TiO_2/N-doped rGO	hydrothermal 200 °C/20 h	187	-	[337]
TiO_2/rGO	solvothermal with $Ti(OBu)_4$	153	1000 (100)	[89]
TiO_2/rGO	hydrothermal 150 °C/14 h	236	100 (100)	[338]
TiO_2/rGO	hydrothermal 180 °C/20 h	235	200 (1000)	[327]
TiO_2-carbon-rGO	hydrothermal 160 °C/24 h	158	1000 (100)	[348]
TiO_2/rGO	sonication for 5 min	143	100 (100)	[349]
R-TiO_2/rGO	hydrothermal 180 °C/12 h	90	1680 (1000)	[336]
TiO_2/rGO	hydrothermal 160 °C/16 h	130	1680 (1000)	[341]
TiO_2/rGO	hydrothermal 180 °C/12 h	180	500 (2000)	[329]
TiO_2-carbon-rGO	UV photocatalysis (254 nm)	191	40 (100)	[347]
TiO_2/rGO	thermal reduction	161	170 (50)	[350]
TiO_2(B)–CNTs–GO	hydrolysis + hydrothermal	190	1C (200)	[340]
TiO_2/rGO (9.9% rGO)	hydrothermal + annealing	254	168 (600)	[333]
TiO_2/rGO (10% rGO)	aerosol-assisted spray-drying	174	1C (200)	[339]
N-doped TiO_2/rGO	hydrothermal + annealing	210	100 (2000)	[355]
Si@TiO_2@rGO	sol-gel	1135	200 (100)	[356]
TiO_2/rGO	solvothermal alcoholysis	176	1675 (1000)	[352]
TiO_2/rGO	microwave hydrothermal process	250	0.2C (200)	[342]
TiO_2/rGO	coprecipitation $Ti_3O_7^{2-}$ + GO	245	1000 (1000)	[353]

4.5.2. $Li_4Ti_5O_{12}$-Based Composites

$Li_4Ti_5O_{12}$ (LTO) can interact with Li ions by an intercalation/deintercalation process up to 3Li delivering a theoretical capacity of 175 mAh g^{-1} with negligible volume expansion (<0.2%). However, this spinel framework has a poor electrical conductivity, which can be mitigated through the introduction of carbonaceous material [357,358].

Since 2011, great efforts have been devoted for the in-situ synthesis of LTO anode materials combined with graphene-based compounds. For example, Shen et al. [359] employed a three-step process with the hydrolysis of tetrabutyl titanate in the presence of GO to produce TiO_2/GO hybrid, which was then transformed into Li-Ti-O/rGO by a hydrothermal method, and finally to LTO/rGO by a post-heating treatment. It is noteworthy that the specific capacity of 82.7 mAh g^{-1} was obtained at a high rate of 60C. Kim et al. [360] utilized a similar microwave assisted, two-step method with titanium ethoxide, LiOH, and GO to obtain Li-Ti-O/rGO hybrid, which was then transformed to LTO/rGO by post annealing. The phase-pure LTO/rGO nanocomposite delivered a reversible capacity of 168 mA h g^{-1} at 1 C-rate and a remarkable rate capability with 59% capacity retention at 50 C-rate.

Chen et al. [361] prepared a nanohybrid electrode of mesoporous single crystalline $Li_4Ti_5O_{12}$ deposited on rGO (MSCs-LTO/rGO) via a simple hydrothermal reaction of TiO_2/rGO and LiOH with subsequent annealing in Ar at 600 °C. This MSCs-LTO/rGO anode yielded a specific capacity of 171 mAh g^{-1} at 0.5C rate with CE of 95.6%, a rate capability of 132 mAh g^{-1} at high rate of 40C and 85% capacity retention after 2000 cycles. A scalable synthesis of LTO/rGO composite was proposed by Ni et al. [362]. The as-prepared hybrid presented LTO nanoparticles uniformly immobilized on the rGO sheets and showed outstanding performance, i.e., good cycle ability and excellent rate capability with specific capacities of 154 and 149 mAh g^{-1} at 10C and 20C rate, respectively. Cycle stability of LTO/rGO after 200 cycles at 5C (98.9% capacity retention) was much better than that of bare LTO (93%). Di et al. fabricated an LTO/rGO through a simple hydrothermal process, which demonstrated a capacity retention of 86.6% after 2000 cycles at 5C [363]. The capacity delivered at 50C and 100C were still 132 and 97.5 mAh g^{-1}, respectively. Chen et al. reported that even a small amount of rGO (1.2 wt%) effectively prevents grain growth and particles aggregation of LTO and enhances the specific surface area of the anode material [364]. The Li||LTO/rGO half-cell could deliver the specific capacity of 187 mAh g^{-1} at 1C rate and the high-rate discharge capacity of 128 mAh g^{-1} at 80C operating for 2000 cycles. Zhang et al. fabricated a $Li_4Ti_5O_{12}$ microspheres/rGO composite by hydrolysis of titanium butoxide with subsequent hydrothermal reaction at 180 °C for 36 h of TiO_2 precursor with GO and LiOH, followed by a heat treatment at 600 °C in Ar atmosphere [365]. The 3 wt% rGO-coated LTO composite presented a high reversible Li-ion insertion capability with a specific discharge capacity of 131.6 mAh g^{-1} at 5C rate and 97% capacity retention after 500 cycles. A porous $Li_4Ti_5O_{12}$/*N*-doped rGO composites was synthesized, while using cyanamide as the nitrogen source prevented the rGO restacking and increased the electronic conductivity to 1.6 S cm^{-1} [366]. The $Li_4Ti_5O_{12}$/*N*-doped rGO composite with a BET specific surface area of 35.8 m^2 g^{-1} demonstrated a specific discharge capacity of 117.8 mAh g^{-1} at 30C rate. The work by Cao et al. [367] shows that LTO/rGO composite grown via one-pot way (hydrothermal process at 180 °C for 36 h) displays higher rate capacity and larger discharge capacity than the bare LTO sample. The small rGO ratio-containing composite (~6.2 wt%) delivered a reversible specific capacity of 196.4 mAh g^{-1} at 1C rate and good cycle ability with 98.1% retention after 100 cycles. The rate capability tests showed discharge capacities of 175, 167, and 160 mAh g^{-1} at 10C, 15C, and 20C, respectively. After 500 cycles at 20C, the discharge capacity retained 154.5 mAh g^{-1} (96.5% retention). Ge et al. [368] reported the synthesis of LTO/GO and LTO/rGO composites by a facile one-step hydrothermal route at 180 °C for 24 h using $Ti(SO_4)_2$ raw material. The reduction of GO to rGO was realized by the hydroxyl groups of glucose, which prevented LTO particle aggregation and led to a mesoporous structure (~5 nm pore size). The reversible specific capacity of 193 mAh g^{-1} at 0.5C rate was delivered by this nanocomposite anode and a capacity of 168 mAh g^{-1} was retained at superior rate of 30C (Figure 11).

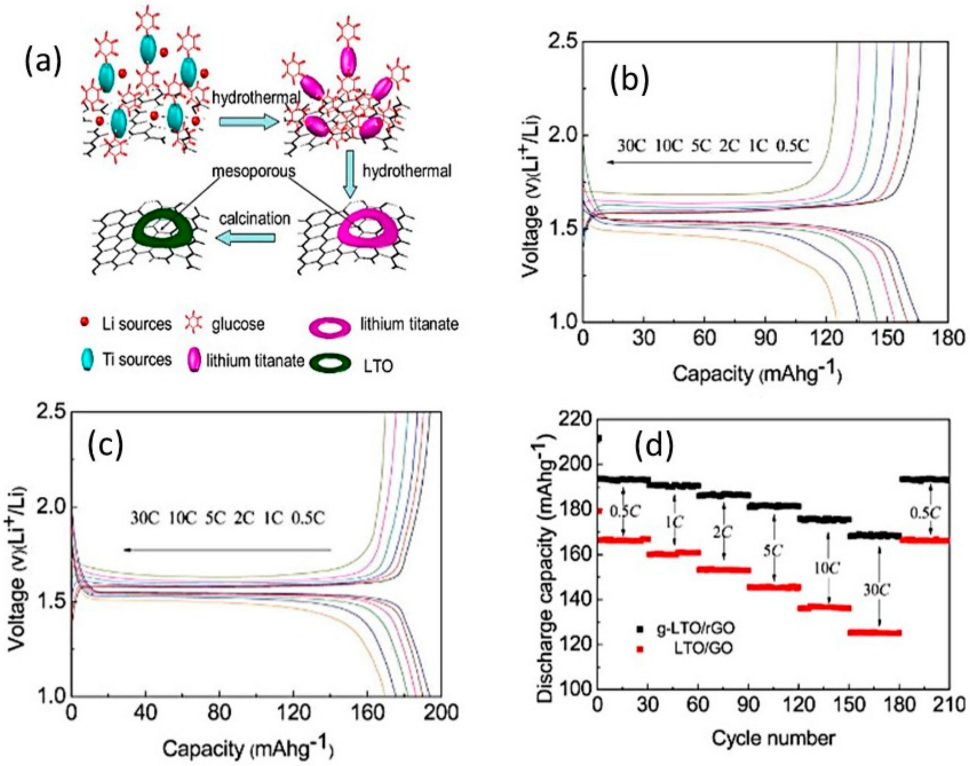

Figure 11. (**a**) Schematic illustration of the synthesis of LTO/rGO composite. (**b**) Galvanostatic charge–discharge profiles of LTO/GO at different current densities. (**c**) Galvanostatic charge–discharge profiles of LTO/rGO at different current densities. (**d**) Comparison of the rate capabilities of LTO/GO and LTO/rGO composites from 0.5 to 30C. Reproduced with permission of [368]. Copyright 2016 American Chemical Society.

The LTO/rGO composite with a "fishnet-like" hierarchical porous structure was fabricated via a gas-foaming method [369]. LTO particles of 50–100 nm were obtained with the NH_4Cl concentration of 1 mg mL^{-1}. Electrochemical tests demonstrated a specific capacity of 176.6 mAh g^{-1} at a rate of 1C, a rate capability of 167 and 143 mAh g^{-1} at 3C and 10C, respectively, and a capacity retention of 95.4% after 100 cycles at 10C. Pender et al. [370,371] reported the fabrication and electrochemical performance of metal-foil free $Li_4Ti_5O_{12}$ (LTO) and $LiNi_{1/3}Mn_{1/3}Co_{1/3}O_2$ (NMC) electrodes supported on conductive and porous reduced graphene oxide/poly(acrylic acid) (rGO-PAA) aerogels. This 3D nanocomposite had a low density (~5 mg cm^{-3}) and high porosity (99.6% void space) [370]. When applied as a free-standing, 3D current collector in LIBs, the highly porous rGO-PAA substrate increased the effective electrode−electrolyte contact area 2.5- fold (16 mg cm^{-2} loading) by increasing the electrode surface roughness and thus improving the lithiation/delithiation kinetics of a commercial LFP cathode [372]. The use of rGO-PAA instead of conventional metal-foil (CMF) showed a 25% increase in energy density over similar electrodes built with CMF current collector, i.e., high volumetric energy densities of 1723 Wh L^{-1} for NMC and 625 Wh L^{-1} for LTO [371].

Recently, an in-situ supramolecular self-assembly assisted synthesis combining spray drying and high-temperature calcination was employed to prepare $Li_4Ti_5O_{12}$-carbon-rGO microspheres for LIBs. During the sol formation, GO was connected with $Ti(OH)_4$ coated by polydopamine [373]. The as-prepared composite consisted of small size LTO particles (~50 nm) wrapped in 3D rGO nanosheets. The LTO/C/rGO hybrid anode exhibited a reversible capacity of 184 mAh g^{-1} at 1C rate and a capacity retention of 94.5% after 500 cycles at 20C rate. These results compared well with those reported by Chen et al. on LTO/CNTs/graphene composite prepared by ball-milling, which exhibits a discharge capacity of 132 mAh g^{-1} at 20C rate [374].

More recently, the ternary microspherical C/LTO/rGO, which consisted of ethylene glycol-derived in-situ carbon-coated $Li_4Ti_5O_{12}$ nanoparticles and rGO sheets, was synthesized by polyol-mediated spray drying method [375]. The as-fabricated C/LTO/rGO composite tested as anode material for LIBs showed 94% capacity retention after 3000 cycles at 10C and 93% capacity retention after 1000 cycles at 60 °C. This electrode was also studied as anode for sodium-ion batteries showing 95% capacity retention after 1000 cycles at 5C for Na^+ storage at room temperature. An LTO/rGO nanolayered composite was synthesized by electrophoretical co-deposition onto Cu substrate using a suspension of 2D-lithium titanate hydrate and GO nanosheets followed by a controlled annealing at 600 °C for 6 g using a ramping temperature of 5 °C min^{-1} [376]. Galvanostatic experiments performed at 1C (175 mA g^{-1}) showed a retention capacity of ~135 mAh g^{-1} after 150 cycles. The rate capability test demonstrated a specific capacity of 50 mAh g^{-1} at high rate of 50C.

4.6. Iron-Based Oxide Composites

4.6.1. Fe_3O_4-Based Composites

Magnetite (Fe_3O_4) proved to be a rechargeable conversion electrode material that reacts with 8 Li ions per formula unit leading a theoretical specific capacity of about 926 mAh g^{-1} [377]. While cells using iron oxides present voltage hysteresis from 0.7 to 1.0 V, the use of rGO reduces the overpotential to ~0.7 V. In 2010, the study of a micro-structured graphene nanosheets/Fe_3O_4 composite has shown the superior performance with the addition of graphene with a reversible specific capacity approaching 1026 mAh g^{-1} after 30 cycles at 35 mA g^{-1} and 580 mAh g^{-1} after 100 cycles at 700 mA g^{-1} [62]. Since 2011, numerous works have been devoted to the investigation of GO-ferrite composite. Fe_3O_4/rGO composites are not only mostly synthesized using the popular hydrothermal method with subsequent annealing process [378–382] but also employing other techniques such as chemical precipitation [383–385], one-pot microwave reduction [386], electrophoretic deposition [387], and redox reaction [388].

Li et coworkers prepared Fe_3O_4/rGO nanocomposites through a chemical co-precipitation of Fe^{2+} and Fe^{3+} in the presence of GO in alkaline solution. After a thermal reduction, the composite was composed of Fe_3O_4 nanoparticles homogeneously dispersed on the rGO sheet surface [383]. Tested in half-cell, this composite displayed a reversible capacity of about 200 mAh g^{-1} even at a high charge/discharge rate of 10C (9260 mA g^{-1}). The rGO/Fe_3O_4||$LiNi_{1/3}Mn_{1/3}Co_{1/3}O_2$ full-cell exhibited a capacity of 80 mAh g^{-1} when discharged at 0.2C rates over 10 cycles. Zhu et al. [384] reported the fabrication of Fe_2O_3/rGO composite using a facile two-step synthesis by homogeneous co-precipitation of $FeCl_3$ in a suspension of GO platelets with urea, with subsequent reduction of the GO with hydrazine under microwave irradiation. The composite has a curled morphology consisting of a thin, wrinkled, "paperlike" structure. Such rGO platelets decorated with Fe_2O_3 nanoparticles (~60 nm in diameter) showed discharge and charge capacities of ~1355 and 982 mAh g^{-1}, respectively, based on the total mass of the composite, at a current density of 100 mA g^{-1} over 50 cycles. A three-dimensional Fe_3O_4/rGO composite was constructed by anchoring Fe_3O_4 nanoparticles encapsulated within carbon shells onto reduced graphene oxide sheet [58]. The two-step synthesis consisted in the mixture of an aqueous solutions of $Fe(NO_3)_3{\cdot}6H_2O$ and polyvinylpyrrolidone (PVP, M_W = 40,000) with the aqueous suspension of graphene oxide (GO) and an aqueous solution of glucose and urotropine (1:1) followed by a calcination to 500 °C in Ar flow. The final black powders exhibit a BET specific surface area of 104.2 m^2 g^{-1}. This Fe_3O_4/rGO composite, tested in Li half-cell, displayed an initial specific capacity of 1426 mAh g^{-1} and superior reversible capacity of 842 mAh g^{-1} after 100 cycles at 200 mA g^{-1} current rate.

A Fe_3O_4/rGO composite was fabricated by a microwave-assisted combustion synthesis of porous Fe_3O_4 particles followed by decoration of Fe_3O_4 by rGO. The material was porous with specific surface area and pore volume of 81.87 m^2 g^{-1} and 0.16 cm^3 g^{-1}, respectively [389]. Electrochemical results revealed a reversible capacity of 612, 543, and 446 mAh g^{-1} at current rates of 1C, 3C, and 5C, respectively, with a coulombic efficiency of 98% after 50 cycles, which emphasized the importance of the composite porosity and the improved electronic conductivity by rGO grafting. A Fe_3O_4/rGO composite was prepared by Liang et al. via coprecipitation, with Fe_3O_4 nanoparticles of size 9nm [390]. As an anode containing 44.9 wt% Fe_3O_4, it delivered a capacity of 300 mAh g^{-1} at 1 A g^{-1} after 100 cycles. Kumar et al. [386] designed and synthesized an interconnected hybrid network constituted by faceted Fe_3O_4 nanoparticles embedded in 3D rGO nanosheets by one-pot microwave approach. The electrochemical properties of these as-synthesized Fe_3O_4/rGO hybrids were analyzed by cyclic voltammetry, galvanostatic charge/discharge measurements, and electrochemical impedance spectroscopy. These hybrids demonstrated superior performance as electrostatic capacitors (ESC) with a specific capacitance of 455 F g^{-1} at the scan rate of 8 mV s^{-1}. Moreover, the 3D composite exhibited good cycling stability with a retention of 91.4% up to 9600 cycles. Liang et al. [391] investigated the effect of Fe_3O_4 loading on the cycling behavior of Fe_3O_4/rGO hybrid anode for LIBs. The composite was prepared by co-precipitation method using Fe_3O_4 nanoparticles (grain size of ca. 9 nm) and different amount of GO followed by reduction. The best cycling capacity of 300 mAh g^{-1} at 1 Ag^{-1} current density was obtained after 100 cycles for the Fe_3O_4/rGO composite electrode containing 44.9 wt% Fe_3O_4. $Fe(OH)_3$ nanoparticles were embedded in rGO nanosheets via a pre-reduction with hydrazine followed by a hydrothermal process at 180 °C for 12 h and a subsequent heating at 500 °C for 2 h in an Ar atmosphere with a heating rate of 5 C min^{-1}, to yield Fe_3O_4/rGO composite with Fe_3O_4 nanoparticles of ~6 nm in size. The as-prepared samples showed a uniform porous morphology with a high BET specific surface area of 114.7 m^2 g^{-1}. Galvanostatic charge–discharge measurements showed that the Fe_3O_4/rGO||Li half-cell delivers a reversible specific capacity of 1108 mAh g^{-1} at a current density of 0.5 A g^{-1} even after 400 cycles and maintains a reversible capacity of 593 mAh g^{-1} at 5 A g^{-1} current rate [378]. The Fe_3O_4/rGO composites consisting of well-crystallized Fe_3O_4 nanoparticles (10–30 nm in diameter) are tightly and homogeneously anchored on the flexible graphene substrate were synthesized through a redox reaction between highly oxidized GO and ferrous salt ($FeSO_4{\cdot}4H_2O$) under basic atmosphere (ammonia), followed by a stabilization treatment ranging from 5 min to 5 h [388]. The optimized Fe_3O_4/rGO composite obtained after 2-h annealing delivers a reversible capacity of 1024 mAh g^{-1} at 1 A g^{-1} current rate and retains 584 mAh g^{-1} at 5 A g^{-1} even after 450 cycles (Figure 12). A super-mesoporous Fe_3O_4/rGO anode material was prepared by a poly(methacrylic acid) (PMAA)-induced self-assembly process, which provided a sample with high porosity by optimizing the dispersion state of PMAA-stabilized Fe_3O_4/GO sheets at different surrounding pH values. The mesoporous composite showed a high specific surface area of 338.8 m^2 g^{-1} with a large amount of 10–40 nm mesopores. The corresponding Fe_3O_4/rGO anode delivered specific-charge capacity of 740 mAh g^{-1} after 100 cycles at 0.5 A g^{-1} and decreases to 200 mAh g^{-1} at 10 A g^{-1} [391].

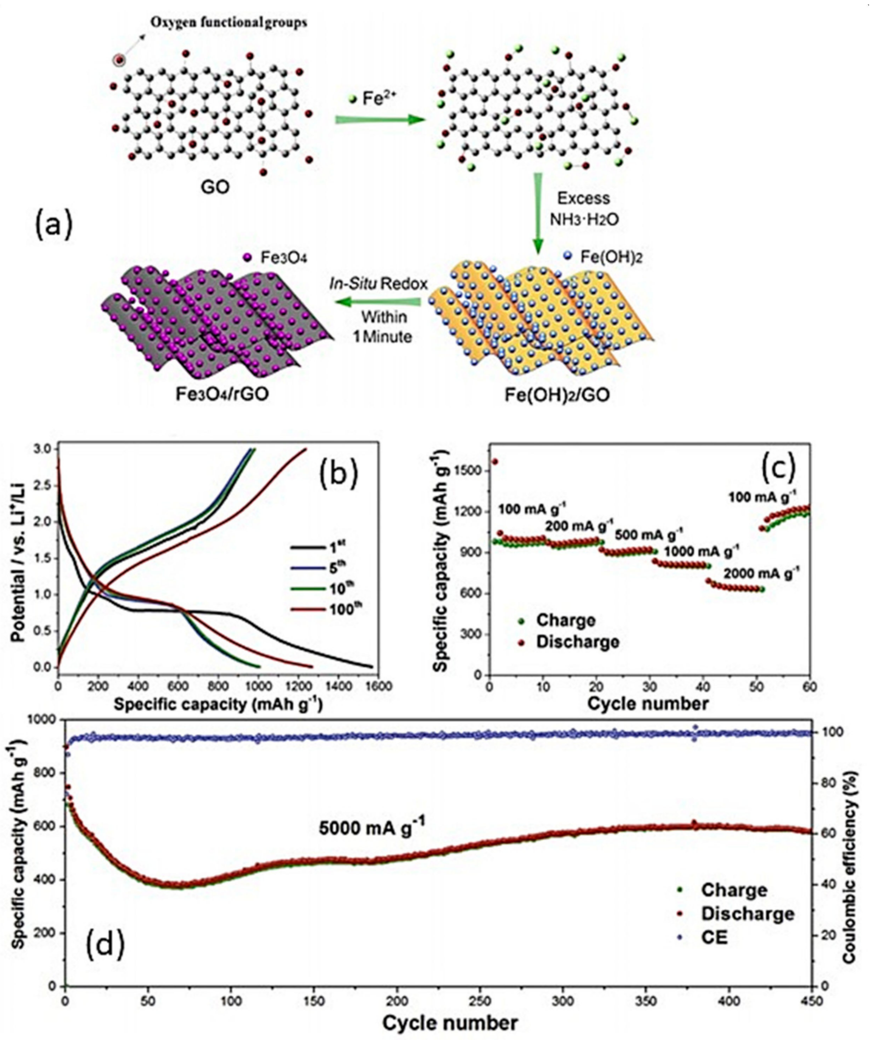

Figure 12. (**a**) Schematic illustration of the procedure for the synthesis of Fe_3O_4/rGO composites. (**b**) Charge–discharge profiles of Fe_3O_4/rGO||Li cell performed at 1 A g^{-1} current rate with the composite anode obtained after 2-h annealing. (**c**) Rate capability. (**d**) Long-term cyclic capability at a current density of 5 mA g^{-1}. Reproduced with permission form [388]. Copyright 2018 Elsevier.

Several studies are related to Fe-based ternary composite electrodes showing superior electrochemical properties. The Fe_3O_4/CNTs/rGO composite electrode as a binder-free anode was prepared by electrophoretic deposition. This robust sandwich-like architecture consisted of Fe_3O_4 nanoparticles interconnected by CNTs between rGO layers [387]. The resultant Fe_3O_4/CNTs/rGO hybrid electrode demonstrated enhanced electrochemical properties with high reversible capacity of 540 mAh g^{-1} at a high current density of 10 A g^{-1}, and a remarkable capacity retention of 1080 mAh g^{-1} after 450 cycles at 1 A g^{-1}. Xiao et al. [392] constructed a multilayered composite rGO/Fe_3O_4@polydopamine (PDA) hydrogel, in which the PDA layer plays the role of artificial SEI onto Fe_3O_4 nanoparticles. The electrochemical tests of the rGO/Fe_3O_4@PDA||Li half-cell showed high specific capacity of 1358 mAh g^{-1} after 300 cycles at 1 A g^{-1} current rate, satisfying rate capability (~600 mAh g^{-1} at 3C), and fast charge/discharge rate (712 mAh g^{-1} after 2000 cycles at 3 A g^{-1}). Rice crust-like structure of thin carbon layer (~2 nm thick) coated Fe_3O_4 nanoparticles (~15 nm) uniformly covering rGO sheets was obtained via solvothermal process with subsequent annealing at 600 °C for 1 h under flowing Ar gas (100 sccm) [393]. This Fe_3O_4@C/rGO composite showed a specific capacity of ~970 mAh g^{-1} at 0.2 A g^{-1}. At higher current rate (5 A g^{-1}), it exhibited a capacity of 420 mAh g^{-1}, which is much higher than that of the composite Fe_3O_4/rGO without carbon coating. The Fe_3O_4@C/rGO anode cycled 1000 times at 5 A g^{-1} delivered 594 mAh g^{-1} with a CE of 99.4%. The authors stated that the charge/discharge process occurs with two reactions: A conversion reaction (above 0.8 V) and a surface adsorption (below 0.8 V), which is attributed to the pseudocapacitance contribution calculated at 89%, originating from the carbon coated nanostructure. A ternary Fe_3O_4-MoO_3/rGO nano-composite prepared by microwave hydrothermal method was deposited on carbon cloth (CC) [394]. The detailed morphological studies showed that Fe_3O_4-MoO_3 nanoparticles were decorated on thin sheets of rGO with a resolution of 50 nm. The as-prepared Fe_3O_4-MoO_3/rGO-@CC electrode showed a specific capacitance of 1666 F g^{-1} at a current density of 2.5 A g^{-1} and a capacitance retention of 95% after 5000 cycles. A NiO/Fe_3O_4/rGO composite obtained via a solvothermal route consisted of Fe_3O_4 nanospheres (average size ~150 nm) and rod-shaped NiO particles (about 300 nm) distributed on the surface of rGO. The porous NiO/Fe_3O_4/rGO sample exhibits a BET specific surface and average pore diameter of 497 m^2 g^{-1} and 1.2 nm, respectively. The initial discharge capacity was 841 mAh g^{-1} and maintained 647 mAh g^{-1} after 200 cycles at the current density of 0.5 Ag^{-1}. Rate capability tests showed that the discharge capacity was still 582 mAh g^{-1} after 200 cycles at 1 A g^{-1} [395].

Recently, Xiao et al. [396] reported the fabrication of multi-layered graphene oxide-Fe_3O_4@polydopamine-polyacrylamide (rGO-Fe_3O_4@PDA-PAM) composites through a green and scalable strategy. In this assembly, Fe_3O_4 nanoparticles (NPs) were confined by the PDA shell and rGO sheets. Gao et al. [397] developed a simple one-step hydrothermal method to prepare Fe_3O_4/FeS/rGO composite with a uniform deposition of octahedral Fe_3O_4/FeS particles on the rGO. This structural design delivered a reversible capacity of 744 mAh g^{-1} at 0.1C rate after 50 cycles showing excellent interface stability. Using broccoli-like multichannel $FeCO_3$ microspheres as raw material, the Fe_3O_4 nanoflakes/rGO composites were realized via a low temperature hydrolysis reaction in the presence of graphene and hydrazine. The Fe_3O_4 NFs/rGO electrode exhibited a satisfied capacity of 925.3 mAh g^{-1} with 68.8% retention and retained a capacity of 636.1 mAh g^{-1} after 1000 cycles at 0.5 A g^{-1} [380].

Fe_3O_4 was intercalated into rGO and conductive carbon layers to form a 3D sandwich-like C/Fe_3O_4/rGO architecture. The composite, prepared by one-pot solvothermal process, exhibited excellent electrochemical performance as anode in LIB with specific capacity of 844 mAh g^{-1} at 0.2 A g^{-1} after 300 cycles and high-rate cyclic performance (i.e., 363 mAh g^{-1} at 4 A g^{-1} after 300 cycles. Meanwhile, when used as ESC electrode, the C/Fe_3O_4/rGO hybrid showed a pseudocapacitance of 77% when scan rate is 5 mV s^{-1} [398]. Liang and Lu developed a new technique for the fabrication of Fe_3O_4/rGO nanocomposites, namely the gamma-irradiation method, in which the iron(III) hydroxide and GO are reduced to Fe_3O_4 and rGO by the reducing species generated from the radiolysis of the solvent [399]. The electrochemical performances of the Fe_3O_4/rGO composite containing various amounts of Fe_3O_4 evaluated in coin-type cells yielded good cycling stability at a low current density of 50 mA g^{-1}. The specific discharge capacity of with 78.8 wt% Fe_3O_4/rGO remained at 568.6 mAh g^{-1} after 100 cycles, while the 74.7 wt% Fe_3O_4/rGO electrode exhibited a sustained discharge capacity is 738.5 mAh g^{-1} after 100 cycles at current density of 500 mA g^{-1}. Copper-ferrite-based composites, namely $CuFeO_2$/rGO and Cu/$CuFeO_2$/rGO were proposed by Wang et al. [400] as high-performance anode materials for LIBs. A four-step synthesis consisted in: (i) The formation of the $CuFeO_2$ delafossite crystals in an alcoholic solution containing $Fe(NO_3)_3$ and $Cu(NO_3)_2$ dissolved species, and (ii) the mixture of the GO suspension and the $CuFeO_2$-like solution with control of the pH at 12 by 6 mol L^{-1} NaOH, (iii) an hydrothermal process at 180 °C for 12 h, and finally (iv) a calcination in a tube furnace at 400 °C for 2 h under a N_2 atmosphere. The TEM images of the as-prepared hybrids revealed that ultrafine nanoparticles (15–25 nm in diameter) decorated the graphene nanosheets. When tested in the voltage range 0.02–3.0 V vs. Li^{+}/Li at 200 mA g^{-1} current rate, the sheet-on-sheet $CuFeO_2$/rGO electrode displayed a reversible capacity of 587 mAh g^{-1} after 100 cycles, while the Cu/$CuFe_2O_4$@rGO hybrid, containing combined nano-copper and rGO, manifested a superior rate capability of 723 and 560 mAh g^{-1} at 0.8 and 3.2 A g^{-1}, respectively and a cyclability of 1102 mAh g^{-1} after 250 cycles at 800 mA g^{-1} rate. Table 7 summarizes the electrochemical performances of iron oxide/rGO composites.

Table 7. Summary of electrochemical performances of iron oxide/rGO composites. Relevant cycle number is displayed in brackets.

Material	Synthesis	Specific Capacity ($mAh\ g^{-1}$)	Current Density ($A\ g^{-1}$)	Ref.
Fe_3O_4/rGO	co-precipitation + annealing	200	9.26	[383]
Fe_3O_4/rGO	microwave-assisted combustion	446	5C (50)	[389]
Fe_3O_4/rGO	coprecipitation	300	1.0 (100)	[390]
Fe_3O_4/rGO	hydrothermal + heating	593	5.0 (400)	[378]
Fe_3O_4/rGO	redox reaction	584	5.0 (450)	[388]
Fe_3O_4/CNTs/rGO	electrophoretic deposition	1080	1.0 (450)	[387]
rGO/Fe_3O_4@PDA	hydrothermal + calcination solvothermal	712	3.0 (2000)	[392]
Fe_3O_4@C/rGO	hydrothermal + calcination	594	5.0 (1000)	[393]
Fe_3O_4/FeS/rGO	hydrolysis	744	1C (50)	[397]
Fe_3O_4 NFs/rGO	gamma-irradiation method	636	0.5 (1000)	[380]
78.8 wt%Fe_3O_4/rGO	gamma-irradiation method	568	0.05 (100)	[399]
74.7 wt%Fe_3O_4/rGO	solvothermal	738	0.5 (100)	[399]
NiO/Fe_3O_4/rGO	electrostatic assembly	580	1.0 (200)	[395]
CP/Fe_3O_4/rGO	solvothermal	1160	0.5 (1000)	[401]
Fe_3O_4/rGO	PMAA-induced self-assembly	992	0.15 (100)	[402]
Fe_3O_4/rGO	hydrothermal + calcination	740	0.5 (200)	[391]
$CuFeO_2$/rGO	one-pot solvothermal	587	0.2 (100)	[400]
C/Fe_3O_4/rGO		844	0.2 (300)	[398]

4.6.2. Fe_2O_3-Based Composites

Fe_2O_3 (a-phase) has the advantages of rich ores, low price, and high theoretical capacity of 1007 mAh g^{-1} according the lithiation process, that is the conversion reaction $Fe_2O_3 + 6Li^+ + 6e^- \leftrightarrow 3Li_2O + 2Fe^0$. In the anodic polarization process, the broad anodic peak at around 1.55 V is related to the reverse de-conversion process of Li_2O with metallic iron. Since 2011, a-Fe_2O_3/rGO hybrids were recognized as important electrode materials for energy storage devices [403–407]. For example, Wang and his collaborators were one of the first researchers who demonstrated the enhanced performances of a-Fe_2O_3/rGO nanocomposites as anode materials for LIBs, showing a high discharge capacity of 660 mAh g^{-1} during up to 100 cycles at the current density of 160 mA g^{-1} [408].

In 2015, Wang et al. [409] fabricated cells with 3D mesostructured Ni scaffolded Fe_2O_3 electrodes. The voltage hysteresis was 0.62 V at 100 mA g^{-1} and was further reduced to 0.42 V at elevated temperature (45 °C). Zhu et al. [384] prepared Fe_2O_3/rGO composite using a co-precipitation/microwave technique. The as-prepared electrode exhibited a specific capacity of 1355 mAh g^{-1} after 50 cycles at 100 mA g^{-1}. Liu et al. [410] built a nanocomposite of a-Fe_2O_3 nanoplates imbedded in graphene networks using a one-step hydrothermal method with water and glycerin as hydrothermal solvents. In this hybrid, the a-Fe_2O_3 nanoplates, with a size of 20–30 nm, were well wrapped and closely connected by the flexible conductive network. The a-Fe_2O_3/rGO composite anode demonstrated high discharge capacities of ~896 mAh g^{-1} up to 200 cycles at 5C rate and ~429 mAh g^{-1} up to 1000 cycles even at a 10 C rate. Lee et al. [411] prepared a-Fe_2O_3 hollow nanobarrels (a-HNBs, ~200 nm in diameter, ~360 nm in length) deposited on rGO using a one-step microwave-assisted hydrothermal process. The as-synthesized a-HNBs/rGO composite yielded superior electrochemical properties such as a reversible capacity of 1279 mAh g^{-1} at 0.5C rate after the first cycle, a long-term cycle ability of 478 mAh g^{-1} after 1000 cycles, and a high rate capability of 403 mAh g^{-1} even at 10C rate. The g-Fe_2O_3/RGO composite electrode materials was prepared by the reduction of few layer GO to rGO by iron metal in aqueous solution under ambient conditions; the final product was obtained by calcination at 600 °C for 2 h under N_2 atmosphere [412]. The g-Fe_2O_3 nanoparticles formed by the oxidation of iron were uniformly dispersed on the surface of rGO sheets. The g-Fe_2O_3/RGO composite anode, tested in the voltage range 0.01–3.0 V at 500 mA g^{-1} current rate, delivered an initial specific capacity of 850 mAh g^{-1}, maintained at of ~800 mAh g^{-1} after 300 cycles. When cycled at 15 A g^{-1} performance, the capacity remains stable at 200 mAh g^{-1}.

Recently, Liu and coworkers [413] focused on the development of facile and low-cost synthetic method to grow Fe_2O_3/rGO hybrids. They used $FeCl_3$ as the raw material and adopted different one-step hydrothermal methods (i.e., hydrothermal in-situ method, PVP-assisted hydrothermal in-situ method, or oleic acid-assisted hydrothermal in-situ method). A comparison of the electrochemical performance of the Fe_2O_3/rGO anodes prepared by these three processes shows that the oleic acid-assisted hydrothermal method is best. With this process, the initial specific discharge capacity was 1431 mAh·g^{-1} at a current density of 100 mA·g^{-1}, and, remained at 478 mAh·g^{-1} after 50 cycles. Within similar conditions, capacities of 435 and 225 mAh·g^{-1} were delivered by the anodes prepared by hydrothermal in-situ and PVP-assisted hydrothermal in-situ method, respectively.

4.6.3. FeO-Based Composites

Exfoliated graphene oxide (EGO)/iron (II) oxide (FeO) composite was prepared by graphenothermal reduction process at 650 °C for 5 h in argon [414]. This composite displayed a measured BET of 11 m^2 g^{-1}, pore diameter of 10.6 nm and average pore volume of ~0.064 cm^3 g^{-1}. Electrochemical tests showed a reversible capacity of 857 mAh g^{-1} at a current rate of 50 mA g^{-1} in the voltage range 0.005–3.0 V vs. Li^+/Li with a high coulombic efficiency of 98% up to 60 cycles. As a cathode material for LIBs, $LiFePO_4$/graphene oxide (LFP/GO) composite was prepared by spray-drying and annealing processes, in which nanoparticles were wrapped homogeneously and loosely with the graphene 3D network facilitating electron migration throughout the secondary particles and fast Li^+ diffusion in the voids. The LFP/GO composite could deliver a specific capacity of 70 mAh g^{-1} at 60C discharge rate. After 1000 cycles, the capacity decay rate of <15% was measured under 10C charging and 20C discharging [415]. One type of Li-ion storage material with fast faradaic surface redox reaction offers high power density but limited in some extent of energy contribution. Qi et al. demonstrated that in-situ pulverized FeOOH rods on rGO sheets exhibit a pseudocapacitance storage behavior (82% of the total capacity). The FeOOH/rGO composite achieved specific capacities of 1135 and 783 mAh g^{-1} at current rate of 1.0 and 5.0 A g^{-1}, respectively, over 200 cycles [416].

4.7. Vanadium-Based Oxide Composites

Vanadium oxides (VO_x) exist in various compositions (e.g., V_2O_5, V_3O_7, V_4O_9, V_6O_{13}, VO_2, V_2O_3, etc.), depending on the oxidation state (5^+ to 2^+) of vanadium. They have attracted considerable attention as potential electrode materials for energy storage devices (LIBs, SIBs, ESCs) [417].

4.7.1. VO_2-Based Composites

Since the 1980s, vanadium oxides VO_{2+y} ($0 \leq y \leq 0.5$) are known for lithium storage applications [418]. VO_2(R) is the most stable phase, which crystallizes in the rutile-like structure (monoclinic, $C2/m$ space group). Nanocrystalline VO_2(B) is a metastable, which crystallizes in the monoclinic structure with a fibrous morphology owing to its V_4O_{10}-type double layers to form V-O tunnels perpendicular to the *c*-axis for rapid lithium-ion insertion/deinsertion process. Typically, VO_2/rGO composites are synthesized by either freeze-drying or a solvothermal method. In the freeze-drying, a dispersed suspension is obtained by mixing graphene oxide and ammonium vanadate in water and freeze in liquid nitrogen; finally, the VO_2/rGO composite is grown after calcination at 500 °C for 5 h under Ar conditions. During this process, NH_4VO_3 is converted into VO_2 ($NH_4VO_3 + C \rightarrow NH_3 + VO_2 + CO_2 + H_2O$) with simultaneous reduction of GO to rGO [419]. In the solvothermal method, the VOC_2O_4 clear dark blue solution formed by the mixture vanadium pentoxide and oxalic acid (molar ratio 1:3) in water is added to a GO dispersion and hydrothermally treated in butanol at 200 °C for 8 h. Finally, the VO_2/rGO composite is obtained after alcohol washing at 80 °C for 8 h [420]. In a two-step hydrothermal reaction, well-dispersed VO_2(B) nanorods with diameter of 40 nm and length of 150 nm are grown using V_2O_5 as raw material and rod-like vanadyl ethylene glycolate as intermediate product, separately. The 3D VO_2(B)/rGO composite is obtained by adding GO. Electrochemical test shows that the close connection between rGO sheets and VO_2(B) NRs improved the cycling stability [421].

VO_2(B)/rGO nanocomposite was synthesized via a one-step microwave-assisted solvothermal process fromVOC_2O_4 obtained by dissolution of V_2O_5 in the presence of oxalic acid [422]. The VO_2(B)/rGO hybrid reveals good performance as an anode in lithium-ion batteries with an initial capacity of 400 mAh g^{-1} and a reversible specific capacity of 200 mAh g^{-1} over 400 cycles in the potential range 3.0–0.05 V vs. Li^+/Li. Nethravathi et al. [423] performed a hydrothermal reaction of a mixture of a colloidal dispersion of GO and NH_4VO_3, which yielded a VO_2(B)/GO hybrid. The nanotubular morphology of VO_2(B) wrapped between graphene sheets improved the charge transfer and achieved ~450 mAh g^{-1} at 40 mA g^{-1} current rate. Song et al. [424] investigated an rGO supported VO_2(M) nanocomposite prepared via a one-step sol-gel assisted hydrothermal process. A GO-dispersed V_2O_5 gel was reduced with an appropriate hydrazine monohydrate ($N_2H_4 \cdot H_2O$) as strong reductant and hydrothermally treated at 220 °C for 24 h. From this synthesis, the as-prepared M-phase VO_2 nanoparticles (20 50 nm in size) well dispersed in rGO exhibits the monoclinic ($P2_1/c$ space group) structure. The discharge capacity of VO_2(M)/rGO electrode is 283 mAh g^{-1} at a current density of 60 mA g^{-1} over 200 cycles. The rate capability showed a capacity of 210 mAh g^{-1} at 300 mA g^{-1}. Choi et al. [425] prepared VO_2-decorated rGO balls using a one-pot spray-pyrolysis process from a colloidal spray solution of well-dispersed GO and NH_4VO_3 followed by post-treatment at 300 °C in an air atmosphere. The as-prepared VO_2(B) nanorods (~200 nm in diameter) are encapsuled by rGO nanosheets. The rGO/VO_2 composite with 5 wt% graphene showed an initial discharge and charge capacities of 148 and 135 mAh g^{-1}, respectively, at 300 mA g^{-1} current rate. A free-standing $VO_{2.07}$/rGO film was fabricated through hydrothermal process using $NH_4VO_3 \cdot$and GO in 1 mol L^{-1} HNO_3 aqueous solution [426]. The as-prepared nanoribbons (30 nm thick, 50 µm long) were annealed at 300 °C in N_2 atmosphere and tested as cathode material (mass loading of 1.2 mg cm^{-2}) in Li cell. The $VO_{2.07}$/rGO intertwining network exhibits a reversible specific capacity of 160 mAh g^{-1} and good cycling stability of 133 mAh g^{-1} after 200 cycles at a current density of 70 mA g^{-1} in the voltage range between 2.0 and 3.5 V.

Xiao et al. [427] prepared VO_2/rGO composites by a simple one-step hydrothermal method. Samples consist of VO_2 flakes anchored with rGO. When used as anode for Li-ion battery, this VO_2/rGO composite yields a high capacity of ~622 mAh g^{-1} at 100 mA g^{-1} and maintains a capacity of 256 mAh g^{-1} after 300 cycles at 2 A g^{-1} with capacity retention of almost 100%. Yan et al. [420] encapsuled VO_2 nanospheres (average diameter of ~500 nm) into crumpled rGO using a one-step rapid and scalable solvothermal approach at 200 °C for 8 h. The as-prepared sample has a BET specific surface area of 130.4 m^2 g^{-1}. The sodiation reaction of VO_2/rGO composites tested in the voltage range of 3.0 to 0.01 V vs. Na^+/Na results in a reversible capacity of 383 mAh g^{-1} at 0.1 A g^{-1} and 214 mAh g^{-1} at 4 A g^{-1}, and long-term stability over 2000 cycles at 4 A g^{-1} with a capacity fade of 0.013% per cycle. Dai et al. [419] demonstrated a highly reversible zinc/vanadium dioxide system, where freestanding reduced graphene oxide/vanadium dioxide (rGO/VO_2) composite films were used as the cathodes of Zn-ion batteries. When cycled at 4 A g^{-1}, the rGO/VO_2 hybrid exhibit an excellent discharge capacity of 240 mAh g^{-1} with a coulombic efficiency ~100% and ~100% capability retention over 1000 cycles.

Graphene woven VO_2 nanoribbons synthesized using in-situ hydrothermal method show high discharge capacity (380 mAh g^{-1}) and 99% capacity retention after 50 cycles [428]. Dai et al. [419] investigated the electrochemical performance of VO_2/rGO films in Zin-ion batteries. The composites synthesized by freeze-drying method delivers a specific capacity of 276 mAh g^{-1} at a current rate of 0.1 A g^{-1} in the potential range of 0.3–1.3 V (energy density of 65 Wh kg^{-1}) and exhibits excellent capacity retention of 99% after 1000 cycles. A considerable capacity of 120 mAh g^{-1} was still obtained at high rate of 35 A g^{-1}. Recently, Cui et al. [429] designed a cathode material for Zn-ion batteries consisting in VO_2(B) nanobelts uniformly deposited on to rGO nanoflakes via a one-step hydrothermal route. The VO_2(B)/rGO composite presents a specific capacity of 456 mAh g^{-1} at 0.1 A g^{-1}. Cycling performance shows an excellent capacity retention of 72% after 1600 cycles at 5 A g^{-1}. Zhao et al. [430] investigated VO_x/rGO composites as cathode materials for Li-ion batteries using a facile hydrothermal method at 190 °C for 48 h. Black precursor heat treated at 500 °C for 2 h produced a V_2O_5/rGO composite (BET surface area of 64 m^2 g^{-1}), while treat at 550 °C for 2 h in N_2 atmosphere resulted in a VO_2/rGO hybrid material (BET surface area of 35 m^2 g^{-1}) with the VO_2(R) phase. The obtained VO_2 had a uniform lamellar 3D structure with thickness of 20 nm. The VO_2/rGO cathode exhibited an initial specific capacity of 115 mAh g^{-1} with a retention of 74% after 100 cycles.

VO_2(B)/rGO composite formed by the assembly of VO_2(B) nanoparticles and rGO were also used as electrodes for ESCs [431–437]. VO_2(B) nanobelts/rGO composite films were fabricated as electrodes for high-performance flexible all-solid-state supercapacitors [421]. The assembly composed of nanobelts with length of 3-5 μm and width of 40-150 nm, provide the maximum power density of 7152 W kg^{-1} at the energy density of 3.13 Wh kg^{-1}. Lee et al. examined the effect of the ultra-large graphene transverse dimension (47 ± 22 μm) on the electrochemical properties of VO_2(B)/rGO composites for ESC. The hybrid electrode with ultra-large rGO performs lower sheet resistance (0.57 kW sq^{-1}) than the composite with rGO of 0.8 μm lateral size. Excellent capacitive performance of 769 F g^{-1} was reported [431]. A 2D nanocomposite was built by the uniform distribution of 3D VO_2(B) flowers on N-doped GO (N-GO) [436]. The anchoring of the VO_2(B) flowers to N-GO results in high surface area of 71 m^2 g^{-1} and shows enhanced electrochemical performance, i.e., after 50 cycles, the hybrid retained 251 mAh g^{-1} (60% retention). GO-coated VO_2(B) nanomaterials were synthesized from a $VOSO_4$ sol using a hydrothermal approach [437]. The functionalized GO-coated VO_2(B) exhibits an urchin-like spherical shape (10–50 nm). Investigated as cathode materials deposited on stainless-steel mesh within a voltage range 1.5–4.0 V vs. Li/Li^+ at current density 100 mA g^{-1}, these GO-coated VO_2(B) nanomaterials exhibit a discharge capacity of 240 mAh g^{-1}. Cycling performance of 220 mAh g^{-1} was achieved after 20 cycles (10% capacity loss). Hierarchical VO_2(B)/rGO composite, synthesized through the hydrothermal route at 180 °C for 24 h, was investigated as an anode and activated carbon on carbon cloth (CC) as a cathode in battery-supercapacitor hybrid (BSH) device taking advantage of the mixed valency of V (V^{3+} and V^{4+}) inside the as-prepared VO_2 matrix, which facilitates redox reaction in working potential of 0.01–3.0 V vs. $Li^{+/}$Li. The VO_2(B)/rGO heterostructure yields a high specific capacity of 1214 mAh g^{-1} at current rate of 0.1 A g^{-1} after 120 cycles, with a high rate capability and stability [434]. The kinetic activation of the composite toward the electrochemical reaction during the activation period for Li-ion penetration resulting in the unconventional increase in the specific capacitance was observed with the increase in the number of cycles. Lv and coworkers [435] constructed a porous-type VO_2(B)/rGO framework formed of flexible rGO sheets and VO_2(B) nanobelts intertwined together, which exhibits a specific capacitance of 353 F g^{-1} at 1 A g^{-1} current rate. The increased transport of ions and electrons by the porous structures allows a capacitance retention of 78% after 10,000 cycles at 10 A g^{-1}. Recently, Kang et al. [438] developed a mesoporous VO_2(B)/rGO composite, which had facile access of Li ions to storage site. The composite electrode with a large specific surface area and pore volume of 335 m^2 g^{-1} and 3.09 cm^3 g^{-1}, respectively, achieves a specific capacity of 226 mAh g^{-1} at 50 mA g^{-1} current density and superior capacity retention of 67.5% over 40 cycles at current density up to 2000 mA g^{-1} (Figure 13). Electrochemical performance of VO_2/rGO composites as anodes or cathode for LIBs from the recent literature are summarized in Table 8.

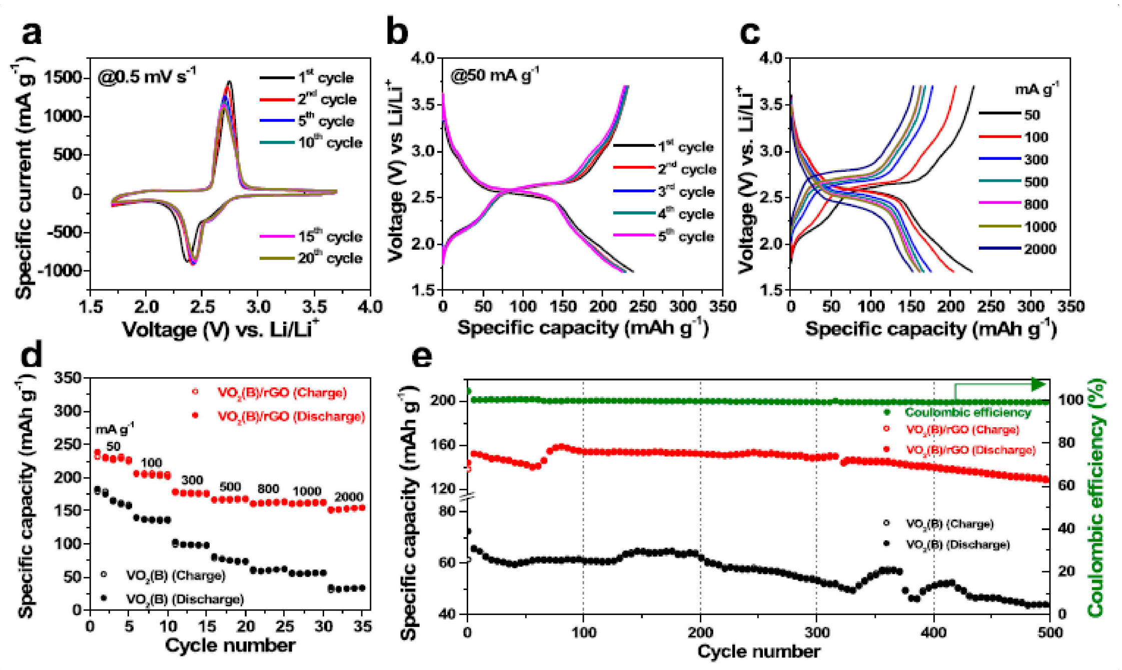

Figure 13. Electrochemical analysis of VO_2(B)/rGO composite. (**a**) CV curves for 20th cycles. (**b**) GCD profiles at 50 mA g^{-1}, (**c**) GCD profiles at various current densities from 50 to 2000 mA g^{-1}. (**d**) Rate capability. (**e**) Cyclic stability test at 1000 mA g^{-1}of VO_2(B)/rGO composite compared with bare VO_2(B). Reproduced with permission from [438]. Copyright 2021 Elsevier.

Although the present work focuses on the graphene-based composite electrodes for Li-ion batteries, it should also be noted that VO_2/rGO was also successful as a cathode for lithium sulfur batteries. The chemistry of such batteries is different, since the major difficulty is to solve the so-called shuttle effect of lithium polysulfides, but a VO_2/rGO proved to be able to solve this problem. The polar VO_2 can chemically anchor and catalyze the conversion of polysulfides and thus avoid their dissolution, while the rGO provides efficient transport pathways. The rGO/VO_2/S cathode with rGO wrapped yolk–shell VO_2 sphere hybrid host delivered a capacity of 718.6 mAh g^{-1} initially, and 516.1 mAh g^{-1} over 400 cycles at 1C [439].

Table 8. Summary of the electrochemical performance of VO_2(B)/rGO composites. Relevant cycle number is given in brackets.

Material	Synthesis	Specific Capacity (mAh g^{-1})	Current Density (mA g^{-1})	Ref.
Cathode				
VO_2(B)/rGO	hydrothermal 150 °C/12 h	250	50 (50)	[440]
VO_2(B)/GO	sonication + hydrothermal	350	40 (20)	[436]
$VO_{2.07}$/rGO	hydrothermal 180 °C/20 h	133	70 (200)	[426]
VO_2(R)rGO	hydrothermal 190 °C/48 h	85	20 (100)	[430]
VO_2(B)/rGO	hydrothermal 180 °C/24 h	130	1000 (500)	[438]
VO_2(B)/rGO	single-step hydrothermal	250	5000 (1600)	[429]
Anode				
VO_2(B)/rGO	microwave-assisted solvothermal	400	200 (400)	[422]
VO_2(M)/rGO	sol-gel assisted hydrothermal	283	60 (200)	[424]
GO-coated VO_2(B)	sol-gel + calcination	220	100 (20)	[437]
VO_2(B)/rGO	hydrothermal 180 °C/24 h	1214	100 (120)	[434]

4.7.2. V_2O_3-Based Composites

V_2O_3 has been considered as anode material because of its high theoretical capacity of 1070 mAh g^{-1} and low discharge potential, but its application is hindered by the low conductivity and drastic volume change [441,442]. Leng et al. [443] prepared 3D V_2O_3/rGO gels through a hydrothermal reaction and annealing process using GO and NH_4VO_3. These composites show a discharge capacity of 786 mAh g^{-1} under 0.07 A g^{-1} current density and good cycle stability. V_2O_3/rGO composites were fabricated by through a facile solvothermal method and annealing process; V_2O_3 nanoparticles (NPs, sizes of 5–40 nm) are uniformly dispersed on rGO sheets without aggregation [444]. The V_2O_3/rGO nanocomposites achieves a reversible specific capacity of 823 mAh g^{-1} under the current density of 0.1 A g^{-1} in the potential range 0.01–3.0 V and maintains 407 mAh g^{-1} under the high current density of 4.0 A g^{-1}. Using vanadyl oxalate (VOC_2O_4) and GO prepared by a modified Hummers' method as starting precursors, V_2O_3/rGO composites were synthesized via solvothermal process in ethylene glycol and hydrothermal route at 200 °C for 12 h with subsequent annealing at 600 °C for 4h in H_2/Ar (8:92) mixed atmosphere. Another specimen V_2O_3/GO was obtained by heat treatment in 100% Ar ambient (i.e., without reducing atmosphere) [445]. The V_2O_3–rGO electrode yields a stable capacity of 380 mAh g^{-1} after 50 cycles at a current density of 0.1 A g^{-1}, much higher than 280 mAh g^{-1} of V_2O_3–GO. The rate capability as anode electrode provided capacities of 150, 108, and 97 mAh g^{-1} at current densities of 3, 9, and 15 A g^{-1}, respectively. Liu and coworkers [446] performed an in-situ synthesis of V_2O_3 nanorods adhered to rGO via hydrothermal route and heat-treatment. Electrochemical features endow V_2O_3/rGO composite as advanced anode material for LIBs with good cycling stability, i.e., 675 mAh g^{-1} after 300 cycles at 0.5 A g^{-1} and excellent rate capability, i.e., 428 mAh g^{-1} at 2 A g^{-1}. Xiao and coworkers [444] have successfully prepared V_2O_3/rGO nanocomposites through a solvothermal method and annealing process. The V_2O_3 nanoparticles (NPs, 5–40 nm in size) were uniformly dispersed and encapsulated by rGO sheets, which inhibits volume changes, improves the ion, and electronic conductivity of highly resistive V_2O_3 and avoids NPs aggregation. The electrochemical properties of V_2O_3/rGO investigated in the potential range 0.01–3.0 V show a reversible specific capacity of 823 mAh g^{-1} under the current density of 0.1 A g^{-1}, and 407 mAh g^{-1} under the high current density of 4.0 A g^{-1}.

4.7.3. V_2O_5-Based Composites

Vanadium pentoxide is a typical layered material, which is crystallized with the orthorhombic structure (*Pmmn* space group). V_2O_5 is a promising cathode material because of its 2D architecture, abundant sources, and high theoretical specific capacity (294 mAh g^{-1} for 2Li uptake into g-$Li_xV_2O_5$) but shows limiting electrochemical performance in regard to the low ionic diffusivity (10^{-12}–10^{-13} cm^2 s^{-1}) and moderate electrical conductivity (10^{-2}–10^{-3} S cm^{-1}) [447]. Liu et al. [448] fabricated V_2O_5/rGO composites with two different morphologies, i.e., nanosheet or nanoparticle-assembled subunits (50–100 nm in-plane size) by adjusting the solvothermal solution as cathode materials for lithium-ion batteries. In the voltage range of 2.5–4.0 V vs. Li^+/Li, the nanosheet-assembled V_2O_5/GO hybrid delivered an initial capacity of 142 mAh g^{-1} at 2C rate and retained 85% of their original capacity at 1C rate after 500 cycles, while the nanoparticle-assembled V_2O_5/GO hybrid retained only 80 mAh g^{-1}. The V_2O_5/rGO composites exhibited better rate capability and long-term cycling stability; they delivered capacities of 122 mAh g^{-1} at 64C rate. A two-step solvothermal method followed by vacuum annealing was employed to prepare mesoporous hybrids of V_2O_5 nanoparticles anchored on rGO. This hybrid obtained by slow hydrolysis of vanadium oxytriisopropoxide ($C_9H_{24}O_4V$) had a hierarchical structure with 20–30 nm V_2O_5 nanoparticles uniformly deposited on rGO nanosheets, leading to a surface area of 24 m^2 g^{-1} and average pore size of 20 nm. The V_2O_5/rGO mesoporous hybrids were used as electrodes in symmetrical ESC (specific capacitance of ~466 F g^{-1} in 1 mol L^{-1} Na_2SO_4 electrolyte) and cathode of lithium battery (specific capacity of 295 and 132 mAh g^{-1} at C/9 and 10C rate, respectively). They showed excellent cycling stability with discharge capacity retention of ~83% after 150 cycles at 1C rate [449]. Luo et al. prepared the GO/V_2O_5-coated $LiNi_{0.5}Co_{0.2}Mn_{0.3}O_2$ (GO/VO/NCM) cathode material by a wet chemical method [450]. The composite consisted of a V_2O_5 inner layer of 5 nm and a GO outer layer of 5–9 nm thick. The double-layer-coated NCM cathode material (initial discharge capacity of ~180 mAh g^{-1}) showed improved electrochemical performance with a capacity retention of 74.2% after 50 cycles in a range of 2.5–4.5 V vs. Li^+/Li at 55 °C. Liu et al. developed a method to introduce GO sheets into V_2O_5 nanoribbons via sol-gel route [451]. The 2 wt% GO containing composite delivered a specific capacity of 315 mAh g^{-1} at 1C rate and showed good cyclability over 200 cycles with a capacity decay of 0.13 mAh g^{-1} per cycle. For the micro-nanosized V_2O_5/rGO composites that were fabricated by the hydrothermal treatment of the mixture of V_2O_5, cetyltrimethyl ammonium bromide, and GO dispersed in aqueous solution kept at 190 °C for 48 h [430], the initial charge capacity was 235 mAh g^{-1} at 20 mA g^{-1} current rate and 235 mAh g^{-1} was retained after 100 cycles. A simple solvothermal technique was used to prepare self-assembled V_2O_5 nanosheets (NSs)/rGO nanocomposite with high specific area of 40 m^2 g^{-1}. The V_2O_5 NSs/rGO anode cycled at 3 and 15 A g^{-1} current densities delivered specific capacities of 138 and 76 mAh g^{-1}, respectively. When discharged at 2C rate a discharge capacity of 102 mAh g^{-1} was obtained after 160 cycles [452]. Highly porous polycrystalline V_2O_5/rGO hybrids were grown through heterogeneous nucleation of V_2O_5 nanoparticles (10–50 nm) on rGO sheets by using a solvothermal method followed by an annealing process [453]. In the voltage range of 4.0–2.0 V, the cathode performance of the as-prepared V_2O_5/rGO (46 wt%) was 102 mAh g^{-1} at a high current density of 5700 mA g^{-1} after 2000 cycles. A V_2O_5-reduced graphene ball composite was formed by the post-annealing of VO_2/rGO hybrid at 300 °C in air [425]. Hu and coworkers [454] synthesized uniform wrinkle V_2O_5/GO flexible thin films via a drop-casting technique with subsequent annealing process. The optimized films with mass ratio (8:1) of V_2O_5 and GO exhibited a specific capacitance of 397 F g^{-1} at a current density of 1 A g^{-1} and cycling stability with 98% retention over 2000 cycles at 5 A g^{-1} rate. With 5 wt% graphene, the initial discharge capacity of V_2O_5/rGO was 282 mAh g^{-1} with a coulombic efficiency of 99%. This cathode material delivered a capacity of 214 mAh g^{-1} at 1 A g^{-1} after 100 cycles. V_2O_5/rGO composites were formed by wet mixing the electrospun V_2O_5 nanowires (100–200 nm in diameter and µm length) [455]. The V_2O_5/rGO composite with 1 wt% rGO showed the 1st and 60th discharge capacities of 225 and 125 mAh g^{-1}, respectively, at C/5 rate. Recently, Kurc et al. [456] investigated the impact of the addition V_xO_y nanoparticles (50–150 nm) in TiO_2/rGO composite electrode synthesized by solvothermal method. Incorporation of 4.5 wt% V_xO_y in TiO_2/rGO was beneficial in terms of the cell stability. This electrode showed a reversible capacity of 182 mAh g^{-1} at 50 mA g^{-1} current density and 118 mAh g^{-1} at 500 mA g^{-1}. A full cell with $LiFePO_4$//V_xO_y-TiO_2/rGO electrochemical chain showed good cycle ability while providing a capacity of 120 mAh g^{-1}. The cell did not lose significant capacity upon extended cycling. Electrochemical performance of V_2O_5/rGO composites as electrodes for LIBs from the recent literature are summarized in Table 9.

Table 9. Comparison of the V_2O_5/rGO-type materials with preparation methods. Relevant cycle number is given in brackets.

Material	Synthesis	Specific Capacity (mAh g^{-1})	Current Rate (mA g^{-1})	Ref.
V_2O_5/GO/NCM	wet chemistry	125	55	[450]
V_2O_5/rGO	solvothermal solution	122	64C (500)	[448]
V_2O_5/rGO	two-step solvothermal	205	1C (120)	[449]
V_2O_5/GO (2 wt%)	sol-gel	240	1C (200)	[451]
V_2O_5/rGO (3.2%)	hydrothermal	175	20 (100)	[430]
V_2O_5 NSs/rGO	solvothermal	141	600 (160)	[452]
V_2O_5/rGO	solvothermal	102	5700 (200)	[453]
V_2O_5 NRs/rGO	hydrothermal + reflux	140	150 (100)	[457]
V_2O_5/rGO	post-annealing of VO_2/rGO	214	1000 (100)	[425]
V_2O_5/rGO	electrospinning	125	C/5 (60)	[455]
V_xO_y-TiO_2/rGO	solvothermal	180	50 (20)	[456]

Yan et al. [458] reported the fabrication of a crumpled rGO (c-rGO) encapsulated 3D hollow V_2O_5 nano/microspheres using one-step solvothermal process followed by subsequent annealing. The as-prepared c-rGO/V_2O_5 composite containing 5 wt% rGO delivered reversible capacities of 289 and 163 mAh g^{-1} at current densities of 0.1 and 5.0 A g^{-1}, respectively, as well as a capacity retention of about 94% after 200 cycles at 2 A g^{-1} in the potential range 2.0–4.0 V vs. Li$^+$/Li. Wang et al. [459] investigated the V_2O_5 nanobelts/rGO composites as positive electrode for aqueous zinc-ion battery (ZIB). While the commercial V_2O_5 powders show poor cycle stability and low specific capacity of 30 mAh g^{-1} after 200 cycles, V_2O_5/rGO nanocomposites delivered a high specific capacity of 135 mAh g^{-1} after 200 cycles at a current density of 0.1 A g^{-1}. The rate capability test yielded a capacity of 113 mAh g^{-1} when a current density of 1 A g^{-1} was applied. Du et al. [460] developed GO/V_2O_5 composites as cathode materials for rechargeable magnesium batteries via solvothermal synthesis using vanadium oxytriisopropoxide and graphene oxide. The composites attain a high discharge capacity of 178 mAh g^{-1} at 0.2C rate and 140 mAh g^{-1} after 20 cycles in the potential range 1.0–2.8 V. The GO/V_2O_5 composite can host 0.6 Mg ions per formula unit.

The V_3O_7/GO nanocomposites, with the V_3O_7 nanobelts of 12 nm in width and several µm in length were prepared by a hydrothermal method. The electrochemical tests of these electrode in Li cells showed a first discharge capacity of 352 mAh·g^{-1}at the current density of 100 mA·g^{-1} and a good cycling performance with 87% and 91% capacity retention upon 50 cycles at the current density of 400 and 800 mA·g^{-1}, respectively [461].

Numerous reports are related to the V_2O_5/rGO composites applied as electrodes of electrochemical ESCs. Ramadoss et al. reported the fabrication of a V_2O_5/rGO electrode, which displayed a maximum specific capacitance of 250 F g^{-1} at 5 mV s^{-1} scan rate retaining 95% of its initial value after 5000 cycles [462]. A bifunctional composite hydrogel containing rGO nanosheets and V_2O_5 nanobelts (rGO/V_2O_5) was successfully prepared by a hydrothermal method at 180 °C for 12 h with GO and aqueous V_2O_5 precursors as raw materials followed by a freeze-drying process [463]. The rGO/V_2O_5 composite exhibited outstanding performance for ESCs, providing a specific capacitance of ~320 F g^{-1} at a current density of 1 A g^{-1} for V_2O_5 mass loading of 67.3 wt%. Foo et al. [464] eliminated the need for current collectors or additives and reducing resistance (sheet resistance 29.1 Ω sq^{-1}) by constructing V_2O_5/rGO free-standing hybrid electrodes for ESC applications. The effective exfoliation of rGO achieved high areal capacitance of 511 mF cm^{-2} coupled with high mass loadings. An asymmetric flexible supercapacitor based on the rGO/V_2O_5-rGO configuration delivered a low equivalent series resistance (ESR) of 3.36 Ω. Zhang et al. [465] prepared V_2O_5-rGO composites using a two-step reduction method with V_2O_5 nanowires (as long as ~1 mm) as the skeleton and rGO nanosheets as the additive. The product had an electrical conductivity of 1.62 S cm^{-1}, which is higher than that of the pure V_2O_5 nanowire (0.049 S cm^{-1}). Studied as cathode for Li-ion battery, the free-standing V_2O_5/rGO composite showed a reversible specific areal capacity of 885 µAh cm^{-2} at 0.09 mA cm^{-2}. When tested at a high current rate of 0.9 mA cm^2, it gave excellent cycling performance with a retention of ~69% after 1000 cycles. Table 10 summarizes the electrochemical performance of V_2O_5/graphene composites as electrodes for supercapacitors

Table 10. Comparison of the V_2O_5/graphene composites as electrodes for electrochemical supercapacitors (ESCs).

Material	Synthesis	Capacitance (F g^{-1})	Rate (mA g^{-1})	Electrolyte	Ref.
V_2O_5/rGO	solvothermal	537	1000	8 M LiCl	[466]
VO_2/rGO	hydrothermal	225	250	0.5M K_2SO_4	[467]
VO_x NTs/rGO	hydrothermal	210	1000	1M Na_2SO_4	[468]
VO_2 NBs/rGO	hydrothermal	426	1000	0.5M K_2SO_4	[469]
V_2O_5 NWs/rGO	hydrothermal	80	500	1M LiTFSI	[470]
$VO_{x/}$rGO	solvothermal	183	500	0.5M Na_2SO_4	[471]
V_2O_5/rGO	hydrothermal	130	100	1M $LiClO_4$	[464]
V_2O_5/rGO	coprecipitation	484	500	0.5M K_2SO_4	[472]
V_2O_5/rGO	solvothermal	450	500	1M Na_2SO_4	[449]
V_2O_5 NRs/rGO	sol-gel	218	5000	1M Na_2SO_4	[473]

4.7.4. VPO_4-Based Composites

Among the polyanionic anode materials, vanadyl phosphate, VPO_4, is considered as a promising anode material because of the excellent chemical activity of vanadium with a relatively high theoretical specific capacity (550 mAh g^{-1}) [474]. The lithiation/delithiation mechanism is a conversion reaction involving three electrons. Combined with rGO, VPO_4 as electrode of both LIBs and ESCs has shown significant improvement in their electrochemical performances [475,476]. Lu et al. [476] developed a 3D hydrangea-like vanadium phosphate microspheres embedded in the interlaced multiporous rGO scaffold (VPO_4/rGO) to form self-supporting porous anodes for lithium-ion batteries. The VPO_4/rGO samples were synthesized by in-situ solvothermal reduction method using a mixture of GO and $VOPO_4 \cdot 2H_2O$ acting as reductant and dispersant followed by a hydrothermal treatment at 180 °C for 24 h. The porous microspheres with 80% VPO_4 had a specific surface area of ~87 m_2 g^{-1} and half pore width of ~35 nm. The as prepared VPO_4/rGO-80% electrode displayed a fast-charging specific capacity of 537 mAh g^{-1} at 0.1 A g^{-1} (weight based on whole electrode), and long-life performance of 318 mAh g^{-1} after 3000 cycles at 2 A g^{-1} (Figure 14). Through differentiating the contribution from pseudocapacitance and diffusion-controlled process, the authors demonstrated that the charge–discharge mechanism was dominated by the pseudocapacitance.

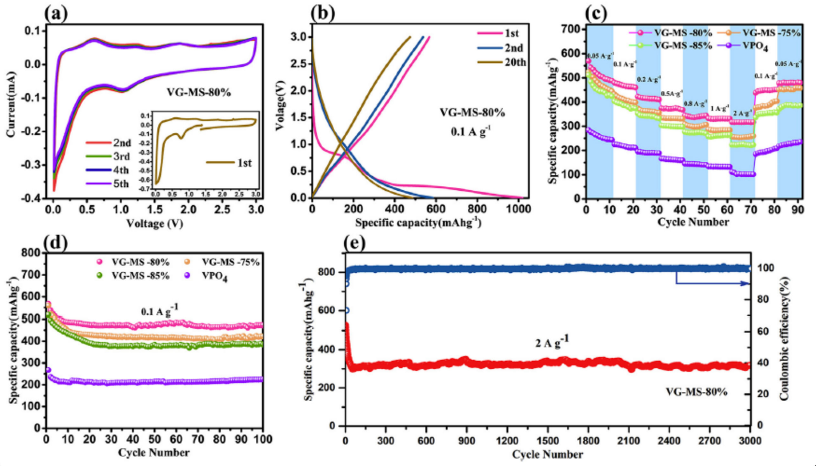

Figure 14. Electrochemical properties of VPO_4/rGO-80% composites. (**a**) Cyclic voltammograms for the first five cycles, (**b**) charge–discharge voltage profiles for selected cycles at a current density of 0.1 A g^{-1}, (**c**) rate, and (**d**) cycling performance of VG-MS-75%, VG-MS-80%, VG-MS-85%, and VPO_4, (**e**) cycling and efficiency performance of VG-MS-80% at 2 A g^{-1}. All the specific capacity values are calculated based on the weight of the composite of VG-MS (also the weight of the electrode). Reproduced with permission from [476]. Copyright 2020 Elsevier.

4.8. Cobalt-Based Oxide Composites

4.8.1. Co_3O_4-Based Composites

Co_3O_4 has attracted extensive interest due to its high specific capacity of 890 mAh g^{-1} (i.e., electrochemical conversion reaction $Co_3O_4 + 8Li^+ + 8e^- \leftrightarrow 3Co + 4Li_2O$ to form lithium oxide and metal nanoparticles). However, similarly to other TM oxides, Co_3O_4 suffers from large volume expansion/contraction and loss of interparticle contact due to electrode pulverization upon lithiation [477].

The most common technique utilized for the synthesis of Co_3O_4/rGO composite is the hydrothermal method, which follows the preparation of a primary solution of GO with the cobalt precursor. For example, Kumar et al. [478] fabricated a ternary Co_3O_4/rGO/CNTs nanocomposite for supercapacitor application using a three-step procedure: (i) Mixture of $Co(NO_3)_2 \cdot 6H_2O$ with a GO/CNTs dispersion and urea as reducing agent for GO with adjustment of the pH at 10 using ammonia, (ii) hydrothermal process at 180 °C for 8 h and (iii) after washing and drying then an annealing treatment at 300 °C in N_2 environment for 3 h yields the final product. Another popular technique of fabrication is the one-pot microwave-assisted synthesis. Typical experiments are carried out in a domestic microwave at a power of 1600 W for 30 min [479].

A rough comparison of early reports indicates that the Co_3O_4/rGO composite displayed superior electrochemical performances. The Co_3O_4/rGO sheet-on-sheet nanocomposite prepared by microwave-assisted synthesis presents a capacity of 931 mAh g^{-1} at a large current rate of 5C (4450 mA g^{-1}) and better cycling behavior with reversible capacity of ~1065 mAh g^{-1} after 30 cycles [480]. Yang et al. [481] have described a self-assembly approach to prepare tailored graphene-encapsulated, mesoporous Co_3O_4 microspheres. The nanocasting method produces a composite with full wrapping by graphene shells, which delivers a first discharge capacity of 1533 mAh g^{-1} and rapidly stabilizes. A high reversible capacity of about 820 mAh g^{-1} was achieved after 35 cycles at a current of 100 A g^{-1}. Wu et al. [482] synthesized the composite of Co_3O_4 nanoparticles (10–30 nm in size) anchored on conducting rGO sheets via a one-step approach. The Co_3O_4/rGO hybrid anode displays a discharge capacity of 935 mAh g^{-1} was obtained after 30 cycles. Zhang et al. [483] also reported the deposition of Co_3O_4 and the exfoliation of graphene sheets in a one-step electrochemical process. The Co_3O_4/rGO composite as an anode material yields a reversible discharge capacity of about 880 mAh g^{-1} for 40 cycles at 0.3C rate.

Using a convenient PVP (polyvinylpyrrolidone)-assisted method under reflux conditions, Pan et al. [484] prepared a Co_3O_4/rGO composite, which consists of uniform Co_3O_4 nanoparticles (~100 nm) tightly enwrapped by rGO in the presence of the PVP surfactant. The Co_3O_4 NPs/rGO/PVP composite exhibits superior Li-battery performance with large discharge capacity of 860 mAh g^{-1} during 120 cycles at 40 mA g^{-1} rate. Mesoporous Co_3O_4 nanosheets (Co_3O_4-NSs) and nitrogen-doped reduced graphene oxide (N-rGO) were prepared through a facile hydrothermal approach, and the N-rGO/Co_3O_4-NSs composite was fabricated using an infiltration procedure. The 2D/2D nanostructured mesoporous N-rGO/Co_3O_4-NSs composite was evaluated in a half-cell as an anode material delivering a reversible capacity of 1305 and 1501 mAh g^{-1} at a current density of 80 mA g^{-1} for the 1st and 50th cycles, respectively [27]. Lou et al. [485] prepared a Co_3O_4/rGO anode material with a specific surface area of 149.5 m^2 g^{-1} composed of ultra-small Co_3O_4 nanoparticles (~12.5 nm in size) anchored on rGO nanosheets. The Co_3O_4/rGO containing ~40 wt% rGO nanocomposite shows excellent electrochemical performances with a high reversible discharge capacity of 830 mAh g^{-1} after 75 cycles at 200 mA g^{-1}, and a reversible capacity of 681 mAh g^{-1} after 30 cycles at 200 mA g^{-1} and 100 consecutive cycles at 500 mA g^{-1}. Rate capability measurements displays reversible specific capacities of about 1153, 961.0, 851, and 736 mAh g^{-1} after each eight cycles at 50, 100, 200, and 500 mA g^{-1}, respectively.

Cho et al. [486] highlighted the enhanced conversion reaction of the Co_3O_4 NFs@rGO composite composed of 1D Co_3O_4 nanofibers (NFs, 150–200 nm in diameter) covered with low content (~3.5 wt%) rGO ultrathin sheets (~3 nm) by electrostatic self-assembly. To ensure efficient graphene wrapping, the surface of the Co_3O_4 NFs was functionalized to amine group poly(allylamine hydrochloride) (PAH). The Co_3O_4 NFs/rGO composite presents a high reversible capacity of 615 mAh g^{-1} and 92% capacity retention after 400 cycles at 4.0 Ag^{-1} and displays excellent rate capability. Kesavan et al. [487] fabricated a nanocomposite anode composed of hollow Co_3O_4 nanospheres (h-Co_3O_4 NSs) combined with CNTs and rGO using a sonication method followed by a hydrothermal treatment. The h-Co_3O_4 NSs (27 nm in size) were prepared by self-assembly process using poly(styrene–b–2-vinylpyridine–b–ethylene oxide) micelle as a soft template and $(NH_4)_2Co(SO_4)_2{\cdot}6H_2O$ as cobalt source. The nanocomposite h-Co_3O_4 NSs/CNT/rGO electrode exhibits higher charge/discharge capacities of ~943 mAh g^{-1} when compared to pristine h-Co_3O_4 NSs-based electrode (~678 mAh g^{-1}) after 50 cycles. Park et al. [488] utilized a one-pot microwave-assisted hydrothermal method for the preparation of Co_3O_4/rGO nanocomposites. The Co_3O_4 nanoparticles (10–30 nm in size) uniformly decorated the surface of rGO sheets, which act as 2D template. The Co_3O_4/rGO hybrid anode containing 79 wt% Co_3O_4 was tested galvanostatically in the voltage range 0.01–3.0 V using a 2032-type coin cell. It delivers a first discharge capacity of 947 mAh g^{-1} at 1 A g^{-1} current rate. The excellent cyclability was observed after 100 cycles at 0.5 A g^{-1} rate, and the specific discharge capacity is still as high as 683 mAh g^{-1}, which is almost the second discharge capacity (685 mAh g^{-1}). The suitability of Co_3O_4/rGO hybrid as cathode material of rechargeable aluminum-ion batteries has been demonstrated by Zhang et al. [489]. The composite was synthesized by a spontaneous self-assembly process using precursor made from the coprecipitation of the Co^{2+} - hexacyanocobaltate (II) metal-organic framework. The self-assembled Co_3O_4/rGO products were further annealed at 500 °C in Ar atmosphere for 2 h. After the initial activation phase, an Co_3O_4/rGO||Al cell retains discharge capacity of 168 mAh g^{-1} and coulombic efficiency of 76% over 500 cycles of charge/discharge.

More recently, Mussa et al. [490] used a microwave irradiation technique to prepare Co_3O_4/rGO/hexagonal boron nitride (h-BN) nanocomposites as anodes for high-temperature LIBs. The addition of h-BN not only enhances the thermal stability but also increases the specific surface area (191 m^2 g^{-1}) of composites. The Co_3O_4/rGO/h-BN electrode cycled at 208 mA g^{-1} in the voltage range 0.5–2.7 V displays a first specific capacity of 758 mAh g^{-1} maintained at 266 mAh g^{-1} after 100 cycles higher than 186 mAh g^{-1} for the Co_3O_4/rGO hybrid.

The use nitrogen-doped rGO (N-rGO) is a promising strategy for the development of anode materials for LIBs with high electrochemical performance [491,492]. Li et al. [492] designed a Co_3O_4/N-rGO composite, in which ultrafine Co_3O_4 nanocrystals (5–10 nm) are homogeneously attached without aggregation to N-rGO sheets by hydrothermal method. In this synthesis, ammonia acts as nitrogen dopant. The charge/discharge cycling performance of the Co_3O_4/N-rGO anode shows a capacity of 882 mAh g^{-1} at the 6th cycle at 400 A g^{-1}, which gradually decreases down 766 mAh g^{-1} at the 50th cycle. Rate capability tests show discharge capacities of 1100, 950, 860, 670, and 460 mAh g^{-1} at different current densities of 100, 200, 400, 1000, and 2000 mA g^{-1}, respectively.

Hierarchically well-developed porous graphene nanofibers comprising N-doped graphitic carbon (NGC)-coated cobalt oxide hollow nanospheres were tested as anodes for high-rate Li-ion batteries [493]. This nanostructured composite delivers a discharge capacity of 823 mAh g^{-1} after 500 cycles at 3.0 A g^{-1} current density with a low decay rate of 0.092% per cycle. The rate capability is also noteworthy as the structure exhibits high discharge capacities of 422 and 222 mAh g^{-1} at current densities of 50 and 100 A g^{-1}, respectively. Co_3O_4/rGO composite powder with the nanobubble-decorated rGO sphere structure was prepared by spray pyrolysis with a reduction process under a mixture of H_2 and Ar gas (i.e., nanoscale Kirkendall diffusion process [494]. Tested as anode for Li-ion battery at the current density of 2 A g^{-1} for 200 cycles before and after the nanoscale Kirkendall diffusion, the Co_3O_4/rGO composite powders show discharge capacities of 932 and 1156 mAh g^{-1}, respectively, with capacity retention of 89% and 99%, respectively, at the second cycle.

4.8.2. CoO-Based Composites

Cobalt monoxide including nanoparticles, nanorods, and mesoporous nanowires have been under prime study because its theoretical capacity of 716 mAh g^{-1} (following the conversion reaction CoO + $2Li^+ + 2e^- \leftrightarrow Co^0 + Li_2O$) and its long cycling stability when combined with rGO [495]. Fu and coworkers [496] elaborated a series of CoO/rGO composites with different proportions via an in-situ hydrothermal method and investigated them as an additive for the nickel-based alkaline secondary battery cathode. The Ni electrode including 5 wt% of CoO/rGO (5:5) delivered a high discharge capacity 208.6 mAh g^{-1} at 10C rate.

Bindumadhavan et al. [497] fabricated a cobalt oxide decorated reduced graphene oxide (CoO/rGO) nanocomposites prepared by simultaneous reduction of GO and Co^{2+} in the presence of $NaBH_4$. The addition of 15 wt% rGO led to a narrow size distribution of ultra-fine CoO NPs. For loading ratios of rGO of 5, 15, 25, and 35 wt%, the BET specific surface area of CoO/rGO increases to 81, 87, 94 and 117 m^2 g^{-1}, respectively. Later, the same group has developed a facile and simple route for the preparation of ultrafine CoO/rGO nanohybrids with tunable particle size and crystallinity. The homogeneous and ultrafine CoO NPs (4.5 nm in size) were intimately attached onto rGO surface after an optimized calcination time of 60 min forming CoO/rGO flakes ~30 nm thick. These CoO/rGO composite anodes delivered a specific capacity of 520 mAh g^{-1} at current rate of 2.0 A g^{-1}, and the capacity was recovered to 900 mAh g^{-1} at 150 mA g^{-1} after 60 cycles [498]. The CoO/rGO composite developed by Wang et al. [499] was synthesized using a hydrothermal process (160 °C, 6 h) of a GO suspension mixed with a $Co(NO_3)_2$ solution followed by an annealing at 500 °C for 2h under nitrogen ambient. The as-fabricated composite anode exhibited a first discharge capacity of 1312 mAh g^{-1} at a current density of 100 mA g^{-1}. The results of long-term cycling demonstrated a capacity of 557 mAh g^{-1} at a high current density of 10 A g^{-1} after 300 cycles.

The CoO-based composite anode proposed by Sun et al. [500] was composed of CoO-Co_3O_4 heterostructure nanoribbons (~50 nm) sandwiched between rGO nanosheets through a solvothermal technique and a sintering process at 350 °C in N_2 atmosphere for 1 h. The CoO-Co_3O_4/rGO composite with a specific surface area of 150 m^2 g^{-1} and average pore size of 4.2 nm delivered a reversible capacity of 994 mAh g^{-1} at a current density of 100 mA g^{-1} after 200 cycles and presented good cyclability of 395 mAh g^{-1} after 500 cycles even at a high charge–discharge rate of 1 A g^{-1}. The rate capability of the CoO-Co_3O_4/rGO anode carried out at 100, 200, 500, 1000, 2000, 5000, and 100 mA g^{-1} after each 10 cycles at each current density was 1210, 1060, 890, 730, 578, 392, and 915 mAh g^{-1}, respectively. Cao et al. [501] assembled a CoO/rGO hybrid for LIBs by using oleic acid as particle shape controller. The composite with 19.wt% carbon had a BET specific surface area of 183.6 m^2 g^{-1} and pore size in the range 5–10 nm. It delivered a highest capacity of 1309 mAh g^{-1} after 100 cycles at 0.1 A g^{-1} current rate. The diffusion coefficient of Li ions in the CoO/rGO network determined from EIS measurements was 4.37 × 10^{-15} cm^2 s^{-1} (Figure 15).

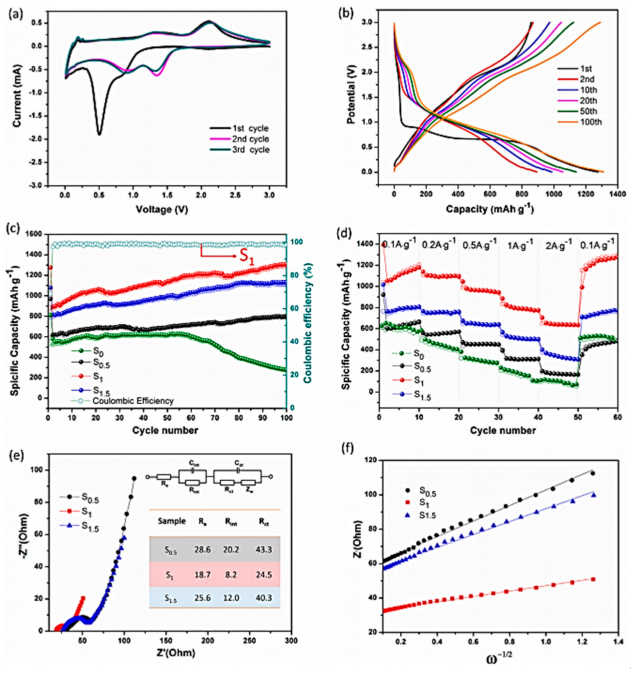

Figure 15. Electrochemical analysis of Co/rGO composites synthesized via hydrothermal route using oleic acid (OA) as particle shape controller (samples are marked as S_x, where x (0, 0.5, 1, 1.5) represented the content of OA in the precursor materials). (**a**) The first three CV curves of S1 electrode at a scan rate of 0.1 mV·s^{-1} from 0.005 V to 3 V. (**b**) The galvanostatic charge/discharge (GCD) profiles of S1-based anode cycled between 0.005 and 3 V at a current of 0.1 A·g^{-1}. (**c**) Cycling performance of S0, S0.5, S1, S1.5 electrodes and corresponding coulombic efficiency of S1 electrode at a specific current of 0.1 A·g^{-1}. (**d**) Rate capability of S0, S0.5, S1, and S1.5 electrodes. (**e**) Nyquist plots of S0.5, S1, and S1.5 electrodes after 10 cycles. (Inset is the equivalent circuit model used to simulate the spectra and the corresponding impedance parameters). (**f**) The relationship between Z′ and $\omega^{-1/2}$ at low frequencies for S0.5, S1, and S1.5 electrodes. Reproduced with permission from [501]. Copyright 2018 Elsevier.

Leng et al. [502] reported the synthesis of rGO/CoO nanowires (diameter of 10–20 nm and length of several μm) mutually supporting porous structure using an in situ method by annealing self-assembled GO/$Co(CO_3)_{0.5}(OH)\cdot 0.11H_2O$ nanowires in N_2 environment. The as-prepared CoO/rGO anode material (BET specific surface area of 66.1 m^2 g^{-1}) presented a high reversible capacity of 994 mAh g^{-1} even after 100 cycles with 96.3% capacity retention of the first discharge capacity, and superior rate capability (262 mAh g^{-1} 10 A g^{-1}). This electrode sustained a capacity of 520 mAh g^{-1} at a current rate of 3 A g^{-1} after 750 cycles. More recently, Yin et al. [503] designed a new CoO/Co_2B/rGO nanocomposite anode with large capacitive contribution for high-efficiency and durable lithium storage. The composite was synthesized by a combination of precipitation method and pyrolysis. Initial discharge/charge capacities of 889/669 mAh g^{-1} with a high ICE of 75.28% at 0.1C rate are delivered for the CoO/Co_2B/rGO composite with primary particles of 20–60 nm. The proportion of the capacitive contribution deduced from cyclic voltammetry is calculated to be 89.2%. Table 11 summarizes the electrochemical performance of CoO/rGO composites as anodes for LIBs from the recent literature.

Table 11. Electrochemical performance of Co/rGO composite anode materials. Relevant cycle number is given in brackets.

Material	Synthesis	Specific Capacity (mAh g^{-1})	Current Density (mA g^{-1})	Ref.
Co hollow cube/rGO	sacrificial-template + annealing	1170	150 (60)	[504]
m-CoO NRs/rGO	hydrothermal + calcination	960	100 (50)	[505]
CoO/3D rGO hydrogel	hydrothermal + calcination	962	200 (80)	[506]
Co/rGO	simultaneous reduction	690	600 (60)	[497]
CoO/rGO flakes	simultaneous reduction	900	150 (60)	[498]
CoO-Co_3O_4/rGO	solvothermal + sintering	994	100 (200)	[500]
CoO/Co_2B/rGO	precipitation + pyrolysis	276	10C	[503]
CoO/rGO	one-pot in situ solution	577	100 (435)	[507]
CoO/CuO/rGO	hydrothermal	1364	200 (100)	[508]
CoO/rGO	hydrothermal + calcination	557	10000 (300)	[499]
CoO/rGO	hydrothermal (oleic acid)	1039	100 (100)	[501]
CoO/rGO NWs	in situ self-assembly	520	3000 (750)	[502]

4.9. Copper-Based Oxide Composites

Song et al. [509] manufactured a three-dimensional CuO/GO aerogel cylindrical composite as a super-capacitor electrode material through a one-step self-assembly hydrothermal procedure at 180 °C for 8 h using $Cu(NO_3)_2$ as Cu precursor and citric acid as reducing agent. The as-prepared product exhibited specific capacitance of 211 F g^{-1} at current density of 1 A g^{-1}. Liu et al. [510] reported the synthesis of sponge-like porous GO/CNTs/CuO hybrid aerogel as anode material for lithium-ion batteries. The samples were prepared as a flocculent suspension obtained by adding a GO suspension and oxidized water-soluble CNTs treated with nitric acid in a CuO colloidal solution followed by a hydrothermal reduction at 180 °C for 10 h. The galvanostatic charge–discharge tests carried out in the voltage range of 0.01–3.0 V under a constant current density of 67 mA g^{-1} (0.1 C) demonstrated the excellent cyclic retention of the binder-free GO/CNTs/CuO hybrid with the specific capacity of 636.9 mAh g^{-1} after 80 cycles. Zhu and coworkers [511] designed three-dimensional CuO/PANI/rGO ternary hierarchical architectures (where PANI is polyaniline) using an in-situ polymerization method combined with hydrothermal route at 180 °C for 12 h. The CuO/PANI/rGO hybrid was reversibly cycled as electrode for supercapacitor in a high voltage region up to 1.2 V with 97.4% specific capacitance retention after 10,000 cycles. It exhibited a maximum specific capacitance of 634 F g^{-1} and a high energy density of 126.8 Wh kg^{-1} with a power density of 114.2 kW kg^{-1} at a current density of 1.0 A g^{-1}. Zhao et al. [512] reported the synthesis of CuO/GO composites in the water–N,N-dimethylformamide without an extra reducing agent, which provided mesoporous sample with high BET surface area of 235 m^2 g^{-1}. Zhu et al. [513] reported the synthesis of CuO/GO hybrids by aligning CuO nanoparticles onto GO sheets in the water–isopropanol media. The authors suggested that the formation mechanism of these CuO/GO nanocomposites occurred as intercalation and adsorption of Cu^{2+} ions onto the GO sheets, followed by the nucleation and growth of the CuO crystallites. The CuO/rGO nanocomposite anode was prepared via microwave-assisted method within short reaction times (<20 min) and subsequent sintering at 500 °C for 5 h by Rai et al. [514]. The first discharge capacity of the nanocomposite (40–65 nm particle size and specific surface area of 37.7 $m^2 g^{-1}$) with 10 wt% graphene was reported at 1043 mAh g^{-1} with reversible capacity retention of 516 mAh g^{-1} after 45 cycles at 0.1 mA cm^{-2} over the potential range of 0.01–3.0 V vs. Li^+/Li. These results compared well with the theoretical specific capacity of 670 mAh g^{-1} based on the electrode conversion reaction, i.e., $CuO + 2Li^+ + 2e^- \leftrightarrow Cu^0 + Li_2O$. Xu and coworkers [515] reported the fabrication of core–shell structured Cu_2O@GO composite consisting of Cu_2O microspheres encapsulated by GO nanosheets. These anode materials delivered a reversible capacity of 458 mAh g^{-1} at a current density of 100 mA g^{-1} after 50 cycles and a reversible capacity of 240 mAh g^{-1} after 200 cycles even at a high charge–discharge rate cycling of 1 A g^{-1}. The rate capability evaluated by the ratio of capacity at 100/1000 mA g^{-1} was 49% for the Cu_2O@GO hybrid, against 25% for a bare Cu_2O anode.

In 2016, Sun et al. [516] reported the synthesis of Cu_2O-CuO-RGO composites as anode materials by a self-assembly solvothermal method in a water-ethanol mixture, which delivered a reversible capacity of 842 mAh g^{-1} after 80 cycles at a current density of 100 mA g^{-1}. The capacity measured every 10 cycles at current densities of 100, 200, 500, 1000, 2000, 5000, and 100 mA g^{-1} were 840, 723, 511, 402, 336, 224, and 703 mAh g^{-1}, respectively. These greatly improved electrochemical behaviors are closely related to the sandwich-like and mesoporous structure of the composite, which had a high specific surface area of 132.1 $m^2 g^{-1}$ and typical pore sizes in a wide range (2.5–20 nm). Sheikhzadeh et al. [517] fabricated nanocomposite foam layer of CuO/GO by the deposition of GO particles on electroplated CuO foam layers through electrophoretic deposition providing samples with BET surface area of 99.2 $m^2 g^{-1}$ and average pore diameter of 29 nm. By embedding GO particles on CuO during 7 min, a specific capacitance of 334 F g^{-1} was obtained. A 3D Ni-Cu foam/rGO composite was prepared by the electrochemical deposition of rGO nanosheets on Ni-Cu foam (0 to −1.5 V vs. SCD) and the subsequent reduction by cyclic voltammetry under different sweep rates in the range of 10–100 mV s^{-1} [518]. The Ni-Cu foam/rGO hybrid deposited electrochemically at the sweep rate of 50 mV s^{-1} presented the specific capacitance of 1380 F g^{-1} at a discharge rate of 2 A g^{-1} and an energy density of 30 Wh kg^{-1} at a power density of 10.2 kW kg^{-1}.

4.10. Nickel-Based Oxide Composites

Nickel monoxide has received widespread attention because of its high theoretical specific capacity of 718 mAh g^{-1} for 2 Li^+ uptake from the conversion reaction $NiO + 2Li^+ + 2e^- \leftrightarrow Ni^0 + Li_2O$. In addition, it is a low-cost, safe, and environmentally friendly compound. Several synthesis techniques are used to fabricated NiO/rGO composites including hydrothermal method [519], thermal decomposition [520], solvothermal [521], in situ ultrasonic agitation [522,523], and heterogeneous assembly approach with subsequent in-situ thermal reduction [524].

Liu et al. reported the formation of hierarchical NiO/rGO nanohybrids with tunable microstructures through the thermal decomposition of $Ni(OH)_2$/rGO formed by the electrostatic attraction between exfoliated $Ni(OH)_2$ and GO nanosheets [520]. Ren et al. [525] reported the hydrothermal synthesis and lithium storage performance of binary NiO NWs/rGO and ternary NiO/rGO/PPy hybrids as anode materials for LIBs. The ternary composite was prepared by chemical oxidation polymerization of pyrrole monomer with a template of the binary hybrid. The NiO/rGO/PPy hybrid delivered the first discharge capacity of 1080 mAh g^{-1} at 0.2C rate and the first charge capacity reached 830 mAh g^{-1}. After 40 cycles, the discharge capacity is maintained at 499 mAh g^{-1}. Li et coworkers [519] designed a hybrid NiO/rGO structure with flower-like NiO wrapped homogeneously by rGO sheets via a facile and controllable hydrothermal treatment of the suspension formed with $Ni(NO_3)_2{\cdot}6H_2O$, $CO(NH_2)_2$, NH_4F, and GO and subsequent annealing at 400 °C for 2 h in Ar ambient. The NiO/RGO nanocomposites exhibited a reversible specific capacity of 702 mAh g^{-1} after 100 cycles at a current density of 100 mA g^{-1}. NiO-ZnO/rGO composites with NiO-ZnO nanoflakes were obtained by thermal annealing of sonically mixed Ni $(OH)_2$-Zn $(OH)_2$/rGO precursor [526]. The as-prepared porous anode material, which exhibited a specific surface area of 110.49 m^2 g^{-1} and pore size distribution in the range 30–80 nm, delivered a reversible capacity of 1017 mAh g^{-1} at a current density of 100 mA g^{-1} after 200 cycles and a specific capacity of 458 mAh g^{-1} at 500 mA g^{-1} even after 400 cycles. A specific capacity of 185 mAh g^{-1} was reached at a current density of 2000 mA g^{-1} (Figure 16). The double-layer $NiFe_2O_4$@NiO-hollow-nanosphere (mean size of 14 nm) decorated rGO composite was prepared by spray pyrolysis with nanoscale Kirkendall diffusion. The first discharge capacities of the nanosphere-decorated rGO composite powders with filled $NiFe_2O_4$/NiO and hollow $NiFe_2O_4$@NiO, at a current density of 1 A g^{-1}, are 1168 and 1319 mAh g^{-1}, respectively, which decrease to 597 and 951 mAh g^{-1}, respectively, after 100 cycles. For repeated lithium-ion discharge at the high current density of 4 A g^{-1} for the 400th cycle, a capacity of 789 mA h g^{-1} is delivered by the $NiFe_2O_4$@NiO/rGO hybrid [527].

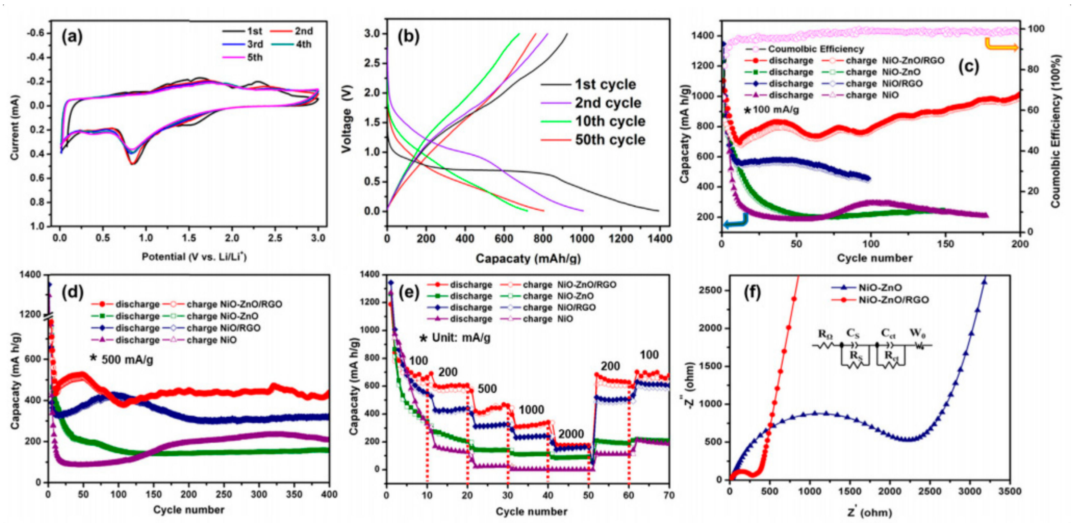

Figure 16. Electrochemical analysis of the NiO-ZnO/RGO composite. (**a**) CV curves at a scan rate of 0.1 mV s^{-1}. (**b**) GCD profiles at a current density of 100 mA g^{-1}. (**c**,**d**) Comparison of cycling performance of NiO, NiO/ZnO, NiO/RGO, and NiO-ZnO/RGO composite at current densities of 100 and 500 mA g^{-1}, respectively. (**e**) Rate capability of the four samples at various current densities. (**f**) Nyquist plots of NiO-ZnO and NiO-ZnO/RGO fresh electrodes at 3.0 V vs. Li^+/Li. Reproduced with permission from [526]. Copyright 2018 Elsevier.

Recently, Tian et al. [521] used metal organic frameworks as NiO precursor for the fabrication of NiO/rGO anode, which provided a modest specific capacity of 440 mAh g^{-1} at 1C rate after 200 cycles. In situ ultrasonic agitation method followed by heat calcination in N_2 atmosphere was carried out for the synthesis of NiO nanoflakes/rGO hybrid, which delivered reversible capacity of 825 mAh g^{-1} after 50 cycles at 100 mA g^{-1}, higher than that of the pure NiO flakes (197 mAh g^{-1}) [518]. Ma and coworkers [523] studied the lithium storage properties of NiO/rGO composites derived from different degrees of GO through an ultrasonic agitation technique. The reversible capacity of these anode materials increased gradually to 1046 mAh g^{-1} and then declined to 956 mAh g^{-1} after 50 cycles at 100 mA g^{-1} current rate. Another Ni-based complex with spinel structure was optimized by Li et al. [528], namely the $NiFe_2O_4$/rGO composite, which was fabricated via a hydrothermal-annealing procedure. The $NiFe_2O_4$/rGO with $NiFe_2O_4$ nanoparticles 20 nm diameter retained a specific capacity of 1105 mAh g^{-1} at a current density of 100 mA g^{-1} over 50 cycles.

5. Anode Materials for Na-Ion Batteries

To obtain anodes with high performances, it is important to exploit the entire graphene layer—which provides favorable sites for energy storage—and to construct the overall conductivity of the graphene networks. In this regard, CNTs can bridge the vertical defects for electron transfer in the graphene layers and increase the distance between graphene sheets. Therefore, when CNTs and graphene are combined with transition-metal chalcogenides (TMCs), synergistic effects on the anodes are expected by the bridging graphene and the suppression of the restacking of graphene sheets during repeated charge and discharge processes. Golden bristlegrass-like unique nanostructures comprising rGO matrixed nanofibers entangled with bamboo-like N-doped CNTs containing $CoSe_2$ nanocrystals at each node (N-CNT/rGO/$CoSe_2$) are designed as anodes for high-rate sodium-ion batteries (SIBs). During a simple etching process, the defects in the N-CNTs allow the complete phase conversion of Co into $CoSe_2$ through the efficient penetration of H_2Se gas inside the CNT walls. The N-CNT/rGO/$CoSe_2$ hybrid, tested as anode material for sodium-ion batteries (SIBs), delivers a discharge capacity of 264 mAh g^{-1} after 10,000 cycles at a high current density of 10 A g^{-1}, and the capacity retention of 89% at the 100th cycle. The rate capability tests show discharge capacities of 395, 263, and 151 mAh g^{-1} at 1, 10, and 20 A g^{-1} current densities, respectively [529].

Mesoporous WSe_2/rGO composites as anode materials for SIBs were prepared by spray pyrolysis and subsequent selenization. The composite particles exhibit both well-dispersed rGO nanosheets and well-faceted WSe_2 nanocrystals with plenty of folded edges. The WSe_2/rGO composite and bare WSe_2 deliver discharge capacities of the 238 and 36 mAh g^{-1}, respectively, for the 100th cycle at a current density of 0.5 A g^{-1}. The WSe_2/rGO composite shows much lower onset potential and larger current density (36.5 mA cm^{-2} at η = 300 mV) than those of the bare WSe_2 particles (0.61 mA cm^{-2} at η = 300 mV) [530]. Through the treatment of Fe_3O_4/rGO powders under H_2Te gas, the $FeTe_2$/rGO hybrid powders were prepared via spray pyrolysis. Electrochemically tested as the anode materials for sodium-ion batteries (SIBs), the $FeTe_2$/rGO composite containing 5 wt% rGO delivered discharge capacities of 493 and 293 mAh g^{-1} for the 1st and 80th cycles, respectively. The Na-ion storage mechanism for $FeTe_2$ in SIBs is described by $FeTe_2 + 4Na^+ + 4e^- \leftrightarrow Fe + 2Na_2Te$ (i.e., the discharge process forms metallic Fe nanocrystals and Na_2Te by a conversion reaction) [531]. Hybrid of graphene-wrapped $NiSe_2$/C porous nanofibers ($NiSe_2$/rGO-C) were prepared via electrospinning and a subsequent selenization process with optimum amount of amorphous carbon obtained from the polystyrene to polyacrylonitrile ratio of 1:4. The electrochemical tests in sodium cell at a current density of 200 mA g^{-1} show initial discharge capacities of the $NiSe_2$-rGO-C composite (nanofibers of 27 nm) and bare $NiSe_2$ nanofibers of 717 and 755 mAh g^{-1}, respectively, which decrease to 468 and 35 mAh g^{-1} after 100 cycles [532]. A 1D nanohybrid comprised of conductive graphitic carbon (GC)-coated hollow $FeSe_2$ nanospheres decorating reduced graphene oxide (rGO) nanofiber ($FeSe_2$@GC–rGO) was designed as an efficient anode material for SIBs [533]. The hollow nanosphere $FeSe_2$@GC–rGO hybrid nanofibers deliver a discharge capacity of 412 mAh g^{-1} at a current density of 1 A g^{-1} for the 150th cycle bare, which is much higher than 63 mAh g^{-1} for $FeSe_2$ nanofibers. Even at high current density of 10 A g^{-1}, a discharge capacity of 352 mAh g^{-1} was achieved, which arose from the synergetic effects of the $FeSe_2$ hollow morphology and highly conductive rGO matrix. $FeSe_x$/rGO composite, in which hollow $FeSe_x$ nanoparticles are uniformly distributed throughout the rGO matrix, was prepared by spray pyrolysis applying the nanoscale Kirkendall diffusion process. The powders had mixed crystal structures of FeSe and $FeSe_2$ phases. The $FeSe_x$/rGO composite has superior sodium-ion storage properties compared to those of the Fe_2O_3/rGO hybrid with similar morphological characteristics. The discharge capacities of the $FeSe_x$/rGO and Fe_2O_3/rGO composites deliver discharge capacities of 434 and 174 mAh g^{-1}, respectively, after 200 cycles at 0.3 A g^{-1} current rate. The $FeSe_x$/rGO hybrid had a high discharge capacity of 311 mAh g^{-1} for the 1000th cycle at a high current density of 1 A g^{-1} [534].

6. Concluding Remarks

In this review, attention was focused on advanced anode composite materials showing efforts currently made towards the technological development of nanostructured electrodes. For the sake of comparison and discussion, the best electrochemical properties obtained with the components have been reported. The advantages and disadvantages of a series of anode materials are highlighted.

The constant progress experienced these last five years evidenced here demonstrates that the rGO-based composites are good candidates as anode materials for rechargeable batteries providing high specific capacity that allows high energy density. They compete with the conventional graphite anodes in terms of rate capability, cycle ability, and safety. Owing to their very good mechanical properties in addition to their good electrical conductivity, remarkable improvement of the electrochemical properties of the anodes are observed with amounts of rGO as small as 1–5 wt%. For mobile applications, such as batteries for EVs, and for static utilization, to buffer the intermittence problem and integration of the production of wind and solar plants to the grid energy storage, the rGO-based hybrids are efficient to improve the structural stability of the electrochemically active materials.

The choice of rGO instead of graphene, which exhibits superior electrical conductivity, is guided by its great hydrophylic behavior and easy deposition on any surface with any method. The simple and fast preparation of rGO by reduction of GO suggest its low-cost and scalable production. Chemical reduction of GO can be eco-friendly achieved using reducing mild agents derived from natural fruits or vegetables. In addition, the oxygen functionalities anchored on the surface of rGO render ability to functionalize graphene with desirable properties and engineer them into diverse morphologies. In contrast, the preparation of graphene without defects is not trivial and is costly in terms of mass production (one needs a CVD system and carbon precursor gases (i.e., CH_4). Actually, mass production remains a bottleneck for the production of high-quality graphene derivatives. The reduction of GO to rGO is thus considered as the most promising route for mass production in the near future, sustained by many applications, not only in the framework of energy storage, but also for biosensors, organic solar cells, actuators, and touch panels [535]. In addition, the performance of Si@graphene and Si @rGO anodes reported in this review for comparison do not evidence a clear advantage to graphene. Interestingly, a more detailed comparison between graphene and rGO-based nanoplatforms on electrochromic switching kinetics show that improved electrochromic switching kinetics is observed on reduced graphene oxide in comparison to the pristine graphene sheets, possibly due to the more heterogeneous electron transfer in graphene [536]. This phenomenon might also explain the remarkable results obtained with rGO-supported materials as anodes for the LIBs.

Owing to their excellent electrochemical performance, composites formed with a single element (silicon, germanium, tin) or with metal oxides MO_x with M = Si, Ti, Mo, Mn, Co, Ni, Cu, etc., have been the most studied hybrid anodes, which can deliver high specific capacity (at least twice the graphite value of 372 mAh g^{-1}). However, anode materials that are electrochemically active by conversion reaction suffered for a long time from the huge variation of volume during cycling. The superior performance of composite in batteries originates from the addition of reduced graphene oxide and their architecture (i.e., from 1D to 3D), which boost the reaction kinetics and electrode stability. The introduction of rGO facilitates the continuous and rapid electron transport and prevent the collapse of nanostructures and aggregation of the active materials. In addition, the strategies adopted in the design of nanocomposites are effective methods to mitigate the large volume changes and low electrical conductivities often met in the bare anodes.

Herewith, we have given many examples according to which such electrodes are better performing. For each composite, we have identified, as possible as it was, the electrochemical properties in relation with its morphology (i.e., particle size, specific surface area, porosity, etc.). Alloying materials such as Si, Ge, SiO_x, and SnO_2 and compounds based on conversion reaction MO_x can provide much larger capacities, and energy densities than the Ti-O oxides based on insertion reaction (i.e., TiO_2, Li_3TiO_4, $Li_4Ti_5O_{12}$). Si, SnO_2, and Mn-based oxides are the most promising elements of this family, while germanium is expensive and not abundant in nature. The big challenge of such nanostructured composite anodes is now the cost, and a scalable production. With the composites of rGO with metal oxides being presently prepared only at the laboratory scale, hopefully the recent results suggest that the one-pot in-situ hydrothermal process is a viable method for the large-scale production for battery electrodes. Today, this technology has the capability to fabricate many composites, which can deliver a capacity superior to 500 mAh g^{-1} and even more for thousands of cycles. Therefore, the rGO holds great promise for use as composite element in electrode for advanced rechargeable batteries such as lithium-sulfur batteries, lithium-air batteries, aluminum-ion batteries, etc. Undoubtedly, the future of rGO-based composites as anode materials for energy storage devices remains very promising and exciting.

Author Contributions: Conceptualization, C.M.J. and S.S.I.; investigation, P.S., A.A.; writing—original draft preparation, C.M.J.; writing—review and editing, A.M. All authors have read and agreed to the published version of the manuscript.

Funding: This research received no external funding.

Conflicts of Interest: The authors declare no conflict of interest.

References

1. Zaghib, K.; Mauger, A.; Julien, C. Rechargeable lithium batteries for energy storage in smart grids. *Recharg. Lithium Batter.* **2015**, *81*, 319–351.
2. Mauger, A.; Armand, M.; Julien, C.M.; Zaghib, K. Challenges and issues facing lithium metal for solid-state rechargeable batteries. *J. Power Sources* **2017**, *353*, 333–342. [CrossRef]
3. Reddy, M.V.; Rao, G.V.S.; Chowdari, B.V.R. Metal oxides and oxysalts as anode materials for Li ion batteries. *Chem. Rev.* **2013**, *113*, 5364–5457. [CrossRef] [PubMed]
4. Ji, L.; Lin, Z.; Alcoutlabi, M.; Zhang, X. Recent developments in nanostructured anode materials for rechargeable lithium-ion batteries. *Energy Environ. Sci.* **2011**, *4*, 2682–2699. [CrossRef]
5. Zhang, W.-J. A review of the electrochemical performance of alloy anodes for lithium-ion batteries. *J. Power Sources* **2011**, *196*, 13–24. [CrossRef]
6. Goriparti, S.; Miele, E.; De Angelis, F.; Di Fabrizio, E.; Zaccaria, R.P.; Capiglia, C. Review on recent progress of nanostructured anode materials for Li-ion batteries. *J. Power Sources* **2014**, *257*, 421–443. [CrossRef]
7. Hassoun, J.; Scrosati, B. Review—Advances in anode and electrolyte materials for the progress of lithium-ion and beyond lithium-ion batteries. *J. Electrochem. Soc.* **2015**, *162*, A2582–A2588. [CrossRef]
8. Lu, J.; Chen, Z.; Pan, F.; Cui, Y.; Amine, K. High-performance anode materials for rechargeable lithium-ion batteries. *Electrochem. Energy Rev.* **2018**, *1*, 35–53. [CrossRef]
9. Yang, S.; Feng, X.; Ivanovici, S.; Müllen, K. Fabrication of graphene-encapsulated oxide nanoparticles: Towards high-performance anode materials for lithium storage. *Angew. Chem. Int. Ed.* **2010**, *49*, 8408–8411. [CrossRef]
10. Sun, W.; Wang, Y. Graphene-based nanocomposite anodes for lithium-ion batteries. *Nanoscale* **2014**, *6*, 11528–11552. [CrossRef]
11. Mauger, A.; Xie, H.; Julien, C.M. Composite anodes for lithium-ion batteries: Status and trends. *AIMS Mater. Sci.* **2016**, *3*, 1054–1106. [CrossRef]
12. Novoselov, K.S.; Geim, A.K.; Morozov, S.V.; Jiang, D.; Zhang, Y.; Dubonos, S.V.; Grigorieva, I.V.; Firsov, A.A. Electric field effect in atomically thin carbon films. *Science* **2004**, *306*, 666–669. [CrossRef]
13. Geim, A.K.; Novoselov, K.S. The rise of graphene. *Nat. Mater.* **2007**, *6*, 183–191. [CrossRef] [PubMed]
14. Lee, C.; Wei, X.; Kysar, J.W.; Hone, J. Measurement of the elastic properties and intrinsic strength of monolayer graphene. *Science* **2008**, *321*, 385–388. [CrossRef]
15. Mahmood, N.; Zhang, C.; Yin, H.; Hou, Y. Graphene-based nanocomposites for energy storage and conversion in lithium batteries, supercapacitors and fuel cells. *J. Mater. Chem. A* **2014**, *2*, 15–32. [CrossRef]
16. Han, S.; Wang, J.; Li, S.; Wu, D.; Feng, X. Graphene aerogel supported $Fe_5(PO_4)_4(OH)_3{\cdot}2H_2O$ microspheres as high performance cathode for lithium ion batteries. *J. Mater. Chem. A* **2014**, *2*, 6174. [CrossRef]
17. Li, F.; Jiang, X.; Zhao, J.; Zhang, S. Graphene oxide: A promising nanomaterial for energy and environmental applications. *Nano Energy* **2015**, *16*, 488–515. [CrossRef]
18. Zhu, J.; Yang, D.; Yin, Z.; Yan, Q.; Zhang, H. Graphene and graphene-based materials for energy storage applications. *Small* **2014**, *10*, 3480–3498. [CrossRef]

19. Javed, K.; Oolo, M.; Savest, N.; Krumme, A. A review on graphene-based electrospun conductive nanofibers, supercapacitors, anodes and cathodes for lithium-ion batteries. *Crit. Rev. Solid State Mater. Sci.* **2019**, *44*, 427–443. [CrossRef]
20. Chen, D.; Feng, H.; Li, J. Graphene oxide: Preparation, functionalization and electrochemical applications. *Chem. Rev.* **2012**, *112*, 6027–6053. [CrossRef]
21. Kuila, T.; Mishra, A.K.; Khanra, P.; Kim, N.H.; Lee, J.H. Recent advances in the efficient reduction of graphene oxide and its application as energy storage electrode materials. *Nanoscale* **2012**, *5*, 52–71. [CrossRef] [PubMed]
22. Li, K.; Shua, F.; Guo, X.; Xue, D. High performance porous MnO@C composite anode materials for lithium-ion batteries. *Electrochim. Acta* **2016**, *188*, 793–800. [CrossRef]
23. Gao, F.; Qin, S.-H.; Zang, Y.-H.; Gu, J.-F.; Qu, J. Highly efficient formation of Mn_3O_4-graphene oxide hybrid aerogels for use as the cathode material of high performance lithium ion batteries. *New Carbon Mater.* **2020**, *35*, 121–130. [CrossRef]
24. Wang, X.; Zhou, X.; Yao, K.; Zhang, J.; Liu, Z. A SnO_2/graphene composite as a high stability electrode for lithium ion batteries. *Carbon* **2011**, *49*, 133–139. [CrossRef]
25. Deng, Y.; Fang, C.; Chen, G. The developments of SnO_2/graphene nanocomposites as anode materials for high performance lithium ion batteries: A review. *J. Power Sources* **2016**, *304*, 81–101. [CrossRef]
26. Sun, Y.; Hu, X.; Luo, W.; Huang, Y. Self-assembled hierarchical MoO_2/graphene nanoarchitectures and their application as a high-performance anode material for lithium-ion batteries. *ACS Nano* **2011**, *5*, 7100–7107. [CrossRef] [PubMed]
27. Sennu, P.; Kim, H.S.; An, J.Y.; Aravindan, V.; Lee, Y.-S. Synthesis of 2D/2D structured mesoporous Co_3O_4 nanosheet/N-doped reduced graphene oxide composites as a highly stable negative electrode for lithium battery applications. *Chem. Asian J.* **2015**, *10*, 1776–1783. [CrossRef]
28. Li, X.; Huang, X.; Liu, D.; Wang, X.; Song, S.; Zhou, L.; Zhang, H. Synthesis of 3D hierarchical Fe_3O_4/graphene composites with high lithium storage capacity and for controlled drug delivery. *J. Phys. Chem. C* **2011**, *115*, 21567–21573. [CrossRef]
29. Wang, R.; Xu, C.; Du, M.; Sun, J.; Gao, L.; Zhang, P.; Yao, H.; Lin, C. Solvothermal-induced self-assembly of Fe_2O_3/GS aerogels for high Li-storage and excellent stability. *Small* **2014**, *10*, 2260–2269. [CrossRef]
30. Wu, P.; Wang, H.; Tanga, Y.; Zhou, Y.; Lu, T. Three-dimensional interconnected network of graphene-wrapped porous silicon spheres: In situ magnesiothermic-reduction synthesis and enhanced lithium-storage capabilities. *ACS Appl. Mater. Interfaces* **2014**, *6*, 3546–3552. [CrossRef]
31. Ren, J.-G.; Wu, Q.-H.; Tang, H.; Hong, G.; Zhang, W.; Lee, S.-T. Germanium–graphene composite anode for high-energy lithium batteries with long cycle life. *J. Mater. Chem. A* **2012**, *1*, 1821–1826. [CrossRef]
32. Chockla, A.M.; Panthani, M.G.; Holmberg, V.C.; Hessel, C.M.; Reid, D.K.; Bogart, T.D.; Harris, J.T.; Mullins, C.B.; Korgel, B.A. Electrochemical lithiation of graphene-supported silicon and germanium for rechargeable batteries. *J. Phys. Chem. C* **2012**, *116*, 11917–11923. [CrossRef]
33. Yue, W.; Yang, S.; Liu, Y.; Yang, X. A facile synthesis of mesoporous graphene-tin composites as high-performance anodes for lithium-ion batteries. *Mater. Res. Bull.* **2013**, *48*, 1575–1580. [CrossRef]
34. Wu, Z.-S.; Zhou, G.; Yin, L.-C.; Ren, W.; Li, F.; Cheng, H.-M. Graphene/metal oxide composite electrode materials for energy storage. *Nano Energy* **2012**, *1*, 107–131. [CrossRef]
35. Jana, A.; Scheer, E.; Polarz, S. Synthesis of graphene–transition metal oxide hybrid nanoparticles and their application in various fields. *Beilstein J. Nanotechnol.* **2017**, *8*, 688–714. [CrossRef]
36. Ke, Q.; Wang, J. Graphene-based materials for supercapacitor electrodes—A review. *J. Materiomics* **2016**, *2*, 37–54. [CrossRef]
37. Chee, W.K.; Lim, H.N.; Zainal, Z.; Huang, N.M.; Harrison, I.; Andou, Y. Flexible graphene-based supercapacitors: A review. *J. Phys. Chem. C* **2016**, *120*, 4153–4172. [CrossRef]
38. Park, S.; Ruoff, R.S. Chemical methods for the production of graphenes. *Nat. Nanotechnol.* **2009**, *4*, 217–224. [CrossRef]
39. Brodie, B.C. Sur le poids atomique du graphite. *Ann. Chem. Phys.* **1860**, *59*, 466–472.
40. Becerril, H.A.; Mao, J.; Liu, Z.; Stoltenberg, R.M.; Bao, Z.; Chen, Y. Evaluation of solution-processed reduced graphene oxide films as transparent conductors. *ACS Nano* **2008**, *2*, 463–470. [CrossRef]
41. Hummers, W.S.; Offeman, R.E. Preparation of graphitic oxide. *J. Am. Chem. Soc.* **1958**, *80*, 1339. [CrossRef]

42. Qiu, X.; Liu, Y.; Wang, L.; Fan, L.-Z. Reverse microemulsion synthesis of nickel-cobalt hexacyanoferrate/reduced graphene oxide nanocomposites for high-performance supercapacitors and sodium ion batteries. *Appl. Surf. Sci.* **2018**, *434*, 1285–1292. [CrossRef]
43. Wang, M.-S.; Song, W.-L.; Fan, L.-Z. Three-dimensional interconnected network of graphene-wrapped silicon/carbon nanofiber hybrids for binder-free anodes in lithium-ion batteries. *ChemElectroChem* **2015**, *2*, 1699–1706. [CrossRef]
44. Si, Y.; Samulski, E.T. Synthesis of water soluble graphene. *Nano Lett.* **2008**, *8*, 1679–1682. [CrossRef]
45. Rao, S.; Upadhyay, J.; Polychronopoulou, K.; Umer, R.; Das, R. Reduced graphene oxide: Effect of reduction on electrical conductivity. *J. Compos. Sci.* **2018**, *2*, 25. [CrossRef]
46. Wang, H.; Tian, H.-W.; Wang, X.-W.; Qiao, L.; Wang, S.-M.; Wang, X.-L.; Zheng, W.-T.; Liu, Y.-C. Electrical conductivity of alkaline-reduced graphene oxide. *Chem. Res. Chinese Univ.* **2011**, *27*, 857–861.
47. Tokarczyk, M.; Kowalski, G.; Witowski, A.; Kozinski, R.; Librant, K.; Aksienionek, M.; Lipińska, L.; Ciepielewski, P. Structural and electronic properties of graphene oxide and reduced graphene oxide papers prepared by high pressure and high temperature treatment. *Acta Phys. Pol. A* **2014**, *126*, 1190–1194. [CrossRef]
48. Marquez, C.; Rodríguez, N.; Ruiz, R.; Gamiz, F. Electrical characterization and conductivity optimization of laser reduced graphene oxide on insulator using point-contact methods. *RSC Adv.* **2016**, *6*, 46231–46237. [CrossRef]
49. Shabir, A.; Sehrawat, P.; Julien, C.M.; Islam, S.S. Reversible synthesis of GO: Role of differential bond structure transformation in fine-tuning photodetector response. *Nanotechnology* **2020**, *32*, 045601. [CrossRef]
50. Pei, S.; Cheng, H.-M. The reduction of graphene oxide. *Carbon* **2012**, *50*, 3210–3228. [CrossRef]
51. Dikin, D.A.; Stankovich, S.; Zimney, E.J.; Piner, R.D.; Dommett, G.H.B.; Evmenenko, G.; Nguyen, S.T.; Ruoff, R.S. Preparation and characterization of graphene oxide paper. *Nat. Cell Biol.* **2007**, *448*, 457–460. [CrossRef] [PubMed]
52. Chua, C.K.; Pumera, M. Reduction of graphene oxide with substituted borohydrides. *J. Mater. Chem. A* **2012**, *1*, 1892–1898. [CrossRef]
53. Liu, Y.; Zhang, Y.; Ma, G.; Wang, Z.; Liu, K.; Liu, H. Ethylene glycol reduced graphene oxide/polypyrrole composite for supercapacitor. *Electrochim. Acta* **2013**, *88*, 519–525. [CrossRef]
54. Zhang, J.; Yang, H.; Shen, G.; Cheng, P.; Zhang, J.; Guo, S. Reduction of graphene oxide via *L*-ascorbic acid. *Chem. Commun.* **2010**, *46*, 1112–1114. [CrossRef] [PubMed]
55. Fan, Z.; Wang, K.; Wei, T.; Yan, J.; Song, L.; Shao, B. An environmentally friendly and efficient route for the reduction of graphene oxide by aluminum powder. *Carbon* **2010**, *48*, 1686–1689. [CrossRef]
56. Maddineni, S.B.; Mandal, B.K. Biofabrication of reduction of graphene oxide nanosheets using terminalia Bellirica fruit extract. *Current Nanosci.* **2016**, *12*, 94–102. [CrossRef]
57. Yang, J.; Wang, Y.; Wang, J.; Chan-Park, M.B. Reducing graphene oxide with a modified Birch reaction. *RSC Adv.* **2015**, *5*, 11124–11127. [CrossRef]
58. Li, B.; Cao, H.; Shao, J.; Qu, M. Enhanced anode performances of the Fe_3O_4–carbon–rGO three dimensional composite in lithium ion batteries. *Chem. Commun.* **2011**, *47*, 10374–10376. [CrossRef]
59. Mei, L.; Xu, C.; Yang, T.; Ma, J.; Chen, L.; Li, Q.; Wang, T. Superior electrochemical performance of ultrasmall SnS_2 nanocrystals decorated on flexible RGO in lithium-ion batteries. *J. Mater. Chem. A* **2013**, *1*, 8658–8664. [CrossRef]
60. Patil, S.B.; Nagaraju, G.; Kishore, B.; Nagaraju, G.; Dupont, J.; Nagaraju, G. High capacity MoO_3/rGO nanocomposite anode for lithium ion batteries: An intuition into the conversion mechanism of MoO_3. *New J. Chem.* **2018**, *42*, 18569–18577. [CrossRef]
61. Paek, S.-M.; Yoo, E.; Honma, I. Enhanced cyclic performance and lithium storage capacity of SnO_2/graphene nanoporous electrodes with three-dimensionally delaminated flexible structure. *Nano Lett.* **2009**, *9*, 72–75. [CrossRef] [PubMed]
62. Zhou, G.; Wang, D.-W.; Li, F.; Zhang, L.; Li, N.; Wu, Z.-S.; Wen, L.; Lu, G.Q. (Max); Cheng, H.-M. Graphene-wrapped Fe_3O_4 anode material with improved reversible capacity and cyclic stability for lithium ion batteries. *Chem. Mater.* **2010**, *22*, 5306–5313. [CrossRef]
63. Ma, C.; Xu, J.; Alvarado, J.; Qu, B.; Somerville, J.; Lee, J.Y.; Meng, Y.S. Investigating the energy storage mechanism of SnS_2-rGO composite anode for advanced Na-ion batteries. *Chem. Mater.* **2015**, *27*, 5633–5640. [CrossRef]

64. Zhang, Q.; Karthick, R.; Zhao, X.; Zhang, L.-G.; Shi, Y.; Sun, L.; Su, C.-Y.; Chen, F. Sb nanoparticle decorated rGO as a new anode material in aqueous chloride ion batteries. *Nanoscale* **2020**, *12*, 12268–12274. [CrossRef]
65. Zensich, M.; Jaumann, T.; Morales, G.M.; Giebeler, L.; Barbero, C.; Balach, J. A top-down approach to build Li_2S@rGO cathode composites for high-loading lithium–sulfur batteries in carbonate-based electrolyte. *Electrochim. Acta* **2018**, *296*, 243–250. [CrossRef]
66. Abalonyx. Available online: https://www.abalonyx.no/?cat=42023. (accessed on 17 September 2020).
67. Kimiagar, S.; Rashidi, N.; Ghadim, E.E. Investigation of the effects of temperature and time on reduction of graphene oxide by microwave hydrothermal reactor. *Bull. Mater. Sci.* **2015**, *38*, 1699–1704. [CrossRef]
68. Pimenta, M.A.; Dresselhaus, G.; Dresselhaus, M.S.; Cançado, L.G.; Jorio, A.; Saito, R. Studying disorder in graphite-based systems by Raman spectroscopy. *Phys. Chem. Chem. Phys.* **2007**, *9*, 1276–1290. [CrossRef]
69. Tian, L.; Zhuang, Q.; Yueli, S.; Shigang, S.; Chen, J.; Lu, F.; Sun, S. Mechanism of intercalation and deintercalation of lithium ions in graphene nanosheets. *Chin. Sci. Bull.* **2011**, *56*, 3204–3212. [CrossRef]
70. Datta, D.; Li, J.; Koratkar, N.; Shenoy, V.B. Enhanced lithiation in defective graphene. *Carbon* **2014**, *80*, 305–310. [CrossRef]
71. Lin, K.-H.; Kuo, C.-L. Lithiation mechanisms and lithium storage capacity of reduced graphene oxide nanoribbons: A first-principles study. *J. Mater. Chem. A* **2017**, *5*, 4912–4922. [CrossRef]
72. Pan, D.; Wang, S.; Zhao, B.; Wu, M.; Zhang, H.; Wang, Y.; Jiao, Z. Li Storage properties of disordered graphene nanosheets. *Chem. Mater.* **2009**, *21*, 3136–3142. [CrossRef]
73. Robledo, C.; Otero, M.; Luque, G.L.; Camara, O.; Barraco, D.; Rojas, M.; Leiva, E. First-principles studies of lithium storage in reduced graphite oxide. *Electrochim. Acta* **2014**, *140*, 232–237. [CrossRef]
74. Randviir, E.P.; Banks, C.E. *Graphene and Graphene Oxide for Energy Storage*; Wiley: Hoboken, NJ, USA, 2017; pp. 725–744.
75. Kühne, M. *Lithium Intercalation in Bilayer Graphene Devices*; Springer Science and Business Media LLC: Berlin/Heidelberg, Germany, 2018; pp. 1–92.
76. Matsuo, Y.; Sasaki, T.; Maruyama, S.; Inamoto, J.; Okamoto, Y.; Tamura, N. Electrochemical intercalation behaviors of lithium ions into graphene-like graphite. *J. Electrochem. Soc.* **2018**, *165*, A2409–A2414. [CrossRef]
77. Ji, K.; Han, J.; Hirata, A.; Fujita, T.; Shen, Y.; Ning, S.; Liu, P.; Kashani, H.; Tian, Y.; Ito, Y.; et al. Lithium intercalation into bilayer graphene. *Nat. Commun.* **2019**, *10*, 1–10. [CrossRef]
78. Kheirabadi, N.; Shafiekhani, A. Graphene/Li-ion battery. *J. Appl. Phys.* **2012**, *112*, 124323. [CrossRef]
79. Wang, C.; Li, D.; Too, C.O.; Wallace, G.G. Electrochemical properties of graphene paper electrodes used in lithium batteries. *Chem. Mater.* **2009**, *21*, 2604–2606. [CrossRef]
80. Gedela, V.; Puttapati, S.K.; Nagavolu, C.; Srikanth, V.V.S.S. A unique solar radiation exfoliated reduced graphene oxide/polyaniline nanofibers composite electrode material for supercapacitors. *Mater. Lett.* **2015**, *152*, 177–180. [CrossRef]
81. Puttapati, S.K.; Gedela, V.; Srikanth, V.V.S.S.; Reddy, M.V.; Adams, S.; Chowdari, B.V.R. Unique reduced graphene oxide as efficient anode material in Li ion battery. *Bull. Mater. Sci.* **2018**, *41*, 53. [CrossRef]
82. Kim, H.; Seo, D.-H.; Kim, S.-W.; Kim, J.; Kang, K. Highly reversible Co_3O_4/graphene hybrid anode for lithium rechargeable batteries. *Carbon* **2011**, *49*, 326–332. [CrossRef]
83. Li, B.; Cao, H.; Shao, J.; Li, G.; Qu, M.; Yin, G. Co_3O_4@graphene Composites as Anode Materials for High-Performance Lithium Ion Batteries. *Inorg. Chem.* **2011**, *50*, 1628–1632. [CrossRef]
84. Zhang, F.; Yang, X.; Xie, Y.; Yi, N.; Huang, Y.; Chen, Y. Pyrolytic carbon-coated Si nanoparticles on elastic graphene framework as anode materials for high-performance lithium-ion batteries. *Carbon* **2015**, *82*, 161–167. [CrossRef]
85. Ji, J.; Ji, H.; Zhang, L.L.; Zhao, X.; Bai, X.; Fan, X.; Zhang, F.; Ruoff, R.S. Graphene-encapsulated Si on ultrathin-graphite foam as anode for high capacity lithium-ion batteries. *Adv. Mater.* **2013**, *25*, 4673–4677. [CrossRef] [PubMed]
86. Lin, N.; Zhou, J.; Zhu, Y.; Qian, Y. Embedding silicon nanoparticles in graphene based 3D framework by cross-linking reaction for high performance lithium ion batteries. *J. Mater. Chem. A* **2014**, *2*, 19604–19608. [CrossRef]
87. Chang, J.; Huang, X.; Zhou, G.; Cui, S.; Mao, S.; Chen, J. Three-dimensional carbon-coated Si/rGO nanostructures anchored by nickel foam with carbon nanotubes for Li-ion battery applications. *Nano Energy* **2015**, *15*, 679–687. [CrossRef]

88. Wang, B.; Li, X.; Zhang, X.; Luo, B.; Jin, M.; Liang, M.; Dayeh, S.A.; Picraux, S.T.; Zhi, L. Adaptable silicon–carbon nanocables sandwiched between reduced graphene oxide sheets as lithium ion battery anodes. *ACS Nano* **2013**, *7*, 1437–1445. [CrossRef] [PubMed]
89. Cao, H.; Li, B.; Zhang, J.; Lian, F.; Kong, X.; Qu, M. Synthesis and superior anode performance of TiO_2@reduced graphene oxide nanocomposites for lithium ion batteries. *J. Mater. Chem.* **2012**, *22*, 9759–9766. [CrossRef]
90. Ji, L.; Zheng, H.; Ismach, A.; Tan, Z.; Xun, S.; Lin, E.; Battaglia, V.; Srinivasan, V.; Zhang, Y. Graphene/Si multilayer structure anodes for advanced half and full lithium-ion cells. *Nano Energy* **2012**, *1*, 164–171. [CrossRef]
91. De Guzman, R.C.; Yang, J.; Cheng, M.M.-C.; Salley, S.O.; Ng, K.Y.S. Effects of graphene and carbon coating modifications on electrochemical performance of silicon nanoparticle/graphene composite anode. *J. Power Sources* **2014**, *246*, 335–345. [CrossRef]
92. Wong, D.P.; Tseng, H.-P.; Chen, Y.-T.; Hwang, B.-J.; Chen, L.-C.; Chen, K.-H. A stable silicon/graphene composite using solvent exchange method as anode material for lithium ion batteries. *Carbon* **2013**, *63*, 397–403. [CrossRef]
93. Xiang, H.; Zhang, K.; Ji, G.; Lee, J.Y.; Zou, C.; Chen, X.; Wu, J. Graphene/nanosized silicon composites for lithium battery anodes with improved cycling stability. *Carbon* **2011**, *49*, 1787–1796. [CrossRef]
94. Lee, J.K.; Smith, K.B.; Hayner, C.M.; Kung, H.H. Silicon nanoparticles–graphene paper composites for Li ion battery anodes. *Chem. Commun.* **2010**, *46*, 2025–2027. [CrossRef]
95. Julien, C.M.; Mauger, A.; Vijh, A.; Zaghib, K. *Lithium Batteries: Science and Technology*; Springer: Cham, Switzerland, 2016; pp. 323–429.
96. Chou, S.-L.; Wang, J.-Z.; Choucair, M.; Liu, H.-K.; Stride, J.A.; Dou, S.-X. Enhanced reversible lithium storage in a nanosize silicon/graphene composite. *Electrochem. Commun.* **2010**, *12*, 303–306. [CrossRef]
97. Liu, X.; Zhu, X.; Pan, D. Solutions for the problems of silicon–carbon anode materials for lithium-ion batteries. *R. Soc. Open Sci.* **2018**, *5*, 172370. [CrossRef] [PubMed]
98. Jamaluddin, A.; Umesh, B.; Chen, F.; Chang, J.-K.; Su, C.-Y. Facile synthesis of core–shell structured Si@graphene balls as a high-performance anode for lithium-ion batteries. *Nanoscale* **2020**, *12*, 9616–9627. [CrossRef] [PubMed]
99. Han, X.; Zhang, Z.; Chen, H.; Qiao-Bao, Z.; Chen, S.; Yang, Y. On the interface design of Si and multilayer graphene for a high-performance Li-ion battery anode. *ACS Appl. Mater. Interfaces* **2020**, *12*, 44840–44849. [CrossRef] [PubMed]
100. Huang, Y.; Peng, J.; Luo, J.; Li, W.; Wu, Z.; Shi, M.; Li, X.; Li, N.; Chang, B.; Wang, X.; et al. Spherical Gr/Si/GO/C composite as high-performance anode material for lithium-ion batteries. *Energy Fuels* **2020**, *34*, 7639–7647. [CrossRef]
101. Kim, D.; Luo, Y.; Tiwari, A.P.; Hwang, H.M.; Oh, S.; Lee, K.; Lee, H. Highly stable multi-layered silicon-intercalated graphene anodes for lithium-ion batteries. *MRS Commun.* **2020**, *10*, 25–31. [CrossRef]
102. Park, S.-H.; Kim, H.-K.; Ahn, D.-J.; Lee, S.-I.; Roh, K.C.; Kim, K.-B. Self-assembly of Si entrapped graphene architecture for high-performance Li-ion batteries. *Electrochem. Commun.* **2013**, *34*, 117–120. [CrossRef]
103. Ye, Y.-S.; Xie, X.; Rick, J.; Chang, F.-C.; Hwang, B.-J. Improved anode materials for lithium-ion batteries comprise non-covalently bonded graphene and silicon nanoparticles. *J. Power Sources* **2014**, *247*, 991–998. [CrossRef]
104. Li, Q.; Chen, D.; Li, K.; Wang, J.; Zhao, J. Electrostatic self-assembly bmSi@C/rGO composite as anode material for lithium ion battery. *Electrochim. Acta* **2016**, *202*, 140–146. [CrossRef]
105. Liu, L.; Li, X.; Zhang, G.; Zhang, Z.; Fang, C.; Ma, H.; Luo, W.; Liu, Z. Enhanced stability lithium-ion battery based on optimized graphene/Si nanocomposites by templated assembly. *ACS Omega* **2019**, *4*, 18195–18202. [CrossRef] [PubMed]
106. Reddy, A.L.M.; Srivastava, A.; Gowda, S.R.; Gullapalli, H.; Dubey, M.; Ajayan, P.M. Synthesis of nitrogen-doped graphene films for lithium battery application. *ACS Nano* **2010**, *4*, 6337–6342. [CrossRef] [PubMed]
107. Chang, J.; Huang, X.; Zhou, G.; Cui, S.; Hallac, P.B.; Jiang, J.; Hurley, P.T.; Chen, J. Multilayered Si nanoparticle/reduced graphene oxide hybrid as a high-performance lithium-ion battery anode. *Adv. Mater.* **2013**, *26*, 758–764. [CrossRef] [PubMed]
108. Lin, N.; Zhou, J.; Wang, L.; Zhu, Y.; Qian, Y. Polyaniline-assisted synthesis of Si@C/RGO as anode material for rechargeable lithium-ion batteries. *ACS Appl. Mater. Interfaces* **2014**, *7*, 409–414. [CrossRef]

109. Wang, S.; Liao, J.; Wu, M.; Xu, Z.; Gong, F.; Chen, C.; Wang, Y.; Yan, X. High rate and long cycle life of a CNT/rGO/Si nanoparticle composite anode for lithium-ion batteries. *Part. Part. Syst. Charact.* **2017**, *34*, 1700141. [CrossRef]
110. Kumar, K.T.; Reddy, M.J.K.; Sundari, G.S.; Raghu, S.; Kalaivani, R.; Ryu, S.H.; Shanmugharaj, A. Synthesis of graphene-siloxene nanosheet based layered composite materials by tuning its interface chemistry: An efficient anode with overwhelming electrochemical performances for lithium-ion batteries. *J. Power Sources* **2020**, *450*, 227618. [CrossRef]
111. Dai, J.; Liao, J.; He, M.; Yang, M.; Wu, K.; Yao, W. Si@SnS$_2$-reduced graphene oxide composite anodes for high-capacity Li-ion batteries. *ChemSusChem* **2019**, *12*, 5092–5098. [CrossRef]
112. Deng, B.; Xu, R.; Wang, X.; An, L.; Zhao, K.; Cheng, G.J. Roll to roll manufacturing of fast charging, mechanically robust 0D/2D nanolayered Si-graphene anode with well-interfaced and defect engineered structures. *Energy Storage Mater.* **2019**, *22*, 450–460. [CrossRef]
113. Bian, F.; Yu, J.; Song, W.; Huang, H.; Liang, C.; Gan, Y.; Xia, Y.; Zhang, J.; He, X.; Zhang, W. A new magnesium hydride route to synthesize morphology-controlled Si/rGO nanocomposite towards high-performance lithium storage. *Electrochim. Acta* **2020**, *330*, 135248. [CrossRef]
114. Zhaoa, H.; Xuab, X.; Yaoa, Y.; Lic, Y. Si nanoparticles veiled with ultrathin rGO film reduced directly by precoated Ni template: Fabrication and electrochemical performance. *Appl. Surf. Sci.* **2020**, *528*, 146993. [CrossRef]
115. Wu, J.; Qin, X.; Zhang, H.; He, Y.-B.; Li, B.; Ke, L.; Lv, W.; Du, H.; Yang, Q.-H.; Kang, F. Multilayred silicon embedded porous carbon/graphene hybrid as a high performance anode. *Carbon* **2015**, *84*, 434–443. [CrossRef]
116. Majeed, M.K.; Saleem, A.; Ma, X.; Ma, W. Clay-derived mesoporous Si/rGO for anode material of lithium-ion batteries. *J. Alloys Compd.* **2020**, *848*, 156590. [CrossRef]
117. Fang, R.; Xiao, W.; Miao, C.; Mei, P.; Yan, W.; Zhang, Y.; Jiang, Y. Improved lithium storage performance of pomegranate-like Si@NC/rGO composite anodes by facile in-situ nitrogen doped carbon coating and freeze drying processes. *J. Alloys Compd.* **2020**, *834*, 155230. [CrossRef]
118. Zhang, K.; Xia, Y.; Yang, Z.; Fu, R.; Shen, C.; Liu, Z. Structure-preserved 3D porous silicon/reduced graphene oxide materials as anodes for Li-ion batteries. *RSC Adv.* **2017**, *7*, 24305–24311. [CrossRef]
119. Yu, K.; Zhang, H.; Qi, H.; Liang, J.-C.; Liang, C. High performance of porous silicon/carbon/RGO network derived from rice husks as anodes for lithium-ion batteries. *New J. Chem.* **2018**, *42*, 19811–19817. [CrossRef]
120. Chen, S.; Bao, P.; Huang, X.; Sun, B.; Wang, G. Hierarchical 3D mesoporous silicon-graphene nanoarchitectures for lithium ion batteries with superior performance. *Nano Res.* **2014**, *7*, 85–94. [CrossRef]
121. Men, X.; Kong, X.; Yang, X.; Wang, B.; Wang, Y.; Liu, Y.; Yu, L.; Li, H.; Xu, B. Synthesis of a pomegranate shaped reduced graphene oxide stabilized secondary Si nanoparticles composite anode for lithium ion batteries. *Int. J. Hydrogen Energy* **2020**, *45*, 29492–29504. [CrossRef]
122. Benzait, Z.; Yuca, N. Synergistic effect of carbon nanomaterials on a cost-effective coral-like Si/rGO composite for lithium ion battery application. *Electrochim. Acta* **2020**, *339*, 135917. [CrossRef]
123. Tang, X.; Wen, G.; Zhang, Y.; Wang, D.; Song, Y. Novel silicon nanoparticles with nitrogen-doped carbon shell dispersed in nitrogen-doped graphene and CNTs hybrid electrode for lithium ion battery. *Appl. Surf. Sci.* **2017**, *425*, 742–749. [CrossRef]
124. Zhang, Z.; Du, Y.; Li, H. Engineering of a bowl-like Si@rGO architecture for an improved lithium ion battery via synergistic effect. *Nanotechnology* **2020**, *31*, 095402. [CrossRef]
125. Chen, Y.; Hu, Y.; Shen, Z.; Chen, R.; He, X.; Zhang, X.; Zhang, Y.; Wu, K. Sandwich structure of graphene-protected silicon/carbon nanofibers for lithium-ion battery anodes. *Electrochim. Acta* **2016**, *210*, 53–60. [CrossRef]
126. Pan, Q.; Zuo, P.; Lou, S.; Mu, T.; Du, C.; Cheng, X.; Ma, Y.; Gao, Y.; Yin, G. Micro-sized spherical silicon@carbon@graphene prepared by spray drying as anode material for lithium-ion batteries. *J. Alloys Compd.* **2017**, *723*, 434–440. [CrossRef]
127. He, Z.; Wu, X.; Yi, Z.; Wang, X.; Xiang, Y. Silicon/graphene/carbon hierarchical structure nanofibers for high performance lithium ion batteries. *Mater. Lett.* **2017**, *200*, 128–131. [CrossRef]
128. Lee, S.-H.; Kim, Y.-J.; Nam, Y.-S.; Park, S.-H.; Lee, H.; Hyun, Y.; Lee, C.-S. Synthesis and characterization of silicon/reduced graphene oxide composites as anodes for Lithium secondary batteries. *J. Nanosci. Nanotechnol.* **2018**, *18*, 5026–5032. [CrossRef] [PubMed]

129. Tao, H.; Xiong, L.; Zhu, S.; Zhang, L.; Yang, X. Porous Si/C/reduced graphene oxide microspheres by spray drying as anode for Li-ion batteries. *J. Electroanal. Chem.* **2017**, *797*, 16–22. [CrossRef]
130. Qin, J.; Wu, M.; Feng, T.; Chen, C.; Tu, C.; Li, X.; Duan, C.; Xia, D.; Wang, D. High rate capability and long cycling life of graphene-coated silicon composite anodes for lithium ion batteries. *Electrochim. Acta* **2017**, *256*, 259–266. [CrossRef]
131. Pan, Q.; Zhao, J.; Qu, W.; Liu, R.; Li, N.; Xing, B.; Jiang, S.; Pang, M.; Zhao, L.; Zhang, Y.; et al. Facile synthesis of the 3D framework Si@N-doped C/Reduced graphene oxide composite by polymer network method for highly stable lithium storage. *J. Phys. Chem. Solids* **2019**, *133*, 92–99. [CrossRef]
132. Toçoğlua, U.; Alaf, M.; Akbulut, H. Towards high cycle stability yolk-shell structured silicon/rGO/MWCNT hybrid composites for Li-ion battery negative electrodes. *Mater. Chem. Phys.* **2020**, *240*, 122160. [CrossRef]
133. Xu, H.; Wang, Y.; Chenab, R.; Baiab, Y.; Liab, T.; Jinab, H.; Wanga, J.; Xiaa, H. A green-synthetic spiderweb-like Si@Graphene-oxide anode material with multifunctional citric acid binder for high energy-density Li-ion batteries. *Carbon* **2020**, *157*, 330–339. [CrossRef]
134. Wu, Y.-S.; Yang, C.-C.; Wu, S.; Wu, Z.; Wei, C.; Yang, M.; Lue, S.J. Preparation of ternary hierarchical silicon/reduced graphene oxide/carbon composites as anodes for lithium–ion batteries. *J. Alloys Compd.* **2019**, *793*, 433–445. [CrossRef]
135. Yu, L.; Liu, J.; He, S.; Huang, C.; Gong, Z.; Gan, L.; Long, M. N-doped rGO/C@Si composites using sustainable chitosan as the carbon source for lithium-ion batteries. *Appl. Surf. Sci.* **2020**, *501*, 144136. [CrossRef]
136. Zhu, C.; Zhang, Y.; Ma, Z.; Wang, H.; Sly, G.L. Yolk-void-shell Si-C nano-particles with tunable void size for high-performance anode of lithium ion batteries. *Nanotechnology* **2020**. [CrossRef] [PubMed]
137. Baggetto, L.; Notten, P.H.N. Lithium ion (de)insertion reaction of germanium thin-film electrodes and electrochemical and in-situ XRD study batteries and energy storage. *J. Electrochem. Soc.* **2009**, *156*, A169–A175. [CrossRef]
138. Liu, X.; Wu, X.; Chang, B.; Wang, K.-X. Recent progress on germanium-based anodes for lithium ion batteries: Efficient lithiation strategies and mechanisms. *Energy Storage Mater.* **2020**, *30*, 146–169. [CrossRef]
139. Liang, W.; Yang, H.; Fan, F.; Liu, Y.; Liu, X.H.; Huang, J.Y.; Zhu, T.; Zhang, S. Tough germanium nanoparticles under electrochemical cycling. *ACS Nano* **2013**, *7*, 3427–3433. [CrossRef]
140. Panayotov, V.; Panayotova, M.; Chukharev, S. Recent studies on germanium-nanomaterials for LIBs anodes. *E3S Web Conf.* **2020**, *166*, 06012. [CrossRef]
141. Loaiza, L.C.; Montconduit, L.; Seznzc, V. Si and Ge-based anode materials for Li-, Na-, and K-ion batteries: A perspective from structure to electrochemical mechanism. *Small* **2020**, *16*, 1905260. [CrossRef]
142. Xue, D.-J.; Xin, S.; Yan, Y.; Jiang, K.-C.; Yin, Y.-X.; Guo, Y.-G.; Wan, L.-J. Improving the electrode performance of Ge through Ge@C core–shell nanoparticles and graphene networks. *J. Am. Chem. Soc.* **2012**, *134*, 2512–2515. [CrossRef]
143. Xu, Y.; Zhu, X.; Zhou, X.; Liu, X.; Liu, Y.; Dai, Z.; Bao, J. Ge nanoparticles encapsulated in nitrogen-doped reduced graphene oxide as an advanced anode material for lithium-ion batteries. *J. Phys. Chem. C* **2014**, *118*, 28502–28508. [CrossRef]
144. Wang, B.; Wen, Z.; Jin, J.; Hong, X.; Zhang, S.; Rui, K. A novel strategy to prepare Ge@C/rGO hybrids as high-rate anode materials for lithium ion batteries. *J. Power Sources* **2017**, *342*, 521–528. [CrossRef]
145. Wang, B.; Jin, J.; Hong, X.; Gu, S.; Guo, J.; Wen, Z. Facile synthesis of the sandwich-structured germanium/reduced graphene oxide hybrid: An advanced anode material for high-performance lithium ion batteries. *J. Mater. Chem. A* **2017**, *5*, 13430–13438. [CrossRef]
146. Fang, S.; Shen, L.; Zheng, H.; Zhang, X. Ge–graphene–carbon nanotube composite anode for high performance lithium-ion batteries. *J. Mater. Chem. A* **2014**, *3*, 1498–1503. [CrossRef]
147. Chen, Y.; Ma, L.; Shen, X.; Ji, Z.; Yuan, A.; Xu, K.; Shah, S.A. In-situ synthesis of Ge/reduced graphene oxide composites as ultrahigh rate anode for lithium-ion battery. *J. Alloys Compd.* **2019**, *801*, 90–98. [CrossRef]
148. Zhao, M.; Zhao, D.-L.; Yang, H.-X.; Han, X.-Y.; Duan, Y.-J.; Tian, X.-M.; Meng, W.-J. Graphene-supported cubic hollow carbon shell-coated germanium particles as high-performance anode for lithium-ion batteries. *Ceram. Int.* **2019**, *45*, 13210–13218. [CrossRef]
149. Zhao, F.; Wang, Y.; Zhang, X.; Liang, X.; Zhang, F.; Wang, L.; Li, Y.; Feng, Y.; Feng, W. Few-layer methyl-terminated germanene–graphene nanocomposite with high capacity for stable lithium storage. *Carbon* **2020**, *161*, 287–298. [CrossRef]

150. Meng, W.-J.; Zhao, M.; Yang, H.-X.; Wu, Y.-Q.; Pu, H.; Gao, R.-Z.; Yang, Y.; Zhao, D.-L. Synthesis of CuGeO3/reduced graphene oxide nanocomposite by hydrothermal reduction for high performance Li-ion battery anodes. *Ceram. Int.* **2020**, *46*, 9249–9255. [CrossRef]
151. Wen, C.J.; Huggins, R.A. Thermodynamic study of the lithium-tin system. *J. Electrochem. Soc.* **1981**, *128*, 1181–1187. [CrossRef]
152. Winter, M.; Besenhard, J.O. Electrochemical lithiation of tin and tin-based intermetallics and composites. *Electrochim. Acta* **1999**, *45*, 31–50. [CrossRef]
153. Park, C.-M.; Kim, J.-H.; Kim, H.; Sohn, H.-J. Li-alloy based anode materials for Li secondary batteries. *Chem. Soc. Rev.* **2010**, *39*, 3115–3141. [CrossRef]
154. Zhang, P.; Ma, Z.S.; Jiang, W.; Wang, Y.; Pan, Y.; Lu, C. Mechanical properties of Li–Sn alloys for Li-ion battery anodes: A first-principles perspective. *AIP Adv.* **2016**, *6*, 015107. [CrossRef]
155. Li, H. Nano-alloy anode for lithium ion batteries. *Solid State Ionics* **2002**, *148*, 247–258. [CrossRef]
156. Wang, B.; Luo, B.; Li, X.; Zhi, L. The dimensionality of Sn anodes in Li-ion batteries. *Mater. Today* **2012**, *15*, 544–552. [CrossRef]
157. Wang, G.; Wang, B.; Wang, X.; Park, J.; Dou, S.; Ahn, H.; Kim, K. Sn/graphene nanocomposite with 3D architecture for enhanced reversible lithium storage in lithium ion batteries. *J. Mater. Chem.* **2009**, *19*, 8378–8384. [CrossRef]
158. Luo, B.; Wang, B.; Liang, M.; Ning, J.; Li, X.; Zhi, L. Reduced graphene oxide-mediated growth of uniform tin-core/carbon-sheath coaxial nanocables with enhanced lithium ion storage properties. *Adv. Mater.* **2012**, *24*, 1405–1409. [CrossRef]
159. Wang, H.; Xing, Z.; Hu, Z.; Zhang, Y.; Hu, Y.; Sun, Y.; Ju, Z.; Zhuang, Q. Sn-based submicron-particles encapsulated in porous reduced graphene oxide network: Advanced anodes for high-rate and long life potassium-ion batteries. *Appl. Mater. Today* **2019**, *15*, 58–66. [CrossRef]
160. Botas, C.; Carriazo, D.; Singh, G.; Rojo, T. Sn—And SnO_2–graphene flexible foams suitable as binder-free anodes for lithium ion batteries. *J. Mater. Chem. A* **2015**, *3*, 13402–13410. [CrossRef]
161. Soler-Piña, F.J.; Hernández-Rentero, C.; Caballero, A.; Morales, J.; Rodríguez-Castellón, E.; Canales-Vázquez, J. Highly graphitized carbon nanosheets with embedded Ni nanocrystals as anode for Li-ion batteries. *Nano Res.* **2020**, *13*, 86–94. [CrossRef]
162. Dashairya, L.; Das, D.; Saha, P. Electrophoretic deposition of antimony/reduced graphite oxide hybrid nanostructure: A stable anode for lithium-ion batteries. *Mater. Today Commun.* **2020**, *24*, 101189. [CrossRef]
163. Yang, J.; Takeda, Y.; Imanishi, N.; Capiglia, C.; Xie, J.Y.; Yamamoto, O. SiO_x-based anodes for secondary lithium batteries. *Solid State Ion.* **2002**, *152-153*, 125–129. [CrossRef]
164. Chang, W.-S.; Park, C.-M.; Kim, J.-H.; Kim, Y.-U.; Jeong, G.; Sohn, H.-J. Quartz (SiO_2): A new energy storage anode material for Li-ion batteries. *Energy Environ. Sci.* **2012**, *5*, 6895–6899. [CrossRef]
165. Yamada, Y.; Iriyama, Y.; Abe, T.; Ogumi, Z. Kinetics of electrochemical insertion and extraction of lithium ion at SiO. *J. Electrochem. Soc.* **2010**, *157*, A26. [CrossRef]
166. Xu, X.; Zhang, H.; Chen, Y.; Li, N.; Li, Y.; Liu, L. SiO_2@SnO_2/graphene composite with a coating and hierarchical structure as high performance anode material for lithium ion battery. *J. Alloys Compd.* **2016**, *677*, 237–244. [CrossRef]
167. Zhao, Y.; Zheng, L.; Wu, H.; Chen, H.; Su, L.; Wang, L.; Wang, Y.; Ren, M. Co_2SiO_4/SiO_2/RGO nanosheets: Boosting the lithium storage capability of tetravalent Si by using highly-dispersed Co element. *Electrochim. Acta* **2018**, *282*, 609–617. [CrossRef]
168. Hu, Z.; Cui, H.; Li, J.; Lei, G.; Li, Z. Constructing three-dimensional Li-transport channels within the Fe_3O_4@SiO_2@RGO composite to improve its electrochemical performance in Li-ion batteries. *Ceram. Int.* **2020**, *46*, 18868–18877. [CrossRef]
169. Haeri, S.; Ramezanzadeh, B.; Asghari, M. A novel fabrication of a high performance SiO_2-graphene oxide (GO) nanohybrids: Characterization of thermal properties of epoxy nanocomposites filled with SiO_2-GO nanohybrids. *J. Colloid Interface Sci.* **2017**, *493*, 111–122. [CrossRef] [PubMed]
170. Kasimayan, U.; Nadarajan, A.; Singaravelu, C.M.; Pan, G.-T.; Kandasamy, J.; Yang, T.C.-K.; Lin, J.-H. In-situ DRIFT investigation of photocatalytic reduction and oxidation properties of SiO_2@α-Fe_2O_3 core-shell decorated RGO nanocomposite. *Sci. Rep.* **2020**, *10*, 1–13. [CrossRef]
171. Zhang, J.; Ma, P.; Hou, Z.; Zhang, X.; Li, C. One-step synthesis of SiO_x@graphene composite material by a hydrothermal method lithium-ion batteries anodes. *Energy Fuels* **2020**, *34*, 3895–3900. [CrossRef]

172. Huang, J.; Fam, D.; He, Q.; Chen, H.; Zhan, D.; Faulkner, S.H.; Nimmo, M.; Tok, A.I.Y. The mechanism of graphene oxide as a growth template for complete reduced graphene oxide coverage on an SiO_2 substrate. *J. Mater. Chem. C* **2014**, *2*, 109–114. [CrossRef]
173. Liang, X.; Liu, S.; Song, X.; Zhu, Y.; Jiang, S. Layer-by-layer self-assembled graphene oxide/silica microsphere composites as stationary phase for high performance liquid chromatography. *Analyst* **2012**, *137*, 5237–5244. [CrossRef]
174. Liu, Y.; Zhang, F.R.; Zhu, W.X.; Su, D.; Sang, Z.Y.; Yan, X.; Li, S.; Liang, J.; Dou, S.X. A multifunctional hierarchical porous SiO_2/GO membrane for high efficiency oil/water separation and dye removal. *Carbon* **2020**, *160*, 88–97. [CrossRef]
175. Guo, C.; Wang, D.; Liu, T.; Zhu, J.X.; Lang, X. A three dimensional SiO_x/C@RGO nanocomposite as a high energy anode material for lithium-ion batteries. *J. Mater. Chem. A* **2014**, *2*, 3521–3527. [CrossRef]
176. Guo, X. Reduced Graphene oxide -coated 3D interconnected SiO_2 Nanoparticles with Enhanced Lithium Storage Performance. *Int. J. Electrochem. Sci.* **2018**, *13*, 5645–5653. [CrossRef]
177. Chen, L.; Zheng, J.; Lin, S.; Khan, S.; Huang, J.; Liu, S.; Chen, Z.; Wu, D.; Fu, R. Synthesis of SiO_x/C composite nanosheets as high-rate and stable anode materials for lithium-ion batteries. *ACS Appl. Energy Mater.* **2020**, *3*, 3562–3568. [CrossRef]
178. Idota, Y.; Kubota, T.; Matsufuji, A.; Maekawa, Y.; Miyasaka, T. Tin-based amorphous oxide: A high-capacity lithium-ion-storage material. *Science* **1997**, *276*, 1395–1397. [CrossRef]
179. Zoller, F.; Böhm, D.; Bein, T.; Fattakhova-Rohlfing, D. Tin oxide based nanomaterials and their application as anodes in lithium-ion batteries and beyond. *ChemSusChem* **2019**, *12*, 4140–4159. [CrossRef]
180. Li, Y.; Lv, X.; Lu, J.; Li, J. Preparation of SnO_2-nanocrystal/graphene-nanosheets composites and their lithium storage ability. *J. Phys. Chem. C* **2010**, *114*, 21770–21774. [CrossRef]
181. Zhao, B.; Zhang, G.; Song, J.; Jiang, Y.; Zhuang, H.; Liu, P.; Fang, T. Bivalent tin ion assisted reduction for preparing graphene/SnO_2 composite with good cyclic performance and lithium storage capacity. *Electrochim. Acta* **2011**, *56*, 7340–7346. [CrossRef]
182. Lian, P.; Zhu, X.; Liang, S.; Li, Z.; Yang, W.; Wang, H. High reversible capacity of SnO_2/graphene nanocomposite as an anode material for lithium-ion batteries. *Electrochim. Acta* **2011**, *56*, 4532–4539. [CrossRef]
183. Huang, X.; Zhou, X.; Zhou, L.; Qian, K.; Wang, Y.; Liu, Z.; Yu, C. A facile one-step solvothermal synthesis of SnO_2/graphene nanocomposite and its application as an anode material for lithium-ion batteries. *ChemPhysChem* **2010**, *12*, 278–281. [CrossRef]
184. Xie, J.; Liu, S.Y.; Chen, X.F.; Zhang, Y.X.; Song, W.T.; Cao, G.S.; Zhu, T.J.; Zhao, X.B. Nanocrystal-SnO_2-loaded graphene with improved Li-storage properties prepared by a facile one-pot hydrothermal route. *Int. J. Electrochem. Sci.* **2011**, *6*, 5539–5549.
185. Lim, S.P.; Huang, N.M.; Lim, H.N. Solvothermal synthesis of SnO_2/graphene nanocomposites for supercapacitor application. *Cream. Int.* **2013**, *39*, 6647–6655. [CrossRef]
186. Ding, S.; Luan, D.; Boey, F.Y.C.; Chen, J.S.; Lou, X.W.D. SnO_2 nanosheets grown on graphene sheets with enhanced lithium storage properties. *Chem. Commun.* **2011**, *47*, 7155–7157. [CrossRef] [PubMed]
187. Gao, T.; Huang, K.; Qi, X.; Li, H.; Yang, L.; Zhong, J. Free-standing SnO_2 nanoparticles@graphene hybrid paper for advanced lithium-ion batteries. *Ceram. Int.* **2014**, *40*, 6891–6897. [CrossRef]
188. Cui, D.; Zheng, Z.; Peng, X.; Li, T.; Sun, T.; Yuan, L. Fluorine-doped SnO_2 nanoparticles anchored on reduced graphene oxide as a high-performance lithium ion battery anode. *J. Power Sources* **2017**, *362*, 20–26. [CrossRef]
189. Wang, H.; Pan, Q.; Wu, Q.; Zhang, X.; Huang, Y.-G.; Lushington, A.; Li, Q.; Sun, X. Ultrasmall MoS_2 embedded in carbon nanosheets-coated Sn/SnO_x as anode material for high-rate and long life Li-ion batteries. *J. Mater. Chem. A* **2017**, *5*, 4576–4582. [CrossRef]
190. Tang, J.; Yang, J.; Zhou, L.; Xie, J.; Chen, G.; Zhou, X. Layer-by-layer self-assembly of a sandwich-like graphene wrapped SnO_x@graphene composite as an anode material for lithium ion batteries. *J. Mater. Chem. A* **2014**, *2*, 6292–6295. [CrossRef]
191. Cai, D.; Yang, T.; Liu, B.; Wang, D.; Liu, Y.; Wang, L.; Li, Q.; Wang, T. A nanocomposite of tin dioxide octahedral nanocrystals exposed to high-energy facets anchored onto graphene sheets for high performance lithium-ion batteries. *J. Mater. Chem. A* **2014**, *2*, 13990. [CrossRef]
192. Huang, Y.; Wu, D.; Wang, J.; Han, S.; Lv, L.; Zhang, F.; Feng, X. Amphiphilic polymer promoted assembly of macroporous graphene/SnO_2 frameworks with tunable porosity for high-performance lithium storage. *Small* **2014**, *10*, 2226–2232. [CrossRef]

193. Zhou, X.; Wan, L.-J.; Guo, Y.-G. Binding SnO_2 $_N$anocrystals in nitrogen-doped graphene sheets as anode materials for lithium-ion batteries. *Adv. Mater.* **2013**, *25*, 2152–2157. [CrossRef]
194. Hu, X.; Zeng, G.; Chen, J.; Lu, C.; Wen, Z. 3D graphene network encapsulating SnO_2 hollow spheres as a high-performance anode material for lithium-ion batteries. *J. Mater. Chem. A* **2017**, *5*, 4535–4542. [CrossRef]
195. Wang, S.; Shi, L.; Chen, G.; Ba, C.; Wang, Z.; Zhu, J.; Zhao, Y.; Zhang, M.; Yuan, S. In situ synthesis of tungsten-doped SnO_2 and graphene nanocomposites for high-performance anode materials of lithium-ion batteries. *ACS Appl. Mater. Interfaces* **2017**, *9*, 17163–17171. [CrossRef] [PubMed]
196. Wang, D.; Li, X.; Wang, J.; Ynag, J.; Geng, D.; Li, R.; Cai, M.; Sham, T.-K.; Sun, X. defect-rich crystalline SnO_2 immobilized on graphene nanosheets with enhanced cycle performance for Li ion batteries. *J. Phys. Chem. C* **2012**, *116*, 22149–22156. [CrossRef]
197. Shao, Q.; Tang, J.; Sun, Y.; Li, J.; Zhang, K.; Yuan, J.; Zhu, D.-M.; Qin, L.-C. Unique interconnected graphene/SnO_2 nanoparticle spherical multilayers for lithium-ion battery applications. *Nanoscale* **2017**, *9*, 4439–4444. [CrossRef] [PubMed]
198. Zhang, H.; Xu, P.; Ni, Y.; Geng, H.; Zheng, G.; Dong, B.; Jiao, Z. In situ chemical synthesis of SnO_2/reduced graphene oxide nanocomposites as anode materials for lithium-ion batteries. *J. Mater. Res.* **2014**, *29*, 617–624. [CrossRef]
199. Chen, L.; Ma, X.; Wang, M.; Chen, C.; Ge, X. Hierarchical porous SnO_2/reduced graphene oxide composites for high-performance lithium-ion battery anodes. *Electrochim. Acta* **2016**, *215*, 42–49. [CrossRef]
200. Hou, C.-C.; Brahma, S.; Weng, S.-C.; Chang, C.-C.; Huang, J.-L. Facile, low temperature synthesis of SnO_2/reduced graphene oxide nanocomposite as anode material for lithium-ion batteries. *Appl. Surf. Sci.* **2017**, *413*, 160–168. [CrossRef]
201. Tan, Q.; Kong, Z.; Chen, X.; Zhang, L.; Hu, X.; Mu, M.; Sun, H.; Shao, X.; Guan, X.; Gao, M.; et al. Synthesis of SnO_2/graphene composite anode materials for lithium-ion batteries. *Appl. Surf. Sci.* **2019**, *485*, 314–322. [CrossRef]
202. Liu, R.; Zhang, N.; Wang, X.; Yang, C.; Cheng, H.; Zhao, H. SnO_2 nanoparticles anchored on graphene oxide as advanced anode materials for high-performance lithium-ion batteries. *Front. Mater. Sci.* **2019**, *13*, 186–192. [CrossRef]
203. Jiang, W.; Zhao, X.; Ma, Z.S.; Lin, J.; Lu, C. SnO_2/reduced graphene oxide nanocomposite as anode material for lithium-ion batteries with enhanced cyclability. *J. Nanosci. Nanotechnol.* **2016**, *16*, 4136–4140. [CrossRef]
204. Jiang, S.; Huang, R.; Zhu, W.; Li, X.; Zhao, Y.; Gao, Z.; Gao, L.; Zhao, J. Free-standing SnO_2@rGO hybrid via the anti-solvent-assisted precipitation for superior lithium storage performance. *Front. Chem.* **2019**, *7*, 878. [CrossRef]
205. Wu, Y.-Z.; Brahma, S.; Weng, S.-C.; Chang, C.-C.; Huang, J.-L. Reduced graphene oxide (RGO)-SnO_x (x = 0,1,2) nanocomposite as high performance anode material for lithium-ion batteries. *J. Alloys Compd.* **2020**, *818*, 152889. [CrossRef]
206. Wang, J.; Wang, L.; Zhang, S.; Liang, S.; Liang, X.; Huang, H.; Zhou, W.; Guo, J. Facile synthesis of iron-doped SnO_2/reduced graphene oxide composite as high-performance anode material for lithium-ion batteries. *J. Alloys Compd.* **2018**, *748*, 1013–1021. [CrossRef]
207. Huang, Z.; Chen, Z.; Ding, S.; Chen, C.; Zhang, M. Enhanced electrochemical properties of SnO_2–graphene–carbon nanofibers tuned by phosphoric acid for potassium storage. *Nanotechnology* **2018**, *29*, 375702. [CrossRef] [PubMed]
208. Zoller, F.; Peters, K.; Zehetmaier, P.M.; Zeller, P.; Dçblinger, M.; Bein, T.; Sofer, Z.; Fattakhova-Rohlfing, D. Making ultrafast high-capacity anodes for lithium-ion batteries via antimony doping of nanosized tin oxide/graphene composites. *Adv. Funct. Mater.* **2018**, *28*, 1706529. [CrossRef]
209. Sun, J.; Xiao, L.; Jiang, S.; Li, G.; Huang, Y.; Geng, J. Fluorine-doped SnO_2@graphene porous composite for high capacity lithium-ion batteries. *Chem. Mater.* **2015**, *27*, 4594–4603. [CrossRef]
210. Zhang, Y.; Wang, R.; Zheng, Z.; Li, T.; Tong, Z.; Ai, C. Fluorine-doped SnO_2/reduced graphene oxide-artificial graphite hybrids as lithium-ion battery anodes with stable capacity. *Ionics* **2020**, *26*, 2835–2843. [CrossRef]
211. Dong, W.; Xu, J.; Wang, C.; Lu, Y.; Liu, X.; Wang, X.; Yuan, X.; Wang, Z.; Lin, T.; Sui, M.; et al. A robust and conductive black tin oxide nanostructure makes efficient lithium-ion batteries possible. *Adv. Mater.* **2017**, *29*, 1700136. [CrossRef]

212. Dou, P.; Cao, Z.; Wang, C.; Zheng, J.; Xu, X. Multilayer Zn-doped SnO_2 hollow nanospheres encapsulated in covalently interconnected three-dimensional graphene foams for high performance lithium-ion batteries. *Chem. Eng. J.* **2017**, *320*, 405–415. [CrossRef]
213. Kokubu, T.; Oaki, Y.; Hosono, E.; Zhou, H.; Imai, H. Biomimetic solid-solution precursors of metal carbonate for nanostructured metal oxides: MnO/Co and MnO-CoO nanostructures and their electrochemical properties. *Adv. Funct. Mater.* **2011**, *21*, 3673–3680. [CrossRef]
214. Wu, Y.; Liu, S.; Wang, H.; Wang, X.; Zhang, X.; Jin, G. A novel solvothermal synthesis of Mn_3O_4/graphene composites for supercapacitors. *Electrochim. Acta* **2013**, *90*, 210–218. [CrossRef]
215. Qiu, Y.; Xu, G.-L.; Yan, K.; Sun, H.; Xiao, J.; Yang, S.; Sun, S.; Jin, L.; Deng, H. Morphology-conserved transformation: Synthesis of hierarchical mesoporous nanostructures of Mn_2O_3 and the nanostructural effects on Li-ion insertion/deinsertion properties. *J. Mater. Chem.* **2011**, *21*, 6346–6353. [CrossRef]
216. Li, L.; Raji, A.-R.O.; Tour, J.M. Graphene-wrapped MnO_2-graphene nanoribbons as anode materials for high-performance lithium ion batteries. *Adv. Mater.* **2013**, *25*, 6298–6302. [CrossRef] [PubMed]
217. Yousefi, T.; Golikand, A.N.; Mashhadizadeh, M.H.; Aghazadeh, M. Facile synthesis of α-MnO_2 one-dimensional (1D) nanostructure and energy storage ability studies. *J. Solid State Chem.* **2012**, *190*, 202–207. [CrossRef]
218. Liu, Y.; Yan, D.; Li, Y.; Wu, Z.; Zhuo, R.; Li, S.; Feng, J.; Wang, J.; Yan, P.; Geng, Z. Manganese dioxide nanosheet arrays grown on graphene oxide as an advanced electrode material for supercapacitors. *Electrochim. Acta* **2014**, *117*, 528–533. [CrossRef]
219. Yang, Y.; Ma, G.; Huang, J.; Nan, J.; Zhen, S.; Wang, Y.; Li, A. Hollow MnO_2 spheres/porous reduced graphene oxide as a cathode host for high-performance lithium-sulfur batteries. *J. Solid State Chem.* **2020**, *286*, 121297. [CrossRef]
220. Majid, S.R. Green synthesis of in situ electrodeposited rGO/MnO_2 nanocomposite for high energy density supercapacitors. *Sci. Rep.* **2015**, *5*, 16195. [CrossRef]
221. Sawangphruk, M.; Srimuk, P.; Chiochan, P.; Krittayavathananon, A.; Luanwuthi, S.; Limtrakul, J. High-performance supercapacitor of manganese oxide/reduced graphene oxide nanocomposite coated on flexible carbon fiber paper. *Carbon* **2013**, *60*, 109–116. [CrossRef]
222. Gund, G.S.; Dubal, D.P.; Patil, B.H.; Shinde, S.S.; Lokhande, C.D. Enhanced activity of chemically synthesized hybrid graphene oxide/Mn_3O_4 composite for high performance supercapacitors. *Electrochim. Acta* **2013**, *92*, 205–215. [CrossRef]
223. Wang, L.; Wang, D.-L. Preparation and electrochemical characterization of MnOOH nanowire–graphene oxide. *Electrochim. Acta* **2011**, *56*, 5010–5015. [CrossRef]
224. Chen, T.; Zhiu, Y.; Zhang, J.; Cao, Y. Two-dimensional MnO_2/reduced graphene oxide nanosheet as a high-capacity and high-rate cathode materials for lithium-ion batteries. *Int. J. Electrochem. Sci.* **2018**, *13*, 8575–8588. [CrossRef]
225. Lee, S.-W.; Lee, C.-W.; Yoon, S.-B.; Kim, M.-S.; Jeong, J.H.; Nam, K.-W.; Roh, K.C.; Kim, K.-B. Superior electrochemical properties of manganese dioxide/reduced graphene oxide nanocomposites as anode materials for high-performance lithium ion batteries. *J. Power Sources* **2016**, *312*, 207–215. [CrossRef]
226. Devi, P.; Bansod, B.; Kaur, M.; Bagchi, S.; Nayak, M.K. Co-electrodeposited rGO/MnO_2 nanohybrid for arsenite detection in water by stripping voltammetry. *Sensors Actuators B Chem.* **2016**, *237*, 652–659. [CrossRef]
227. Zhang, L.; Liu, H.; Ruan, H.; Su, Y.; Hu, R.; Tian, L.; Hu, Z.; Li, J. Fabrication of β-MnO_2/rGO composite and its electrochemical properties. *Int. J. Electrochem. Sci.* **2016**, *11*, 10815–10826. [CrossRef]
228. Liu, H. Preparation of (MnO_2/RGO)/$Li_7La_3Zr_2O_{12}$/$LiCoO_2$ Solid State Lithium Ion Batteries and Theirs Electrochemical Performance. *Int. J. Electrochem. Sci.* **2017**, *12*, 11479–11486. [CrossRef]
229. Ali, G.A.; Yusoff, M.; Algarni, H.; Chong, K.F. One-step electrosynthesis of MnO_2/rGO nanocomposite and its enhanced electrochemical performance. *Ceram. Int.* **2018**, *44*, 7799–7807. [CrossRef]
230. Liu, H.D.; Hu, Z.L.; Su, Y.Y.; Ruan, H.B.; Hu, R.; Zhang, L. MnO_2 nanorods/3D-rGO composite as high performance anode materials for Li-ion batteries. *Appl. Surf. Sci.* **2017**, *392*, 777–784. [CrossRef]
231. Cao, Y.; Lin, X.; Zhang, C.; Yang, C.; Zhang, Q.; Hu, W.; Zheng, M.; Dong, Q. MnO_2 nanoflakes anchored on reduced graphene oxide nanosheets as high performance anode materials for lithium-ion batteries. *RSC Adv.* **2014**, *4*, 30150–30155. [CrossRef]

232. Chae, C.; Kim, K.W.; Yun, Y.J.; Lee, D.; Moon, J.; Choi, Y.; Lee, S.S.; Choi, S.; Jeong, S. Polyethylenimine-mediated electrostatic assembly of MnO_2 nanorods on graphene oxides for use as anodes in lithium-ion batteries. *ACS Appl. Mater. Interfaces* **2016**, *8*, 11499–11506. [CrossRef]
233. Zhang, Y.; Liu, H.; Zhu, Z.; Wong, K.; Mi, R.; Mei, J.; Lau, W. A green hydrothermal approach for the preparation of graphene/α-MnO_2 3D network as anode for lithium ion battery. *Electrochim. Acta* **2013**, *108*, 465–471. [CrossRef]
234. Ma, Z.; Zhao, T. Reduced graphene oxide anchored with MnO_2 nanorods as anode for high rate and long cycle Lithium ion batteries. *Electrochim. Acta* **2016**, *201*, 165–171. [CrossRef]
235. Li, Y.; Ye, D.; Liu, W.; Shi, B.; Guo, R.; Pei, H.; Xie, J. A three-dimensional core-shell nanostructured composite of polypyrrole wrapped MnO_2/reduced graphene oxide/carbon nanotube for high performance lithium ion batteries. *J. Colloid Interface Sci.* **2017**, *493*, 241–248. [CrossRef] [PubMed]
236. Li, S.; Zhao, Y.; Liu, Z.; Yang, L.; Zhang, J.; Wang, M.; Che, R. Flexible graphene-wrapped carbon nanotube/graphene@MnO_2 3D multilevel porous film for high-performance lithium-ion batteries. *Small* **2018**, *14*, 1801007. [CrossRef] [PubMed]
237. Kim, S.J.; Yun, Y.J.; Kim, K.W.; Chae, C.; Jeong, S.; Kang, Y.; Choi, S.-Y.; Lee, S.S.; Choi, S. Superior lithium storage performance using sequentially stacked MnO_2/reduced graphene oxide composite electrodes. *ChemSusChem* **2015**, *8*, 1484–1491. [CrossRef] [PubMed]
238. Li, Y.; Ye, D.; Shi, B.; Liu, W.; Guo, R.; Pei, H.; Xie, J. Free-standing reduced graphene oxide/MnO_2–reduced graphene oxide–carbon nanotube nanocomposite flexible membrane as an anode for improving lithium-ion batteries. *Phys. Chem. Chem. Phys.* **2017**, *19*, 7498–7505. [CrossRef] [PubMed]
239. Li, X.; Xu, X.; Xia, F.; Bu, L.; Qiu, H.; Chen, M.; Zhang, L.; Gao, J. Electrochemically active MnO_2/RGO nanocomposites using Mn powder as the reducing agent of GO and the MnO_2 precursor. *Electrochim. Acta* **2014**, *130*, 305–313. [CrossRef]
240. Han, G.; Liu, Y.; Zhang, L.; Kan, E.; Zhang, S.; Tang, J.; Tang, W. MnO_2 nanorods intercalating graphene oxide/polyaniline ternary composites for robust high-performance supercapacitors. *Sci. Rep.* **2015**, *4*, 4824. [CrossRef]
241. Chan, P.Y.; Rusi, R.; Majid, S. RGO-wrapped MnO_2 composite electrode for supercapacitor application. *Solid State Ionics* **2014**, *262*, 226–229. [CrossRef]
242. Zhu, S.; Zhang, H.; Chen, P.; Nie, L.H.; Li, C.-H.; Li, S.K. Self-assembled three-dimensional hierarchical graphene hybrid hydrogels with ultrathin β-MnO_2 nanobelts for high performance supercapacitors. *J. Mater. Chem. A* **2015**, *3*, 1540–1548. [CrossRef]
243. Chen, S.; Zhu, J.W.; Wu, X.D.; Han, Q.F.; Wang, X. Graphene oxide-MnO_2 nanocomposites for supercapacitors. *ACS Nano* **2010**, *4*, 2822–2830. [CrossRef]
244. Lu, L.; Xu, S.; An, J.; Yan, S. Electrochemical performance of CNTs/RGO/MnO_2 composite material for supercapacitor. *Nanomater. Nanotechnol.* **2016**, *6*, 1–7. [CrossRef]
245. Hareesh, K.; Shateesh, B.; Joshi, R.P.; Williams, J.F.; Phase, D.M.; Haram, S.K.; Dhole, S.D. Ultra high stable supercapacitance performance of conducting polymer coated MnO_2 nanorods/rGO nanocomposites. *RSC Adv.* **2017**, *7*, 20027–20036. [CrossRef]
246. Seredych, M.; Bandosz, T.J. Evaluation of GO/MnO_2 composites as supercapacitors in neutral electrolytes: Role of graphite oxide oxidation level. *J. Mater. Chem.* **2012**, *22*, 23525–23533. [CrossRef]
247. Pang, M.; Long, G.; Jiang, S.; Ji, Y.; Han, W.; Wang, B.; Liu, X.; Xi, Y. Rapid synthesis of graphene/amorphous α-MnO_2 composite with enhanced electrochemical performance for electrochemical capacitor. *Mater. Sci. Eng. B* **2015**, *194*, 41–47. [CrossRef]
248. Miniach, E.; Śliwak, A.; Moyseowicz, A.; Fernández-Garcia, L.; González, Z.; Granda, M.; Menendez, R.; Gryglewicz, G. MnO_2/thermally reduced graphene oxide composites for high-voltage asymmetric supercapacitors. *Electrochim. Acta* **2017**, *240*, 53–62. [CrossRef]
249. Chen, J.; Wang, Y.; Cao, J.; Liu, Y.; Ouyang, J.-H.; Jia, D.; Zhou, Y. Flexible and solid-state asymmetric supercapacitor based on ternary graphene/MnO_2/carbon black hybrid film with high power performance. *Electrochim. Acta* **2015**, *182*, 861–870. [CrossRef]
250. Zardkhoshoui, A.M.; Davarani, S.S.H. Flexible asymmetric supercapacitors based on CuO@MnO_2-rGO and MoS_2-rGO with ultrahigh energy density. *J. Electroanal. Chem.* **2018**, *827*, 221–229. [CrossRef]

251. Wang, K.; Li, L.; Xue, W.; Zhou, S.; Lan, Y.; Zhang, H.; Sui, Z. Electrodeposition synthesis of PANI/MnO_2/graphene composite materials and its electrochemical performance. *Int. J. Electrochem. Sci.* **2017**, *12*, 8306–8314.
252. Dong, W.; Meng, L.; Hong, X.; Liu, S.; Shen, D.; Xia, Y.; Yang, S. MnO_2/rGO/CNTs framework as a sulfur host for high-performance Li-S batteries. *Molecules* **2020**, *25*, 1989. [CrossRef]
253. Jie, G.; Michael, A.L.; Hector, D.A. Sponge like nanosized Mn_3O_4 as a high-capacity anode material for rechargeable lithium batteries. *Chem. Mater.* **2011**, *23*, 3223–3227.
254. Su, Q.; Wang, S.; Du, G.; Xu, B.; Ma, S.; Shang, L. Microstructure evolution and conversion mechanism of Mn_3O_4 under electrochemical cyclings. *J. Phys. Chem. C* **2018**, *122*, 2475–2480. [CrossRef]
255. Wang, H.; Cui, L.-F.; Yang, Y.; Casalongue, H.S.; Robinson, J.T.; Liang, Y.; Cui, Y.; Dai, H. Mn_3O_4−graphene hybrid as a high-capacity anode material for lithium-ion batteries. *J. Am. Chem. Soc.* **2010**, *132*, 13978–13980. [CrossRef] [PubMed]
256. Zhou, Y.; Guo, L.; Shi, W.; Zou, X.; Xiang, B.; Xing, S. Rapid production of Mn_3O_4/rGO as an efficient electrode material for supercapacitor by flame plasma. *Materials* **2018**, *11*, 881. [CrossRef] [PubMed]
257. Wang, Y. Coprecipitated 3D nanostructured graphene oxide-Mn_3O_4 hybrid as anode for lithium-ion batteries. *J. Mater. Res.* **2015**, *30*, 484–492. [CrossRef]
258. Li, Q.; Li, Y.; Fulari, A.; Ghodake, G.; Kim, D.; Lohar, G.M. Performance of chemically synthesized Mn_3O_4/rGO nanocomposite for electrochemical supercapacitor: A cost-effective high-performance electrode. *Nanotechnology* **2020**, *31*, 415403. [CrossRef]
259. Wang, L.; Ouyang, Y.; Jiao, X.; Xia, X.; Lei, W.; Hao, Q. Polyaniline-assisted growth of MnO_2 ultrathin nanosheets on graphene and porous graphene for asymmetric supercapacitor with enhanced energy density. *Chem. Eng. J.* **2018**, *334*, 1–9. [CrossRef]
260. Liu, M.; Shi, M.; Lu, W.; Zhu, D.; Li, L.; Gan, L. Core–shell reduced graphene oxide/MnO_x@carbon hollow nanospheres for high performance supercapacitor electrodes. *Chem. Eng. J.* **2017**, *313*, 518–526. [CrossRef]
261. Wang, Y.; Lai, W.H.; Wang, N. A reduced graphene oxide/mixed-valent manganese oxides composite electrode for tailorable and surface mountable supercapacitors with high capacitance and super-long life. *Energy Environ. Sci.* **2017**, *10*, 941–949. [CrossRef]
262. Seong, C.-Y.; Park, S.-K.; Bae, Y.; Yoo, S.; Piao, Y. An acid-treated reduced graphene oxide/Mn_3O_4 nanorod nanocomposite as an enhanced anode material for lithium ion batteries. *RSC Adv.* **2017**, *7*, 37502–37507. [CrossRef]
263. Wang, J.; Guan, C.; Feng, G.; Ke, Q.; Huang, X.; Wang, J. Flexible asymmetric supercapacitor based on structure-optimized Mn_3O_4/reduced Graphene oxide nanohybrid paper with high energy and power density. *Adv. Funct. Mater.* **2015**, *25*, 7291–7299. [CrossRef]
264. Gu, Y.; Wu, J.; Wang, X.; Liu, W.; Yan, S. Producing symbiotic reduced graphene oxide/Mn_3O_4 nanocoposites directly from converting graphite for high-performance supercapacitor electrodes. *ACS Omega* **2020**, *5*, 18975–18986. [CrossRef]
265. Li, Y.; Gai, T.; Shao, L.; Tang, H.; Li, R.; Yang, S.; Wang, S.; Wu, Q.; Ren, Y. Synthesis of sandwich-like Mn_3O_4@reduced graphene oxide nano-composites via modified Hummers' method and its application as uranyl adsorbents. *Heliyon* **2019**, *5*, e01972. [CrossRef] [PubMed]
266. Raj, B.G.S.; Ramprasad, R.N.R.; Asiri, A.M.; Wu, J.J.; Anandan, S. Ultrasound assisted synthesis of Mn_3O_4 nanoparticles anchored graphene nanosheets for supercapacitor applications. *Electrochim. Acta* **2015**, *156*, 127–137. [CrossRef]
267. Park, G.; Bartolome, L.; Lee, K.G.; Lee, S.J.; Kim, D.H.; Park, T.J. One-step sonochemical synthesis of a graphene oxide-manganese oxide nanocomposite for catalytic glycolysis of polu(ethylene terephthalate). *Nanoscale* **2012**, *4*, 3879–3885. [CrossRef] [PubMed]
268. Ayhan, I.A.; Meduri, P.; Oh, H.; Bhimanapati, G.R.; Li, Q.; Yang, G.; Robinson, J.A.; Wang, Q. Effect of Mn_3O_4 nanoparticle composition and distribution on graphene as a potential hybrid anode material for lithium-ion batteries. *RSC Adv.* **2016**, *6*, 33022–33030. [CrossRef]
269. Park, S.-H.; Lee, W.-J. Hierarchically mesoporous CuO/carbon nanofiber coaxial shell-core nanowires for lithium ion batteries. *Sci. Rep.* **2015**, *5*, 9754. [CrossRef] [PubMed]
270. Rosaiah, P.; Zhu, J.; Shaik, D.P.M.D.; Hussain, O.M.; Qiu, Y.; Zhao, L. Reduced graphene oxide/Mn_3O_4 nanocomposite electrodes with enhanced electrochemical performance for energy storage applications. *J. Electroanal. Chem.* **2017**, *794*, 78–85. [CrossRef]

271. Nithya, C.; Vishnuprakash, P.; Gopukumar, S. A Mn_3O_4 nanospheres@rGO architecture with capacitive effects on high potassium storage capability. *Nanoscale Adv.* **2019**, *1*, 4347–4358. [CrossRef]
272. Nam, I.; Kim, N.D.; Kim, G.-P.; Park, J.; Yi, J. One step preparation of Mn_3O_4/graphene composites for use as an anode in Li ion batteries. *J. Power Sources* **2013**, *244*, 56–62. [CrossRef]
273. Luo, Y.; Fan, S.; Hao, N.; Zhong, S.; Liu, W. An ultrasound-assisted approach to synthesize Mn_3O_4/RGO hybrids with high capability for lithium ion batteries. *Dalton Trans.* **2014**, *43*, 15317–15320. [CrossRef]
274. Li, S.; Yu, L.-L.; Shi, Y.-T.; Fan, J.; Li, R.-B.; Fan, G.-D.; Xu, W.-L.; Zhao, J.-T. Greatly Enhanced Faradic Capacities of 3D Porous Mn_3O_4/G Composites as Lithium-Ion Anodes and Supercapacitors by C–O–Mn Bonding. *ACS Appl. Mater. Interfaces* **2019**, *11*, 10178–10188. [CrossRef]
275. Zhang, R.; Wang, D.; Qin, L.-C.; Wen, G.; Pan, H.; Zhang, Y.; Tian, N.; Zhou, Y.; Huang, X. $MnCO_3$/Mn_3O_4/reduced graphene oxide ternary anode materials for lithium-ion batteries: Facile green synthesis and enhanced electrochemical performance. *J. Mater. Chem. A* **2017**, *5*, 17001–17011. [CrossRef]
276. Shah, H.U.; Wang, F.; Javed, M.S.; Shaheen, N.; Saleem, M.; Li, Y. Hydrothermal synthesis of reduced graphene oxide – Mn_3O_4 nanocomposite as an efficient electrode material for supercapacitors. *Ceram. Int.* **2018**, *44*, 3580–3584. [CrossRef]
277. Varghese, S.P.; Babu, B.; Prasannachandran, R.; Antony, R.; Shaijumon, M.M. Enhanced electrochemical properties of Mn_3O_4/graphene nanocomposite as efficient anode material for lithium ion batteries. *J. Alloys Compd.* **2019**, *780*, 588–596. [CrossRef]
278. Petnikota, S.; Srikanth, V.V.S.S.; Nithyadharseni, P.; Reddy, M.V.; Adams, S.; Chowdari, B.V.R. Sustainable graphenothermal reduction chemistry to obtain MnO nanonetwork supported exfoliated graphene oxide composite and its electrochemical characteristics. *ACS Sustain. Chem. Eng.* **2015**, *3*, 3205–3213. [CrossRef]
279. Yuan, T.; Xu, B.; Sun, W.; Xiang, B.; Li, Y.; Yan, M.; Xu, B.; Dou, S. Ever-Increasing Pseudocapacitance in RGO-MnO-RGO Sandwich Nanostructures for Ultrahigh-Rate Lithium Storage. *Adv. Funct. Mater.* **2016**, *26*, 2198–2206. [CrossRef]
280. Cheng, F.; Zhou, X.; Yang, J.; Sun, A.; Wang, H.; Tang, J. MnO nanoparticles sandwiched within 3D graphene-based hierarchical architecture for efficient lithium storage. *Inorg. Chem.* **2019**, *58*, 3329–3337. [CrossRef]
281. Wang, Y.; Wu, H.; Liu, Z.; Zhao, H.; Liu, H.; Zhang, Y. Bottom-up construction of reduced-graphene-oxide-anchored MnO with an nitrogen-doped carbon coating for synergistically improving lithium-ion storage. *Inorg. Chem.* **2018**, *57*, 13693–13701. [CrossRef]
282. Hsieh, C.-T.; Lin, C.-Y.; Lin, J.-Y. High reversibility of Li intercalation and de-intercalation in MnO-attached graphene anodes for Li-ion batteries. *Electrochim. Acta* **2011**, *56*, 8861–8867. [CrossRef]
283. Zhang, K.; Han, P.; Gu, L.; Zhang, L.; Liu, Z.; Kong, Q.; Zhang, C.; Dong, S.; Zhang, Z.; Yao, J.; et al. Synthesis of nitrogen-doped MnO/graphene nanosheets hybrid material for lithium ion batteries. *ACS Appl. Mater. Interfaces* **2012**, *4*, 658–664. [CrossRef]
284. Qiu, D.; Ma, L.; Zheng, M.; Lin, Z.; Zhao, B.; Wen, Z.; Hu, Z.; Pu, L.; Shi, Y. MnO nanoparticles anchored on graphene nanosheets via in situ carbothermal reduction as high-performance anode materials for lithium-ion batteries. *Mater. Lett.* **2012**, *84*, 9–12. [CrossRef]
285. Liu, S.-Y.; Xie, J.; Zheng, Y.-X.; Cao, G.-S.; Zhu, T.-J.; Zhao, X. Nanocrystal manganese oxide (Mn_3O_4, MnO) anchored on graphite nanosheet with improved electrochemical Li-storage properties. *Electrochim. Acta* **2012**, *66*, 271–278. [CrossRef]
286. Mai, Y.; Zhang, D.; Qiao, Y.; Gu, C.; Wang, X.; Tu, J. MnO/reduced graphene oxide sheet hybrid as an anode for Li-ion batteries with enhanced lithium storage performance. *J. Power Sources* **2012**, *216*, 201–207. [CrossRef]
287. Zhang, S.; Zhu, L.; Song, H.; Chen, X.; Zhou, J. Enhanced electrochemical performance of MnO nanowire/graphene composite during cycling as the anode material for lithium-ion batteries. *Nano Energy* **2014**, *10*, 172–180. [CrossRef]
288. Wu, T.; Tu, F.; Liu, S.; Zhuang, S.; Jin, G.; Pan, C. MnO nanorods on graphene as an anode material for high capacity lithium ion batteries. *J. Mater. Sci.* **2013**, *49*, 1861–1867. [CrossRef]
289. Zang, J.; Qian, H.; Wei, Z.; Cao, Y.; Zheng, M.; Dong, Q. Reduced graphene oxide supported MnO nanoparticles with excellent lithium storage performance. *Electrochim. Acta* **2014**, *118*, 112–117. [CrossRef]
290. Jiang, X.; Zhu, X.; Liu, X.; Xiao, L.; Ai, X.; Yang, H.; Cao, Y. Nanospherical-like manganese monoxide/reduced graphene oxide composite Synthesized by rlectron beam radiation as anode Material for high-performance lithium-ion batteries. *Electrochim. Acta* **2016**, *196*, 431–439. [CrossRef]

291. Auborn, J.J.; Barberio, Y.L. Lithium intercalation cells without metallic lithium: $MoO_2/LiCoO_2$ and $WO_2/LiCoO_2$. *J. Electrochem. Soc.* **1987**, *134*, 638–640. [CrossRef]
292. Rogers, D.B.; Shannon, R.D.; Sleight, A.W.; Gillson, J.L. Crystal chemistry of metal dioxides with rutile-related structures. *Inorg. Chem.* **1969**, *8*, 841–849. [CrossRef]
293. Shi, Y.; Guo, B.; Corr, S.A.; Shi, Q.; Hu, Y.-S.; Heier, K.R.; Chen, L.; Seshadri, R.; Stucky, G.D. Ordered mesoporous metallic MoO_2 materials with highly reversible lithium storage capacity. *Nano Lett.* **2009**, *9*, 4215–4220. [CrossRef]
294. Wang, Y.; Huang, Z. A new approach to synthesize MoO_2@C for high-rate lithium ion batteries. *J. Mater. Chem. A* **2015**, *3*, 21314–21320. [CrossRef]
295. Sen, U.K.; Shaligram, A.; Mitra, S. Intercalation anode material for lithium ion battery based on molybdenum dioxide. *ACS Appl. Mater. Interfaces* **2014**, *6*, 14311–14319. [CrossRef] [PubMed]
296. Zhang, H.-J.; Wu, T.-H.; Wang, K.-X.; Wu, X.-Y.; Chen, X.-T.; Jiang, Y.-M.; Wei, X.; Chen, J.-S. Uniform hierarchical MoO_2/carbon spheres with high cycling performance for lithium ion batteries. *J. Mater. Chem. A* **2013**, *1*, 12038–12043. [CrossRef]
297. Petnikota, S.; Teo, K.W.; Chen, L.; Sim, A.; Marka, S.K.; Reddy, M.V.; Srikanth, V.V.S.S.; Adams, S.; Chowdari, B. Exfoliated graphene oxide/MoO_2 composites as anode materials in Lithium-ion batteries: An insight into intercalation of Li and conversion mechanism of MoO_2. *ACS Appl. Mater. Interfaces* **2016**, *8*, 10884–10896. [CrossRef] [PubMed]
298. Hu, S.; Yin, F.; Uchaker, E.; Chen, W.; Zhang, M.; Zhou, J.; Qi, Y.; Cao, G. Facile and green preparation for the formation of MoO_2-GO composites as anode material for lithium-ion batteries. *J. Phys. Chem. C* **2014**, *118*, 24890–24897. [CrossRef]
299. Qian, Y.; Lu, S.; Gao, F. Preparation of MoO_2/graphene composite as electrode material for supercapacitors. *J. Mater. Sci.* **2011**, *46*, 3517–3522. [CrossRef]
300. Huang, J.; Xu, Z.; Cao, L.; Zhang, Q.; Ouyang, H.; Li, J. Tailoring MoO_2/graphene oxide nanostructures for stable, high-density sodium-ion battery anodes. *Energy Technol.* **2015**, *3*, 1108–1114. [CrossRef]
301. Tang, W.; Peng, C.X.; Nai, C.T.; Su, J.; Liu, Y.P.; Reddy, M.V.V.; Lin, M.; Loh, K.P. Ultrahigh capacity due to multi-electron conversion reaction in reduced graphene oxide-wrapped MoO_2 porous nanobelts. *Small* **2015**, *11*, 2446–2453. [CrossRef]
302. Zhu, Y.; Xu, X.; Chen, G.; Zhong, Y.; Cai, R.; Li, L.; Shao, Z. Surfactant-free self-assembly of reduced graphite oxide-MoO2 nanobelt composites used as electrode for lithium-ion batteries. *Electrochim. Acta* **2016**, *211*, 972–981. [CrossRef]
303. Ju, P.; Zhu, Z.; Shao, X.; Wang, S.; Zhao, C.; Qian, X.; Zhao, C. 3D walnut-shaped TiO_2/RGO/MoO_2@Mo electrode exhibiting extraordinary supercapacitor performance. *J. Mater. Chem. A* **2017**, *5*, 18777–18785. [CrossRef]
304. Hwang, J.; Yoon, D.; Kweon, B.; Chang, W.; Kim, J. A simple, one-pot synthesis of molybdenum oxide-reduced graphene oxide composites in supercritical methanol and their electrochemical performance. *RSC Adv.* **2016**, *6*, 108298–108309. [CrossRef]
305. Xu, Z.; Yao, K.; Fu, H.; Shen, X.; Duan, X.; Cao, L.; Huang, J.; Wang, H. Constructing MoO_2 porous architectures using graphene oxide flexible supports for lithium io battery anodes. *Glob. Chall.* **2017**, *1*, 7. [CrossRef]
306. Wang, S.; Liu, B.; Zhi, G.; Xu, G.; Wang, Q.; Zhang, J. 2D layered mesoporous MoO_2/rGO composites for high performance anode materials in lithium-ion battery. *Microporous Mesoporous Mater.* **2017**, *246*, 14–23. [CrossRef]
307. Chen, X.; Liu, R.; Zeng, L.; Huang, X.; Fang, Y.; Liu, J.; Xu, Y.; Chen, Q.; Wei, M.; Qian, Q. Preparation of hierarchical MoO_2@RGO composite and its application for high rate performance lithium-ion batteries. *Mater. Lett.* **2018**, *212*, 198–201. [CrossRef]
308. Li, F.; Li, L.; Wang, W.; Gao, J. A new facile approach to prepare reduced graphene oxide and MoO_2/reduced graphene oxide as electrode materials for oxygen reduction reactions. *J. Colloid Interface Sci.* **2018**, *519*, 194–202. [CrossRef]
309. Liu, C.-L.; Luo, S.-H.; Huang, H.-B.; Zhai, Y.-C.; Wang, Z.-W. Direct growth of MoO_2/reduced graphene oxide hollow sphere composites as advanced anode materials for potassium-ion batteries. *ChemSusChem* **2019**, *12*, 873–880. [CrossRef]

310. Li, M.; Zhu, Y.; Ji, X.; Cheng, S. Facile synthesis of MoO_2/Mo-GO with high initial columbic efficiency and enhanced lithiation ability. *Mater. Lett.* **2019**, *254*, 332–335. [CrossRef]
311. Devina, W.; Hwang, J.; Kim, J. Synthesis of MoO_2/Mo_2C/rGO composite in supercritical fluid and its enhanced cycling stability in Li-ion batteries. *Chem. Eng. J.* **2018**, *345*, 1–12. [CrossRef]
312. Zhang, R.; Tang, Z.; Wang, H.; Sun, D.; Tang, Y.; Xie, Z. The fabrication of hierarchical MoO_2@MoS_2/rGO composite as high reversible anode material for lithium ion batteries. *Electrochim. Acta* **2020**, *364*, 136996. [CrossRef]
313. Xia, F.; Hu, X.; Sun, Y.; Luo, W.; Han, J. Layer-by-layer assembled MoO_2–graphene thin film as a high-capacity and binder-free anode for lithium-ion batteries. *Nanoscale* **2012**, *4*, 4707. [CrossRef]
314. Xu, Y.; Yi, R.; Yuan, B.; Wu, X.; Dunwell, M.; Lin, Q.; Fei, L.; Deng, S.; Andersen, P.; Wang, D.; et al. High capacity MoO_2/graphite oxide composite anode for lithium-ion batteries. *J. Phys. Chem. Lett.* **2012**, *3*, 309–314. [CrossRef]
315. Tang, Q.; Shan, Z.; Wang, L.; Qin, X. MoO_2–graphene nanocomposite as anode material for lithium-ion batteries. *Electrochim. Acta* **2012**, *79*, 148–153. [CrossRef]
316. Seng, K.H.; Du, G.D.; Li, L.; Chen, Z.X.; Liu, H.K.; Guo, Z. Facile synthesis of graphene–molybdenum dioxide and its lithium storage properties. *J. Mater. Chem.* **2012**, *22*, 16072. [CrossRef]
317. Guo, L.; Wang, Y. Standing carbon-coated molybdenum dioxide nanosheets on graphene: Morphology evolution and lithium ion storage properties. *J. Mater. Chem. A* **2015**, *3*, 4706–4715. [CrossRef]
318. Bhaskar, A.; Deepa, M.; Rao, T.; Varadaraju, U. Enhanced nanoscale conduction capability of a MoO_2/graphene composite for high performance anodes in lithium ion batteries. *J. Power Sources* **2012**, *216*, 169–178. [CrossRef]
319. Wang, X.; Xiao, Y.; Wang, J.; Sun, L.; Cao, M. Facile fabrication of molybdenum dioxide/nitrogen-doped graphene hybrid as high performance anode material for lithium ion batteries. *J. Power Sources* **2015**, *274*, 142–148. [CrossRef]
320. Feng, Y.; Liu, H. One-dimensional architecture with reduced graphene oxide supporting ultrathin MoO_2 nanosheets as high performance anodes for lithium-ion batteries. *Nanotechnology* **2019**, *30*, 315602. [CrossRef] [PubMed]
321. Li, Y.; Luo, J.; Hu, X.; Wang, X.; Liang, J.-C.; Yu, K. Fabrication of TiO_2 hollow nanostructures and their application in lithium ion batteries. *J. Alloys Compd.* **2015**, *651*, 685–689. [CrossRef]
322. Zhang, X.; Kumar, P.S.; Aravindan, V.; Liu, H.H.; Sundaramurthy, J.; Mhaisalkar, S.G.; Duong, H.M.; Ramakrishna, S.; Madhavi, S. Electrospun TiO_2-graphene composite nanofibers as a highly durable insertion anode for lithium ion batteries. *J. Phys. Chem. C* **2012**, *116*, 14780–14788. [CrossRef]
323. El-Deen, S.S.; Hashem, A.M.; Ghany, A.E.A.; Indris, S.; Ehrenberg, H.; Mauger, A.; Julien, C.M. Anatase TiO_2 nanoparticles for lithium-ion batteries. *Ionics* **2018**, *24*, 2925–2934. [CrossRef]
324. Wu, F.; Wang, Z.; Li, X.; Guo, H. Simple preparation of petal-like TiO_2 nanosheets as anode materials for lithium-ion batteries. *Ceram. Int.* **2014**, *40*, 16805–16810. [CrossRef]
325. Kucinskis, G.; Bajars, G.; Kleperis, J. Graphene in lithium ion battery cathode materials: A review. *J. Power Sources* **2013**, *240*, 66–79. [CrossRef]
326. Li, B.; Yuan, Z.; Xu, Y.; Liu, J. N-doped graphene as an efficient electrocatalyst for lithium-thionyl chloride batteries. *Appl. Catal. A Gen.* **2016**, *523*, 241–246. [CrossRef]
327. Zhen, M.; Zhu, X.; Zhang, X.; Zhou, Z.; Liu, L. Reduced graphene oxide-supported TiO_2 fiber bundles with mesostructures as anode materials for lithium-ion batteries. *Chem. A Eur. J.* **2015**, *21*, 14454–14459. [CrossRef] [PubMed]
328. He, L.; Ma, R.; Du, N.; Ren, J.; Wong, T.; Li, Y.Y.; Lee, S.T. Growth of TiO_2 nanorod arrays on reduced graphene oxide with enhanced lithium-ion storage. *J. Mater. Chem.* **2012**, *22*, 19061–19066. [CrossRef]
329. Li, J.; Huang, J.; Li, J.; Cao, L.; Qi, H.; Cheng, Y.; Xi, Q.; Dang, H. Improved Li-ion diffusion process in TiO_2/rGO anode for lithium-ion battery. *J. Alloys Compd.* **2017**, *727*, 998–1005. [CrossRef]
330. Zhang, Z.; Zhang, L.; Li, W.; Yu, A.; Wu, P. Carbon-coated mesoporous TiO_2 nanocrystals grown on graphene for lithium-ion batteries. *ACS Appl. Mater. Interfaces* **2015**, *7*, 10395–10400. [CrossRef] [PubMed]
331. Liu, Y.; Yang, Y. Recent progress of TiO_2-based anodes for Li ion batteries. *J. Nanomater.* **2016**, *2016*, 1–15. [CrossRef]
332. Etacheri, V.; Yourey, J.E.; Bartlett, B.M. Chemically bonded TiO_2–bronze nanosheet/reduced graphene oxide hybrid for high-power lithium-ion batteries. *ACS Nano* **2014**, *8*, 1491–1499. [CrossRef]

333. Zhao, X.; Liu, H.; Ding, M.; Feng, Y. In-situ constructing of hollow TiO_2@rGO hybrid spheres as high-rate and long-life anode materials for lithium-ion batteries. *Ceram. Int.* **2019**, *45*, 12476–12483. [CrossRef]
334. Dong, L.; Li, M.; Zhao, M.; Feng, J.; Han, Y.; Deng, J.; Li, X.; Li, D.; Sun, X. Hydrothermal synthesis of mixed crystal phases TiO_2–reduced graphene oxide nanocomposites with small particle size for lithium ion batteries. *Int. J. Hydrogen Energy* **2014**, *39*, 16116–16122. [CrossRef]
335. Yang, M.-C.; Lee, Y.-Y.; Xu, B.; Powers, K.; Meng, Y.S. TiO_2 flakes as anode materials for Li-ion-batteries. *J. Power Sources* **2012**, *207*, 166–172. [CrossRef]
336. Fu, Y.-X.; Dai, Y.; Pei, X.-Y.; Lyu, S.-S.; Heng, Y.; Mo, D.-C. TiO_2 nanorods anchor on reduced graphene oxide (R-TiO_2/rGO) composite as anode for high performance lithium-ion batteries. *Appl. Surf. Sci.* **2019**, *497*, 143553. [CrossRef]
337. Li, D.; Shi, D.; Liu, Z.; Liu, H.K.; Guo, Z. TiO_2 nanoparticles on nitrogen-doped graphene as anode material for lithium ion batteries. *J. Nanopart. Res.* **2013**, *15*, 1674. [CrossRef]
338. Geng, C.; Yu, J.; Shi, F. Synthesis and electrochemical performance of TiO_2/rGO composites with different layers of graphene oxide as anode materials for lithium-ion battery. *IOP Conf. Ser. Mater. Sci. Eng.* **2019**, *585*, 012090. [CrossRef]
339. Mondal, A.; Maiti, S.; Singha, K.; Mahanty, S.; Panda, A.B. TiO_2-rGO nanocomposite hollow spheres: Large scale synthesis and application as an efficient anode material for lithium-ion batteries. *J. Mater. Chem. A* **2017**, *5*, 23853–23862. [CrossRef]
340. Shen, T.; Zhou, X.; Cao, H.; Zheng, C.; Liu, Z. TiO_2(B)–CNT–graphene ternary composite anode material for lithium ion batteries. *RSC Adv.* **2015**, *5*, 22449–22454. [CrossRef]
341. Fang, Y.; Hu, R.; Liu, B.; Zhang, Y.; Zhu, K.; Yan, J.; Ye, K.; Cheng, K.; Wang, G.; Cao, D. MXene-derived TiO_2/reduced graphene oxide composite with an enhanced capacitive capacity for Li-ion and K-ion batteries. *J. Mater. Chem. A* **2019**, *7*, 5363–5372. [CrossRef]
342. Farooq, U.; Ahmed, F.; Pervez, S.A.; Rehman, S.; Pope, M.A.; Fichtner, M.; Roberts, E.P. A stable TiO2–graphene nanocomposite anode with high rate capability for lithium-ion batteries. *RSC Adv.* **2020**, *10*, 29975–29982. [CrossRef]
343. Subaşı, Y.; Somer, M.; Yağcı, M.B.; Slabon, A.; Afyon, S. Surface modified TiO_2/reduced graphite oxide nanocomposite anodes for lithium ion batteries. *J. Solid State Electrochem.* **2020**, *24*, 1085–1093. [CrossRef]
344. Williams, G.; Seger, B.; Kamat, P.V. TiO_2-graphene nanocomposites. UV-assisted photocatalytic reduction of graphene oxide. *ACS Nano* **2008**, *2*, 1487–1491. [CrossRef]
345. Qiu, J.; Zhang, P.; Ling, M.; Li, S.; Liu, P.; Zhao, H.; Zhang, S. Photocatalytic synthesis of TiO_2 and reduced graphene oxide nanocomposite for lithium-ion batteries. *ACS Appl. Mater. Interfaces* **2012**, *4*, 3636–3642. [CrossRef] [PubMed]
346. Tong, X.; Zeng, M.; Li, J.; Li, F. UV-assisted synthesis of surface modified mesoporous TiO_2/G microspheres and its electrochemical performances in lithium ion batteries. *Appl. Surf. Sci.* **2017**, *392*, 897–903. [CrossRef]
347. Zhang, X.; Liu, Y.; Wang, X.; Li, B. Improving the anode performances of TiO_2–carbon–rGO composites in lithium ion batteries by UV irradiation. *New J. Chem.* **2015**, *39*, 9345–9350. [CrossRef]
348. Ren, Y.; Zhang, J.; Liu, Y.; Li, H.; Wei, H.; Li, B.; Wang, X. Synthesis and superior anode performances of TiO_2-carbon-rGO composites in lithium-ion batteries. *ACS Appl. Mater. Interfaces* **2012**, *4*, 4776–4780. [CrossRef]
349. Madhusanka, S.A. TiO_2 microparticles/reduced graphene oxide composite as anode material for lithium-ion battery. *Int. J. Electrochem. Sci.* **2020**, *15*, 2792–2805. [CrossRef]
350. Bai, L.; Fang, F.; Zhao, Y.; Liu, Y.; Li, J.; Huang, G.; Sun, H. A sandwich structure of mesoporous anatase TiO_2 sheets and reduced graphene oxide and its application as lithium-ion battery electrodes. *RSC Adv.* **2014**, *4*, 43039–43046. [CrossRef]
351. Park, J.; Kim, S.; Lee, G.; Choi, J. RGO-coated TiO_2 microcones for high-rate lithium-ion batteries. *ACS Omega* **2018**, *3*, 10205–10210. [CrossRef]
352. Yu, W.-B.; Hu, Z.-Y.; Jin, J.; Yi, M.; Yan, M.; Li, Y.; Wang, H.-E.; Gao, H.-X.; Mai, L.-Q.; Hasan, T.; et al. Unprecedented and highly stable lithium storage capacity of (001) faceted nanosheet-constructed hierarchically porous TiO_2/rGO hybrid architecture for high-performance Li-ion batteries. *Natl. Sci. Rev.* **2020**, *7*, 1046–1058. [CrossRef]
353. Liang, Y.; Xiong, X.; Xu, Z.; Xia, Q.; Wan, L.; Liu, R.; Chen, G.; Chou, S. Ultrathin 2D mesoporous TiO_2/rGO heterostructure for high-performance lithium storage. *Small* **2020**, *16*, 2000030. [CrossRef]

354. Wang, J.; Shen, L.; Li, H.; Wang, X.; Nie, P.; Ding, B.; Xu, G.; Dou, H.; Zhang, X. A facile one-pot synthesis of TiO_2/nitrogen-doped reduced graphene oxide nanocomposite as anode materials for high-rate lithium-ion batteries. *Electrochim. Acta* **2014**, *133*, 209–216. [CrossRef]
355. Li, J.; Huang, J.; Li, J.; Cao, L.; Qi, H.; Cheng, Y. N-doped TiO_2/rGO hybrids as superior Li-ion battery anodes with enhanced Li-ions storage capacity. *J. Alloys Compd.* **2019**, *784*, 165–172. [CrossRef]
356. Fang, R.; Miao, C.; Mou, H.; Xiao, W. Facile synthesis of Si@TiO_2@rGO composite with sandwich-like nanostructure as superior performance anodes for lithium ion batteries. *J. Alloys Compd.* **2020**, *818*, 152884. [CrossRef]
357. Shi, Y.; Wen, L.; Li, F.; Cheng, H.-M. Nanosized $Li_4Ti_5O_{12}$/graphene hybrid materials with low polarization for high rate lithium ion batteries. *J. Power Sources* **2011**, *196*, 8610–8617. [CrossRef]
358. Ri, S.G.; Zhan, L.; Wang, Y.; Zhou, L.; Hu, J.; Liu, H. $Li_4Ti_5O_{12}$/graphene nanostructure for lithium storage with high-rate performance. *Electrochim. Acta* **2013**, *109*, 389–394. [CrossRef]
359. Shen, L.; Yuan, C.; Luo, H.; Zhang, X.; Yang, S.; Lu, X. In situ synthesis of high-loading $Li_4Ti_5O_{12}$–graphene hybrid nanostructures for high rate lithium ion batteries. *Nanoscale* **2011**, *3*, 572–574. [CrossRef]
360. Kim, H.-K.; Jegal, J.-P.; Kim, J.-Y.; Yoon, S.-B.; Roh, K.C.; Kim, K.-B. In situ fabrication of lithium titanium oxide by microwave-assisted alkalization for high-rate lithium-ion batteries. *J. Mater. Chem. A* **2013**, *1*, 14849. [CrossRef]
361. Chen, W.; Jiang, H.; Hu, Y.; Dai, Y.; Li, C. Mesoporous single crystals $Li_4Ti_5O_{12}$ grown on rGO as high-rate anode materials for lithium-ion batteries. *Chem. Commun.* **2014**, *50*, 8856–8859. [CrossRef]
362. Ni, H.; Song, W.-L.; Fan, L.-Z. A strategy for scalable synthesis of Li4Ti5O12/reduced graphene oxide toward high rate lithium-ion batteries. *Electrochem. Commun.* **2014**, *40*, 1–4. [CrossRef]
363. Di, S.; Li, J.; Zhao, Y.; Hou, L.; Ma, Z.; Qin, X.; Shao, G. Hierarchical microspheres assembled from $Li_4Ti_5O_{12}$-TiO_2 nanosheets with advanced lithium ion storage. *Ionics* **2020**, *26*, 2763–2772. [CrossRef]
364. Chen, C.; Huang, Y.; Zhang, H.; Wang, X.; Li, G.; Wang, Y.; Jiao, L.; Yuan, H. Small amount of reduce graphene oxide modified $Li_4Ti_5O_{12}$ nanoparticles for ultrafast high-power lithium ion battery. *J. Power Sources* **2015**, *278*, 693–702. [CrossRef]
365. Zhang, J.; Cai, Y.; Wu, J.; Yao, J. Graphene oxide-confined synthesis of $Li_4Ti_5O_{12}$ microspheres as high-performance anodes for lithium ion batteries. *Electrochim. Acta* **2015**, *165*, 422–429. [CrossRef]
366. Jeong, J.H.; Kim, M.-S.; Kim, Y.-H.; Roh, K.C.; Kim, K.-B. High-rate $Li_4Ti_5O_{12}$/N-doped reduced graphene oxide composite using cyanamide both as nanospacer and a nitrogen doping source. *J. Power Sources* **2016**, *336*, 376–384. [CrossRef]
367. Cao, N.; Wen, L.; Song, Z.; Meng, W.; Qin, X. $Li_4Ti_5O_{12}$/reduced graphene oxide composite as a high-rate anode material for lithium ion batteries. *Electrochim. Acta* **2016**, *209*, 235–243. [CrossRef]
368. Ogechi, O.; Hao, T.; Osgood, H.; Zhang, B.; Chen, L.; Cui, L.; Song, X.-M.; Ogoke, O.; Wu, G. Advanced mesoporous spinel $Li_4Ti_5O_{12}$/rGO composites with increased surface lithium storage capability for high-power lithium-ion batteries. *ACS Appl. Mater. Interfaces* **2016**, *8*, 9162–9169. [CrossRef]
369. Meng, T.; Yi, F.; Cheng, H.; Hao, J.; Shuab, D.; Zhao, S.; He, C.; Song, X.; Zhang, F. Preparation of lithium titanate/reduced graphene oxide composites with three-dimensional "fishnet-like" conductive Structure via a gas-foaming method for high-rate lithium-ion batteries. *ACS Appl. Mater. Interfaces* **2017**, *9*, 42883–42892. [CrossRef]
370. Xiao, H.; Pender, J.P.; Meece-Rayle, M.A.; De Souza, J.P.; Klavetter, K.C.; Ha, H.; Lin, J.; Heller, A.; Ellison, C.J.; Mullins, C.B. Reduced-graphene oxide/poly(acrylic acid) aerogels as a three-dimensional replacement for metal-foil current collectors in lithium-ion batteries. *ACS Appl. Mater. Interfaces* **2017**, *9*, 22641–22651. [CrossRef]
371. Pender, J.P.; Xiao, H.; Dong, Z.; Cavallaro, K.A.; Weeks, J.A.; Heller, A.; Ellison, C.J.; Mullins, C.B. Compact lithium-ion battery electrodes with lightweight reduced graphene oxide/poly(acrylic acid) current collectors. *ACS Appl. Energy Mater.* **2018**, *2*, 905–912. [CrossRef]
372. Ha, H.; Shanmuganathan, K.; Ellison, C.J. Mechanically stable thermally crosslinked poly(acrylic acid)/reduced graphene oxide aerogels. *ACS Appl. Mater. Interfaces* **2015**, *7*, 6220–6229. [CrossRef]
373. Zhang, F.; Yiab, F.; Meng, T.; Gao, A.; Shuab, D.; Chen, H.; Cheng, H.; Zhou, X. In situ supramolecular self-assembly assisted synthesis of $Li_4Ti_5O_{12}$–carbon-reduced graphene oxide microspheres for lithium-ion batteries. *ACS Sustain. Chem. Eng.* **2018**, *7*, 916–924. [CrossRef]

374. Chen, Y.; Zhang, H.; Li, Y.; Chen, Y.; Luo, T. Electrochemical performance of $Li_4Ti_5O_{12}$/carbon nanotubes/graphene composite s an anode material in lithium-ion batteries. *Int. J. Hydrogen Energy* **2017**, *42*, 7195–7201. [CrossRef]
375. Roh, H.-K.; Lee, G.-W.; Haghighat-Shishavan, S.; Chung, K.Y.; Kim, K.-B. Polyol-mediated carbon-coated $Li_4Ti_5O_{12}$ nanoparticle/graphene composites with long-term cycling stability for lithium and sodium ion storages. *Chem. Eng. J.* **2020**, *385*, 123984. [CrossRef]
376. Uceda, M.; Chiu, H.-C.; Gauvin, R.; Zaghib, K.; Demopoulos, G.P. Electrophoretically co-deposited $Li_4Ti_5O_{12}$/reduced graphene oxide nanolayered composites for high-performance battery application. *Energy Storage Mater.* **2020**, *26*, 560–569. [CrossRef]
377. Mitra, S.; Poizot, P.; Finke, A.; Tarascon, J.-M. Growth and electrochemical characterization versus lithium of Fe_3O_4 electrodes made by electrodeposition. *Adv. Funct. Mater.* **2006**, *16*, 2281–2287. [CrossRef]
378. Zhu, S.P.; Fan, L.; Lu, Y.Y. Highly uniform Fe_3O_4 nanoparticle-rGO composites as anode materials for high performance lithium-ion batteries. *RSC Adv.* **2017**, *7*, 54939–54946. [CrossRef]
379. Su, Q.; Xie, D.; Zhang, J.; Du, G.; Xu, B. In situ transmission electron microscopy observation of the coversion mechanism of Fe_2O_3/graphene anode during lithiation-delithiation processes. *ACS Nano* **2013**, *7*, 9115–9121. [CrossRef]
380. Shi, Y.-H.; Wang, K.; Li, H.-H.; Wang, H.-F.; Li, X.-Y.; Wu, X.-L.; Zhang, J.-P.; Xie, H.-M.; Su, Z.-M.; Wang, J.; et al. Fe_3O_4 nanoflakes-RGO composites: A high rate anode material for lithium-ion batteries. *Appl. Surf. Sci.* **2020**, *511*, 145465. [CrossRef]
381. Lian, P.; Zhu, X.; Xiang, H.; Li, Z.; Yang, W.; Wang, H. Enhanced cycling performance of Fe_3O_4-graphene nanocomposite as an anode material for lithium-ion batteries. *Electrochim. Acta* **2010**, *56*, 834–840. [CrossRef]
382. Zhu, S.-P.; Wu, T.; Su, H.-M.; Qu, S.-S.; Xie, Y.-J.; Chen, M.; Diao, G. Hydrothermal synthesis of Fe_3O_4/rGO nanocomposites as anode materials for lithium ion batteries. *Acta Physico Chimica Sin.* **2016**, *32*, 2737–2744. [CrossRef]
383. Ji, L.; Tan, Z.; Kuykendall, T.R.; Aloni, S.; Xun, S.; Lin, E.; Battaglia, V.; Zhang, Y. Fe_3O_4 nanoparticle-integrated graphene sheets for high-performance half and full lithium ion cells. *Phys. Chem. Chem. Phys.* **2011**, *13*, 7170–7177. [CrossRef]
384. Zhu, X.; Zhu, Y.; Murali, S.; Stoller, M.D.; Ruoff, R.S. Nanostructured reduced graphene oxide/Fe_2O_3 composite as a high-performance anode material for lithium ion batteries. *ACS Nano* **2011**, *5*, 3333–3338. [CrossRef]
385. Tan, W.K.; Asami, K.; Maegawa, K.; Kumar, R.; Kawamura, G.; Muto, H.; Matsuda, A. Fe_3O_4-embedded rGO composites as anode for rechargeable FeOx-air batteries. *Mater. Today Commun.* **2020**, *25*, 101540. [CrossRef]
386. Kumar, R.; Singh, R.K.; Vaz, A.R.; Savu, R.; Moshkalev, S.A. Self-assembled and one-step synthesis of interconnected 3D network of Fe_3O_4/reduced graphene oxide nanosheets hybrid for high-performance supercapacitor electrode. *ACS Appl. Mater. Interfaces* **2017**, *9*, 8880–8890. [CrossRef]
387. Yang, Y.; Li, J.; Chen, D.; Zhao, J. A facile electrophoretic deposition route to the Fe_3O_4/CNTs/rGO composite electrode as a binder-free anode for lithium ion battery. *ACS Appl. Mater. Interfaces* **2016**, *8*, 26730–26739. [CrossRef] [PubMed]
388. Zhao, Q.; Liu, J.; Wang, Y.; Tian, W.; Liu, J.; Zang, J.; Ning, H.; Yang, C.; Wu, M. Novel in-situ redox synthesis of Fe_3O_4/rGO composites with superior electrochemical performance for lithium-ion batteries. *Electrochim. Acta* **2018**, *262*, 233–240. [CrossRef]
389. Bhuvaneswari, S.; Pratheeksha, P.M.; Anandan, S.; Rangappa, D.; Gopalan, R.; Rao, T.N. Efficient reduced graphene oxide grafted porous Fe_3O_4 composite as a high performance anode material for Li-ion batteries. *Phys. Chem. Chem. Phys.* **2014**, *16*, 5284–5294. [CrossRef] [PubMed]
390. Liang, C.-L.; Liu, Y.; Bao, R.-Y.; Luo, Y.; Yangb, W.; Xie, B.; Yang, M.-B. Effects of Fe_3O_4 loading on the cycling performance of Fe3O4/rGO composite anode material for lithium ion batteries. *J. Alloys Compd.* **2016**, *678*, 80–86. [CrossRef]
391. Wang, H.; Kalubowilage, M.; Bossmann, S.H.; Amama, P.B. Design of highly porous Fe_3O_4@reduced graphene oxide via a facile PMAA-induced assembly. *RSC Adv.* **2019**, *9*, 27927–27936. [CrossRef]
392. Xiao, Z.C.; Li, Y.; Liang, C.L.; Bao, R.Y.; Yang, M.B.; Yang, W. Scalable synthesis of an artificial polydopamine solid-electrolyte-interface-assisted 3D rGO/Fe_3O_4@PDA hydrogel for a highly stable anode with enhanced lithium-ion-storage properties. *ChemElectroChem* **2019**, *6*, 1069–1077. [CrossRef]

393. Qi, H.; Cao, L.; Li, J.; Huang, J.; Ma, M.; Cheng, Y.; Wang, C.; Dang, H. Rice crust-like Fe_3O_4@C/rGO with improved extrinsic pseudocapacitance for high-rate and long-life Li-ion anodes. *J. Alloys Compd.* **2019**, *804*, 57–64. [CrossRef]
394. Khan, A.J.; Javed, M.S.; Hanif, M.; Abbas, Y.; Liao, X.; Ahmed, G.; Saleem, M.; Yun, S.; Liu, Z. Facile synthesis of a novel Fe_3O_4-rGO-MoO_3 ternary nano-composite for high-performance hybrid energy storage applications. *Ceram. Int.* **2020**, *46*, 3124–3131. [CrossRef]
395. Pei, M.; Wu, Y.; Qi, Z.; Mei, D. Synthesis and electrochemical performance of NiO/Fe_3O_4/rGO as anode material for lithium ion battery. *Ionics* **2020**, *26*, 3831–3840. [CrossRef]
396. Xiao, Z.-C.; Li, Y.; Liang, C.-L.; Bao, R.-Y.; Yang, M.-B.; Yangb, W. Driven by electricity: Multilayered GO-Fe_3O_4@PDA-PAM flake assembled micro flower-like anode for high-performance lithium ion batteries. *Appl. Surf. Sci.* **2020**, *499*, 143934. [CrossRef]
397. Gao, R.; Wang, S.; Xu, Z.; Li, H.; Chen, S.; Hou, H. High-performance anode materials with superior structure of Fe_3O_4/FeS/rGO composite for lithium ion batteries. *Nano* **2020**, *15*, 2050128. [CrossRef]
398. Wu, Q.; Jiang, R.; Liu, H. Carbon layer encapsulated Fe_3O_4@reduced graphene oxide lithium battery anodes with long cycle performance. *Ceram. Int.* **2020**, *46*, 12732–12739. [CrossRef]
399. Liang, Y.; Lu, W. Gamma-irradiation synthesis of Fe_3O_4/rGO nanocomposites as lithium-ion battery anodes. *J. Mater. Sci. Mater. Electron.* **2020**, *31*, 17075–17083. [CrossRef]
400. Wang, J.; Deng, Q.; Qinglin, D.; Jiang, K.; Zhang, J.; Hu, Z.; Chu, J.; Wang, J.; Deng, Q.; Qinglin, D.; et al. Copper ferrites@reduced graphene oxide anode materials for advanced lithium storage applications. *Sci. Rep.* **2017**, *7*, 1–12. [CrossRef]
401. Gao, T.; Xu, C.; Li, R.; Zhang, R.; Wang, B.; Jiang, X.; Hu, M.; Bando, Y.; Kong, D.; Dai, P.; et al. Biomass-derived carbon paper to sandwich magnetite anode for long-life Li-ion battery. *ACS Nano* **2019**, *13*, 11901–11911. [CrossRef]
402. Jiao, Y.; Zhang, H.; Dong, T.; Shen, P.; Cai, Y.; Zhang, H.; Zhang, S. Improved electrochemical performance in nanoengineered pomegranate-shaped Fe_3O_4/RGO nanohybrids anode material. *J. Mater. Sci.* **2016**, *52*, 3233–3243. [CrossRef]
403. Lee, K.K.; Deng, S.; Fan, H.M.; Mhaisalkar, S.; Tan, H.R.; Tok, E.S.; Loh, K.P.; Chin, W.S.; Sow, C.H. α-Fe_2O_3 nanotubes-reduced graphene oxide composites as synergistic electrochemical capacitor materials. *Nanoscale* **2012**, *4*, 2958–2961. [CrossRef]
404. Zhang, Z.-J.; Wang, Y.-X.; Chou, S.-L.; Li, H.-J.; Liu, H.-K.; Wang, J.-Z. Rapid synthesis of α-Fe_2O_3/rGO nanocomposites by microwave autoclave as superior anodes for sodium-ion batteries. *J. Power Sources* **2015**, *280*, 107–113. [CrossRef]
405. Pradhan, G.K.; Padhi, D.K.; Parida, K.M. Fabrication of α-Fe_2O_3 nanorod/RGO composite: A novel hybrid photocatalyst for phenol degradation. *ACS Appl. Mater. Interfaces* **2013**, *5*, 9101–9110. [CrossRef] [PubMed]
406. Qu, J.; Yin, Y.-X.; Wang, Y.-Q.; Yan, Y.; Guo, Y.-G.; Song, W. Layer structured α-Fe_2O_3 nanodisk/reduced graphene oxide composites as high-performance anode materials for lithium-ion batteries. *ACS Appl. Mater. Interfaces* **2013**, *5*, 3932–3936. [CrossRef] [PubMed]
407. Liu, X.; Chen, T.; Chu, H.; Niu, L.; Sun, Z.; Pan, L.; Sun, C.Q. Fe_2O_3-reduced graphene oxide composites synthesized via microwave-assisted method for sodium ion batteries. *Electrochim. Acta* **2015**, *166*, 12–16. [CrossRef]
408. Wang, G.; Liu, T.; Luo, Y.; Zhao, Y.; Ren, Z.; Bai, J.; Wang, H. Preparation of Fe_2O_3/graphene composite and its electrochemical performance as an anode material for lithium ion batteries. *J. Alloys Compd.* **2011**, *509*, L216–L220. [CrossRef]
409. Wang, J.; Zhou, H.; Nanda, J.; Braun, P.V. Three-dimensionally mesostructured Fe_2O_3 electrodes with good rate performance and reduced voltage hysteresis. *Chem. Mater.* **2015**, *27*, 2803–2811. [CrossRef]
410. Liu, S.; Chen, Z.; Xie, K.; Li, Y.; Xu, J.; Zheng, C. A facile one-step hydrothermal synthesis of α-Fe_2O_3 nanoplates imbedded in graphene networks with high-rate lithium storage and long cycle life. *J. Mater. Chem. A* **2014**, *2*, 13942–13948. [CrossRef]
411. Lee, K.S.; Park, S.; Lee, W.; Yoon, Y.S. Hollow nanobarrels of α-Fe_2O_3 on reduced graphene oxide as high-performance anode for lithium-ion batteries. *ACS Appl. Mater. Interfaces* **2016**, *8*, 2027–2034. [CrossRef]
412. Xu, B.; Guan, X.; Zhang, L.Y.; Liu, X.; Jiao, Z.; Liu, X.; Hu, X.; Zhao, X.S. A simple route to preparing γ-Fe_2O_3/RGO composite electrode materials for lithium ion batteries. *J. Mater. Chem. A* **2018**, *6*, 4048–4054. [CrossRef]

413. Liu, Z.; Fu, H.; Gao, B.; Wang, Y.; Li, K.; Sun, Y.; Yin, J.; Kan, J. In-situ synthesis of Fe_2O_3/rGO using different hydrothermal methods as anode materials for lithium-ion batteries. *Rev. Adv. Mater. Sci.* **2020**, *59*, 477–487. [CrossRef]
414. Petnikota, S.; Marka, S.; Banerjee, A.; Reddy, M.; Srikanth, V.; Chowdari, B.; Reddy, M.V. Graphenothermal reduction synthesis of 'exfoliated graphene oxide/iron (II) oxide' composite for anode application in lithium ion batteries. *J. Power Sources* **2015**, *293*, 253–263. [CrossRef]
415. Zhou, X.; Wang, F.; Zhu, Y.; Liu, Z. Graphene modified $LiFePO_4$ cathode materials for high power lithium ion batteries. *J. Mater. Chem.* **2011**, *21*, 3353–3358. [CrossRef]
416. Qi, H.; Cao, L.; Li, J.; Huang, J.; Xu, Z.; Cheng, Y.; Kong, X.; Yanagisawa, K. High Pseudocapacitance in FeOOH/rGO composites with superior performance for high rate anode in Li-ion battery. *ACS Appl. Mater. Interfaces* **2016**, *8*, 35253–35263. [CrossRef] [PubMed]
417. Wu, C.; Xie, Y. Promising vanadium oxide and hydroxide nanostructures: From energy storage to energy saving. *Energy Environ. Sci.* **2010**, *3*, 1191–1206. [CrossRef]
418. Murphy, D.W.; Christian, P.A.; Disalvo, F.J.; Carides, J.N.; Waszczak, J.V. Lithium Incorporation by V_6O_{13} and Related Vanadium (+4, +5) Oxide Cathode Materials. *J. Electrochem. Soc.* **1981**, *128*, 2053–2060. [CrossRef]
419. Dai, X.; Wan, F.; Zhang, L.; Cao, H.; Niu, Z. Freestanding graphene/VO_2 composite films for highly stable aqueous Zn-ion batteries with superior rate performance. *Energy Storage Mater.* **2019**, *17*, 143–150. [CrossRef]
420. Yan, B.; Li, X.; Bai, Z.; Lin, L.; Chen, G.; Song, X.; Xiong, D.; Li, D.; Sun, X. Superior sodium storage of novel VO_2 nano-microspheres encapsulated into crumpled reduced graphene oxide. *J. Mater. Chem. A* **2017**, *5*, 4850–4860. [CrossRef]
421. Li, S.; Wei, Z.; Tang, Y.; Qian, K.; Li, Y.; Ji, S.; Luo, H.; Gao, Y.; Jin, P. Synthesis of reduced graphene oxide carried VO_2(B) Nanorods and their application in lithium-ion batteries. *Sci. Adv. Mater.* **2014**, *6*, 1293–1297. [CrossRef]
422. He, G.; Li, L.; Manthiram, A. VO_2/rGO nanorods as a potential anode for sodium- and lithium-ion batteries. *J. Mater. Chem. A* **2015**, *3*, 14750–14758. [CrossRef]
423. Nethravathi, C.; Viswanath, B.; Michael, J.; Rajamath, M. Hydrothermal synthesis of a monoclinic VO_2 nanotube–graphene hybrid for use as cathode material in lithium ion batteries. *Carbon* **2012**, *50*, 4839–4846. [CrossRef]
424. Song, H.J.; Choi, M.; Kim, J.-C.; Park, S.; Lee, C.W.; Hong, S.-H.; Kim, B.-K.; Kim, D.-W. Enhanced lithium storage in reduced graphene oxide-supported M-phase vanadium(IV) dioxide nanoparticles. *Sci. Rep.* **2016**, *6*, 30202. [CrossRef]
425. Choi, S.H.; Kang, Y.C. Uniform decoration of vanadium oxide nanocrystals on reduced graphene-oxide balls by an aerosol process for lithium-ion battery cathode material. *Chem. A Eur. J.* **2014**, *20*, 6294–6299. [CrossRef] [PubMed]
426. Sun, Y.; Yang, S.-B.; Lv, L.-P.; Lieberwirth, I.; Zhang, L.-C.; Ding, C.-X.; Chen, C.-H. A composite film of reduced graphene oxide modified vanadium oxide nanoribbons as a free standing cathode material for rechargeable lithium batteries. *J. Power Sources* **2013**, *241*, 168–172. [CrossRef]
427. Xiao, Z.; Peng, Z.; Wang, H.; Tang, Y. Synthesis and electrochemical properties of VO_2/rGO composite for high-performance anode materials for Li-ion batteries. *J. Funct. Mater.* **2017**, *48*, 9011–9017.
428. Shi, Y.; Chou, S.L.; Wang, J.Z.; Li, H.J.; Liu, H.K.; Wu, Y.P. In situ hydrothermal synthesis of graphene woven VO_2 nanoribbons with improved cycling performance. *J. Power Sources* **2013**, *244*, 684–689. [CrossRef]
429. Cui, F.; Zhao, J.; Zhang, D.; Fang, Y.; Hu, F.; Zhu, K. VO_2(B) nanobelts and reduced graphene oxides composites as cathode materials for low-cost rechargeable aqueous zinc ion batteries. *Chem. Eng. J.* **2020**, *390*, 124118. [CrossRef]
430. Zhao, H.; Pan, L.; Xing, S.; Luo, J.; Xu, J. Vanadium oxides–reduced graphene oxide composite for lithium-ion batteries and supercapacitors with improved electrochemical performance. *J. Power Sources* **2013**, *222*, 21–31. [CrossRef]
431. Lee, M.; Wee, B.-H.; Hong, J.-D. High Performance flexible supercapacitor electrodes composed of ultralarge graphene sheets and vanadium dioxide. *Adv. Energy Mater.* **2015**, *5*, 1401890. [CrossRef]
432. Xiao, X.; Li, S.; Wei, H.; Sun, D.; Wu, Y.; Jin, G.; Wang, F.; Zou, Y. Synthesis and characterization of VO_2(B)/graphene nanocomposite for supercapacitors. *J. Mater. Sci. Mater. Electron.* **2015**, *26*, 4226–4233. [CrossRef]

433. Zhang, J.; Chen, L.; Wang, Y.; Cai, S.; Yang, H.; Yu, H.; Shi, X.; Huang, C.; Liu, X.; Peng, Y. VO_2(B)/graphene composite-based symmetrical supercapacitor electrode via screen printing for intelligent packaging. *Nanomaterials* **2018**, *8*, 1020. [CrossRef]
434. Sahoo, R.; Lee, T.H.; Pham, D.T.; Luu, T.H.T.; Lee, Y.H. Fast-charging high-energy battery–supercapacitor hybrid: Anodic reduced graphene oxide–vanadium(IV) oxide sheet-on-sheet heterostructure. *ACS Nano* **2019**, *13*, 10776–10786. [CrossRef]
435. Lv, W.; Yang, C.; Meng, G.; Zhao, R.; Han, A.; Wang, R.; Liu, J. VO_2(B) nanobelts/reduced graphene oxide composites for high-performance flexible all-solid-state supercapacitors. *Sci. Rep.* **2019**, *9*, 1–8. [CrossRef] [PubMed]
436. Nethravathi, C.; Rajamathi, C.R.; Rajamathi, M.; Gautam, U.K.; Wang, X.; Golberg, D.; Bando, Y. N-Doped graphene–VO_2(B) nanosheet-built 3D flower hybrid for lithium ion battery. *ACS Appl. Mater. Interfaces* **2013**, *5*, 2708–2714. [CrossRef] [PubMed]
437. Reddy, C.S.; Ravichandran, D.; Rambabu, B.; Holze, R. Carbon and functionalized graphene oxide coated vanadium oxide electrodes for lithium ion batteries. *Appl. Surf. Sci.* **2014**, *305*, 596–602. [CrossRef]
438. Kang, M.S.; Park, S.K.; Nakhanivej, P.; Shin, K.H.; Yeon, J.S.; Park, H.S. Mesoporous VO_2(B) nanorods deposited onto graphene architectures for enhanced rate capability and cycle life of Li ion battery cathodes. *J. Alloys Compd.* **2020**, *855*, 157361. [CrossRef]
439. Song, Z.; Lu, X.; Hu, Q.; Lin, D.; Zheng, Q. Construction of reduced graphene oxide wrapped yolk–shell vanadium dioxide sphere hybrid host for high-performance lithium–sulfur batteries. *Dalton Trans.* **2020**, *49*, 14921–14930. [CrossRef] [PubMed]
440. Mahadi, N.B.; Park, J.-S.; Park, J.-H.; Chung, K.Y.; Yi, S.Y.; Sun, Y.-K.; Myung, S.-T. Vanadium dioxide−reduced graphene oxide composite as cathode materials for rechargeable Li and Na batteries. *J. Power Sources* **2016**, *326*, 522–532. [CrossRef]
441. Jiang, L.; Qu, Y.; Ren, Z.; Yu, P.; Zhao, D.; Zhou, W.; Wang, L.; Fu, H. In situ carbon-coated yolk–shell V_2O_3 microspheres for lithium-ion batteries. *ACS Appl. Mater. Interfaces* **2015**, *7*, 1595–1601. [CrossRef]
442. Song, H.J.; Choi, M.; Kim, J.-C.; Park, S.; Lee, C.W.; Hong, S.-H.; Kim, D.-W. Li-electroactivity of thermally-reduced V_2O_3 nanoparticles. *Mater. Lett.* **2016**, *180*, 243–246. [CrossRef]
443. Leng, J.; Mei, H.; Zhan, L.; Wang, Y.; Yang, S.; Song, Y. V_2O_3 nanoparticles anchored onto the reduced graphene oxide for superior lithium storage. *Electrochim. Acta* **2017**, *231*, 732–738. [CrossRef]
444. Xiao, B.; Zhang, B.; Tang, L.-B.; An, C.-S.; He, Z.-J.; Tong, H.; Yu, W.-J.; Zheng, J. V_2O_3/rGO composite as a potential anode material for lithium ion batteries. *Ceram. Int.* **2018**, *44*, 15044–15049. [CrossRef]
445. Zhang, Y.; Pan, A.; Liang, S.; Chen, T.; Tang, Y.; Tan, X. Reduced graphene oxide modified V_2O_3 with enhanced performance for lithium-ion battery. *Mater. Lett.* **2014**, *137*, 174–177. [CrossRef]
446. Liu, X.; Zhang, D.; Li, G.; Xue, C.; Ding, J.; Li, B.; Chen, D.; Li, L. In situ synthesis of V_2O_3 nanorods anchored on reduced graphene oxide as high-performance lithium ion battery anode. *ChemistrySelect* **2018**, *3*, 12108–12112. [CrossRef]
447. Ramana, C.V.; Smith, R.J.; Hussain, O.M.; Massot, M.; Julien, C.M. Surface analysis of pulsed laser-deposited V_2O_5 thin films and their lithium intercalated products studied by Raman spectroscopy. *Surf. Interface Anal.* **2005**, *37*, 406–411. [CrossRef]
448. Liu, Y.; Cao, G.; Zhang, Y.; Zhou, J.; Pan, A. Controllable preparation of V_2O_5/graphene nanocomposites as cathode materials for lithium-ion batteries. *Nanoscale Res. Lett.* **2016**, *11*, 549. [CrossRef]
449. Pandey, G.P.; Liu, T.; Brown, E.; Yang, Y.; Li, Y.; Sun, X.S.; Fang, Y.; Li, J.; Brown, J.E. Mesoporous hybrids of reduced graphene oxide and vanadium pentoxide for enhanced performance in lithium-ion batteries and electrochemical capacitors. *ACS Appl. Mater. Interfaces* **2016**, *8*, 9200–9210. [CrossRef]
450. Luo, W.; Zheng, B. Improved electrochemical performance of $LiNi_{0.5}Co_{0.2}Mn_{0.3}O_2$ cathode material by double-layer coating with graphene oxide and V_2O_5 for lithium-ion batteries. *Appl. Surf. Sci.* **2017**, *404*, 310–317. [CrossRef]
451. Liu, Q.; Li, Z.-F.; Liu, Y.; Zhang, H.; Ren, Y.; Sun, C.-J.; Lu, W.; Zhou, Y.; Stanciu, L.; Stach, E.A.; et al. Graphene-modified nanostructured vanadium pentoxide hybrids with extraordinary electrochemical performance for Li-ion batteries. *Nat. Commun.* **2015**, *6*, 6127. [CrossRef]
452. Cheng, J.; Wang, B.; Xin, H.L.; Yang, G.; Cai, H.-Q.; Nie, F.; Huang, H. Self-assembled V_2O_5 nanosheets/reduced graphene oxide hierarchical nanocomposite as a high-performance cathode material for lithium ion batteries. *J. Mater. Chem. A* **2013**, *1*, 10814–10820. [CrossRef]

453. Rui, X.; Zhu, J.; Sim, D.; Xu, C.; Zeng, Y.; Hng, H.H.; Lim, T.M.; Yan, Q. Reduced graphene oxide supported highly porous V_2O_5 spheres as a high-power cathode material for lithium ion batteries. *Nanoscale* **2011**, *3*, 4752–4758. [CrossRef]
454. Hu, B.; Xiang, Q.; Cen, Y.; Li, S.; Liu, L.; Yu, D.; Chen, C. In situ constructing flexible V_2O_5@GO composite thin film electrode for superior electrochemical energy storage. *J. Electrochem. Soc.* **2018**, *165*, A3738–A3747. [CrossRef]
455. Pham-Cong, D.; Ahn, K.; Hong, S.W.; Jeong, S.; Kim, D.-H.; Doh, C.; Jin, J.; Jeong, E.; Cho, C.R. Cathodic performance of V_2O_5 nanowires and reduced graphene oxide composites for lithium ion batteries. *Curr. Appl. Phys.* **2014**, *14*, 215–221. [CrossRef]
456. Kurc, B.; Wysokowski, M.; Rymaniak, L.; Lijewski, P.; Piasecki, A.; Fuc, P. The Impact of the vanadium oxide addition on the physicochemical performance stability and intercalation of lithium ions of the TiO_2-rGO-electrode in lithium ion batteries. *Materials* **2020**, *13*, 1018. [CrossRef] [PubMed]
457. Chen, D.; Quan, H.; Luo, S.; Luo, X.; Luoab, X.; Jiang, H. Reduced graphene oxide enwrapped vanadium pentoxide nanorods as cathode materials for lithium-ion batteries. *Phys. E Low-Dimens. Syst. Nanostruct.* **2014**, *56*, 231–237. [CrossRef]
458. Yan, B.; Li, X.; Bai, Z.; Zhao, Y.; Dong, L.; Song, X.; Li, D.; Langford, C.; Sun, X. Crumpled reduced graphene oxide conformally encapsulated hollow V_2O_5 nano/microsphere achieving brilliant lithium storage performance. *Nano Energy* **2016**, *24*, 32–44. [CrossRef]
459. Wang, S.; Zhu, K.; Yang, L.; Li, H.; Wang, S.; Tang, S.; Zhang, M.; Abliz, A.; Zhao, F. Synthesis and study of V_2O_5/rGO nanocomposite as a cathode material for aqueous zinc ion battery. *Ionics* **2020**, *26*, 1–9. [CrossRef]
460. Du, X.; Huang, G.; Qin, Y.-L.; Wang, L. Solvothermal synthesis of GO/V_2O_5 composites as a cathode material for rechargeable magnesium batteries. *RSC Adv.* **2015**, *5*, 76352–76355. [CrossRef]
461. Xu, J.; Li, Z.; Zhang, X.; Huang, S.; Jiang, S.; Zhu, Q.; Sun, H.; Zakharova, G.S. Self-assembled V_3O_7/graphene oxide nanocomposites as cathode material for lithium-ion batteries. *Int. J. Nanotechnol.* **2014**, *11*, 808. [CrossRef]
462. Ramadoss, A.; Saravanakumar, B.; Kim, S.-J. Vanadium pentoxide/reduced graphene oxide composite as an efficient electrode material for high-performance supercapacitors and self-powered systems. *Energy Technol.* **2015**, *3*, 913–924. [CrossRef]
463. Zhang, H.; Xie, A.; Wang, C.; Wang, H.; Shen, Y.; Tian, X. Bifunctional reduced graphene oxide/V_2O_5 composite hydrogel: Fabrication, high performance as electromagnetic wave absorbent and supercapacitor. *ChemPhysChem* **2013**, *15*, 366–373. [CrossRef]
464. Foo, C.Y.; Sumboja, A.; Tan, D.J.H.; Wang, J.; Lee, P.S. Flexible and highly scalable V_2O_5-rGO electrodes in an organic electrolyte for supercapacitor devices. *Adv. Energy Mater.* **2014**, *4*, 1400236. [CrossRef]
465. Zhang, Y.; Wang, Y.; Xiong, Z.; Hu, Y.; Song, W.; Huang, Q.-A.; Cheng, X.; Chen, L.-Q.; Sun, C.; Gu, H. V_2O_5 nanowire composite paper as a high-performance lithium-ion battery cathode. *ACS Omega* **2017**, *2*, 793–799. [CrossRef] [PubMed]
466. Li, M.; Sun, G.; Yin, P.; Ruan, C.; Ai, K. Controlling the formation of rodlike V_2O_5 nanocrystals on reduced graphene oxide for high-performance supercapacitors. *ACS Appl. Mater. Interfaces* **2013**, *5*, 11462–11470. [CrossRef] [PubMed]
467. Deng, L.; Zhang, G.; Kang, L.; Lei, Z.; Liu, C.; Liu, Z. Graphene/VO_2 hybrid material for high performance electrochemical capacitor. *Electrochim. Acta* **2013**, *112*, 448–457. [CrossRef]
468. Fu, M.; Ge, C.; Hou, Z.; Cao, J.; He, B.; Zeng, F.; Kuang, Y. Graphene/vanadium oxide nanotubes composite as electrode material for electrochemical capacitors. *Phys. B Condens. Matter* **2013**, *421*, 77–82. [CrossRef]
469. Wang, H.; Yi, H.; Chen, X.; Wang, X. One-step strategy to three-dimensional graphene/VO_2 nanobelt composite hydrogels for high performance supercapacitors. *J. Mater. Chem. A* **2014**, *2*, 1165–1173. [CrossRef]
470. Perera, S.D.; Liyanage, A.D.; Nijem, N.; Ferraris, J.P.; Chabal, Y.J.; Balkus, J.K.J. Vanadium oxide nanowire—Graphene binder free nanocomposite paper electrodes for supercapacitors: A facile green approach. *J. Power Sources* **2013**, *230*, 130–137. [CrossRef]
471. Li, H.; Wei, J.; Qian, Y.; Zhang, J.; Yu, J.; Wang, G.; Xu, G. Effects of the graphene content and the treatment temperature on the supercapacitive properties of VO_x/graphene nanocomposites. *Colloids Surf. A Physicochem. Eng. Asp.* **2014**, *449*, 148–156. [CrossRef]

472. Saravanakumar, B.; Purushothaman, K.K.; Muralidharan, G. Fabrication of two-dimensional reduced graphene oxide supported V_2O_5 networks and their application in supercapacitors. *Mater. Chem. Phys.* **2016**, *170*, 266–275. [CrossRef]
473. Govindarajan, D.; Shankar, V.U.; Gopalakrishnan, R. Supercapacitor behavior and characterization of RGO anchored V_2O_5 nanorods. *J. Mater. Sci. Mater. Electron.* **2019**, *30*, 16142–16155. [CrossRef]
474. Zhang, B.; Han, Y.-D.; Zheng, J.; Zhang, J.-F.; Shen, C.; Ming, L.; Yuan, X.-B.; Li, H. $VOPO_4$ nanosheets as anode materials for lithium-ion batteries. *Chem. Commun.* **2014**, *50*, 11132–11134. [CrossRef]
475. He, Y.; Yang, X.; Bai, Y.; Zhang, J.; Kang, L.; Lei, Z.; Liu, Z. Vanadyl phosphate/reduced graphene oxide nanosheet hybrid material and its capacitance. *Electrochim. Acta* **2015**, *178*, 312–320. [CrossRef]
476. Lu, W.; Cong, L.; Liu, Y.; Liu, J.; Mauger, A.; Julien, C.M.; Sun, L.; Xie, H. Pseudocapacitance controlled fast-charging and long-life lithium ion battery achieved via a 3D mutually embedded VPO_4/rGO electrode. *J. Alloys Compd.* **2020**, *812*, 152135. [CrossRef]
477. Yao, Z.; Kim, S.; Aykol, M.; Li, Q.; Wu, J.; He, J.; Wolverton, C. Revealing the conversion mechanism of transition metal oxide electrodes during lithiation from first-principles. *Chem. Mater.* **2017**, *29*, 9011–9022. [CrossRef]
478. Kumar, N.; Huang, C.-W.; Yen, P.-J.; Wu, W.-W.; Wei, K.-H.; Tseng, T.Y. Probing the electrochemical properties of an electrophoretically deposited Co_3O_4/rGO/CNTs nanocomposite for supercapacitor applications. *RSC Adv.* **2016**, *6*, 60578–60586. [CrossRef]
479. Bankole, O.M.; Olaseni, S.E.; Adeyemo, M.A.; Ogunlaja, A.S. Microwave-assisted synthesis of cobalt oxide/reduced graphene oxide (Co_3O_4–rGo) composite and its sulfite enhanced photocatalytic degradation of organic Dyes. *Z. Phys. Chem.* **2020**, *234*, 1681–1708. [CrossRef]
480. Chen, S.Q.; Wang, Y. Microwave-assisted synthesis of a Co_3O_4–graphene sheet-on-sheet nanocomposite as a superior anode material for Li-ion batteries. *J. Mater. Chem.* **2010**, *20*, 9735–9739. [CrossRef]
481. Yang, X.; Fan, K.; Zhu, Y.; Shen, J.; Jiang, X.; Zhao, P.; Li, C. Tailored graphene-encapsulated mesoporous Co_3O_4 composite microspheres for high-performance lithium ion batteries. *J. Mater. Chem.* **2012**, *22*, 17278–17283. [CrossRef]
482. Wu, Z.-S.; Ren, W.; Wen, L.; Gao, L.; Zhao, J.; Chen, Z.; Zhou, G.; Li, F.; Cheng, H.-M. Graphene anchored with Co_3O_4 nanoparticles as anode of lithium ion batteries with enhanced reversible capacity and cyclic performance. *ACS Nano* **2010**, *4*, 3187–3194. [CrossRef]
483. Zhang, W.; Zeng, Y.; Xiao, N.; Hng, H.H.; Yan, Q. One-step electrochemical preparation of graphene-based heterostructures for Li storage. *J. Mater. Chem.* **2012**, *22*, 8455–8461. [CrossRef]
484. Pan, L.; Zhao, H.; Shen, W.; Dong, X.; Xu, J. Surfactant-assisted synthesis of a Co_3O_4/reduced graphene oxide composite as a superior anode material for Li-ion batteries. *J. Mater. Chem. A* **2013**, *1*, 7159–7166. [CrossRef]
485. Lou, Y.; Liang, J.; Peng, Y.; Chen, J. Ultra-small Co_3O_4 nanoparticles–reduced graphene oxide nanocomposite as superior anodes for lithium-ion batteries. *Phys. Chem. Chem. Phys.* **2015**, *17*, 8885–8893. [CrossRef] [PubMed]
486. Cho, S.-H.; Jung, J.-W.; Kim, C.; Kim, I.-D. Rational design of 1-D Co_3O_4 nanofibers@low content graphene composite anode for high performance Li-ion batteries. *Sci. Rep.* **2017**, *7*, srep45105. [CrossRef] [PubMed]
487. Kesavan, T.; Gunawardhana, N.; Senthil, C.; Kundu, M.; Maduraiveeran, G.; Yoshio, M.; Sasidharan, M. Fabrication of hollow Co_3O_4 nanospheres and their nanocomposites of CNT and rGO as high-performance anodes for lithium-ion batteries. *ChemistrySelect* **2018**, *3*, 5502–5511. [CrossRef]
488. Park, S.-H.; Kim, H.-K.; Roh, K.C.; Kim, K.-B. Co_3O_4-reduced graphene oxide nanocomposite synthesized by microwave-assisted hydrothermal process for Li-ion batteries. *Electron. Mater. Lett.* **2015**, *11*, 282–287. [CrossRef]
489. Zhang, K.; Lee, T.H.; Cha, J.H.; Jang, H.W.; Choi, J.-W.; Mahmoudi, M.; Shokouhimehr, M. Metal-organic framework-derived metal oxide nanoparticles@reduced graphene oxide composites as cathode materialf for rechargeable aluminum-ion batteries. *Sci. Rep.* **2019**, *9*, 13739. [CrossRef]
490. Mussa, Y.; Ahmed, F.; Arsalan, M.; Alsharaeh, E.H. Two dimensional (2D) reduced graphene oxide (RGO)/hexagonal boron nitride (h-BN) based nanocomposites as anodes for high temperature rechargeable lithium-ion batteries. *Sci. Rep.* **2020**, *10*, 1882. [CrossRef]
491. Liang, Y.; Li, Y.; Wang, H.; Zhou, J.; Wang, J.; Regier, T.; Dai, H. Co_3O_4 nanocrystals on graphene as a synergistic catalyst for oxygen reduction reaction. *Nat. Mater.* **2011**, *10*, 780–786. [CrossRef]

492. Li, D.; Shi, D.; Chen, Z.; Liu, H.K.; Jia, D.; Guo, Z. Enhanced rate performance of cobalt oxide/nitrogen doped graphene composite for lithium ion batteries. *RSC Adv.* **2013**, *3*, 5003–5008. [CrossRef]
493. Lee, J.S.; Jo, M.S.; Saroha, R.; Jung, D.S.; Seon, Y.H.; Lee, J.S.; Kang, Y.C.; Kang, D.-W.; Cho, J.S. Hierarchically well-developed porous graphene nanofibers comprising N-doped graphitic C-coated cobalt oxide hollow nanospheres as anodes for high-rate Li-ion batteries. *Small* **2020**, *16*, 2002213. [CrossRef]
494. Park, G.D.; Cho, J.S.; Kang, Y.C. Novel cobalt oxide-nanobubble-decorated reduced graphene oxide sphere with superior electrochemical properties prepared by nanoscale Kirkendall diffusion process. *Nano Energy* **2015**, *17*, 17–26. [CrossRef]
495. Sun, Y.; Hu, X.; Luo, W.; Huang, Y. Ultrathin CoO/graphene hybrid nanosheets: A highly stable anode material for lithium-ion batteries. *J. Phys. Chem. C* **2012**, *116*, 20794–20799. [CrossRef]
496. Fu, G.; Chang, K.; Shangguan, E.; Tang, H.; Li, B.; Chang, Z.; Yuan, X.-Z.; Wang, H. Synthesis of CoO/reduced graphene oxide composite as an alternative additive for the nickel electrode in alkaline secondary batteries. *Electrochim. Acta* **2015**, *180*, 373–381. [CrossRef]
497. Bindumadhavan, K.; Yeh, M.-H.; Chou, T.-C.; Chang, P.-Y.; Andoongc, R.-. Ultrafine CoO Embedded reduced graphene oxide nanocomposites: A high rate anode for Li-ion battery. *ChemistrySelect* **2016**, *1*, 5758–5767. [CrossRef]
498. Bindumadhavan, K.; Chang, P.-Y.; Yeh, M.-H.; Andoongc, R.-. Ultra-small CoO nanocrystals anchored on reduced graphene oxide for enhanced lithium storage in lithium ion batteries. *MRS Commun.* **2017**, *7*, 236–244. [CrossRef]
499. Wang, L.; Zhao, D.; Liu, X.; Yu, P.; Fu, H. Hydrothermal for synthesis of CoO nanoparticles/graphene composite as Li-ion battery anodes. *Acta Chim. Sin.* **2017**, *75*, 231. [CrossRef]
500. Sun, L.; Deng, Q.; Li, Y.; Mi, H.; Wang, S.; Deng, L.; Ren, X.; Zhang, P. CoO-Co_3O_4 heterostructure nanoribbon/RGO sandwich-like composites as anode materials for high performance lithium-ion batteries. *Electrochim. Acta* **2017**, *241*, 252–260. [CrossRef]
501. Cao, L.; Kang, Q.; Li, J.; Huang, J.; Cheng, Y. Assembly control of CoO/reduced graphene oxide composites for their enhanced lithium storage behavior. *Appl. Surf. Sci.* **2018**, *455*, 96–105. [CrossRef]
502. Leng, X.; Ding, X.; Hu, J.; Wei, S.; Jiang, Z.; Lian, J.; Wang, G.; Jiang, Q.; Liu, J. In situ prepared reduced graphene oxide/CoO nanowires mutually-supporting porous structure with enhanced lithium storage performance. *Electrochim. Acta* **2016**, *190*, 276–284. [CrossRef]
503. Yin, J.; Sun, P.; Qu, G.; Xiang, G.; Hou, P.; Xu, X. A new CoO/Co_2B/rGO nanocomposite anode with large capacitivecontribution for high-efficiency and durable lithium storage. *Appl. Surf. Sci.* **2020**, *508*, 144698. [CrossRef]
504. Guan, X.; Nai, J.; Zhang, Y.; Wang, P.; Yang, J.; Zheng, L.; Zhang, J.; Guo, L. CoO hollow cube/reduced graphene oxide composites with enhanced lithium storage capability. *Chem. Mater.* **2014**, *26*, 5958–5964. [CrossRef]
505. Zhu, W.; Huang, H.; Gan, Y.; Tao, X.; Xia, Y.; Zhang, W. Mesoporous cobalt monoxide nanorods grown on reduced graphene oxide nanosheets with high lithium storage performance. *Electrochim. Acta* **2014**, *138*, 376–382. [CrossRef]
506. Zhang, M.; Wang, Y.; Jia, M. Three-dimensional reduced graphene oxides hydrogel anchored with ultrafine CoO nanoparticles as anode for lithium ion batteries. *Electrochim. Acta* **2014**, *129*, 425–432. [CrossRef]
507. Zhang, M.; Jia, M.; Jin, Y.; Shi, X. Synthesis and electrochemical performance of CoO/graphene nanocomposite as anode for lithium ion batteries. *Appl. Surf. Sci.* **2012**, *263*, 573–578. [CrossRef]
508. Zhang, H.; Wang, Y.-F.; Liu, W.-L.; Kong, F.; Ren, M.; Wang, S.-J.; Wang, X.-Q.; Duan, X.-L.; Peng, D. Designed synthesis of CoO/CuO/rGO ternary nanocomposites as high-performance anodes for lithium-ion batteries. *JOM* **2018**, *70*, 1793–1799. [CrossRef]
509. Song, Z.; Liu, W.; Sun, N.; Wei, W.; Zhang, Z.; Liu, H.; Liu, G.; Zhao, Z. One-step self-assembly fabrication of three-dimensional copper oxide/graphene oxide aerogel composite material for supercapacitors. *Solid State Commun.* **2019**, *287*, 27–30. [CrossRef]
510. Liu, Y.; Cai, X.; Shi, W. Free-standing graphene/carbon nanotubes/CuO aerogel paper anode for lithium ion batteries. *Mater. Lett.* **2016**, *172*, 72–75. [CrossRef]
511. Zhu, S.; Wu, M.; Ge, M.-H.; Zhang, H.; Lia, S.; Li, C.-H. Design and construction of three-dimensional CuO/polyaniline/rGO ternary hierarchical architectures for high performance supercapacitors. *J. Power Sources* **2016**, *306*, 593–601. [CrossRef]

512. Zhao, Y.; Song, X.; Song, Q.; Yin, Z. A facile route to the synthesis copper oxide/reduced graphene oxide nanocomposites and electrochemical detection of catechol organic pollutant. *CrystEngComm* **2012**, *14*, 6710–6719. [CrossRef]
513. Zhu, J.; Zeng, G.; Nie, F.; Xu, X.; Chen, S.; Han, Q.; Wang, X. Decorating graphene oxide with CuO nanoparticles in a water–isopropanol system. *Nanoscale* **2010**, *2*, 988–994. [CrossRef]
514. Rai, A.K.; Anh, L.T.; Gim, J.; Mathew, V.; Kang, J.; Paul, B.J.; Singh, N.K.; Song, J.; Kim, J. Facile approach to synthesize CuO/reduced graphene oxide nanocomposite as anode materials for lithium-ion battery. *J. Power Sources* **2013**, *244*, 435–441. [CrossRef]
515. Xu, Y.-T.; Guo, Y.; Li, C.; Zhou, X.-Y.; Tucker, M.C.; Chen, J.; Sun, R.; Wong, C.-P. Graphene oxide nano-sheets wrapped Cu_2O microspheres as improved performance anode materials for lithium ion batteries. *Nano Energy* **2015**, *11*, 38–47. [CrossRef]
516. Sun, L.; Deng, Q.; Li, Y.; Deng, L.; Wang, Y.; Ren, X.; Zhang, P. Solvothermal synthesis of ternary Cu_2O-CuO-RGO composites as anode materials for high performance lithium-ion batteries. *Electrochim. Acta* **2016**, *222*, 1650–1659. [CrossRef]
517. Sheikhzadeh, M.; Sanjabi, S.; Gorji, M.; Khabazian, S. Nano composite foam layer of CuO/graphene oxide (GO) for high performance supercapacitor. *Synth. Met.* **2018**, *244*, 10–14. [CrossRef]
518. Mirzaiey, V.; Dehghanian, C.; Bokati, K.S. One-step electrodeposition of reduced graphene oxide on three-dimensional porous nano nickel-copper foam electrode and its use in supercapacitor. *J. Electroanal. Chem.* **2018**, *813*, 152–162. [CrossRef]
519. Li, X.; Fan, L.; Li, X.; Shan, H.; Chen, C.; Yan, B.; Xiong, D.; Li, D. Enhanced anode performance of flower-like NiO/RGO nanocomposites for lithium-ion batteries. *Mater. Chem. Phys.* **2018**, *217*, 547–552. [CrossRef]
520. Liu, A.; Zhang, H.; Wang, G.; Zhang, J.; Zhang, S. Sandwich-like NiO/rGO nanoarchitectures for 4 V solid-state asymmetric-supercapacitors with high energy density. *Electrochim. Acta* **2018**, *283*, 1401–1410. [CrossRef]
521. Tian, S. Preparation of RGO/NiO Anode for Lithium-ion Batteries. *Int. J. Electrochem. Sci.* **2019**, *14*, 9459–9467. [CrossRef]
522. Ma, L.; Pei, X.-Y.; Mo, D.-C.; Heng, Y.; Lyu, S.-S.; Fu, Y.-X. Facile fabrication of NiO flakes and reduced graphene oxide (NiO/RGO) composite as anode material for lithium-ion batteries. *J. Mater. Sci. Mater. Electron.* **2019**, *30*, 5874–5880. [CrossRef]
523. Ma, L.; Lyu, S.-S.; Dai, Y.; Pei, X.-Y.; Mo, D.-C.; Fu, Y.-X. Lithium storage properties of NiO/reduced graphene oxide composites derived from different oxidation degrees of graphite oxide. *J. Alloys Compd.* **2019**, *810*, 151954. [CrossRef]
524. Li, Q.; Wei, Q.; Xie, L.; Chen, C.; Lu, C.; Su, F.; Zhou, P. Layered NiO/reduced graphene oxide composites by heterogeneous assembly with enhanced performance as high-performance asymmetric supercapacitor cathode. *RSC Adv.* **2016**, *6*, 46548–46557. [CrossRef]
525. Ren, Y.; Wang, J.; Ding, J. The synthesis and lithium storage performance of NiO/rGO/PPy anode materials. *J. Changzhou Univ. (Nat. Sci.)* **2015**, *27*, 18–23.
526. Ma, L.; Pei, X.-Y.; Mo, D.-C.; Lyu, S.-S.; Fu, Y.-X. Fabrication of NiO-ZnO/rGO composite as an anode material for lithium-ion batteries. *Ceram. Int.* **2018**, *44*, 22664–22670. [CrossRef]
527. Park, G.D.; Cho, J.S.; Kang, Y.C. Multiphase and double-layer $NiFe_2O_4$@NiO-hollow-nanosphere-decorated reduced graphene oxide composite powders prepared by spray pyrolysis applying nanoscale Kirkendall diffusion. *ACS Appl. Mater. Interfaces* **2015**, *7*, 16842–16849. [CrossRef] [PubMed]
528. Li, C.; Wang, X.; Li, S.; Li, Q.; Xu, J.; Liu, X.; Liu, C.; Xu, Y.; Liu, J.; Li, H.; et al. Optimization of $NiFe_2O_4$/rGO composite electrode for lithium-ion batteries. *Appl. Surf. Sci.* **2017**, *416*, 308–317. [CrossRef]
529. Jo, M.S.; Lee, J.S.; Jeong, S.Y.; Kim, J.K.; Kang, Y.C.; Kang, D.-W.; Jeong, S.M.; Cho, J.S. Golden bristlegrass-like hierarchical graphene nanofibers entangled with N-doped CNTs containing $CoSe_2$ nanocrystals at each node for high-performance anodes in sodium-ion batteries. *Small* **2020**, *16*, 2003391. [CrossRef] [PubMed]
530. Cho, J.S.; Park, S.-K.; Jeon, K.M.; Piao, Y.; Cho, J.S. Mesoporous reduced graphene oxide/WSe_2 composite particles for efficient sodium-ion batteries and hydrogen evolution reactions. *Appl. Surf. Sci.* **2018**, *459*, 309–317. [CrossRef]
531. Cho, J.S.; Lee, S.Y.; Lee, J.-K.; Kang, Y.C. Iron telluride-decorated reduced graphene oxide hybrid microspheres as anode materials with improved Na-ion storage properties. *ACS Appl. Mater. Interfaces* **2016**, *8*, 21343–21349. [CrossRef]

532. Cho, J.S.; Lee, S.Y.; Kang, Y.C. First introduction of $NiSe_2$ to anode material for sodium-ion batteries: A hybrid of graphene-wrapped $NiSe_2$/C porous nanofiber. *Sci. Rep.* **2016**, *6*, 23338. [CrossRef]
533. Cho, J.S.; Lee, J.-K.; Kang, Y.C. Graphitic carbon-coated $FeSe_2$ hollow nanosphere-decorated reduced graphene oxide hybrid nanofibers as an efficient anode material for sodium ion batteries. *Sci. Rep.* **2016**, *6*, 23699. [CrossRef]
534. Park, G.D.; Cho, J.S.; Lee, J.-K.; Kang, Y. Na-ion storage performances of $FeSe_x$ and Fe_2O_3 hollow nanoparticles-decorated reduced graphene oxide balls prepared by nanoscale Kirkendall diffusion Process. *Sci. Rep.* **2016**, *6*, 22432. [CrossRef]
535. Mohan, V.B.; Lau, K.-T.; Hui, D.; Bhattacharyya, D. Graphene-based materials and their composites: A review on production, applications and product limitations. *Compos. Part B Eng.* **2018**, *142*, 200–220. [CrossRef]
536. Gadgil, B.; Damlin, P.; Kvarnström, C. Graphene vs. reduced graphene oxide: A comparative study of graphene-based nanoplatforms on electrochromic switching kinetics. *Carbon* **2016**, *96*, 377–381. [CrossRef]